Numerical modelling of the impact of tidal currents over the long-term : application to Holocene sedimentary records from the bay of Brest

Matthieu Guillaume Olivier

DOCTORAT SCIENCES BRETAGNE DE LA MER LOIRE ET DU LITTORAL

UBO
Université de Bretagne Occidentale

Ifremer

ifp Energies nouvelles

THESE DE DOCTORAT DE

L'UNIVERSITE
DE BRETAGNE OCCIDENTALE

ECOLE DOCTORALE N° 598
Sciences de la Mer et du littoral
Spécialité : Géosciences Marines

Par
Matthieu Guillaume OLIVIER

Numerical modelling of the impact of tidal currents over the long-term: application to Holocene sedimentary records from the bay of Brest.

Thèse présentée et soutenue à Plouzané, le 10 mai 2022
Unité de recherche : Laboratoire Geo-ocean, UMR6538 (UBO, CNRS, IFREMER)
IFPEN, Direction des Sciences de la Terre et Technologie de l'Environnement

Rapporteurs avant soutenance :

Jean-Yves REYNAUD
Professeur, Université de Lille1, France
Xavier BERTIN
Directeur de Recherche, CNRS, La Rochelle Université

Composition du Jury :

Jean-Yves REYNAUD – Rapporteur – **Président du Jury**
Professeur, Université de Lille1, France
Xavier BERTIN – Rapporteur
Directeur de Recherche, CNRS, La Rochelle Université

Bernadette TESSIER – Examinatrice
Directrice de recherche, CNRS, Université de Caen, France
Mattias GREEN – Examinateur
Professor, Bangor University, United Kingdom
Pascal Le Roy – Examinateur
Directeur de recherche, IUEM, France

Marina RABINEAU – Directrice de Thèse
Directrice de recherche, CNRS, IUEM, France
Estelle LEROUX – Co-encadrement de thèse
Chercheuse, IFREMER, France
Héloïse MULLER – Co-encadrement de thèse
Chercheuse, IFREMER, France

Invités
Didier GRANJEON – Promoteur de la thèse
Chercheur, IFPEN, France
Pierre Le Hir– Co-encadrement de thèse
Chercheur, IFREMER, FRANCE

Acknowledgement

This part of the manuscript is intended mainly for French people and for this reason it is written in French. All the scientific parts are written in English. I would like to take this opportunity to thank Jean-Yves Reynaud and Xavier Bertin for agreeing to be examiners for this thesis. I want to thank also Bernadette Tessier, Mattias Green and Pascal Le Roy for accepting to be part of the jury. I hope that the reading will not be too long or redundant, as the thesis contains two articles. I hope you will appreciate the message it carries and I look forward to hearing your feedbacks.

Remerciements

Je souhaite remercier l'IFREMER, ainsi que l'IFPEN d'avoir rendu possible ces travaux de thèse en les finançant, ainsi que l'UBO et l'EDSML (spécialement Elodie et Elisabeth) pour le cadre et le suivi de la thèse.

Je souhaite remercier en tout premier lieu Estelle, tu as été le pilier de cette thèse. Depuis les premiers jours, tu es au front pour batailler contre mes difficultés à me faire comprendre à l'écrit. Tu as subi des marées de versions d'articles et de chapitres à s'arracher les cheveux depuis maintenant trois ans, sur des notions dont tu n'es pas forcément spécialiste. Je dis bravo, bravo d'avoir su déchiffrer mes idées au milieu des phrases à rallonge, sans verbe, et j'en passe… Je te remercie d'avoir été un soutien, parfois dure certes (je me souviendrai toujours de ce commentaire écrit dans la discussion d'un article : « puff… c'est nul on s'ennuie »), mais infaillible, pour ton jeune et maladroit Padawan. Merci pour tout Estelle, je te dois beaucoup.

Un gros merci également à Didier, tu as essuyé de nombreuses expériences similaires. Ta faculté à être toujours positif, ta pédagogie, ta patience, ta vitesse de compréhension (hallucinante) font de toi un encadrant remarquable. J'ai appris énormément à tes côtés, et merci de t'être creusé la tête jusqu'aux derniers moments avec moi sur les concepts les plus complexes de cette thèse.

Je souhaite remercier chaleureusement Héloïse, tu as dû gérer et former un géologue qui s'essaye à l'hydrodynamique à des échelles de temps et de façon… spéciales ! Sans toi je n'aurais jamais réussi à mettre en place cette modélisation. Il est important de souligner ta patience et ta gentillesse, tu ne t'es pas découragée quand je te demandais de l'aide sur les post traitements et concepts hydrodynamiques les plus simples au début. Merci beaucoup !

Je te remercie chaleureusement Marina, pour ton soutien et ton expertise toujours pertinente. Tu fais partie de ces gens sur lesquels on peut compter et qui n'ont pas peur de prendre les choses en main. Tu as toujours réagi sans délai pour régler les problèmes les plus épineux. Pour ne citer que deux exemples : quand mon premier article a été publié sans que l'on ait pu voir un pre-print, tu n'as pas hésité une seconde à appeler les responsables en Inde à plusieurs reprises, ou encore, à calmer les esprits quand je m'emportais contre notre hiérarchie. Merci pour toutes nos discussions, ton soutien et tes corrections efficaces (sans toi j'aurais toujours une coquille de bivalve à la place d'une carotte en exemple dans mon état de l'art).

Un gros merci à Pierre également, tu as été un des acteurs majeurs de cette thèse. Tes connaissances en modélisation hydro-sédimentaire sans limites ont nettement amélioré la qualité des simulations réalisées et des discussions sur les processus hydrodynamiques et hydro-sédimentaires. Tu mets toujours la barre un peu plus haute, à chaque nouvelle simulation, version d'article, etc… Au premier

abord, cela peut sembler dur mais, à mon avis, tu le fais par passion pour ton domaine et le résultat est une amélioration indiscutable des résultats et des discussions. Merci pour ton aide et tes commentaires avisés.

Je souhaite également remercier Laure, Axel, Pascal, Gwen et Nicolas pour tous les précieux conseils et avis que vous m'avez donnés au cours de cette thèse.

Merci à Laure, Bernadette, Pascal et François d'avoir participé aux comités de thèse, vos conseils ont été très précieux pour garder le cap dans ce très vaste sujet de thèse.

Merci également à Maryline, pour ton aide lors de mon stage de Master et pour avoir été une cheffe aussi attentive et bienveillante.

Cette thèse a été fortement affectée par la crise sanitaire et tout ce qui en a découlé. Dans ces temps difficiles, un lieu nous a recueilli pour sauver nos esprits et nos papilles de la déprime : le restaurant le Mille et Une Lunes. Véritable lieu de culte de la science et de l'approche holistique, au fil des semaines, le chef Daniel a su faire de son restaurant une véritable terre d'accueil pour les thésards en déroute. Le mercredi est ainsi devenu la date clef de nos emplois du temps. En nous réunissant autour d'un repas (gastronomique +++), Daniel et Marina, sans oublier Wagyu, ont permis aux thésards de maintenir ce lien si important entre eux et de voir leurs encadrants en direct. A ce moment-là, c'était quelque chose de précieux ! Daniel tu as accompli le joli paradoxe de me faire voyager pendant la crise sanitaire grâce à tes plats. En vérité, je ne sais même pas comment vous remercier tellement cette initiative a été importante pour moi. Je vous remercie également pour ce magnifique stage sur l'île de Bailleron qui restera inoubliable, merci également à Agnès, Bernadette, et Hélène.

Malheureusement, la crise sanitaire ne m'a pas permis de passer beaucoup de temps à Rueil-Malmaison (IFPEN), cependant je tiens à remercier chaleureusement toute l'équipe R16. Tous ses membres ont toujours montré beaucoup de bienveillance à mon égard et d'intérêt pour mes travaux. Je garderai un excellent souvenir des trop courtes périodes passées à leurs côtés. Une pensé spéciale pour toi, Marc, avec qui j'ai passé la plupart de ces moments.

Je souhaite remercier tous les doctorants et post doctorants (ou contrat d'intérim incompréhensible, oui je pense à toi Alissia), vous m'avez tous apporté quelque chose à votre façon. Massimo et Denovan, vous avez été mes plus belles découvertes, deux super amis que je ne perdrai jamais de vu. Cette dernière année sans vous a été dure. Que de bons moments passés ensemble en soirée, à surfer et à ne rien faire par de beaux après-midis ensoleillés. Merci à vous deux. Merci à toi Romain pour nos sessions, et d'être comme tu es, toujours souriant, positif, motivé… Tu es un bloc de positive attitude, et un excellent surfeur de longboard je dois l'admettre ! Merci à Renaud et Océane, j'ai passé de supers moments avec vous, c'est vraiment dommage que vous soyez partis si vite. Merci à Maël et Léa pour toutes les bières/sessions ou sessions/bières que nous avons fait ensemble. Un gros merci à toi Aurélien, j'ai adoré les soirées et moments passés ensemble. Bonne chance en Corée et reviens vite nous voir. Thomas, tu as été une vraie belle rencontre également ! Tes blagues nulles et ta bonne humeur me manquent déjà (à très vite sur Age of empire, j'espère que tu t'es entrainé pendant que je rédigeais). Je remercie toute la team du volley de l'Ifremer, vous m'avez permis de me défouler dans une super ambiance. Merci à toi Claire, depuis le début on a toujours été tous les deux. Ça a été un vrai plaisir de faire ma thèse avec toi. A l'ancienne team, Pierre, Shray, Florent, Marie, Marie, Arthur, Maude, Ruth, Jean, merci pour tous ces bons moments. A la nouvelle team, Manon, Thomas, Quentin, Méril, Alissia, Edouard, Raph, merci également pour tous ces bons moments. Merci à Brice d'être venu me rendre visite si souvent à Brest et de m'avoir soutenu en direct quand mon congrès en ligne était un échec (je parle de l'organisation, ma présentation je n'en sais rien personne n'a pu poser de question).

Je tiens à remercier également tous mes amis qui m'ont permis d'avoir un toit et de savourer pleinement ma vie de nomade à Paris. Mamad et Vanessa, ça a été un plaisir de pouvoir à nouveau parler espagnol avec vous. On a passé de supers moments, même si on a un peu forcé sur les restaurants ! Antoine un gros merci à toi mon pote, de m'avoir hébergé et d'être parti vadrouiller en Grèce avec moi. Je garde un très bon souvenir de nos semaines « sportives » pour l'élection des bureaux à centrale Lille et de chez tes parents dans le sud. Adrien, un gros merci pour les moments partagés avec tes potes et tes colocataires. J'ai hâte de refaire des Brodredi avec vous ! Jessica notre colombienne/parisienne, c'était un vrai plaisir de boire du vin avec toi et ta colocataire en écoutant un savoureux mix de reggaeton et de jazz. Un très gros merci à Anouck qui m'a permis de me ressourcer dans le luxe au cours de ces périodes plus ou moins confortables. Je tenais à le mettre noir sur blanc : Hôtel Anouck 5 étoiles, j'attends le lien tripadvisor pour donner mes commentaires ! Merci à tous mes autres amis qui m'ont soutenu pendant cette thèse : Solène, Gabin, Alerig, Caro, Tangi et toute la bande d'école et de Master : Etienne, Samy, Emma, Marie, Cécile, Karl, Victor, Sarah, Pierro, Julien (alias poilu), Tanguy, Samuel, Vincent, …

Je tiens tout spécialement à remercier mon frère, Quentin, tu as toujours été là pour me changer les idées quand j'en avais besoin. Merci à mes parents, pour votre soutien moral, administratif, logistique et financier (j'en oublie sûrement beaucoup d'autres). Mon parcours d'étudiant n'aurait jamais été possible sans vous. Merci à mes grands-parents paternels, pour votre soutien et toutes vos attentions, j'ai hâte de retourner vous voir. Je remercie chaleureusement ma grand-mère maternelle, pour tout ce que tu as fait pour moi et mes cousins. Après mûre réflexion, tu n'es peut-être pas étrangère à mon choix de me lancer dans une thèse, même si ce n'est pas un doctorat en médecine. Je suis fière d'avoir suivi les traces de mon grand-père maternel dans la recherche. Je souhaite lui dédier en partie cette thèse, et espère qu'elle fera honneur à sa carrière et sa mémoire. Je souhaite également remercier tous mes cousins : Vincent, avec qui j'ai surfé de nombreuses heures pour oublier cette thèse, Thomas et Tanguy, à nos nombreuses soirées jeux de société et fiesta (notamment chez toi Thomas). Un gros merci à Tiphaine, la chatelaine de Plouhinec qui nous accueille toujours avec plaisir dans son domaine. J'en profite pour remercier Katel, qui fait partie de la famille maintenant. Merci à Marie et Thomas de m'avoir accueilli si souvent chez vous (dans une si grande diversité de maisons et appartements brestois), avec leurs amis et ta famille Thomas. Je tiens également à remercier mon ami Romario avec qui j'ai partagé mon expérience patagonienne, merci pour tout mon ami. Je te dis à bientôt, l'Amérique latine me manque ! Un gros merci à Léna, ma chérie, on a traversé cette même expérience ensemble, mais malheureusement trop souvent à distance. J'espère ne pas avoir été trop agaçant sur la fin. Je te souhaite bon courage pour ton manuscrit et j'ai hâte que tu me fasses visiter un peu plus l'Italie !

Table of contents

Table of illustrations

1 General introduction

Estuaries and deltas are located at the interface between rivers and oceans (Fig. 1). They differ each other by their morphology, facies and related hydrodynamic processes:

1. Deltas are characterized by strong fluvial inputs, which makes the "depositional formation to protrude from the general outline of the coast" (Bird, 2011), as "the rate of sedimentation at the mouth exceeds the rate at which sediments are eroded and dispersed by waves and currents" (Bird, 2011). Deltas thus prograde (advance towards the sea) and display a prominent shape compared to the coast (e.g. Nile, Mississippi, Ganges, Ebro deltas…). Sediment dynamics within deltas is therefore strongly influenced by river discharge, but also by waves and tides (see the classification of river dominated, tidal-dominated or wave dominated deltas and all the continuous spectrum of mixed cases Galloway, 1975).
2. In the opposite, estuaries can be defined as "the seaward part of a drowned valley system subject to tidal fluctuations and the meeting and mixing of fresh river water with salt water from the sea and receiving sediment from its catchment and from marine sources" (Bird, 2011). Estuaries are characterised by "inlet" or funnel-shaped morphology, i.e. a seaward widening which is often related to the coastline retrogradation since the formation of the previous valley. It means a landward retreat of the shoreline, that is correlated to relatively small rivers inputs compared to deltas (e.g. Gironde, Suances, Shanghai, Scheldt estuaries…).

Most of sediments, resulting from continental erosion, or pollution, resulting from anthropic activities, are transported by rivers flows and pass or transit through estuaries and deltas before reaching seas and ocean basins. Moreover, this interface between rivers and oceans is often a very rich environment in term of biodiversity. Some ecosystems only develop within estuaries and deltas under specific salinity and hydro-sedimentary conditions (Pasquaud et al., 2015; Douglas et al., 2019). The characteristics and geographical locations of estuaries and deltas conduct to harbour constructions and large anthropisation (e.g. Langouët and Daire, 2009; Dauble et al., 2012; see also the main harbour locations, https://www.worldshipping.org/top-50-ports). Fast evolution of hydrodynamic conditions of coastal areas has already led to the abandonment of cities during the mid-Holocene period, such as some prehistoric Chinese cities located in coastal plains (Wang et al., 2020).

In the context of global warming, understanding the evolution of coastal hydrodynamics and sediment dynamics as a function of sea-level is getting more and more relevant. Either at an anthropic time scale (a few years to centuries) to study the pollution of the seas (e.g. plastic), or over geological time scale (a few centuries to a few thousands of years) to understand the evolution of sedimentary systems, estuaries and deltas are thus key areas from a source-to-sink point of view (Milliman and Syvitski, 1992; Sømme et al., 2009). Understanding the hydro-sedimentary evolution of these environments is therefore a high-stake issue for the sustainability of a large part of coastal infrastructures, but also for marine resources preservation, as they are very sensitive to environmental changes induced for example by climatic (Tu et al., 2019), geological (Wells et al., 2007b), anthropic (Grasso and Le Hir, 2019), or biological (Ganthy, 2011; Beudin et al., 2013) variations. Indeed, in such coastal areas, erosion, transport and deposition of sediment are governed by a multitude of physical forcings (e.g. tides, waves, winds, river discharges...), which induce very different hydrodynamics. Locations and architectures of the deposits are closely connected to hydrodynamics forcings (Boyd et al., 1992; Boyd et al., 2006; Clifton, 2006; Bird, 2011), but these mixed influence of multiple physical forcings strongly complicate the understanding and quantification of the respective influence of each forcing.

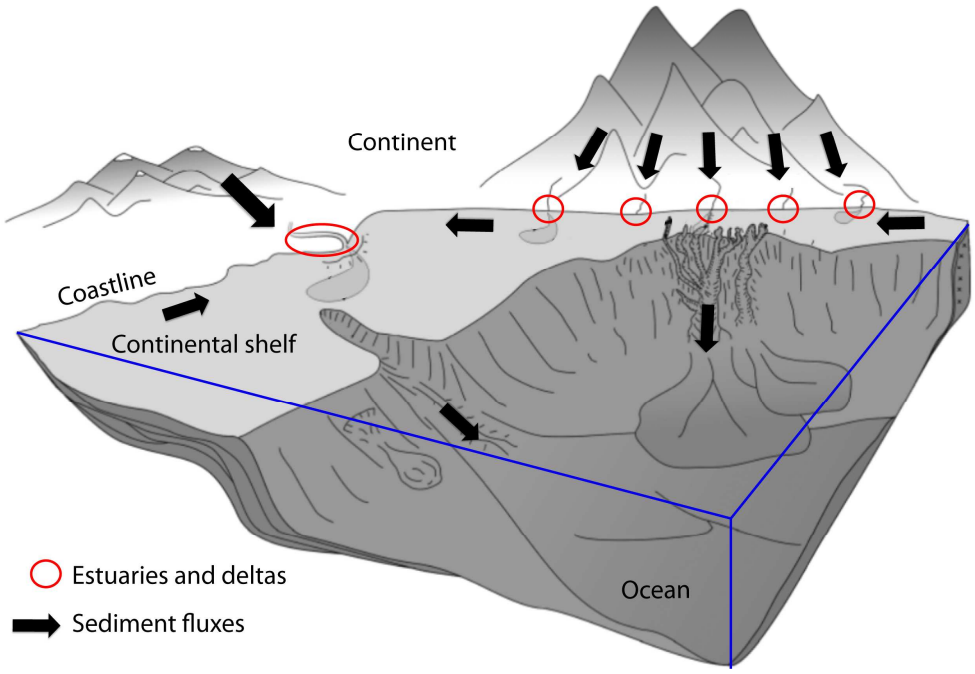

Fig. 1: Conceptual scheme showing the position of deltas and estuaries in global sediment transit from land erosion to ocean (modified after Sømme et al., 2009).

The impact of different hydrodynamic forcings on deltas and estuaries is getting better and better understood since the twentieth century, thanks to complementary approaches of sedimentological studies and hydrodynamic modelling. The naturalistic approach of geologists links sedimentary facies and stratigraphy, with transport and depositional environment (e.g. Trentesaux et al., 1994; Dias et al., 2002; Barnard et al., 2012), while physical oceanographers try to explain the erosion and sedimentation induced by hydrodynamics (e.g. Ji et al., 2007; Toublanc et al., 2014; Lemoine and Le Hir, 2021) and even to simulate erosion/transport/deposition processes with numerical process-based modelling.

However, hydrodynamic and morphodynamic evolutions of estuaries during a sea-level transgression or regression (about 10 to 100 ka, Miller et al., 2011) is poorly understood as these two dynamics operate and are observed over very different time scales. Hydrodynamic time-scale in estuaries varies from a few days to a few months (Webb and Marr, 2016), while morphodynamic time-scale are about a few decades to centuries. Making the link between these two time-scales is not easy. On one hand, the longest tidal gauge data has been recorded in Brest, but covered only a time interval of 300 years and only the sea surface heights were recorded. There is no long-term record of hydrodynamic data such as currents velocities. On the other hand, sedimentological studies have to deal with sediment hiatus, i.e. deposited sediments are not always preserved. A significant part of sediments (sometimes the whole) that are deposited during a tidal cycle is remobilized by the subsequent cycles. It is therefore very complicated to discretize the different tidal events and understand the evolution of the system (Tessier et al., 2012). Moreover, most of estuaries' sediment infill show only isolated, sparse records (in time and space). It is unusual to observe the longitudinal variation of facies deposits, even in the presence of a large dataset (e.g. cores, seismic, outcrops; Tessier, 2012).

All three main controlling factors in estuarine systems (rivers, waves and tides) act over short time-scales and face the same lack of data in the past. In the case of rivers, two main extreme regimes can be distinguished over one year: drought and flood. Rivers mainly induce a unidirectional flow, that can be summarized over a few centuries with many different statistical methods, depending on the degree of influence and the frequency of the identified regimes (Zhang et al., 2019), to estimate the flood of

the century, or of the millennium. Waves can also be simplified over large period, it is based on preferential direction and the recurrence of most intense events (van Vliet-Lanoë et al., 2014; Goslin and Clemmensen, 2017). Their impact on sediment erosion/transport/deposition can be summarized in turbulent unidirectional flows, depending on preferential direction of waves or storms (Al-Salmi et al., 2019; Busson et al., 2019). For tides, no specific period or threshold exist to describe the main impact of tides on sediments over long time intervals and it is thus difficult to synthetise its impact. In fact, there is no consensus in the scientific community about (preserved) tidal deposits over centuries or larger time-scales: are they the results of only spring tides, or the cumulative effect of all the tides (neap, spring), or a specific condition of tide? Moreover, tides are much more complicated to classify into statistical groups, as they induce hourly variations of bidirectional currents (ebb and flood), with various, changing daily amplitudes. Until now, upscaling instantaneous tide impact on sediment distribution over large time-scales (centuries to ten thousands of years) is not possible.

The coupled numerical simulation of estuarine hydrodynamics and its associated sedimentation over hundreds of years is very complex (Coco et al., 2013). The numerical simulation of hydrodynamic processes requires very small time steps to capture temporal variations of water flows of the order of minutes to hours, while morphodynamic numerical simulation requires longer time step, on the order of months to years, to reproduce the evolution of seafloor (or about hundred years for metric variations). Two kinds of numerical tools are dedicated for modelling sedimentary processes: the stratigraphic and the hydro-sedimentary models.

1. Stratigraphic forward models are designed for geological purposes and seek to model the sediment infilling stratigraphy of basins over long time-scales (thousands to millions of years). Stratigraphic models do not consider the path of each individual grain, but aims to represent an average of all different sediment processes, in order to simulate the long-term evolution of geometries (Leroux, 2012). They mainly consider the accommodation space (calculated from vertical movement – subsidence or uplift – and sea-level variations) and the land sediment supply. Water flows from drainage area to ocean basin, in relation to gravity laws that follow the steepest basin slope (channelized flow) or by simple advective flows. Sediment transport is then ruled using empirical laws, relating sediment transport capacity to water flow velocity. Finally, erosion and deposition of sediment are calculated from the mass balance principle. These stratigraphic forward models have been applied and validated on numerous fluvial, deltaic and marine case studies, but unfortunately never in tidal-dominated sedimentary systems, as (1) tidal currents very rarely follow the steepest slope, and (2) tidal processes vary in time and space over very short time intervals (half-a-day for semi-diurnal tide).
2. Hydro-sedimentary models provide accurate and high resolution (seconds) representation of tidal currents and induced erosion or sedimentation, but only over a few months to a few years. These models seek to physically describe the hydro-sedimentary processes acting in estuaries, which implies the use of assumptions, necessary for the application of fluid dynamics equations, and many processes are described by empirical formulations. As a result, simulations drift progressively from the reality, which leads to uncertainties that increase with simulations time span. A very small change in the input parameters of the numerical model, such as a gentle change of the topography or sediment supply, leads to a different result in the simulation outputs. For this reason, they are systematically used to complement in-situ data.

Because of the different time and space scales they deal with, these two types of models are not used for the same purposes (Joseph et al., 2016). That is why none of these numerical models is able to simulate the tidal process over long time-scale, i.e. at least centuries to tens of thousands of years. Long-term tidal modelling is yet an important issue for the understanding of estuaries infill. Neither sedimentological or numerical modelling studies achieved to explore the hydro-sedimentary response of estuaries (induced by the tide) to long-term parameters (seafloor and sea-level evolution), over a

transgression. They are respectively limited by the sediment records preservation and hydro-sediment simulations temporal limit (secular scale). Thus, very important questions remain about tide-dominated estuaries infilling: How do tidal currents evolve according to long-term parameters, such as sea-level and seafloor variations? What are the consequences of hydrodynamical evolution on sediment dynamics, in terms of erosion and deposition patterns and sediment grain-sizes classes distribution? What does hydrodynamics imply for the preservation of sedimentary units in tide-dominated estuaries? How do the muddy/sandy sediments and the erosion/deposition limits evolve in response to a rise in sea-level? What are the main triggering parameters of hydro-sediment dynamics evolution? Previous studies investigated these issues at secular scales (Dam et al., 2016; Franz et al., 2017; Le Tu et al., 2019; Elmilady et al., 2020 and more), however the use of continuous modelling did not allow to reach the time scale of an estuary infilling (about ten thousand years).

This PhD focuses on the impact of the tidal process on long-term sedimentation (about 10 ka) in tide-dominated estuaries. Rivers and waves may have a major role in estuarine hydro-sedimentary dynamics. In order to focus our study on the action of the tidal process, this study explores its impact in a tide-dominated estuary: the Bay of Brest, and in particular the scientific issue of the upscaling of the tide impact on sediments, in order to understand tide-dominated estuaries infill.

For that purpose, a specific methodology based on sedimentology and numerical hydro-sedimentary modelling is set. The aims are to identify, rebuild and simulate each key period of the Bay of Brest Holocene infill. It intends to explore the tidal hydrodynamic and hydro-sedimentary responses to key paleoenvironmental changes such as seafloor and sea-level.

Tidal currents at each key period are then simulated (and validated), simulations results are analysed to determine if morphodynamic changes (i.e. sediment volume variations in the Bay of Brest), could be described by the action of one or a few specific tidal conditions. The determination of such morphogen tides characteristics would allow to perform long-term hydro-sedimentary and stratigraphic simulations to reproduce the interactions between sedimentary units and better understand the formation of sedimentary structures under the action of tides (e.g. dunes, sand ridges and bars, mud flats).

The principal expectations of this study are thus:

1. to test the relevance of the methodology to study the tide impact on sediment erosion/transport/deposition;
2. to explore how do sedimentation patterns evolve in tide-dominated estuaries in response to paleoenvironmental changes (seafloor and sea-level variations);
3. to determine if one or more morphogen tides can be defined to characterize the evolution of a tide-dominated estuary over long time interval (about 10 ka).

To answer those scientific questions, the manuscript is organized in the following ways. The second chapter (after this introduction) aims to provide a state of the art on the knowledge about present-day tides, and an overview about past tidal characteristics. Then, the chapter 2 focuses on the tide impact on sedimentary processes in modern and recent natural systems. It also describes the basic principles of numerical stratigraphic and hydro-sedimentary modelling, as well as the time-scale issue of numerical modelling. Chapter 3 is dedicated to data and methods: the chosen study area and data are described as well as the modelling strategy we used. The results are presented in the three following chapters (4, 5, 6) : hydrodynamics (Chapter 4-published paper in Continental Shelf Research, Olivier et al., 2021), hydro-sedimentary dynamics (Chapter 5-submitted paper) and the preliminary investigations towards the long-term representation of the tidal processes (Chapter 6). Finally, the main conclusions are synthetized and perspectives are drawn in Chapter 7.

2 State of the art: Tidal implications on estuaries infilling

This study focuses on the tide effects on sedimentation in estuarine environments. Sea surface tide induced variations generate currents and the displacement of water masses. The energy of these currents induces erosion, transport or deposition of sediments. Given the short time between a consecutive low and high tide (~6:12 hours for semi-diurnal tide), the induced changes on sediment transport are of very high frequency. These fast variations make it difficult to analyse and model effect of tides on sediment deposition over geological time (ka or Ma).

The filling of sedimentary basins is the result of multiple long-scale processes, such as tectonics, subsidence or eustatism, and also of short-scale processes that mainly concern transport, such as tides, fluvial discharge or waves. This chapter aims to explain the tidal processes and the associated sediment transport. However, in order to describe sediment transport, two times scales have to be considered: short- and long-term. The short-term is considered here to range between the day and year, i.e. the time-scale of the tidal process. The long-term scale is the scale of geological interest, i.e. the formation of sediment layers leading to the infilling of an estuary (thousands to millions years). This time gap between these processes periods of actions leads to two different ways of studying estuaries. The naturalist approach of geologists aims at observing, describing and analysing the deposits of sediment layers to interpret the processes and their drivers, on both long- and short-time scales. However, only some deposits are preserved in estuaries: sediment is often remobilised after its deposits by daily variations of tidal currents, or subsequent hydrodynamics in particular related to extreme events (e.g. storm or flood) or mean sea level variations that can generate important erosion. Oceanographers focus on resolving physical processes to interpret the deposits. They are interested in sediment transport at, event, seasonal and even interannual time-scales, to answer questions related to these time-scales. e.g. What are the effects of dredging on hydro-sediment dynamics? What are the factors driving suspended matters flows and river's area of maximum turbidity migration? What is the effect of sedimentation on human infrastructures and conversely? In this context and in the absence of hydrodynamic data in the past, estuaries hydrodynamics are mostly studied at present-day over short time scales. The objectives of oceanographers' approach are the understanding of physical processes and the prediction of their future impacts.

These different objectives motivate the development of numerical models. The stratigraphic models of geologists consider the formation of long-term sediment layers, whereas the hydro-sediment models used by oceanographers consider the short-term movement of sediment.

This chapter aims to give an overview of the tidal process and its impact on sediment deposits over both time-scales. It is organized in the following way: first, the description of the tidal hydrodynamic process for present and past, and ways to explore it (2.1); then the tide impacts on sedimentation inside estuaries is developed at both short-and long term (2.2); the last section focuses on the key concepts of the two main numerical tools for modelling sediment deposits: stratigraphic models and hydro-sediment models, including their limitations to simulate long-term tidal deposits in estuaries (2.3).

2.1 Tides

Tide is the sea surface variation due mainly to the gravitational action of the Moon, the Sun, and the centrifugal force against gravity. At human scale, the tidal phenomenon makes the *water* either go *up* or *down* at the shore. Although this phenomenon was discovered through sea surface elevation changes, it affects all terrestrial fluids and solids (lithosphere to the earth's core). In this study, tide refers only to the ocean tide. It was observed since a very long time, but due to the

complexity and the quantity of drivers at the origin of the tidal phenomenon, it remained without explanation until the mathematician Wallis proposed to take into account the influence of the Moon in 1666 (Wallis J., 1966). This changed the tidal analysis at a local scale. A review of historical advances in the comprehension of tide is proposed by Cartwright (1999). At the end of the 20th century a global interpretation of the tidal wave was developed, thanks to the advent of numerical modelling (Hansen, 1966; Cartwright, 1999). Tide is a wave induced by astronomical movements through the attractive and centrifugal forces, that propagate in the oceans (Laplace, 1775, 1799, 1825). The propagation of this wave depends on the size and shape of oceans and its action is very unequal across the globe, in terms of amplitude, frequency and propagation (Simon, 2007). It implies that the tides were different in the past, as the sea level changed and the continents moved. The following section focuses on the tidal process near the coast and is therefore divided in two parts: first the tidal process is described for the present-day, secondly the ways to explore the tidal wave propagation in the past are discussed.

2.1.1 Present-day tide

The ocean tide is the movement of water masses, which induces variations of sea surface elevation and propagates as a wave across the oceans. The tidal wave has not the same amplitude and frequency everywhere on earth and the classification of the tide type is based on the properties of the signal, represented by a sea surface variation curve (Fig. 2).

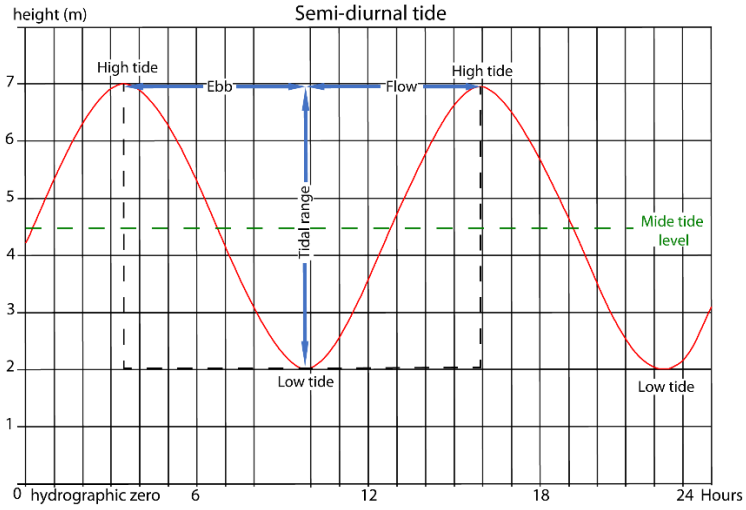

Fig. 2: Tidal amplitude over 2 cycles of comparable spring tides (Brest tidal gauge, modified after Simon, 2007).

The greatest amplitudes are observed in shallow water areas of the seas connected to oceans and the lowest in close and semi-enclosed seas, where the tidal wave cannot enter (e.g. Mediterranean sea, Fig. 3). The amplitude hardly exceeds 2m in the deep ocean, but near the coast the amplitude between high and low tide can reach 16 m (Bay of Fundy). Tides in coastal areas are classified according to the maximum tidal range, defined as the height difference between high (maximum) and low tide (minimum, Fig. 2). Coastal areas can be microtidal (tidal range smaller than 2 m), mesotidal (between 2 and 4 m) and macrotidal (greater than 4 m). The spatial distribution of tidal ranges varies very rapidly and particularly near the coast (Fig. 3). For example, in the Bay of Mont Saint Michel (France) the tidal range can reach 14m during exceptional spring tides and in Sainte Marie du Mont (80 km away, NE) its maximum is 7.5m under the same conditions (SHOM).

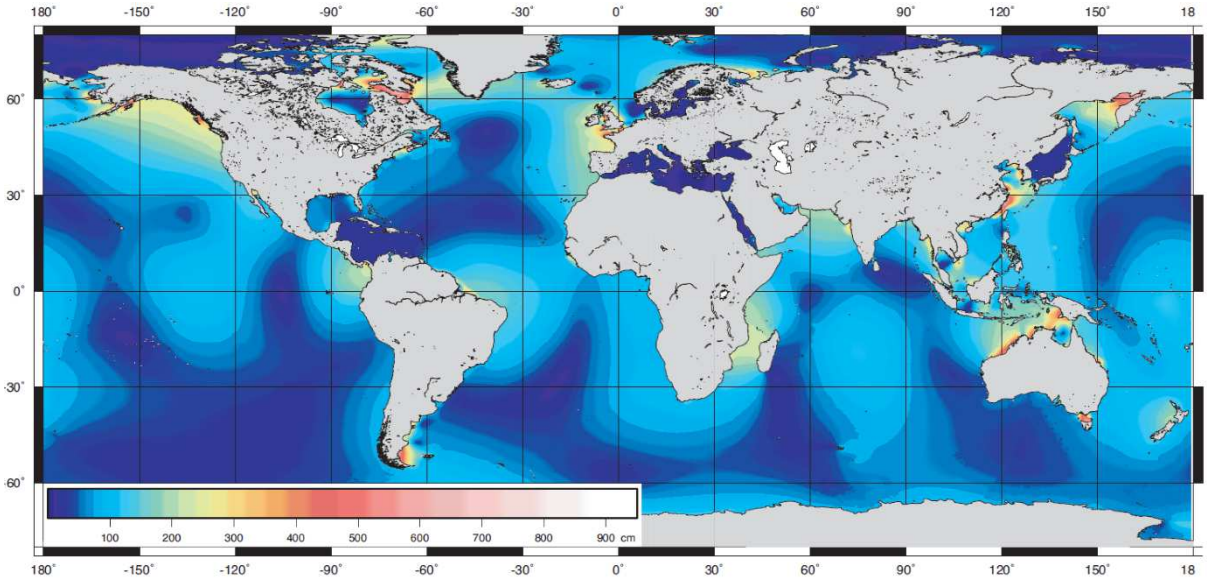

Fig. 3 : Tidal range distribution in the world (Simon, 2007).

Tides are also classified according to the period of tidal cycles, i.e. one low and one high tide. The period is defined as the time between two maximum (or minimum) amplitudes. A tidal cycle can last 12 hours and 25 minutes (semi-diurnal, Fig. 2) or 24 hours and 50 minutes (diurnal). It exists 4 types of tidal behaviour classified according to their period and amplitude (Figs. 4 and 5, Simon, 2007):

- semi-diurnal type: two high and two low tides per day of approximately equal height.
- semi-diurnal type with diurnal inequality: two high and two low tides per day, but the high and low tides are very different in height.
- mixed type: sometimes two high tides and two low tides per day, sometimes only one.
- diurnal type: always one high and one low tide per day

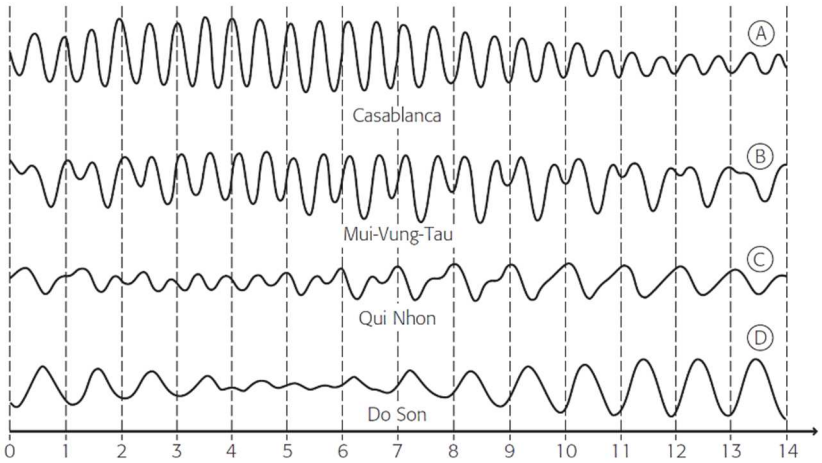

Fig. 4: Tidal curve over 14 days at 4 points. A: semi-diurnal tide, B: diurnal inequality tide, C: semi-diurnal tide with diurnal inequality, D: diurnal tide (Simon, 2007).

The differences between these tidal regimes are due to astronomical forcings and the shape of oceans. This is highlighted for the first time by Laplace, who introduced the tidal generating potential (1775). The theory is then improved by Laplace himself, with his treatise on celestial mechanics (1799 and 1825). The concept is that the tidal generating potential moves as waves through the oceans according to their shape, depth and the nature of the environment. These waves are superimposed by reflection, refraction, dissipation and form the tidal phenomenon. The interaction of these waves (or component) can attenuate or amplify the tidal signal. This concept has never been questioned, but the tidal generating potential were recalculated by Doodson (1921) and by Cartwright and Tayler (1971). Tide is the result of all gravitational forces acting on the earth, however some of the components dominate the tidal spectrum (e.g., M2, S2, K1, O1). The repartition of the different behaviour (Fig. 5) is mostly linked to the earth and the Moon relative position, and the shape of continental shelves. It was observed that semi-diurnal tides are the dominant pattern on earth and the three other behaviours occur only where the semi-diurnal components are weak (Simon, 2007). Comparing the tidal type and amplitude maps, it appears that the areas affected by the highest tidal amplitudes are often semi-diurnal, especially in the Atlantic (Figs. 3 and 5). It is the case for the Bay of Brest (Fig. 2).

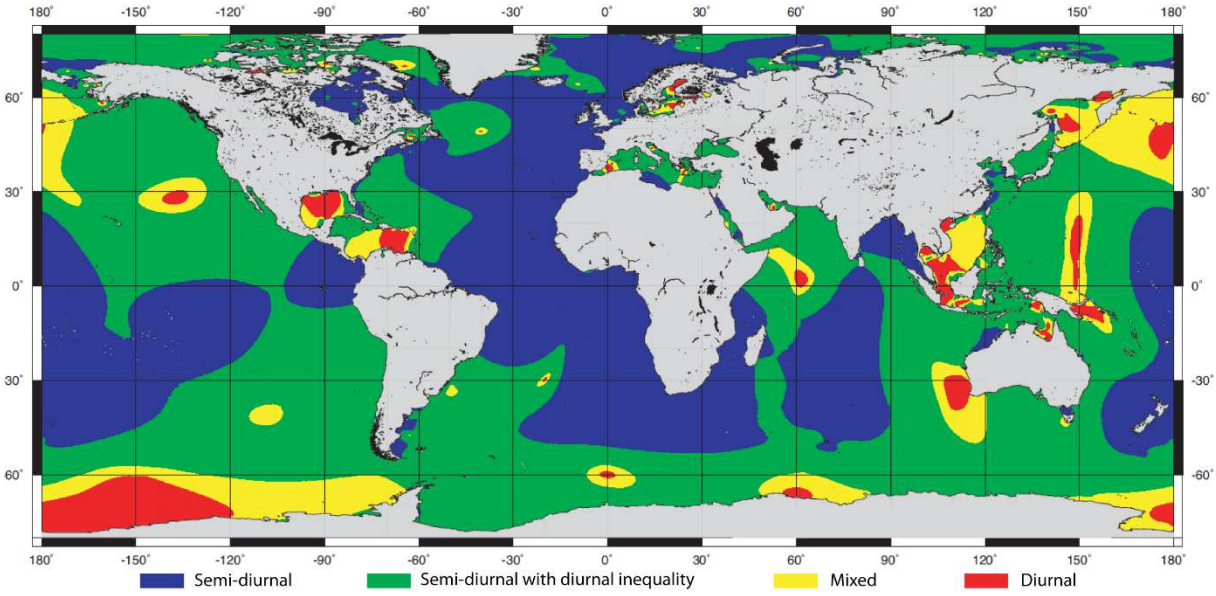

Fig. 5: Distribution of the four tidal types in the world (Simon, 2007).

In deep oceans the tidal signal has a sinusoidal shape, because the rotation of the earth and the relative movements of earth, sun and moon have a cyclical character. Theoretically the tide is not periodic, because some component of the tidal spectrum have an incommensurable frequency (Simon, 2007). However, it was shown that there are periods of time after which these conditions are more or less fulfilled (Ray and Cartwright, 2007). The most known is the saros, which regulates the return of eclipses, and corresponds approximately to 6 585 days, or 18 years and 11 days. At the end of this period, the Moon, the Sun and elements of their apparent orbit are approximately in the same relative positions. The tidal impact on oceans returns approximately to the same values. This does not mean, that the saros is a period of the tide, because after several saros the tide resemblance with the initial one deteriorates more and more. Oceans tides are thus not really symmetric due to the superposition of certain tidal components with mutually related frequencies and show a difference between the periods of rising and falling tide called tidal asymmetry.

When the tidal wave reaches shallow water areas (continental shelves), the tidal signal is notably distorted and the tidal asymmetry can be much more important. When the tidal range is high compared to mean water depth, nonlinear hydrodynamic processes distort the tidal wave (e.g. fig. 6). These processes are insignificant in the deep ocean, but notably modify the tidal wave propagation in shallow coastal areas, due to the generation of shallow-water overtides. The periodic components of the tide, coming from the generating force, combine with each other over shallow depths, creating harmonics that can propagate independently. The distortion of the tide can be so strong that an important difference can be observed between ebb and flow durations and their flow velocities.

The distortion of the tide is related to a different propagation speed of the high-water crest of the tidal wave and the low-water trough. High water level propagates faster than low water level and thus the duration of rising tide shortens while the duration of falling tide is lengthened. Consequently, the tidal wave front will steepen progressively and in extreme cases that phenomenon generates tidal bores. This tidal asymmetry increases with the relative tidal amplitude (*wave crest heigh/depth*), but the propagation the propagation of the tidal wave is closely link to others parameters in shallow areas, such as friction and coastal basin morphology. This behaviour described more along-shore tidal wave evolution, displaying similar bathymetry, but cross-shore propagation experience much more bathymetric and morphologic variations and implies a more complex distortion of the tidal wave.

The evolution of friction is much more important towards the coast. Friction increases with decreasing depth, resulting in a flow shorter than the ebb (Fig. 6). The difference between their periods increases with increasing friction (Fig. 6). Tidal velocity is mainly determined by the water surface slope and thus in the absence of a significative river plume, flow velocities are higher than ebb velocities. However, friction is influenced by many factors such as density stratification, small bed forms, the nature of the seafloor and its morphology. Thus, friction influence on the tidal wave distortion is often not linear, as friction is not uniform close to the coast. In addition, important bathymetric variations along the coast induce a difference of friction over space inside coastal basins that distorts the tidal wave.

The amplitude of the tidal wave deformation is also dependent on the shape of the coastline in coastal basins. For example, the expansion of the tidal flood wave over large intertidal areas decreases its height and propagation speed. The opposite occurs when the tide propagates into a tidal channel that becomes progressively narrower in up-channel direction. In a simplified way, the longer the length over which a large ratio *wave crest heigh/depth* is maintained, the greater the deformation will be. For short coastal basins, these effects are partially offset by the reflected tidal wave on basin coastline.

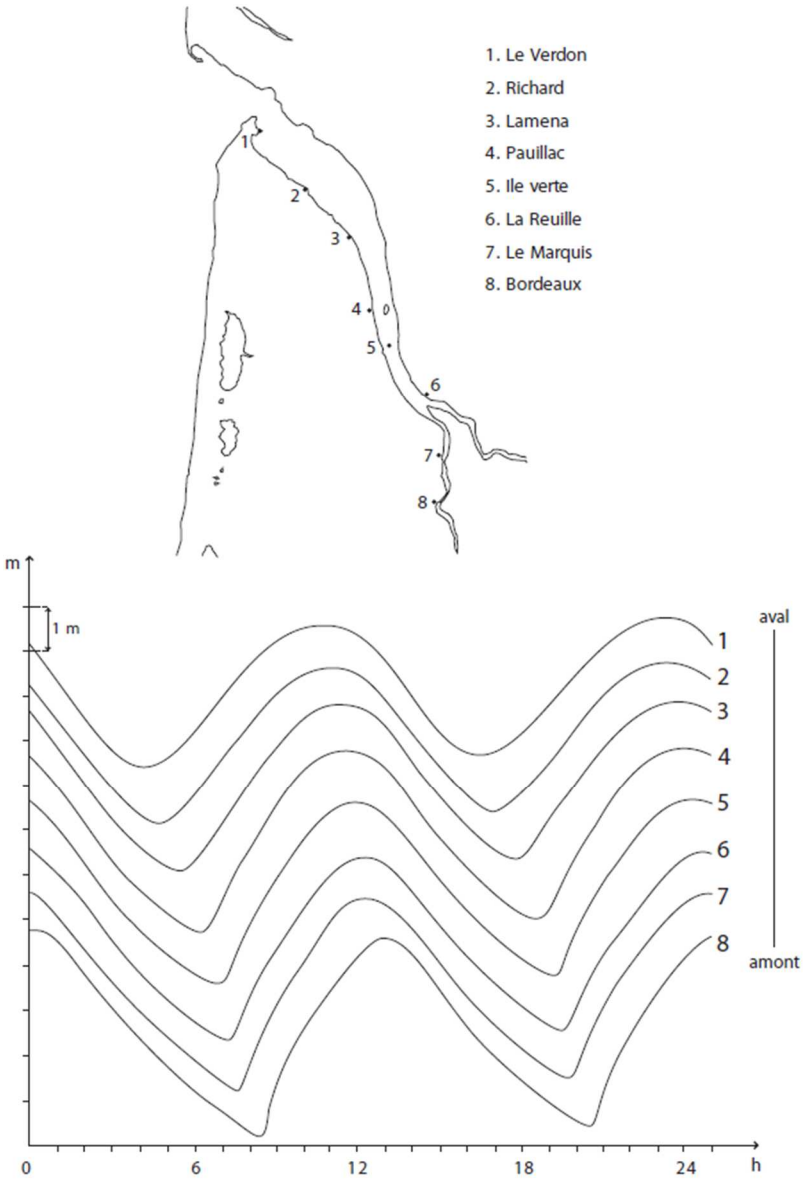

Fig. 6: Tidal curves (prediction) over 24 hours at 8 points along the Gironde estuary, France (Simon, 2007).

All these characteristics and particularities of the tide were recently highlighted, with the help of numerical modelling and the development and multiplication of data acquisition tools, like the Global Sea Level Observing System (GLOSS) (Intergovernmental Oceanographic Commission., 1997). The increase in computing power made possible to simulate this process, which requires short computing time steps and fine grid cells close to the coast. Tidal data acquisition increased enormously with the installation of tidal gauges, boys, ADCP. The second major advance in oceanographic data comes from satellites, which are able to collect a wide range of data, with a high degree of accuracy, but above all, everywhere on the planet. This led to the development of tide tables and current maps, which predict the height of water and tidal current velocities with high temporal and spatial accuracy (minute, cm, cm/s) over years. However, data are available only for the present-day. Beyond the lake of data, the "most difficult of all celestial mechanics" according to Laplace, is even more complicated to represent in the past or the future cases, because of the complexity of stars movements inducing the phenomenon (mostly the Sun and the Moon), and also the evolution of the shape of oceans and coastal basins.

2.1.2 Past tides

Understanding and representing tides in the past remains a challenge for oceanographers, given the quantity of parameters to be taken into account. First, it is difficult to predict the evolution of the Moon and the Sun positions far from the present (past or future) and therefore to predict tidal amplitudes. Moreover, modern technological advances offer the possibility to understand the tide thanks to the record of a lot of data. The oldest available data goes back to 300 years maximum and comes from the Brest harbour's tidal gauge. As presented by Laplace, celestial mechanics are not the only parameters to consider. Oceans shape evolution and eustatic movements (paleoenvironments) are very important. And contrary to tidal amplitudes and currents, a lot of information are available in the sedimentary record for paleoenvironmental reconstruction. It is thus possible to explore theorical past tide relying on both numerical models and paleoenvironmental reconstructions. Those reconstructions are a key step in the study of past tides and are mainly based on geology. Paleoenvironmental evolution is the result of vertical and horizontal movements. There are three main parameters influencing the shape of oceans: kinematic movements (plate tectonics, magmatic production linked to it, uplifts and subsidence), sea-level variations, and sedimentation.

Close to the coast, vertical movements induced by sediment accumulations (or erosion) and tectonics can quickly modified the local propagation of the tide (years to hundreds of years). Tidal wave propagation is much more sensitive to geomorphological changes on the continental shelf. However, over larger time scales (millions of years) ocean basins can accumulate tens of kilometres of sediment, like in the Gulf of Bengal or the Gulf of Mexico (Fig. 7) and also display large morphological changes. The record of sediment thicknesses comes from seismic acquisition and drillings.

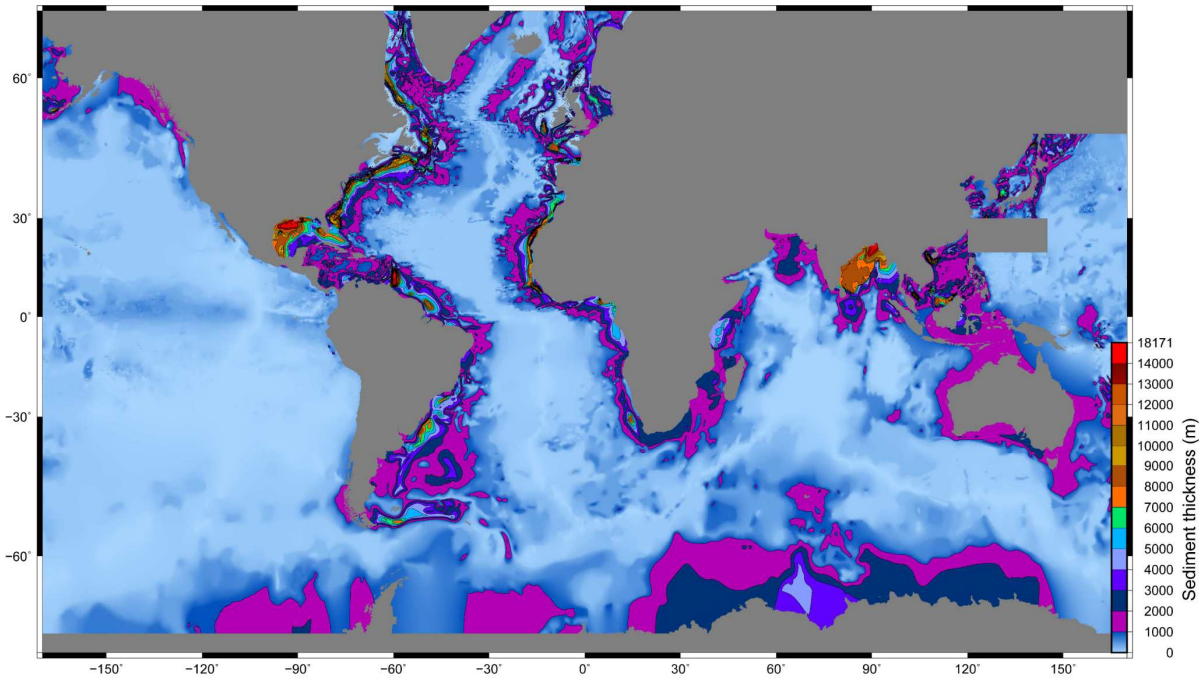

Fig. 7: Global sediment thickness distribution (data from NOAA, Straume et al., 2019).

Sea-level variations induce important vertical variations of the water depth, from metres to hundreds of metres. The factors influencing eustatic movements are numerous, but do not have the same impact on the sea-level variations and act at different time-scales (Fig. 8). They are separated into two categories, processes acting at short time-scale (1 to 100 ka, Miller et al., 2011): thermal expansion of the oceans, discharge of fresh water from lakes or groundwaters, and melting or formation of ice sheets; and processes acting at large time-scale (100 ka to 100 Ma, Miller et al., 2011): ocean crust production, sedimentation, continental collision. Short time-scale variations of the mean sea-level are mostly linked with climatic processes and geological processes act on those variations over longer time-scale. The main reason is that climatic processes affect the volume of water available in oceans and geological processes modify the oceans shapes. Glacio-eustatism and ocean crust production are the main parameters, responsible for the largest (of the order of 100 m) sea-level variations (Fig. 8). However, ice sheets volume variations are much quicker than oceanic crust production (respectively 10 ka and 10 Ma). 10 ka represents therefore a key duration over which it is particularly interesting to understand the impact of sea-level variation on tide and on the subsequent sedimentation in estuaries. Sea-level variations are deduced from numerous proxies, such as: isotopes (Oxygen, Neodymium), sediment facies, fossils, pollens… Numerous reconstructions of sea-level evolution were carried out from global (see Miller et al., 2011 for further details) to local scales (e.g Goslin et al., 2015).

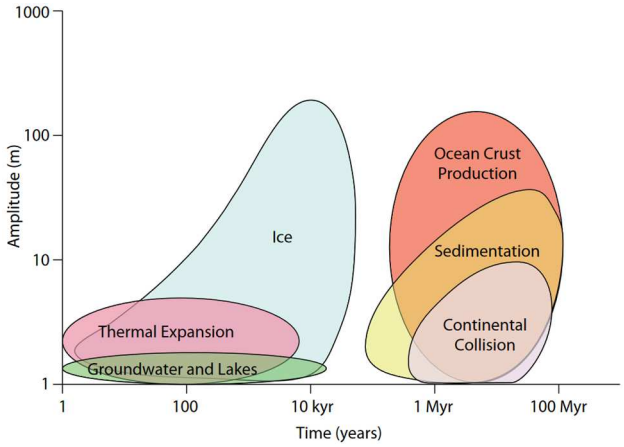

Fig. 8: Mechanisms for sea-level change (Miller et al., 2011).

Kinematic motions of plates (Plate tectonics) also play a major role in the propagation of the tidal wave. They determine the shape, size and depth of the oceans. It seems obvious that the tidal propagation will be completely different in the present-day configuration (five oceans) and in the case of a super-continent bordered by a single ocean for example. For studies over long past time-scales (millions of years) plate tectonic reconstructions will be crucial and need to be taken into account to reconstruct past tidal processes. Plate tectonics implies horizontal movements such as the opening and closing of oceans (position of the continents) and vertical movements (uplift or subsidence) ranging from meters to kilometres (e.g. continental collision, subduction, oceans floor cooling).

Plate tectonic take place over periods of the order of a million years, but much more rapid kinematic movements can deeply modify the shape of the oceans (e.g. Messinian crisis, see Bellucci, 2021). The importance of geological processes for paleoenvironmental reconstructions is very dependent on the time scale considered and the local geological history. Depending on the study area and the time period chosen, the reconstructions present uncertainties that are not negligible. Generally, the

uncertainty increases with the age of the reconstructions and can reach hundreds of kilometres of differences depending on the interpretation in geodynamics for example (Aslanian et al., 2009). For reconstruction younger than around a million of years, the position of the continents can be considered similar as the present-day configuration and can be neglected (except in specific locations). For reconstruction younger than around 10 ka, sedimentation and sea-level variations are the main parameters of paleoenvironmental reconstructions (except in specific locations). The further back in time the reconstructions go, the lower the resolution will be as more phenomena have to be considered and as the uncertainties increase.

Many studies used paleo-bathymetric reconstructions to explore past tides. The following paragraphs seek to present the range of time and space scales considered in reconstructions, as well as the aims and results of previous studies simulations. Four main spatial scales are considered in reconstructions: local (coastal area), regional (continental shelf), single-oceanic scale and global (world-wide). Most of those studies are dedicated to coastal areas: shallow areas are the place where tidal propagation is very sensitive to paleoenvironmental changes and these changes can directly impact coastal populations. Tokyo estuary was studied by Uehara and Saito (2019), in order to determine M2 component evolution (influence of the Moon, main semi-diurnal component) through the last 10 ka. Nine different bathymetries were used and one simulation is run for each context. This study highlighted the impact of sea-level change on past tide amplitude at the scale of an estuary (Fig. 9). Sea-level variations strongly modify the estuary morphology and therefore the propagation of the tidal wave (Fig. 9). Tidal amplitude and induced current repartition over the estuary are closely connected to the flooded surface morphology, near the coast.

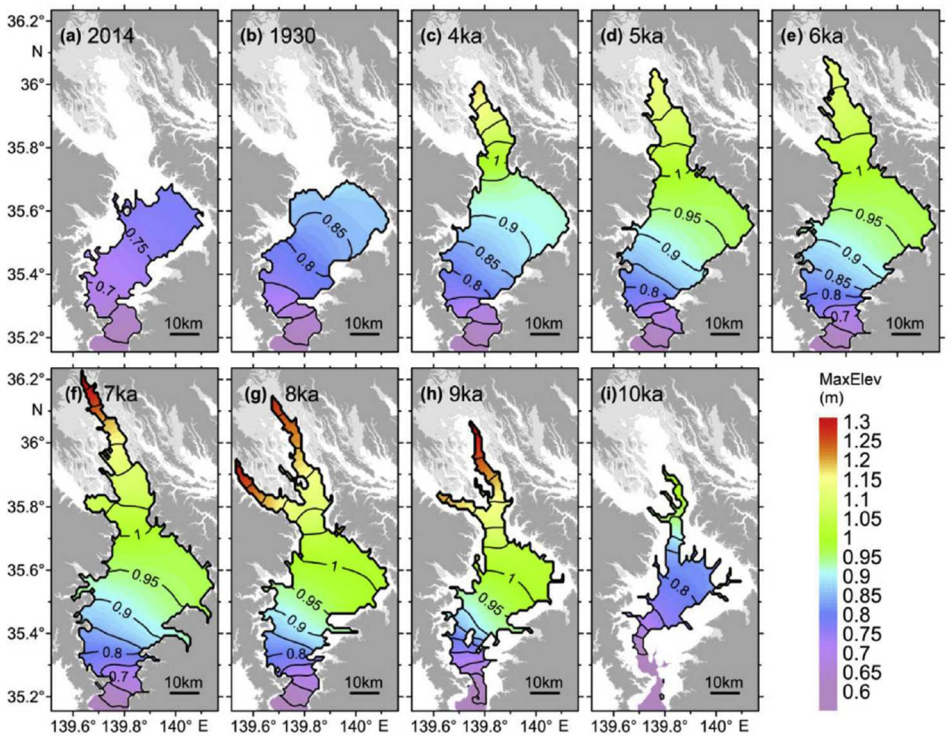

Fig. 9: Horizontal distribution of the maximum elevation predicted by the numerical model in Tokyo estuary for 9 different bathymetric reconstructions. The contour interval is 0.05 m (Uehara and Saito, 2019).

Local approaches are numerous and most of the time aim at exploring the evolution of forcings according to the paleo-environmental evolution. In Goslin et al. (2015) the evolution of the principal semidiurnal (M2 and S2) tidal constituents were simulated to describe “mean” spring and neap ranges around westernmost Brittany (Finistère, France). The aim was to simulate the tidal response to a new local sea-level variation curve (Goslin et al., 2015, Fig. 10). This study shows a relatively weak influence of sea-level variations on the amplitude of tidal paleo-ranges on the continental shelves of Western Brittany from 8 ka to present-day (Fig. 10). The tidal range remains similar between 6 ka and the present-day and is about 0.5 m lower at 8 ka compared to present-day over the three sites.

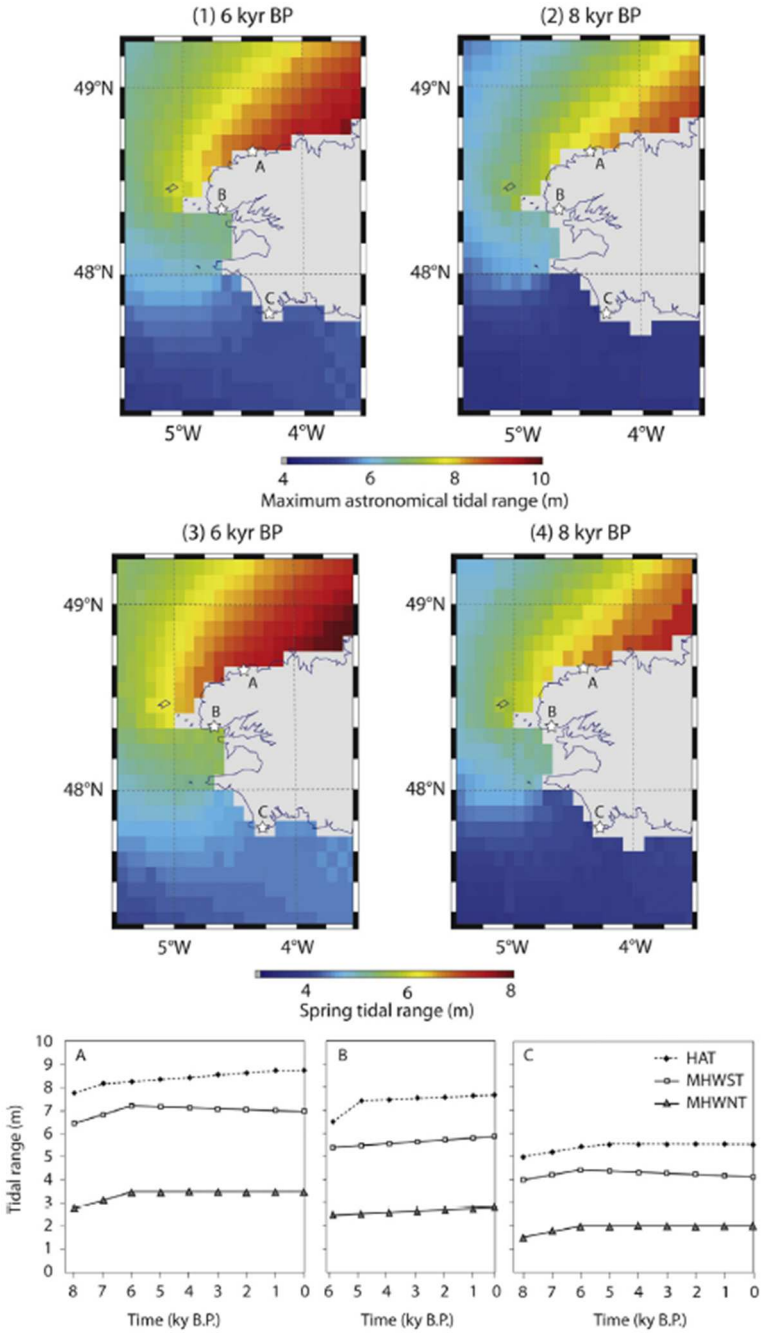

Fig. 10: Paleo tidal model outputs of the maximum annual tidal range (maps 1 & 2) and Spring tidal ranges (maps 3 & 4) around Brittany point for 8 ka and 6 ka cal. B.P. Stars show the locations of the Guisseny-Tresseny (A), Porsmilin (B) and Treffiagat (C) sites. Example plots of the 8 ka to present-day evolution of the local max. annual spring and neap tidal ranges are shown (Goslin et al., 2015).

Tidal propagation over the continental shelf, in relation to larger glacio-eustatic variations (last 20 ka, glacial to interglacial conditions), is an important issue studied through reconstructions. For example, paleo-tides were explored over continental shelf of northern Europe, since 16 ka by Uehara et al. (2006) and since the last glacial maximum (21 ka) by Ward et al. (2016). Those studies focus on the major semi-diurnal (main regime in the Atlantic Ocean) harmonic component, M2 (Fig. 11). The tide induced current velocities were also calculated for each stage. Between 21 and 14 ka amplitudes get greater and greater along the Atlantic coast (Fig. 11). Then, 12 and 10 ka present similar patterns, greatest amplitudes are located inside the English Channel and between England and Ireland (Fig. 11). When the North Sea is mostly emerged (10 ka) the location of amphidromic points and the amplitudes of M2 are significantly different (Fig. 11). Globally higher amplitudes are simulated at 10 ka than at 8 ka along the French coast and around England. This study shows similar amplitudes on the continental shelf from present day to 8 ka (Fig. 11). The opening of the English Channel seems to be a key factor for tide evolution. It allowed the tide to propagate into the North Sea, reducing the tidal over the continental shelf and increasing the tidal dissipation due to friction effects in the relatively shallow channel, thus reducing the tidal amplitude (Ward et al., 2016).

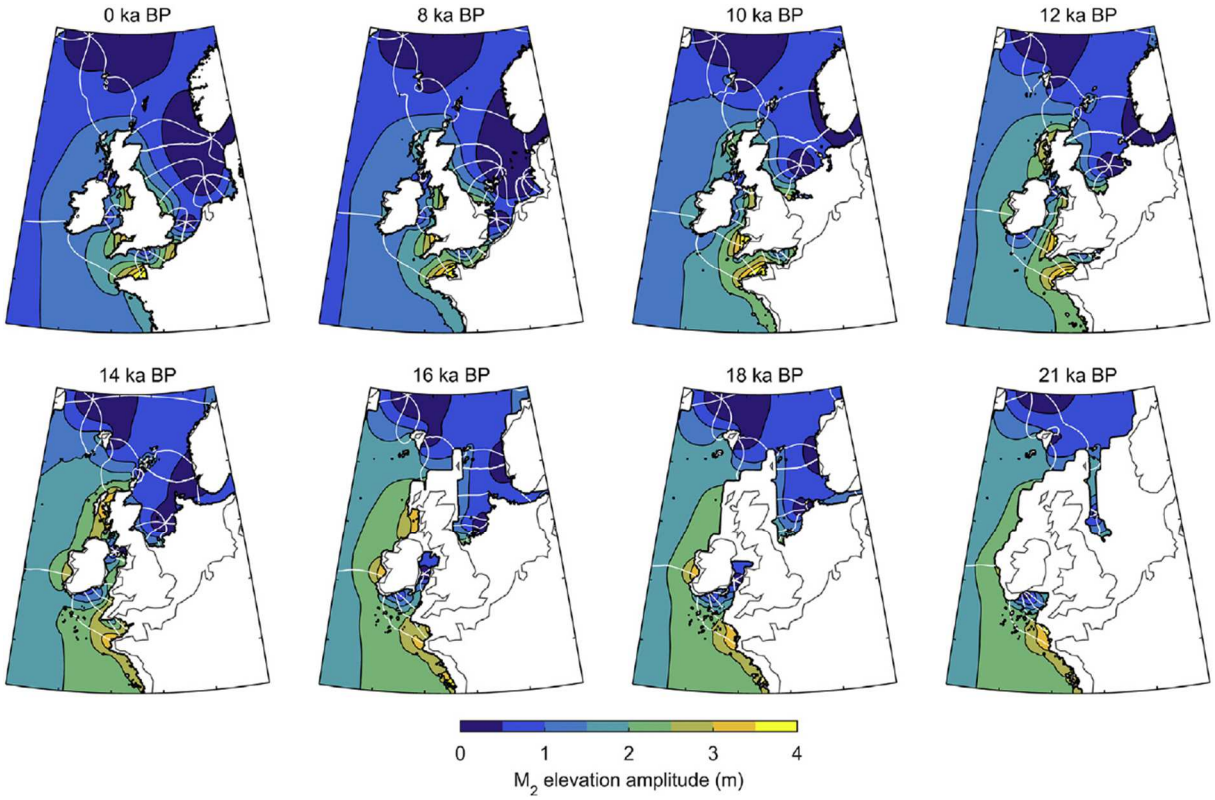

Fig. 11: Simulated M2 elevation amplitudes (colour scale, 0-4 m) and phases (white lines) for selected time slices from the ROMS + Bradley simulations. The black line is the paleo-coastline, the white areas are land/ice and the present-day coastline is provided for reference (grey line, Ward et al., 2016).

Uehara et al. (2006) reconstructed also the co-tidal chart of the M2 component over the entire North Atlantic, for the last 16 ka. A new bathymetry is applied each 1 ka in order to explore sea-level evolution (due to ice melt mostly) impact on M2 amplitude distribution (Fig. 12). The gap of 10 ka is also visible over the north Atlantic Ocean. Main location of amphidromic points changed between 8 ka and 10 ka

(Fig. 12). Between those simulations a large part of North America and Europe are flooded and it significantly changes amphidromic points distributions and M2 amplitudes.

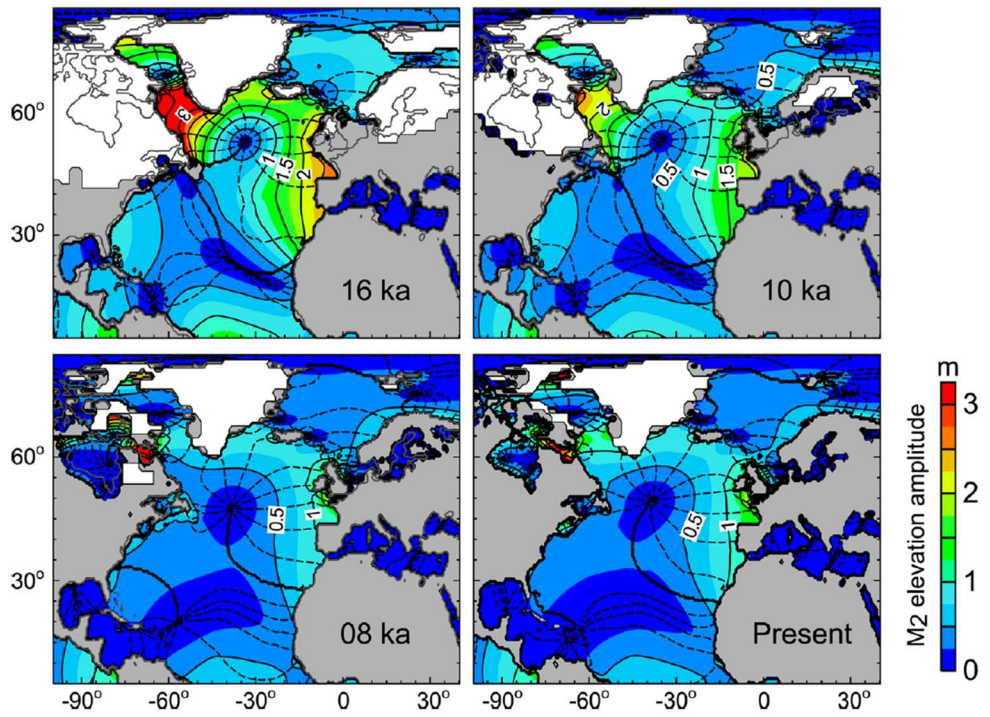

Fig. 12: Co-tidal charts for the evolution of the M2 ocean tide used as boundary forcing for the shelf model. Contour interval is 0.5m for M2 amplitude (solid lines) and 30 degrees for phase (dashed lines). White areas denote the range of ice sheets (Uehara et al., 2006).

Egbert et al. (2004) exposed also the differences of M2 elevations between the last glacial maximum and the present-day, but at global scale. Main amplitude changes between 20 ka and 0 are located in the continental shelves as observed in Uehara et al. (2006, Fig. 12). The results revealed also a greater M2 kinetic energy at 20 ka than at the present-day. All those studies focus on the period between the last glacial maximum (21 ka) and the present-day, which facilitate considerably the reconstructions. This period is too short to observe significant tectonic plates movements and only the seafloor evolution close to the coast and sea-level variations need to be taken into account.

When paleoenvironments are older than 1 Ma, the plate tectonic needs to be considered. However, as highlighted by Green and Huber (2013), due to uncertainties many simulations need to be run to test the sensitivity of the model to several parameters (e.g. sea-level, geodynamic reconstruction, water stratification). Green and Huber (2013) aimed to explore the tidal dynamics during the early Eocene at global scale (55 Ma). Because of uncertainties linked to the age of the reconstruction, all paleoenvironmental parameters are tested, in order to observe their potential influence on Eocene tides. The imperial college carried out a lot of pioneer work about old tides modelling. Wells et al. (2010) proposed a representation of semi-diurnal main components (M2+S2) and diurnal main components (K1+O1) of the tide at global scale during the Aptian (Lower Cretaceous, 125 Ma to 113 Ma, Fig. 13).

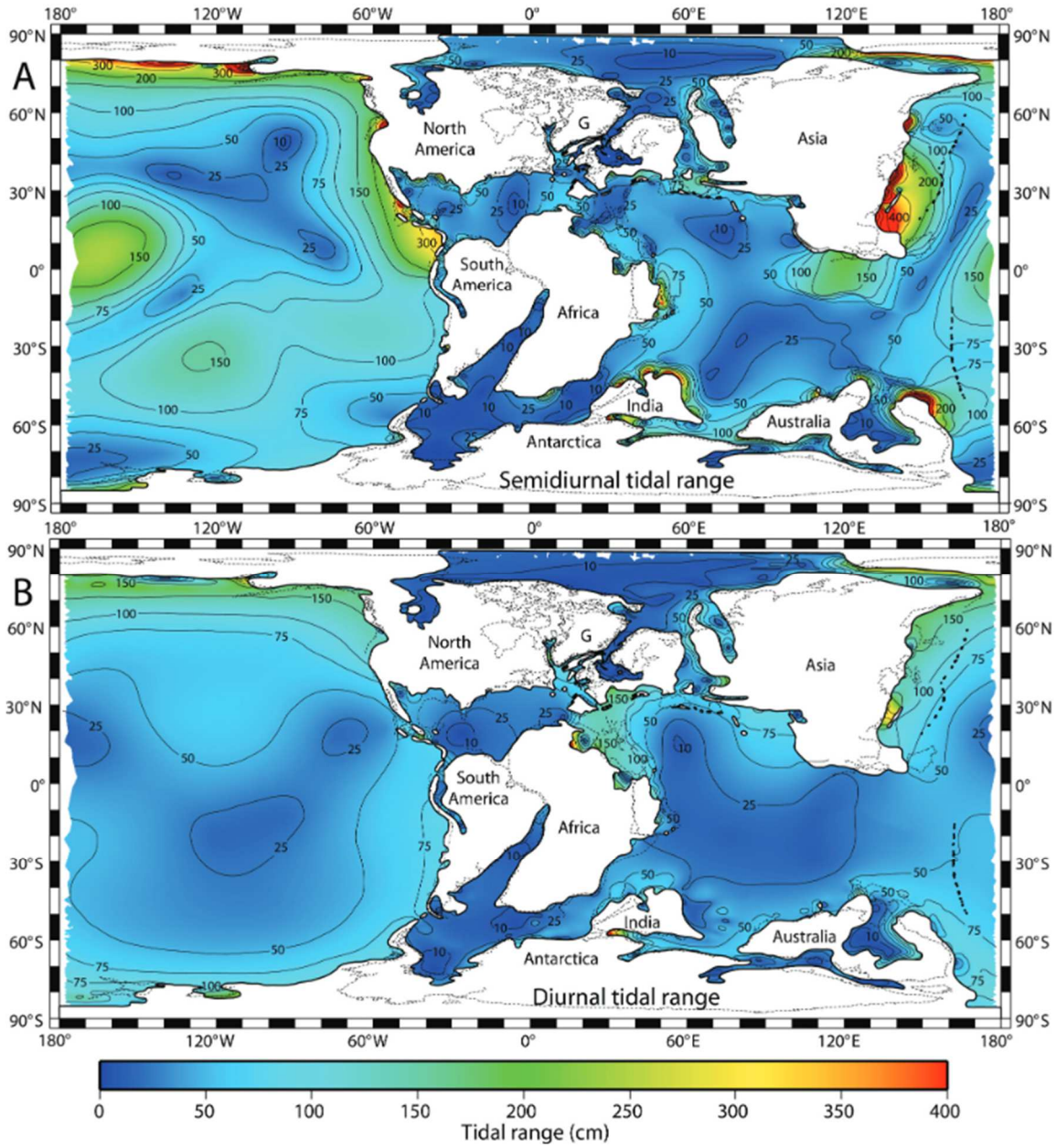

Fig. 13: ICOM (Imperial College Ocean Modelling) results for the Aptian global ocean paleo-tidal model. Tidal range of A) the semidiurnal tidal constituents (M2 + S2), and B) the diurnal tidal constituents (K1 + O1). Contours are drawn at 10 cm, 25 cm, 50 cm, 75 cm, 100 cm, 150 cm, 200 cm, then at 100 cm intervals, extending beyond the upper limit of the colour bar. G, Greenland (Wells et al., 2010).

The results show a completely different tide compared to the present-day, which is probably due to the presence of the Neotethys ocean and the separation of the Atlantic Ocean in two distinct parts (closed at the level of the equator, Fig. 13). It demonstrated the importance of oceans size and straits on tidal amplitudes distribution. The highest amplitudes are located at the edges of the Pacific Ocean (Fig. 13). The Imperial College also focused on continental platforms (shallow water), like the opening of epicontinental sea. Wells et al. (2007b; 2007a) simulated potential tides in the early and the late Pennsylvanian Seaway of NW Eurasia. Investigations through different sea-level (high stand and low stand) over the late Pennsylvanian (298.9 to 323.2 Ma) led to very different propagations of semi-diurnal and diurnal main components depending on the geological reconstitutions (replacing or nor the Ancestral Rocky Mountains with a shallow water, i.e. 20–50 m, platforms). Simulations of very old

contexts are thus very dependent on the plate tectonic reconstruction. Other studies explored recent and old paleoenvironment impact on tides, such as Reynaud and Dalrymple (2012, Holocene and Lower Cretaceous; Zuchuat et al., 2022, lower Oxfordian).

The main conclusion about past tide simulations is that its propagation or amplitude is mainly modified by variation of the oceans, continental platforms or basins shapes, depending on the spatial scale considered. For old reconstructions, kinematics motions must be taken into account. The older the reconstructions are, the more different the propagation of the tidal wave will be. There is less data and information for old stages than for younger ones. Even if they are probably not a reproduction of the reality, these simulations provide very important information about past tides behaviour and factors influencing changes in global to local tidal dynamics.

Over shorter period of time (hundreds of years to tens of thousands of years), sea-level variations and morphological changes (through mainly erosion/sedimentation, local to regional scale) are responsible of main tide evolution. However, as there is still no hydrodynamic record older than 300 years ago, numerical modelling is the only way to obtain valuable information about tide evolution and its main triggers.

2.2 Tide impact on estuaries sediment infilling

The propagation of the tidal wave induces currents of varying strength, depending on the tidal amplitude and bathymetry. When reaching the continental shelf, the bathymetry decreases and tidal currents increase. In tidal seas the strongest currents are located nearby shoals and the coast. It is therefore at the land/sea interface that the tide has the greatest influence on sediment transport. Other hydrodynamic forcings act along the coast such as waves and river flows. The dominance of one of those forcings can vary rapidly along the coast (in time or space), i.e. their impact on coastal currents varies quickly. Tidal currents are an important factor in coastal basins, as they directly influence erosion, transport and deposition of sediments. It is also at the land/sea interface, more precisely in estuaries and deltas, that the transfer of sediments from continental erosion to deep basins takes place. Estuaries (and deltas) are thus key areas in global understanding of coastal to deep basins infilling and therefore to the source-to-sink approach.

2.2.1 Short-term impact of tide

In order to explain sediment movements induced by the tide, two main technics exist. On one hand, the naturalistic approach of geologists interprets sediment structures and facies in term of transport and deposition processes. On the other hand, the physical approach of oceanographers, based on the resolution of physical processes, uses numerical modelling to simulate transport/deposition/erosion processes and measurements (currents velocities, free surface elevation, salinity, temperature…).

The naturalistic approach is based on the identification of depositional morphologies. These latter are classified according to observations made in many estuaries (e.g. tidal flats domains, Flemming, 2012, Fig. 14).

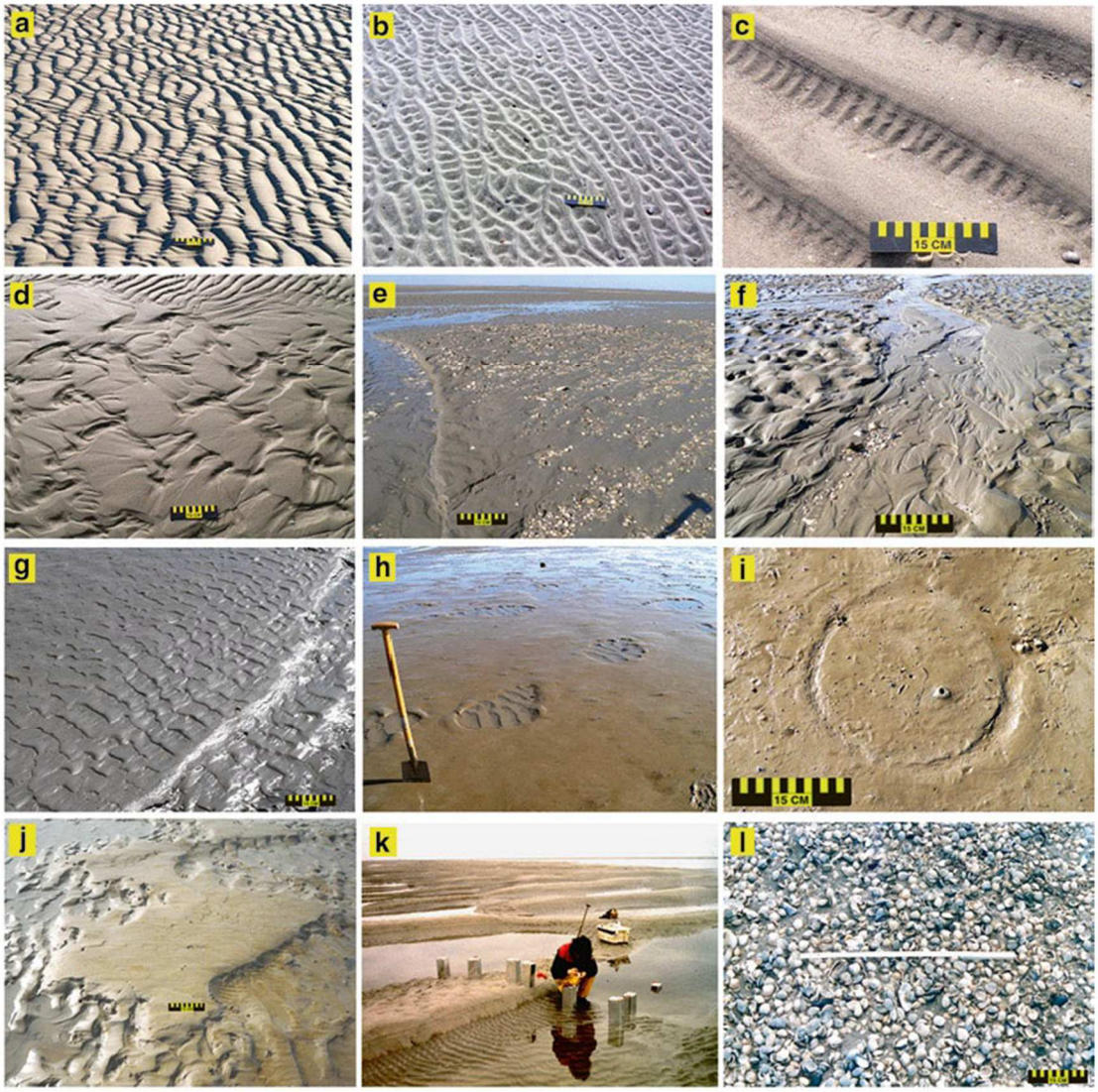

Fig. 14: Physical surface structures frequently observed on tidal flats. (a) Asymmetrical wave ripples; (b) Ladderback ripples; (c) Small wave ripples in the troughs of larger ripples and water level marks; (d) Late-stage runoff with linguoid current ripples dissecting a field of flat-crested wave ripples; (e) Shallow intertidal creek with small sand ribbons over shell pavement; (f) Late-stage runoff features; (g) Current ripples in mud; (h) Thin fluid mud sheet with scour windows displaying ripples on the surface of underlying sand. (i) Circular tool mark formed by the rotation of a protruding polychaete tube. Note the bird tracks surrounding the structure; (j) Rippled sand bed with patchy wash-outs formed shortly before emergence; (k) Intertidal dunes; (l) Shell pavement (Flemming, 2012).

The currents inducing these deposits are interpreted according to several criteria: the grain-size characteristics, the organisation of the grains between them (structure of the deposits) and the global repartition of these two parameters over the whole estuary. Grain characteristics are precious information: for non-cohesive sediments the sphericity of the grain testifies of the travelled distance from the erosion site. High sphericity highlights a long transport to the recorded area and angular grain the opposite, as transport is responsible for the fragmentation of blocks and grains. Grain sorting can also provide information on transport patterns, for example eolian sands are easily recognisable by very well sorted grains showing traces of impact due to saltation movements. The size of the transported grains also gives information on the energy of the currents. The relationship is simple, the heavier the grains are, the greater the energy is required to move them. The alternation of fine and

coarse grains can reveal several directions of currents and a dominance of one of them over the area (Fig. 15).

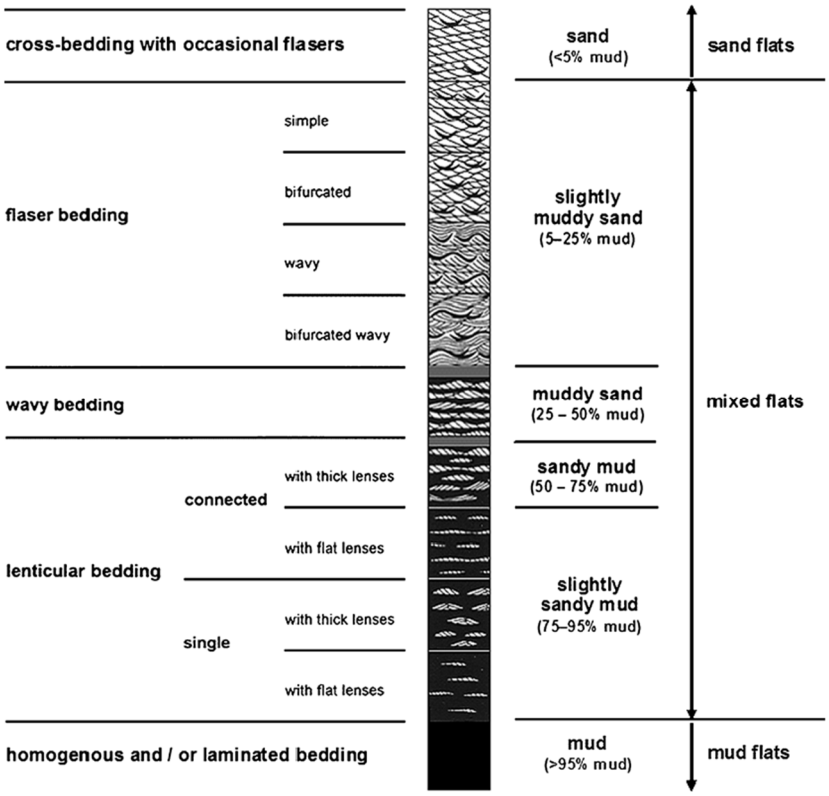

Fig. 15: Synthetic section in which successive sedimentary facies occurring between the low-tide and the high-tide level of intertidal flats (without tidal creeks and bioturbation) have been vertically stacked in an idealized transgressive facies model (Modified after Reineck and Wunderlich, 1968; Flemming, 2012).

The distribution of sand and mud in estuaries was linked to estuaries morphologies by Reineck and Wunderlich (1968). Facies distribution is constantly used as a proxy for currents intensity and the transition between mud and sand dominated facies is indicated in all conceptual models of estuarine sediment dynamic (Dalrymple et al., 1992; Dalrymple and Choi, 2007; Tessier et al., 2012). Details about grain sizes transport and their deposits are discussed by Le Roux and Rojas (2007), including potential limitation of grain sizes interpretation.

Deposits morphology provides many information about current directions. For example, all structures with ridges, i.e. ripple marks or dunes, reveal the axis of the currents. The interpretation of dune fields can give the directions of ebb and flood tide currents (Gregoire, 2016). Dunes are often mobile structures controlled by tidal and wind-induced currents (Le Bot, 2001; Le Bot and Trentesaux, 2004; Ferret et al., 2010). These sediment figures are elongated and display a perpendicular crest to the main axis of currents with an angular variation of 20° (Le Bot, 2001). Those structures show an eroding (Stoss side) and an aggrading (Lee side) side and the asymmetry between the two flanks reflects the orientation of the residual bottom current (Fig. 16, Gregoire, 2016). The rate of dune migration can even be estimated from the calculation of an asymmetry index (Xu et al., 2008).

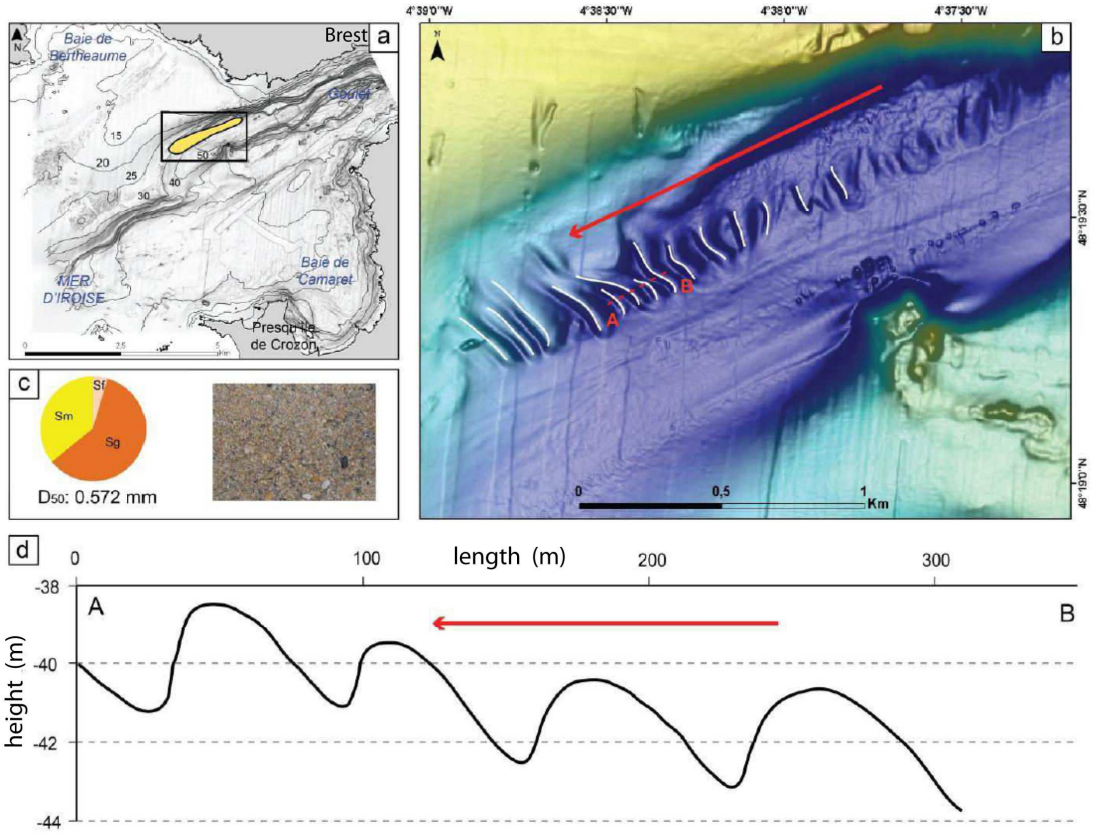

Fig. 16: a: Dune field location (the Bay of Brest). b: Zoom on the dune field. The white lines represent the crests of the dunes, the red arrow represents the transport direction interpreted from dunes asymmetry and the red dashed line represents the cross-section. (c) grain size characteristic of the dune and picture. d: Cross-section A-B to the dune ridges, the red arrow illustrates the transport orientation (Gregoire, 2016).

Comet tails are another example of bottom currents proxy (Bouma et al., 1977). They are sediment structures that develop parallel to bottom currents (Flemming, 1980), behind obstacles. The direction of current can be deduced thanks to the orientation of the accumulation (Fig. 17 and see examples in Gregoire, 2016). The sediment structures induced by tidal currents are very numerous: dunes, tidal channels, many types of ripple marks, sand waves and more (Fig. 14 and see Davis and Dalrymple, 2012). They are better and better imaged and understood thanks to experiments and the development of new tools: high resolution seismic or sub-bottom profilers (chirp), grain-size profiler, multibeam backscatter… (Montereale-Gavazzi et al., 2019).

Then, by combining the information from all proxies, tidal sediment dynamics are reconstructed. That was done by Gregoire (2016) for the Bay of Brest (Fig. 17). Thus, by interpreting the residual sediment movements, areas dominated by ebb and flood tide can be highlighted and different hydro-sedimentary areas (or cells) can be distinguished (Fig. 17).

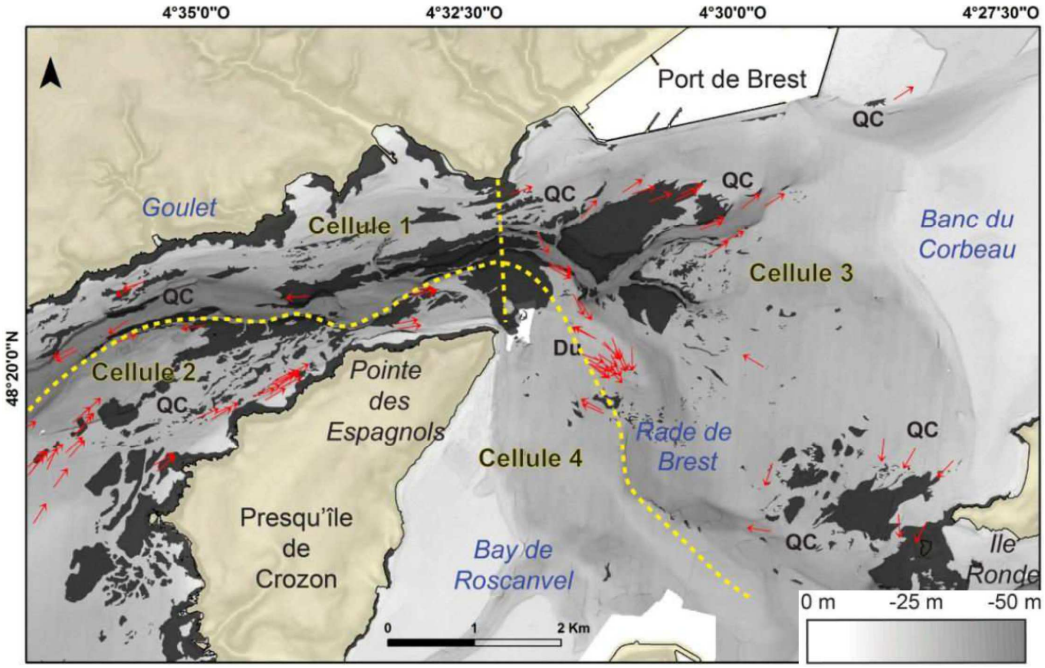

Fig. 17: Resume of morphological indices of transport on the seafloor in the Bay of Brest. Red arrows represent the interpretation of currents directions. Letters represent the sediment structures interpreted: QC are comet tails, Du are dunes (Gregoire, 2016).

The same kind of work was carried out for many estuaries and by many authors (FitzGerald et al., 2000; Kang et al., 2014; Shaw et al., 2014; Gregoire, 2016). Common depositional morphologies (dunes, tidal bars, scour trough…) were linked to specific transport conditions (Hayes, 1980; Dalrymple and Rhodes, 1995; Todd et al., 2014). Tidal bars are an excellent example, located in so-called high-energy zones of tidal estuaries, they form and orient themselves according to the trajectories of the ebb and flood tide currents (Leuven et al., 2016). The observation of those proxies led to the establishment of a conceptual model (Dalrymple et al., 1992; Dalrymple and Choi, 2007). The sediment deposits in tide-dominated estuaries would be organised in the following way (Dalrymple et al., 2012): non-cohesive sediments are located in the centre of the estuary in the form of dunes, tidal bars and so-called high-energy structures; cohesive sediments are deposited towards the flanks and upstream of the estuary (shallower than non-cohesive deposition area and inside the intertidal zone); and in supratidal areas, mostly salt marshes are observed (Fig. 18).

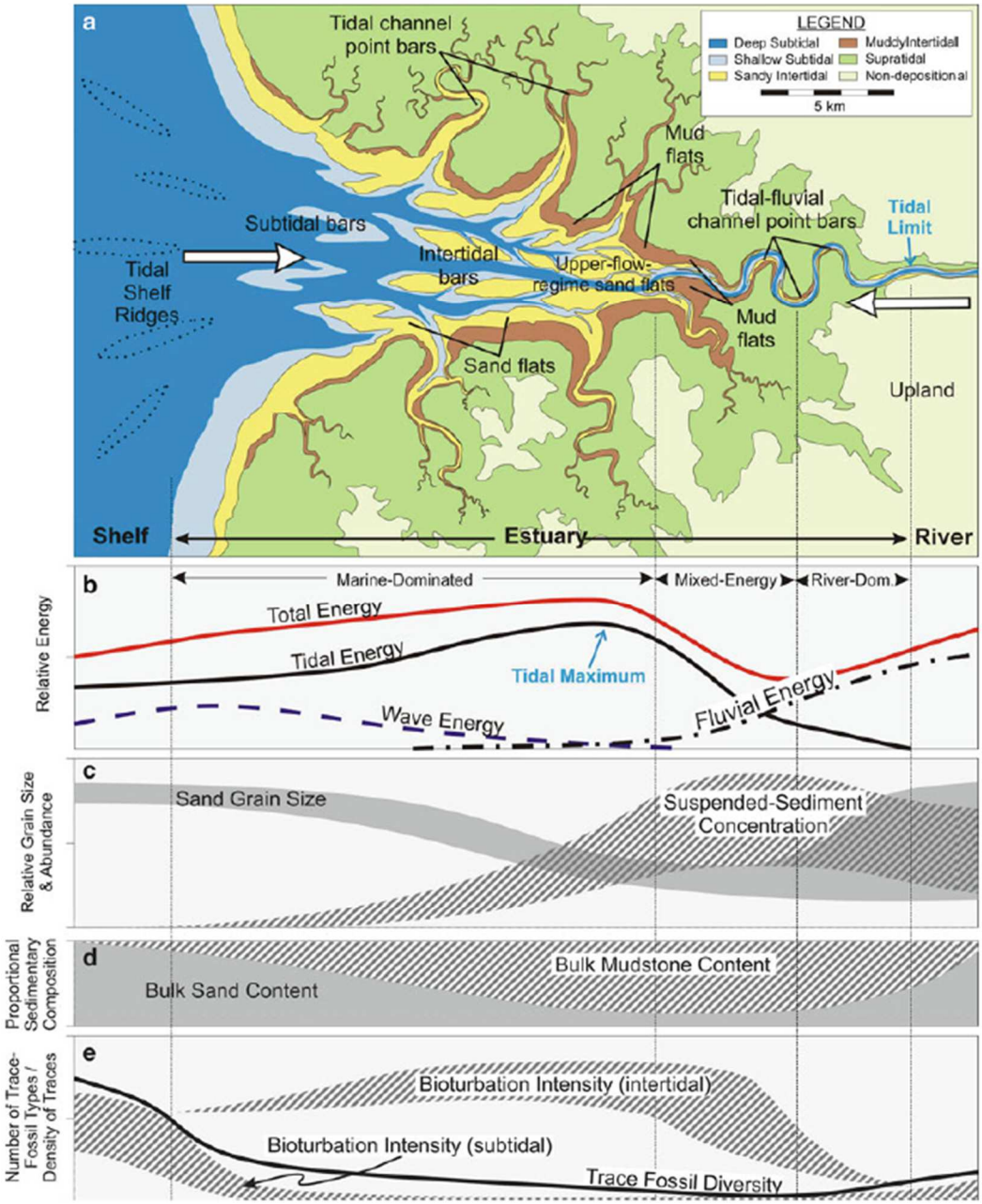

Fig. 18: (a) Schematic map showing the typical distribution of channel forms and subenvironments in a sandy macrotidal estuary, based on systems such as the Cobequid Bay-Salmon River and Bristol Channel-Severn River estuaries. The large white arrows indicate sediment movement into the estuary from both the landward (fluvial) and seaward directions. (b) Longitudinal distribution of wave, tidal and river energy (Modified after Dalrymple et al. (1992) and Dalrymple and Choi (2007). The 'tidal maximum' is the location where the tidal-current speeds are greatest. (c) Longitudinal distribution of bed-material (sand) grain size, showing the presence of a grain-size minimum near the location where flood-tidal and river currents are equal (i.e., the bedload convergence), and of suspended-sediment concentrations, showing the turbidity maximum. (d) Longitudinal distribution of the relative proportion of sand- and mud-sized sediment in the deposits. e) Longitudinal distribution of trace fossil characteristics, based on Lettley et al. (2005) and MacEachern et al. (2005). (Dalrymple et al., 2012).

Oceanographers use a different approach based on the physical representation of hydrodynamic processes acting on the sediment from event to interannual time scales (process-based model). The two approaches are therefore complementary in understanding the present-day sediment dynamics of estuaries. Geologists provide a naturalistic description of sediment deposits and structures, which

is as essential as short term in-situ measurements (e.g., current velocities or suspended matters) for the definition and calibration of the physical processes simulated by oceanographers. Then process-based models provide potential configurations, forcing or processes to explain the observations. Many theoretical and realistic estuaries were modelled. Those works allowed to discretize the processes and to study more precisely the formation of sediment structures already identified by naturalists: tidal bars (Ouahsine et al., 2013; Price and Ruessink, 2013), dunes (van Santen et al., 2011; Davies and Robins, 2017), or tidal flats (Palacio et al., 2005; Hu et al., 2015). It was through conceptual estuary simulations that van de Lageweg and Feldman (2018) demonstrated the relationship between estuary width and tidal bar formation. Tidal bars are more numerous and thicker in wide estuaries and much less numerous and thick in narrow estuaries (Fig. 19).

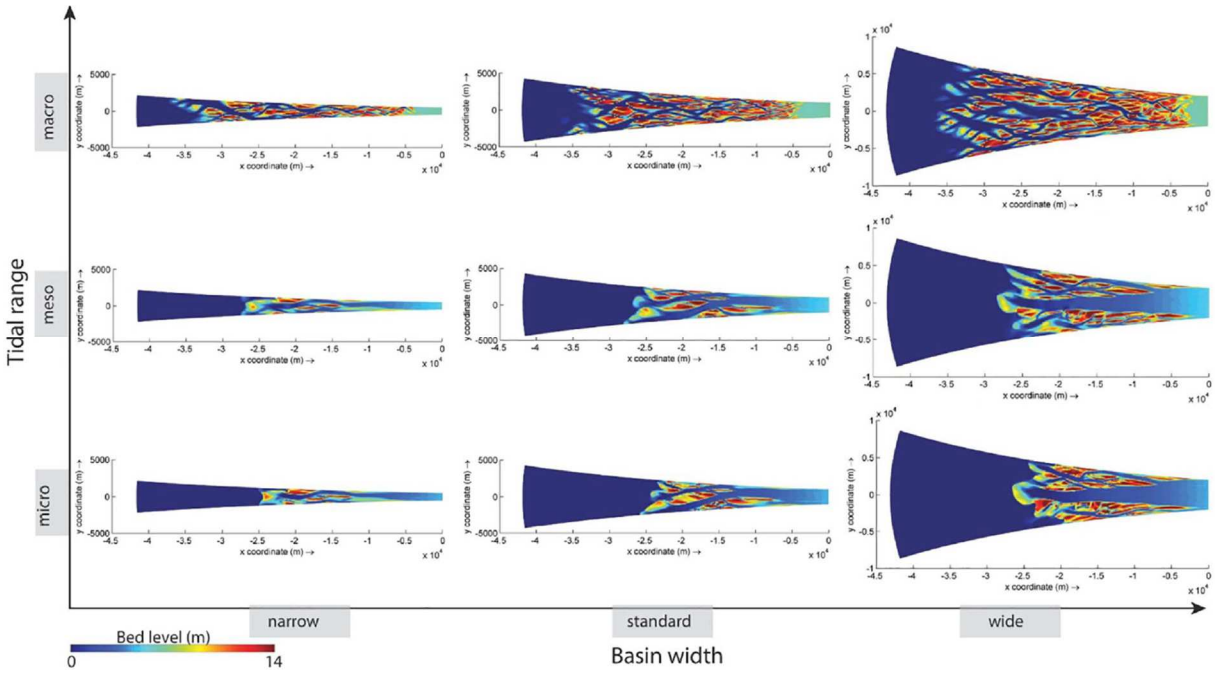

Fig. 19: Variations of bar morphology after one year of mixed fluvial and tidal currents, followed by one year of only tidal currents. (van de Lageweg and Feldman, 2018).

Through the study of conceptual (or idealized) estuaries, the impact of hydrodynamics on sediment structures is increasingly better understood and simulated. Bringing together naturalistic observations and experimental physic investigations (e.g. van Rijn, 1994; Soulsby, 1997 for sand transport) allows to reproduce the complex hydrodynamics that occurs in estuaries. Many realistic estuaries were modelled in order to understand the sediment dynamics and its likely implications for human activities or natural systems. In Grasso and Le Hir (2019) the spread of suspended sediments was studied in the Seine estuary in 1960 and in 2010, for two median flows: 1340 and 340 ($m^3.s^{-1}$). The study shows a very different spread of sediments between these two periods, due to the human modifications of the estuary (Fig. 20). The transfer of sediment is confined to the southern part of the estuary in 2010.

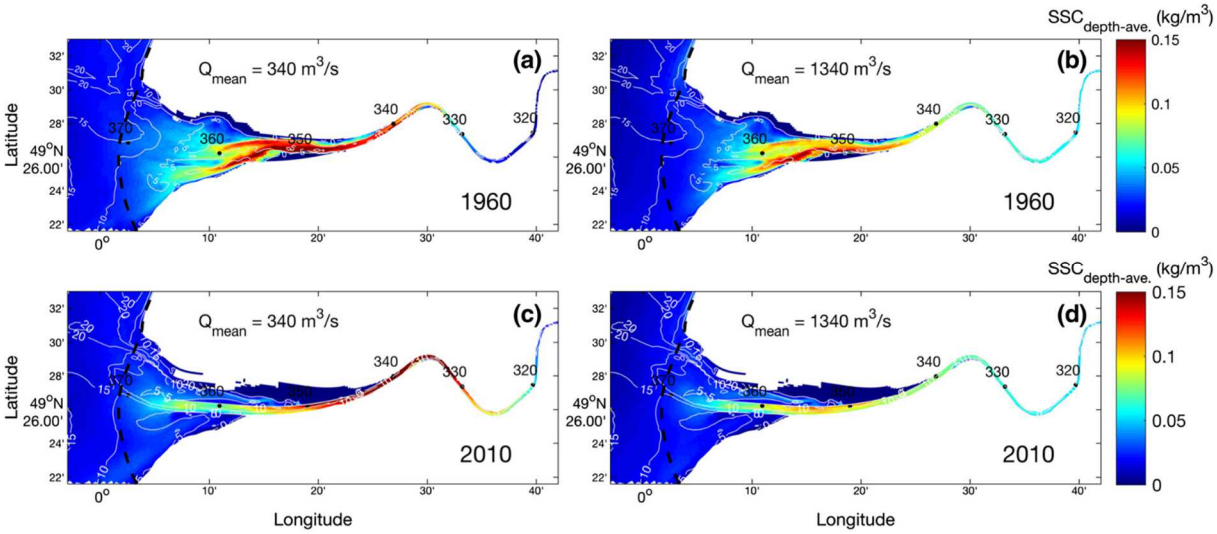

Fig. 20: Spatial distribution of depth-averaged mud SSC (suspended sediment concentration) in the 1960 (top panels) and 2010 (bottom panels) configurations. Median values over a neap-spring tidal period during a, c low river flow (Qmean = 340 m3.s-1) and b, d high river flow (Qmean = 1340 m3.s-1). The white contours represent 5m isobaths, the black dashed line represents the lower-most estuary limit used for SSC analyses (Grasso and Le Hir, 2019).

In the case of a low flow of the Seine river, the concentration of sediments is much higher in the present-day upstream toward the Seine mouth than in 1960 and can disturb the human development of this area (Fig. 20c). The maximum mass of suspended mud does not significantly change with the estuary deepening and narrowing, but its distribution is less extended. The study of Grasso and Le Hir (2019) highlights that the dredging and damping activities have hardly influenced the SSC (suspended sediment concentration) distribution. In the Western Scheldt estuary (Netherlands), Dam et al. (2016) directly explored the morpho-dynamical behaviour, by using a 2-D, high-resolution, process-based model. Thanks to a unique bathymetric dataset they were able to compare the simulated morphological evolution and measurements (thickness of tidal sand bars) over hundred years. The results revealed the same patterns between simulation and data (only minor bathymetric differences are visible, Fig. 21). This consistency between observations and simulations (Fig. 21) testified of the very good representation of the tidal phenomenon in estuaries in hydro-sediment models.

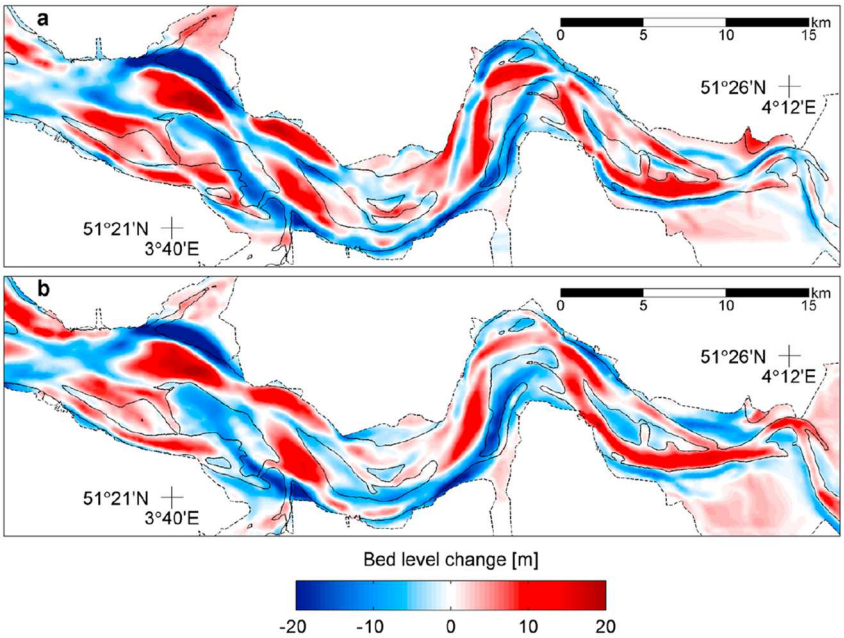

Fig. 21: Erosion and sedimentation patterns over the 1860–1970 period. (a) Measured. (b) Modelled. Black dashed line indicates the 1860 plan form. Black solid line indicates the -5m contour line of the 1860 bed level (Dam et al., 2016).

Over a short period of time and with careful parameterisation, hydro-sediment models can represent the sediment dynamics induced by tide in realistic estuaries. The main difficulty for tide modelling is to discriminate the effects of each forcing at play in the system. An example of mixed system is the Mekong Delta. The study of sediment distribution from the Mekong River along the coast (Tu et al., 2019) needs to take into account tide, waves, the seasonal variability of river discharge and meteorological forcings (monsoon). The simulations are validated with the help of Sea-Surface Temperatures data (SSC) from satellite and in-situ measurements (SSC, waves and salinity). Tu et al. (2019) explored the morphological evolution of the seafloor by calculating the difference of sediment budget between the beginning and the end of the simulation at each point (Fig. 22).

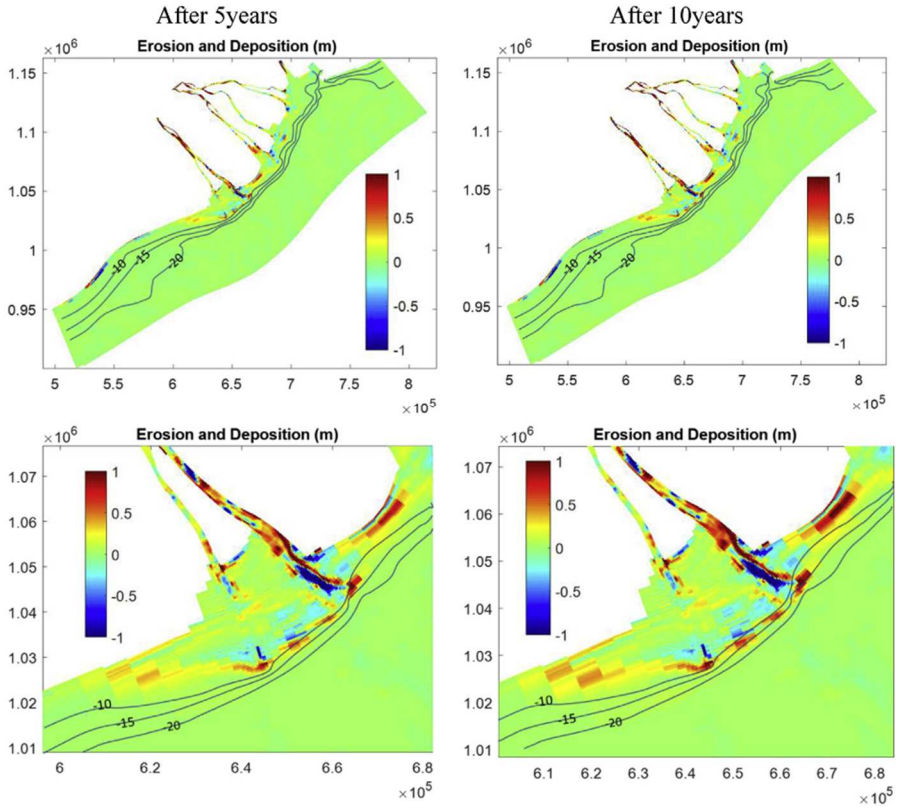

Fig. 22: Morphological changes of the Mekong coast (upper panel) and Bassac estuary (lower panel) after 5 and 10 years of simulation (Tu et al., 2019).

They found that at the river mouths, seasonal sediment transport is strongly modulated by river discharges and monsoons. When sand or mud sedimentation processes are related to seasonal river discharges, the direction of suspended sediment movement depends on the direction of the monsoon. In the estuaries erosion and deposition occurred alternatively, bars were formed in front of the estuaries by tides and rivers, then these bars developed and migrated to the south-west region (Fig. 22). Thus, even in estuaries governed by numerous seasonal and annual forcings, the impact of different events can be identified. In mixed systems, simulations may not be an exact reproduction of sediment movements, but the most important, as for naturalistic approach, is that they help us to understand natural processes and their interactions.

Thanks to the combined approach of these two communities, the present-day sediment dynamics are well understood in estuaries. However, the understanding and simulation of sediment dynamics within an estuary over thousands of years remains a challenging issue.

2.2.2 Long-term impact of tide on sedimentation

Compared to present-day tides, knowledge of the impact of past tides on sediment is very limited. Processes acting on sediment transport in tide-dominated estuaries are very complex, as they are influenced by numerous hydrodynamic and sedimentological factors over a wide range of temporal and spatial scales (Wang, 2012). The study of sedimentary records allows to consider very long temporal scale, i.e., in the order of thousands (ka) to million years (Ma). Contrary to the study of present-day systems, where the information available is horizontal or in 3D, information available for past sedimentary systems is mostly vertical (e.g. outcrop, seismic). Then sedimentary basins can be

considered in 3D thanks to interpolation. For this reason, the interpretation of tidal influenced rocks is mainly based on the cyclicity of the deposits (Kvale, 2012), marked by recurrent grain-size alternation for example (Davis, 2012). Those rocks are the result of thousands of years of a short temporal scale forcing (tidal currents: second/minute). The tide cyclicity is so well marked in some locations (outcrops, cores) that tidal bedding sequences were correlated with paleo-tidal cycles (Fig. 23, Tessier, 1993).

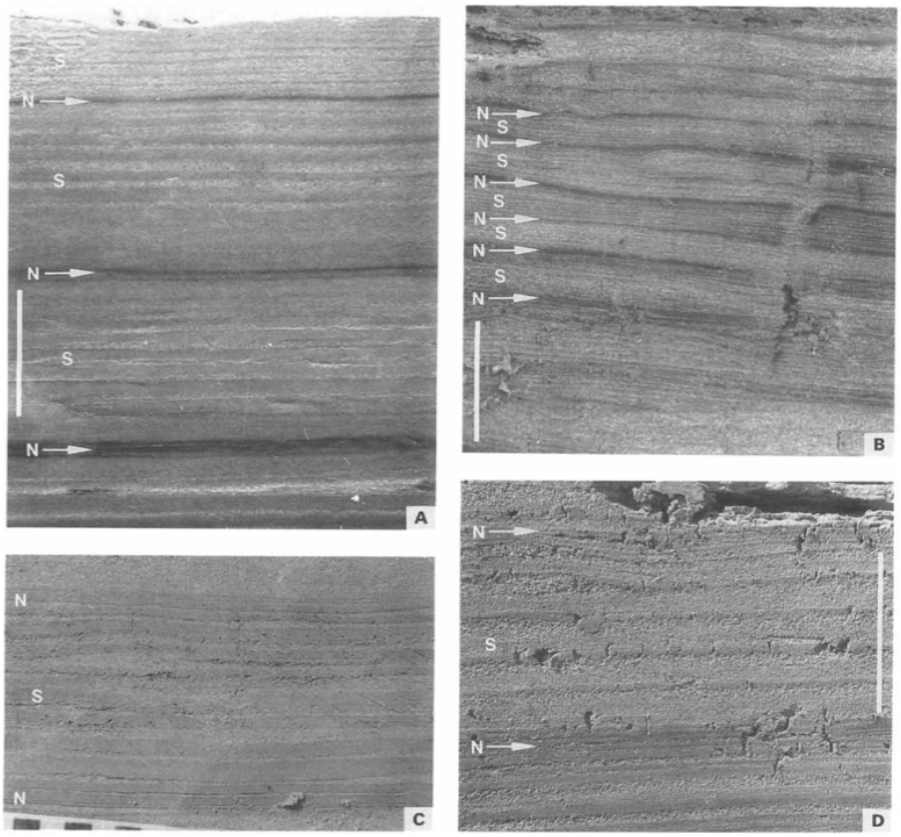

Fig. 23: Some examples of neap/spring cycle records in planar bedding (N= neap: S=spring). (A) neap/spring cycle records with sand-mud centimetre-scale tidal cycles. Notice the well-developed dark beds corresponding to the neap stages. Scale bar= 3 cm; (B) neap/spring cycle records with sand-mud millimetre-scale tidal cycles. Notice the well-developed dark beds corresponding to the neap stages. Scale bar = 10cm; (C) neap/spring cycle record with mud dominated centimetre-scale tidal cycles. Scale in centimetres; (D) neap/spring cycle record with sand dominated centimetre-scale tidal cycles. Scale bar= 5 cm (Tessier, 1993)

This type of pattern can be observed in cores or outcrops only, because it needs a high resolution to be observed. Sedimentary rocks influenced by tide are called tidalites, this term is used at different time-scales and for various sediment structures.

Tidal influence on sediment deposits can also be identified by analogy with present-day coastal environments, i.e. sediment patterns are compared with similar sedimentary system active at present-day (Gingras and MacEachern, 2012). All the sediment structures forming at the present-day (section 2.2.1) can be interpreted in fossil records (Fig. 24, Flemming, 2012).

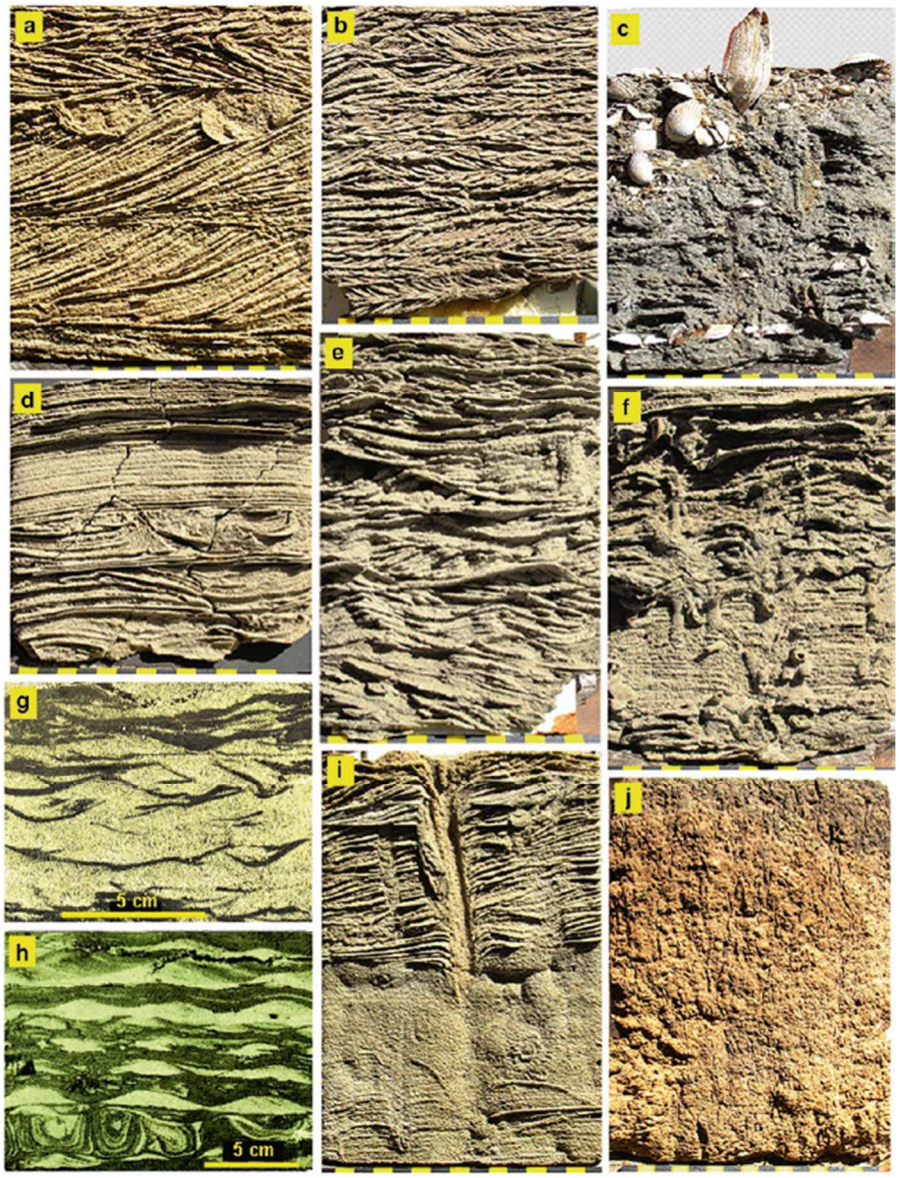

Fig. 24 : Internal sedimentary structures typical for tidal flat deposits. (a) Bidirectional dune cross-bedding with current dominance from right to left; (b) Bidirectional ripple crossbedding with well-developed herringbone structures; (c) Partly bioturbated sand with shell layer at depth and shell lag at the surface. Note partly excavated shell of the bivalve Mya arenaria in live position; (d) horizontally bedded sands above several convoluted bedsets; (e) Multidirectional wave and current ripples in sand. Note the absence of clear herringbone structures; (f) Partly bioturbated, horizontally bedded sand in lower part of core, grading into partly bioturbated rippled sand in upper part; (g) Flaser bedding typical for muddy sand facies; (h) Lenticular bedding typical for sandy mud facies; (i) Weakly laminated sand in lower core, followed by well-preserved lamination in upper core, both penetrated by a large worm tube, possibly of Arenicola marina (u-part hidden); (j) Rooted salt marsh deposit (Flemming, 2012).

Ripple marks, dunes, sand bars and more, are excellent paleo-currents proxies (Fig. 24). Combining the analysis of sediment structures and grain-sizes characteristics, can give paleo-directions of tidal currents and clues about their velocity. Only some outcrops can give a 3D view of those structures. In their absence, these centimetric structures are only visible with high resolution seismic, if they are not too deeply buried. The stratigraphic interpretation of tidal deposits is carried out by analogy with present-day observations (e.g. Reynaud et al., 2006; Shanmugam et al., 2009; Flemming, 2012; Olariu et al., 2012; Reynaud and James, 2012; Lee et al., 2022), which are summarized in conceptual models (e.g. Dalrymple and Choi, 2007; Dalrymple et al., 2012). The interpreted depositional environments are

thus assembled to determine the depth and the influence of hydrodynamics by analogy. They can be then associated with transgressive and regressive cycles: LST (Lowstand System Tract), TST (Transgressive System Tract) and HST (Highstand system tract).

A good example of stratigraphic interpretation of a tidal dominated estuary infill (Mont Saint Michel bay) is provided by Tessier et al. (2012). In this study numerous proxies are combined with a seismic dataset and compared with conceptual models to interpret the sediment infill (Fig. 25). Main sedimentation patterns are then attributed to several forcing or processes.

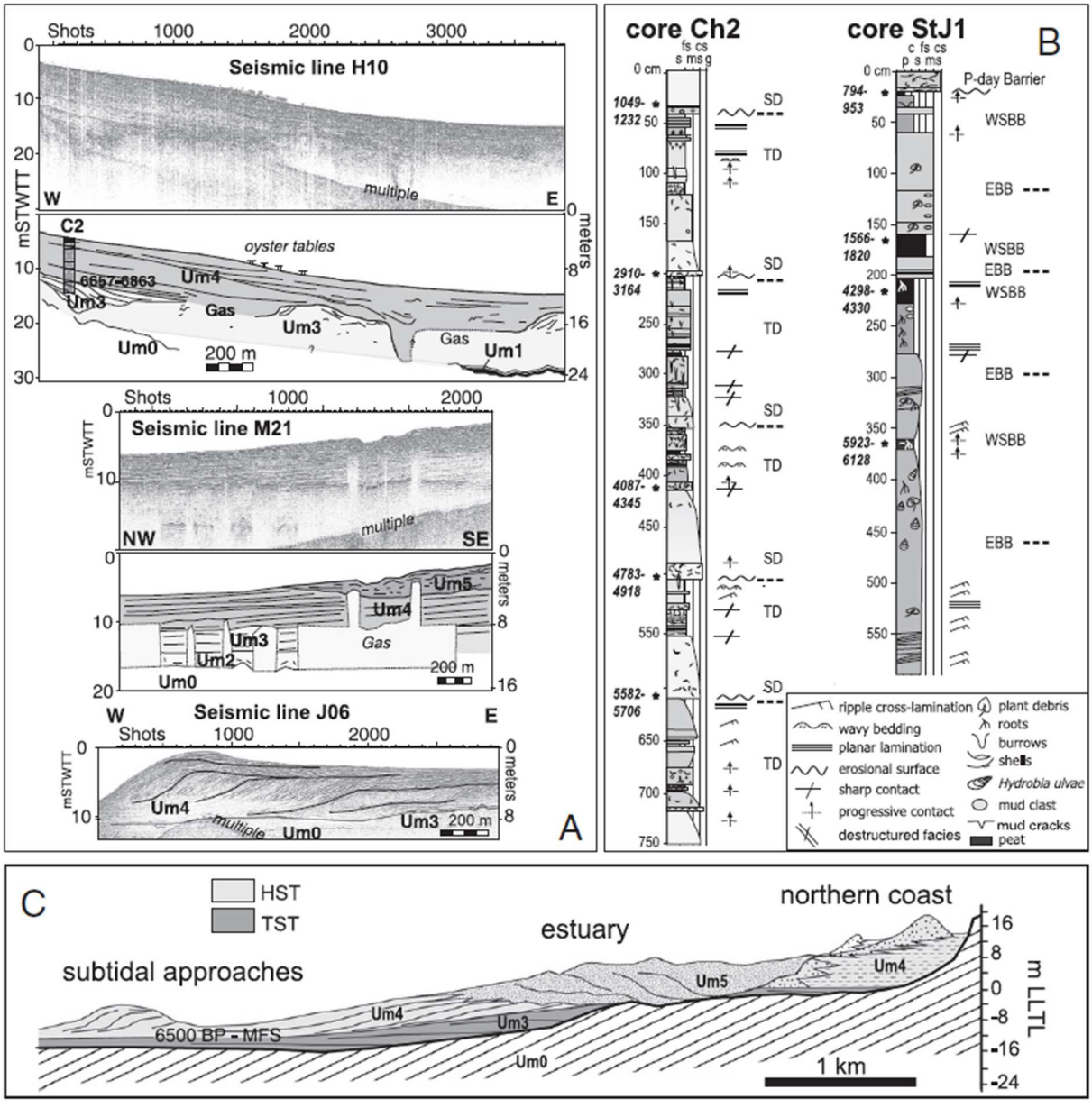

Fig. 25: A) Seismic line samples and B) representative cores collected in the Mont-Saint-Michel bay. C) Illustrative model of infilling with main systems tracts and surfaces according to a longitudinal cross-section (approximately parallel to the incised valley). On B: Ages indicated along the cores are years cal BP; SD: storm dominated facies; TD: tide-dominated facies; WSBB: well-sheltered back-barrier facies; EBB: exposed back barrier facies. Grain-size: p — peat, c — clay, s — silt, fs — fine sand, ms — medium sand, cs —coarse sand, and g —gravel. On C: TST: transgressive systems tract; HST: highstand systems tract, MFS: maximum flooding surface; and LLTL: lowest low tide level (Tessier et al., 2012).

Although all this information is valuable, the question of preservation of the deposits is very important for understanding the infilling of an estuary. Each layer is the result of the balance between erosion and deposition over hundreds to thousands of years (Flemming, 2012) and the sediment dynamics coming after the deposition that could remobilized the previously deposited sediments. Erosion and deposition areas are supposed to change with sea-level variation and seafloor morphology, it is therefore very complicated to discretize the different events and understand the evolution of the system (Tessier et al., 2012). The stratigraphic response of estuaries to sea-level changes is even more complicated to take into account, as it varies with the combination of the rate of sea-level change, sediment supply, bedrock morphology, and hydrodynamics (Tessier, 2012).

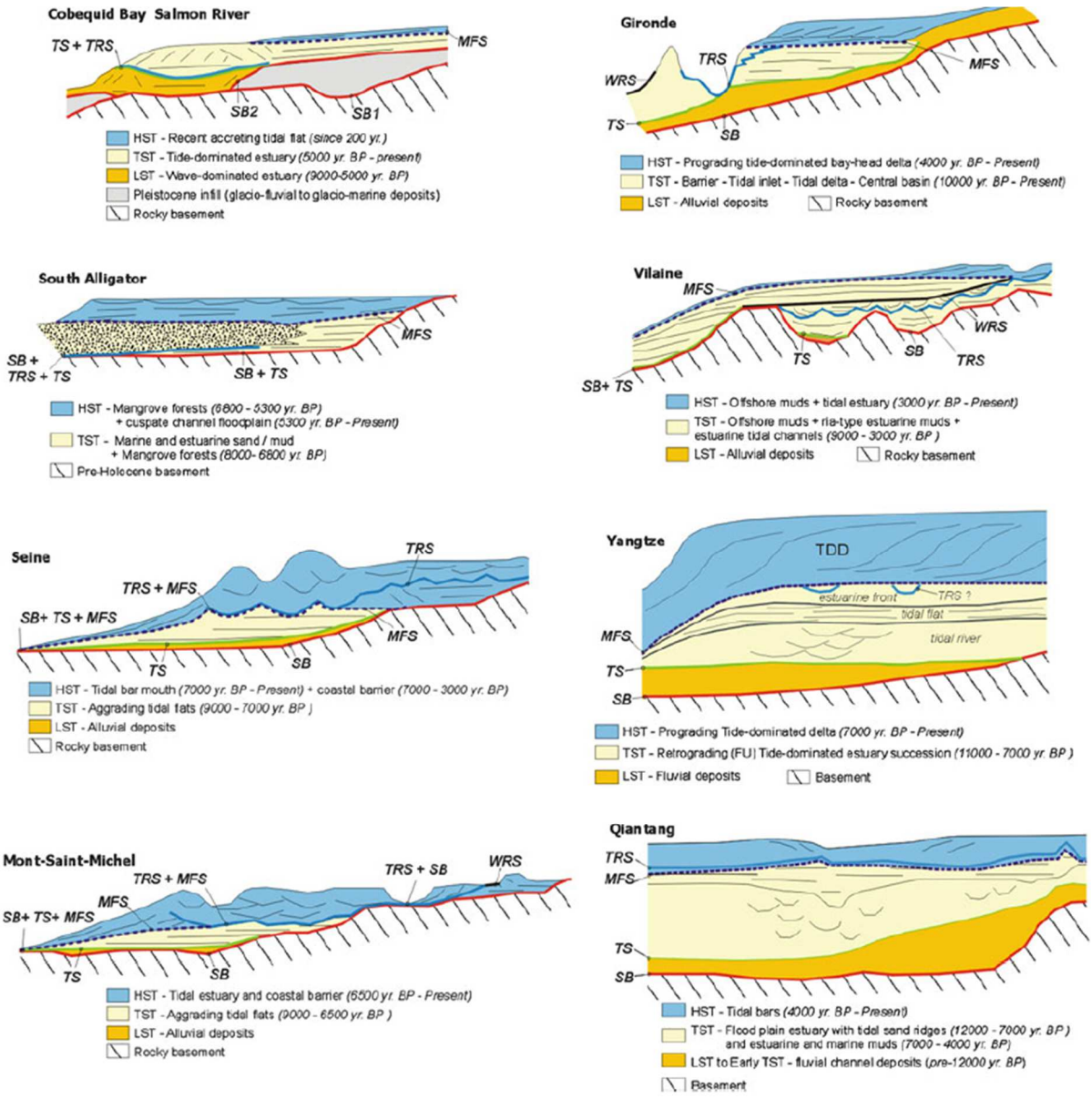

Fig. 26: Stratigraphic organization of the sedimentary infill of the main modern (Holocene) tide-dominated estuaries, including as well the mixed-energy estuary of the Gironde, and the tide-dominated delta of the Yangtze (a tide-dominated estuary during the transgressive systems tract deposition). The Cobequid Bay–Salmon River estuary (Bay of Fundy, Canada). The South Alligator estuary (van Diemen Gulf, North Australia). The Gironde estuary (Central Bay of Biscay, SW France). The Seine estuary (Bay of Seine, NW France). The Mont-Saint-Michel estuary (Norman-Breton Gulf, NW France). The Vilaine estuary (Northern Bay of Biscay, NW France). The early Holocene Yangtze estuary (East China Sea, China). The Qiantang River estuary (Hangzhou Bay, China). SB: Sequence Boundary, TS: Transgressive Surface, TRS: Tidal Ravinement Surface,

WRS: Wave Ravinement Surface, MFS: Maximum Flooding Surface, LST, TST , HST: Lowstand, Transgressive, Highstand Systems Tracts), TDD Tide Dominated Delta (Tessier, 2012 and references).

The filling of tide-dominated estuaries in the Holocene reveals very different depositional morphologies (Fig. 26). The thicknesses and shape of the deposits during the Holocene transgression (sea-level rise) are different in all estuaries. Without common patterns, it is hard to deduce a global impact of the tide on estuaries infill. In estuaries sequence stratigraphy, transgressive or regressive movements are linked with the interpreted evolution of shoreline, which comes from depositional environments interpretation of sedimentary record. For example, if the intertidal mud/sand limit or sand bars (Dalrymple et al., 2012) are found upstream towards flanks of the estuary and river mouths, it will be interpreted as a marine transgression and in this opposite case as a regression. Some particular facies, or facies transition, are used to interpret sea-level variations, as salt marsh (e.g. Goslin et al., 2015). However, due to bad preservation, it is unusual to observe longitudinal variation of facies deposits, even in the presence of a great dataset (e.g. cores, seismic, outcrops, Tessier, 2012). Moreover, designation of the transgressive surface is particularly difficult as many of the prominent surfaces in the estuary fill are diachronous facies boundaries (Dalrymple and Zaitlin, 1994). The combination of diachronous facies boundaries, poor preservation of deposits, and the great variabilities of facies and hydro-sediment processes in estuaries in space and time, complicates a lot the interpretation of the tide impact on sedimentation.

The knowledge about short-term impact of tide on sediment dynamics allows to explain fossil records (e.g. in Davis and Dalrymple, 2012). However, with partially preserved sedimentary records, reconstructing the evolutive tidal influence over the entire history of the infill of the estuary is very complex. With only partial sedimentary records, the only option to explore the evolution of the hydro-sediment dynamic induced by tide is numerical modelling.

2.3. Numerical modelling of sediment deposits

The geological and oceanographic communities seek to understand respectively the infilling of sedimentary basins and the hydro-sediment dynamics. Even if these two objectives are not totally independent, the numerical models developed by each of these communities are thought in a completely different way. To numerically simulate sedimentation two main models are developed: (i) Stratigraphic models are designed to simulate sediment layers and resultant geometries at basin scale and over geologic time-scales. They are therefore designed for geological purposes. (ii) Process-based models that are designed for oceanographers aims, attempt to reproduce the impact of hydrodynamic processes on sediment movements over events or decades. Various models of each type exist.

2.3.1 Stratigraphic modelling

Stratigraphic modelling is designed to represent the infilling of sedimentary basins at geological time-scale (100 ka to 100 Ma) and basin scales (1 Km to 1000 km). This technic uses a deterministic approach based on diffusion, which is the only approach allowing to reach such time and space scales. Sediment transport is considered using a semi-empirical diffusive equation, linking the sediment flux flowing at each point in the basin (transport capacity), to the slope (energy of the water flow), and to a diffusion coefficient (transport efficiency, Granjeon and Joseph, 1999; Granjeon, 2014; Granjeon, 2019). It also allows to take into account the influence of some advective currents, but only

over large time steps (Eq. 1). The amount of sediment deposited or eroded at each point in the basin can be then calculated by coupling those 3 parameters to the principle of mass conservation (Exner, Eq. 2). For example in DionisosFlow, the sediment flow is considered in 3 dimensions with the following equation (Granjeon, 1996; Granjeon, 2014; Granjeon, 2019):

$$\text{Eq. 1: } \overrightarrow{q_s} = -\left(k_{gravity} + k_{water}\, q_w\, S^{n-1}\right) \overrightarrow{\nabla h} + c_s\, d\, \vec{u}$$

$$\overrightarrow{\nabla h} = \begin{bmatrix} \frac{dh}{dx} \\ \frac{dh}{dy} \end{bmatrix}$$

$$S = \left\| \overrightarrow{\nabla h} \right\|$$

$\overrightarrow{q_s}$: the sediment flux (m²/s)

$k_{gravity}$: the gravity-driven diffusion coefficient (m²/s)

k_{water}: the water-driven diffusion coefficient (m²/s)

q_w: relative water flow (dimensionless)

h: elevation (m).

S: bottom slope (altitude gradient)

c_s: marine sediment concentration (suspended matter transported by the currents, kg/m^3)

d: elevation of marine current (m)

$\vec{u}$: current velocity (m.s^{-1})

$$\text{Eq. 2: } \frac{\partial h}{\partial t} = -\vec{\nabla} \cdot \overrightarrow{q_s}$$

Stratigraphic models do not consider the path of each individual grain, but aims to represent an average of all different sediment processes, in order to simulate the long-term evolution of geometries (Leroux, 2012). Stratigraphic models aim to simulate the synthetic result of geological processes over millions of years. They consider mostly long-term processes (1 ka to several Ma) and the resulting effect of some short-term processes over the same time scale using mean averaged values (e.g. river discharge, wave direction). Long-term processes concern mostly the basin shapes, such as tectonic movements with subsidence/uplift, and bathymetric evolution (eustatic movement and sedimentation rate). Short-term processes concern mainly sediment fluxes, such as hydrodynamics. Choosing the right statistical calculation to summarise the effect of short-term processes is very complex. For example, for river discharge it is possible to consider the rivers discharge average, or only flood events, or a mixture of both. The matter is to determine which conditions have the greatest impact on the system. The basic principle of stratigraphic models links the amount of available sediment (from river discharge, erosion and in-situ production) and the accommodation space of the basin, by diffusion (Fig.

27). The accommodation space is established by quantifying tectonics, i.e. subsidence and/or uplift, eustatism, compaction and erosion rates. Accommodation can be defined in two distinct ways: its physical origin defines it as the result of the eustatic and tectonic movements combination, but it can also be understood from the sedimentary record as the sum of the cumulative thickness of the sediments (space filled by sediment) and the paleo-bathymetry (space not filled by sediment, Fig. 27, Granjeon, 1996; Leroux, 2012).

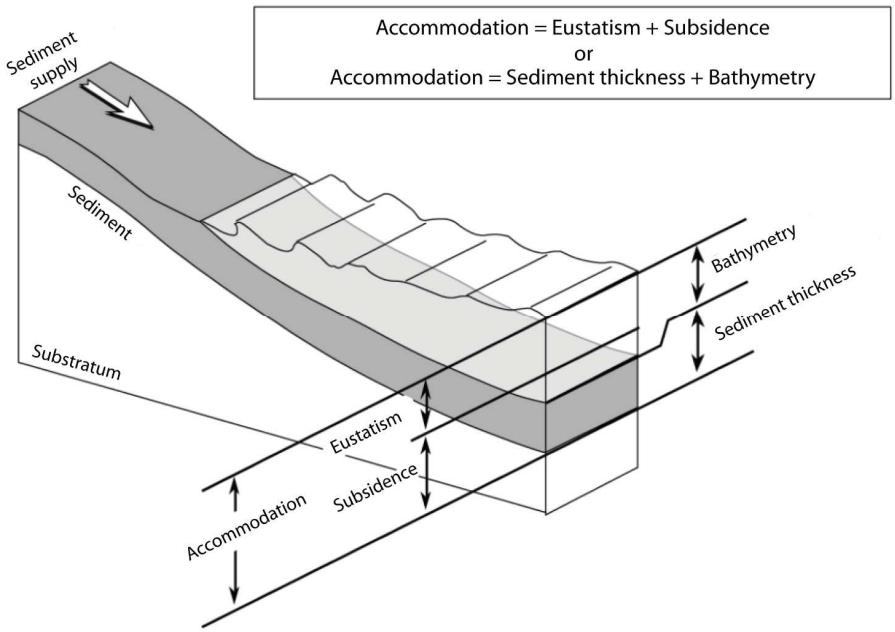

Fig. 27 : Definition of accommodation (Granjeon, 1996)

Stratigraphic models therefore consider the three main factors influencing sedimentation: sediment supply, subsidence and eustatism (Rabineau, 2001). Although these three factors constitute the main triggering parameters of basins infilling, many others influence the sediment deposition, such as hydrodynamic processes or seafloor morphology (Fig. 28).

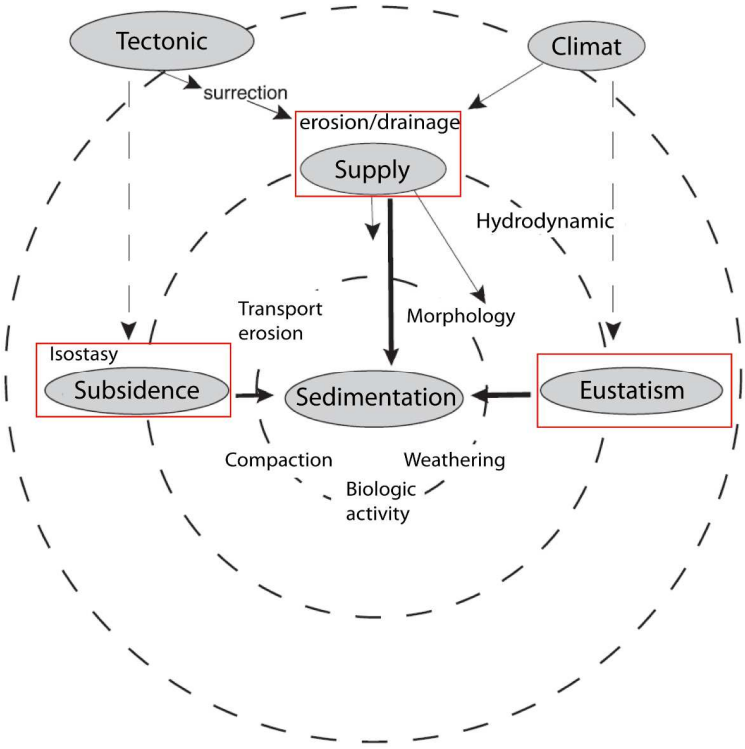

Fig. 28: Hierarchy of factors influencing sedimentation (Rabineau, 2001)

Most of the factors identified in this figure (Fig. 28), are considered by stratigraphic models nowadays. For example, most of them deal with basins and seafloor morphologies, tectonic movements, compaction of sediment layers and erosion/weathering evolution in relation with climatic changes. However, tides and generally hydrodynamics remain a challenge for stratigraphic modelling. Only some of hydrodynamic forcings can be considered by those models: rivers discharge and waves. For example, a predominant direction and height of waves (wave driven-diffusion coefficient) can be implemented in some models. It was used by Busson et al. (2019) in the study of Caribbean carbonate margins and by Al-Salmi et al. (2019) in Northern Oman. It is therefore possible to consider a summarize approach of some hydrodynamic forcings. However, hydrodynamics is rarely taken into account or only in a very simplified way, such as unidirectional mean currents. This type of simplification is representative of some processes such as river discharge or waves impact (in some locations). The rapid variations in speed and direction of tidal currents cannot be represented with this kind of simplification. Moreover, the impact of hundreds of thousands tidal cycles on a sedimentary system is unknown. The tide is therefore not taken into account, which is a major weakness or lack for the coastal application of stratigraphic modelling.

Stratigraphic modelling already showed its effectiveness to reproduce different sedimentary basins filling and studying long-term processes: coral bank formations (Barrett and Webster, 2017), basins fluid dynamic (Vilasi et al., 2009), reservoirs and source rock formations (Bruneau et al., 2017), regressive and transgressive sedimentary bodies (Ainsworth et al., 2000; Storms and Swift, 2003) ... However, environments driven by short time-scale hydrodynamics processes, such as estuaries, cannot be represented by these models. In the case of an estuary affected by tide, the impact of 2 or 20 thousand tidal cycles is unknown and stratigraphic models can not explicitly simulate tidal induced currents.

2.3.2 Hydro-sediment modelling

The hydro-sediment modelling is based on a completely different philosophy. Its objective is to reproduce physical processes of hydrodynamics (currents, water level), the hydrology (salinity, temperature) and their interactions with superficial sediments layer (suspension and re-suspension of sediments, erosion/deposition, morphological evolutions) over short time scales (from event to multiannual scales), related to realistic forcings (tide, wind, wave, river and weather forcing, Fig. 29, Le Hir P. et al., 2001; Waeles, 2005). They are based on the coupling of a hydrodynamic core and a sediment module. The hydrodynamic core reproduces currents and free surface evolution induced by the different forcings thanks to the resolution of fluid dynamics equations. The hydrodynamic core is then coupled with sediment processes: transport (particle advection), erosion and deposition of sediment layers. The hydro-sediment models can take into account the morphological evolution of the seafloor due to the erosion/deposition processes of the sediment layers, which influence the hydrodynamics (Fig. 29). To model tide, free surface elevation variations are imposed at the boundaries of a domain and circulation is allowed to take place. Those variations modify the potential energy between borders and the estuary, and water masses propagate in or out of the estuary by gravity. It means that currents are produced by the propagation of sea surface variations, which are coming from astronomical parameters summarized in a sea surface variations curve (applied at the model oceanic open boundaries). The effect of simulated current on sediments is taken into account to compute the sediment processes on the seafloor and in the water column, considering median diameters of sediment classes.

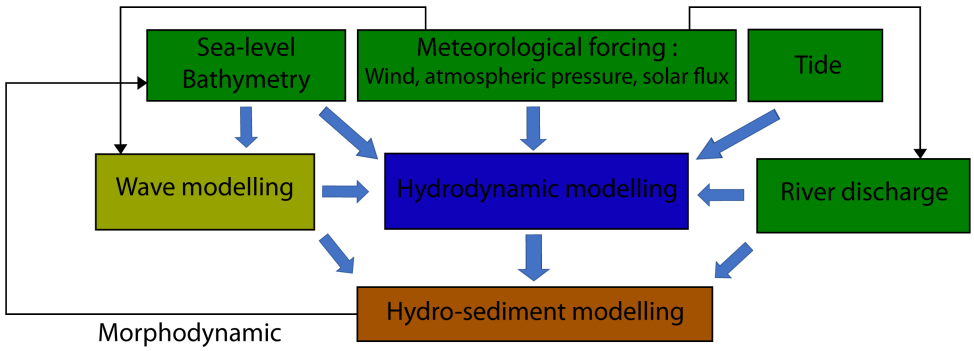

Fig. 29: Schematic representation of the hydro-sedimentary modelling.

These models are calibrated and parameterised with in-situ measurements, such as water height, current velocities, suspended matters, etc. They provide a 3D view of the sediment dynamics over an entire estuary where in situ data can only give punctual information. Then they can be used to test the response of estuaries to different forcing scenarios: different river flows, wave or wind regimes.

Hydro-sediment modelling allows to study the hydrodynamic effects on sedimentation at very fine spatial scale, but only over short-time periods (from hours to years, e.g. Tosic et al., 2019; Diaz et al., 2020). However, it can be used to study very specific processes from the behaviour of a floc population during a tidal cycle (Aggregation and fragmentation of cohesive sediments, Verney et al., 2011), to global considerations such as potential tidal propagation due to paleo-oceans shapes (Aptian, Wells et al., 2010; Holocene and Lower Cretaceous, Reynaud and Dalrymple, 2012; lower Oxfordian, Zuchuat et al., 2022). It allows to study morphological evolution of coastal environment induced by hydrodynamic (e.g. Waeles, 2005; Dam et al., 2016; Grasso and Le Hir, 2019; Tu et al., 2019). The

computational time of hydro-sediment processes limits the simulation to approximatively a decade, unless simplifications of the integration of time-consuming processes are made.

To consider larger time scales, many simplifications were imagined for hydro-sediment modelling. The morphological evolutions of nearshore basins are most often approached by the so-called "reduced complexity models". It is an important topic for society but complex for researchers, because it mixes one second-time scale processes with one-hundred-year time-scale processes. Several methodologies already exist to simplify or schematize the tidal calculation in process-based models. It can be done by extrapolating the computed bed evolution (morphological factor), by increasing the morphological time step (elongated tide), by avoiding the time-consuming re-computation of the hydrodynamics after every transport and bed-evolution step (continuity correction), or by considering the seabed fixed during the computation of hydrodynamics and sediment transport over a tidal cycle (tide-averaging). All those technics are described and illustrated in a synthesis proposed by Roelvink (2006). Simplified considerations of the tidal process are always done in order to achieved hydro-sediment model computing time reduction and rely on strong hypothesis.

The most used technique is to run hydro-sediment models with a multiplicative factor for morphological process. The multiplicative factor (n) is applied on erosion and deposition fluxes, or directly on the amount of gain and loss of sediment, estimated by a hydro-sediment model (Franz et al., 2017; Elmilady et al., 2020). The volumes deposited are therefore the expression of present-day forcing (1 to 10 years) multiplied by n at each time step. These simulations take into account the evolution of the bottom, thanks to regular update of the bathymetry, which modify the propagation of currents. Usually, this technique does not exceed 100 years. However, some studies used much larger factors (e.g. 400 in Braat et al., 2017) to explore morphological evolution over longer time scales.

2.3.3 Modelling long-term tidal impact

Simulating the impact of tide on sedimentation over a long time interval remains a scientific lock. Only sedimentary records give clues about the impact of paleo-tides, as neither geologists nor oceanographers were able to model tidal sediment deposits or tides over long periods. Because of the different time and space scales they deal with, these two types of models are not used for the same purposes (Joseph et al., 2016). Stratigraphic modelling is run for large time scale issues and are parameterized with time steps that are too large to take explicitly into account hydrodynamic processes oscillating as fast as the tide. It could only take into account the cumulative effect of the tide over long periods, which is unknown. Hydro-sediment modelling is designed to reproduce hydrodynamic processes and faithfully represents the tide impact on sediment deposits, but only over short-time scales. This scale issue, well known by the scientific community, prevents any simulation considering both geological and hydrodynamical processes. Time span of simulations is quickly identified as an important limitation to the understanding of the sediment dynamics of estuaries. Many studies seek to increase the simulation time-span of hydro-sediment modelling by simplifying the input conditions (Latteux, 1995; Cayocca, 2001; Visser, 2002) or using a morphological factor (see above) (Franz et al., 2017; Elmilady et al., 2020). Mainly conceptual estuaries were simulated with high morphological factors and they all led to estuary equilibrium configuration (Bolla Pittaluga et al., 2015; Guo et al., 2015; Braat et al., 2017). Simulations of Bolla Pittaluga et al. (2015) indicate that the investigated system always moves toward an equilibrium configuration in which the net sediment flux in a tidal cycle keeps constant throughout the estuary and equal to the constant sediment flux delivered by the river. After around 100 years, the estuary becomes a transfer zone (Fig. 30), but this duration can change with mud and sand proportions (Braat et al., 2017), the size and shape of the

estuary (Lanzoni and Seminara, 2002) and river discharge (Guo et al., 2015). Fig. 30 also questions the use of large morphological factors by showing that only short-term parameters, such as tides, waves and river discharge, cannot explain the long-term morphological evolution of an estuary.

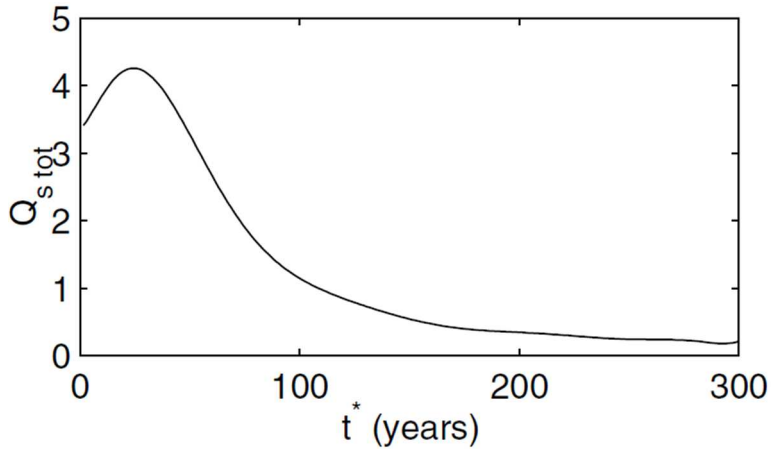

Fig. 30: Temporal evolution of the global dimensionless net sediment flux $Q_{s\,tot}$.

Most of the observed sediment features, such as tidal channels, dunes, tidal flats, are the result of a system seeking to reach its dynamic equilibrium. For example, the incision process (channels formation), which can be rather rapid at the geologic time scale, is the result of the whole morphodynamic system being far from its equilibrium configuration (Coco et al., 2013). However, eustatism or subsidence processes change the conditions to reach this dynamic equilibrium and that is why almost no natural estuary reached it yet. Lanzoni and Seminara (2002) show that hydrodynamic processes dominate for periods within 1 to 100 years, but for longer periods long-term processes (continuously changing the equilibrium conditions) are not negligible to reproduce natural estuaries sedimentation.

The upscale issue rises therefore the question of using "appropriate complexity" (French et al., 2016), which consists of considering (and solving) the processes at the scale of the problem studied. It means that the objective is to summarise the impact of the considered forcing at study timestep. Identifying and modelling the feedbacks at the scale of interest is of critical importance and uttermost difficulty (particularly with respect to the choice of which processes are included/excluded from the model, and how to simplify the representation of these processes, Coco et al., 2013). In the case of the tide, the problem is therefore how to estimate (qualitatively and quantitatively) its impact on sediment deposits. Understanding the evolution of the impact of tidal currents in relation to geological parameters, such as sea-level and seafloor evolution, is therefore a key issue for long-term modelling and sequence stratigraphy interpretation. In other words, the issue is to understand the movements of depositional and erosional zones induced by tidal currents in relation to paleoenvironmental evolution. Numerically modelling the hydro-sediment response of an estuary to geological parameters is the only way to find out if the computation of the tidal impact on sediments can be synthetised/simplified over long time interval.

Chapter 3 will propose a new methodology using Holocene sedimentary records to identify and rebuild successive paleoenvironments (defined as seafloor and sea-level), which stand for all key infilling steps over the estuary Holocene history, in order to run hydro-sediment simulations representative of the past 10 ka.

3 Study area and methodology

3.1 The Bay of Brest

The Bay of Brest is located at the western-end of Brittany (France). It is a semi-enclosed estuary communicating with the Iroise Sea, through a 6 km long and 1.8 km wide strait (Fig. 31). At present-day, the Bay of Brest covers about 180 km². Its coastline is 270 km long (Beudin, 2014) and displays points, peninsula, coves and bays. The Bay of Brest is a macrotidal system, with a mean spring tidal range of 5.9 m and a mean neap tidal range of 2.80 m in Brest harbour (Beudin, 2014). During exceptional spring tide, tidal range can reaches 7.5 to 8 m depending on the location within the Bay (SHOM, 2015a). Hydrodynamic within the Bay of Brest is dominated by tide, as it is naturally protected from oceanic waves thanks to its semi-enclosed configuration (Monbet and Bassoullet, 1989).

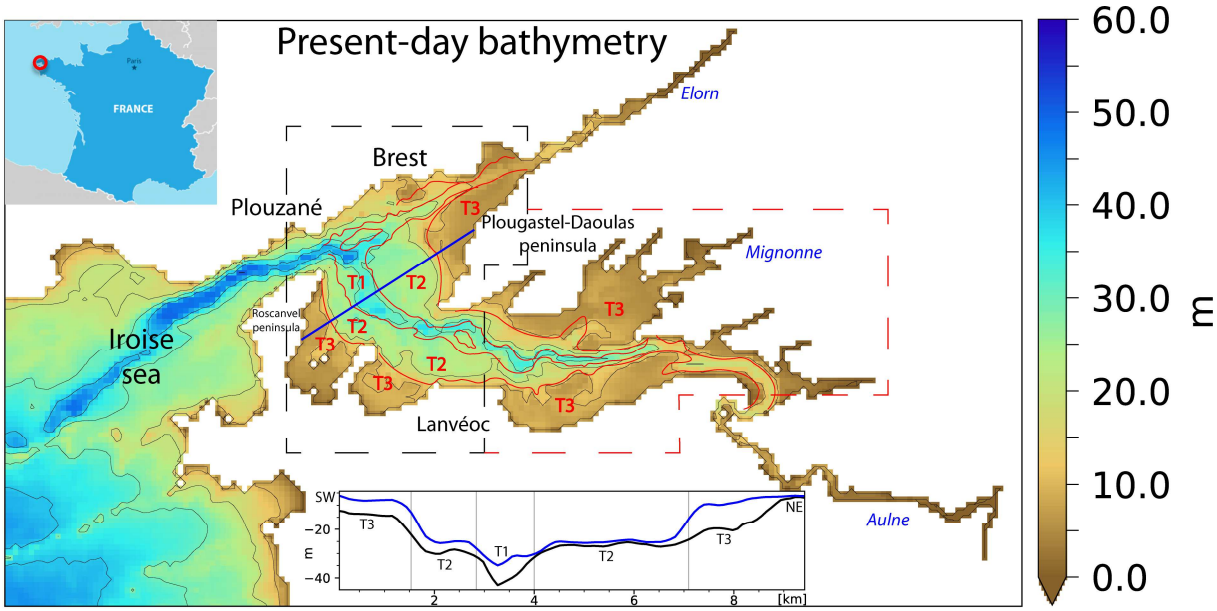

Fig. 31: Present-day bathymetric map of the Bay of Brest, generated from SHOM's data (2015). The inset-bathymetric section is represented by a blue line on the map. Blue line section correspond to the present-day bathymetry and the black one to the beginning of the Holocene filling of the Bay of Brest terraces (9 ka cal.BP). T1: paleo main channel. T2: deepest stage of terraces. T3: shallowest stage of terraces. Black dotted box represents the limits of the central area and red dotted box is the limits of the upper area.

The Bay of Brest displays a particular shape, with a very steep and irregular coastline. This morphology is due to the nature of its basement rocks. The north of the Bay of Brest (Brest) is made of magmatic rocks very difficult to erode, while metamorphosed Paleozoic sedimentary rocks constitute Crozon and Plougastel-Daoulas peninsula (Gumiaux et al., 2004). Along the coastline, many coves and bays are protected by this irregular coastline, which also forms straits. This estuary is divided in two parts: the upper part, located East of the strait between Lanvéoc and Plougastel-Daoulas peninsula (towards the estuary of the Aulne river, Fig. 31) and the central part, located West to the same strait until the strait between Plouzané and Roscanvel peninsula on the Westernmost part (Fig. 31). The outer zone corresponds to the Iroise sea, this area is exposed to a different hydrodynamic regime (e.g. waves, storms) and is not analysed in this study. The shape of the Bay of Brest is a consequence of three major mountain orogens: the Pentevrian (2 Ga to 750 Ma), Cadomian (600 to 530 Ma) and Hercynean (380 to 250 Ma) chains (Ballèvre et al., 2009; 2014). The Hercynian chain was divided into different provinces, separated from each other by faults and shear zones. The South Armorican Shear Zone is located South to the Bay of Douarnenez (South to Crozon). The North Armorican Shear Zone crosses

the study area and formed the bed of the Elorn river and the strait between Plouzané and the Roscanvel peninsula, named “Goulet”. The two main rivers (Aulne and Elorn) result from different formation processes. The Elorn main channel takes place within a tectonic fault (North Armorican Shear Zone), while the Aulne main channel is characterized by a meandering shape, formed by regressive erosion (Fig. 31, Hallegouet et al., 1994). Since the Eocene the Bay of Brest emerged several times (Fig. 32), because of glacio-eustatic movements. As a result the basement was eroded by paleo-rivers during low sea-level stages (Hallegouet et al., 1994).

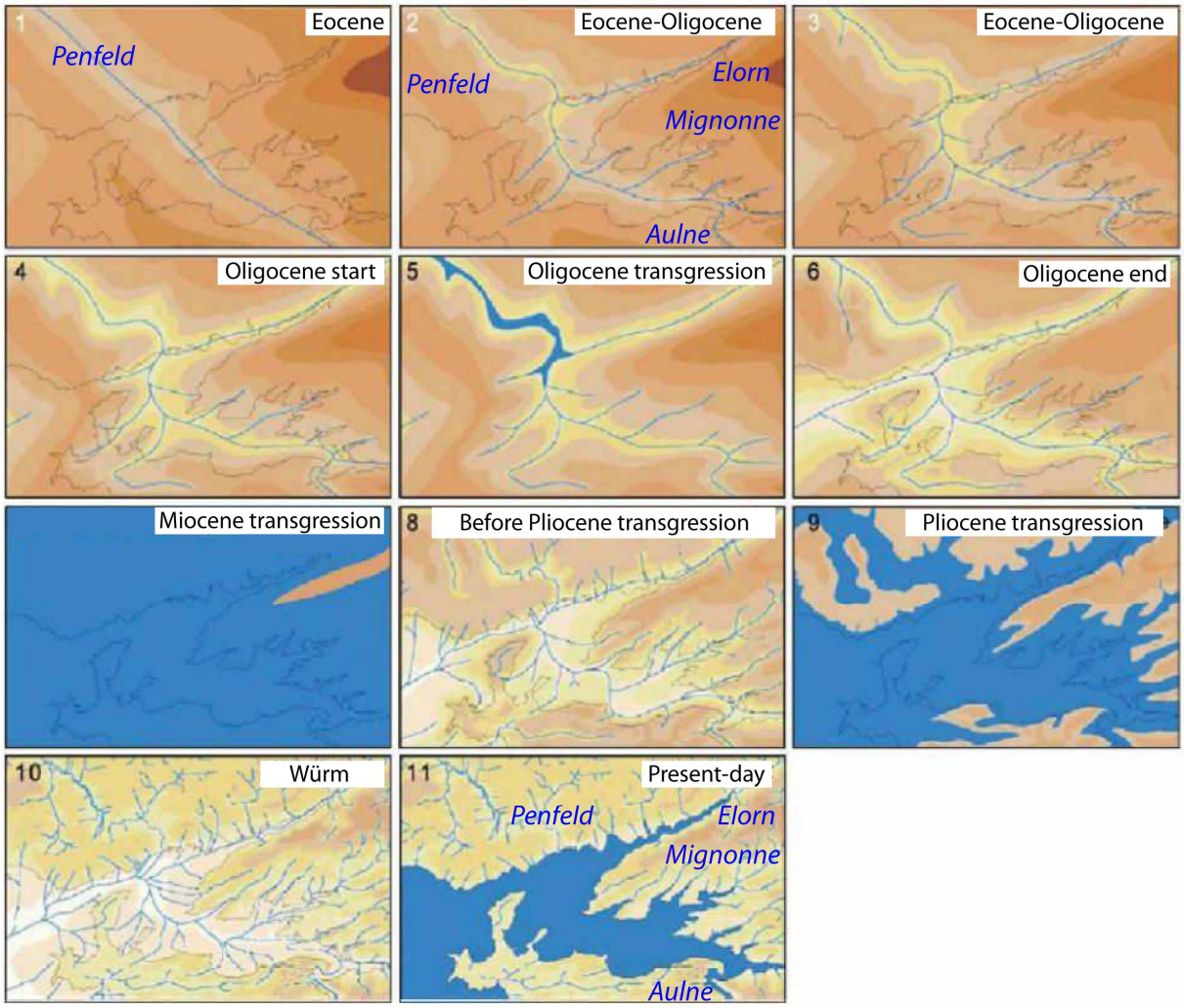

Fig. 32 : Synoptic diagram of the genesis of the Bay of Brest since the beginning of the Tertiary period. Flooded areas are represented in blue. The other colours represent emerged areas from the lowest (white) to the highest (brown, Hallegouet et al., 1994).

During the Eocene, the fluvial paleo-network passed through the Penfeld bed towards the English Channel to the north (Fig. 32). At the end of the Oligocene a drainage network existed at the site of the present-day strait between Plouzané and Roscanvel peninsula, and rivers acquired a configuration (location and flowing direction) similar to present-day (Fig. 32).

Those sea-level variations led to the digging of the Aulne bed and the present-day seafloor morphology. The period of digging occurred during the last glacial maximum (LGM). During the LGM

the sea-level was at least 100 metres lower than the present-day sea-level and Europe and England were separated only the paleo-river Manche (Ehlers and Gibbard, 2004, Fig. 33). At that time Brittany was in a periglacial context and covered by a discontinuous permafrost (Petit-Maire, 1999, Fig. 34).

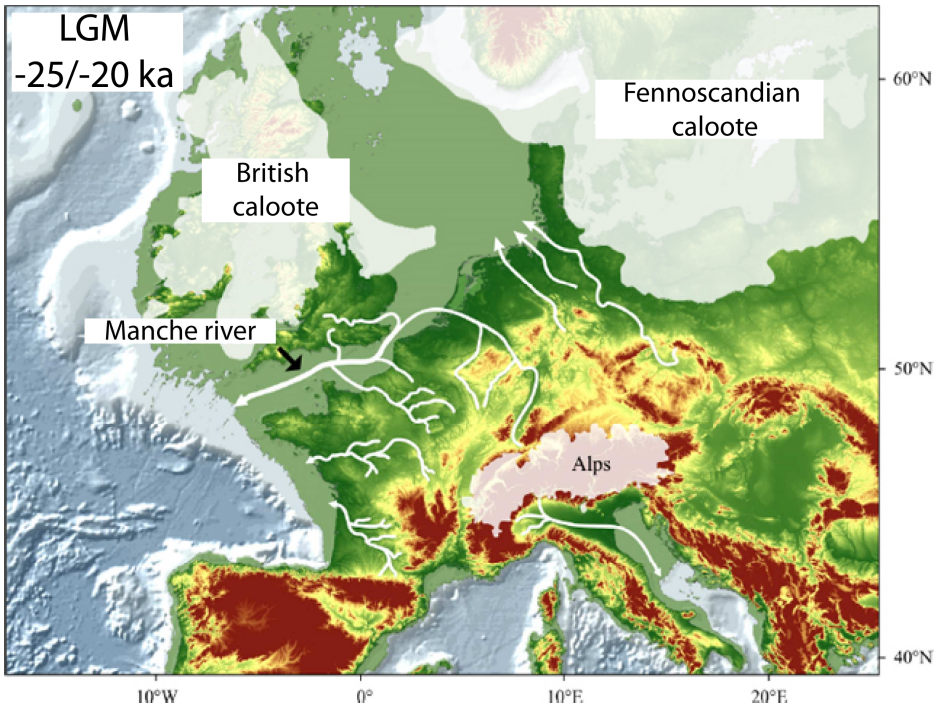

Fig. 33 : Paleogeography during the LGM (Ehlers and Gibbard, 2004)

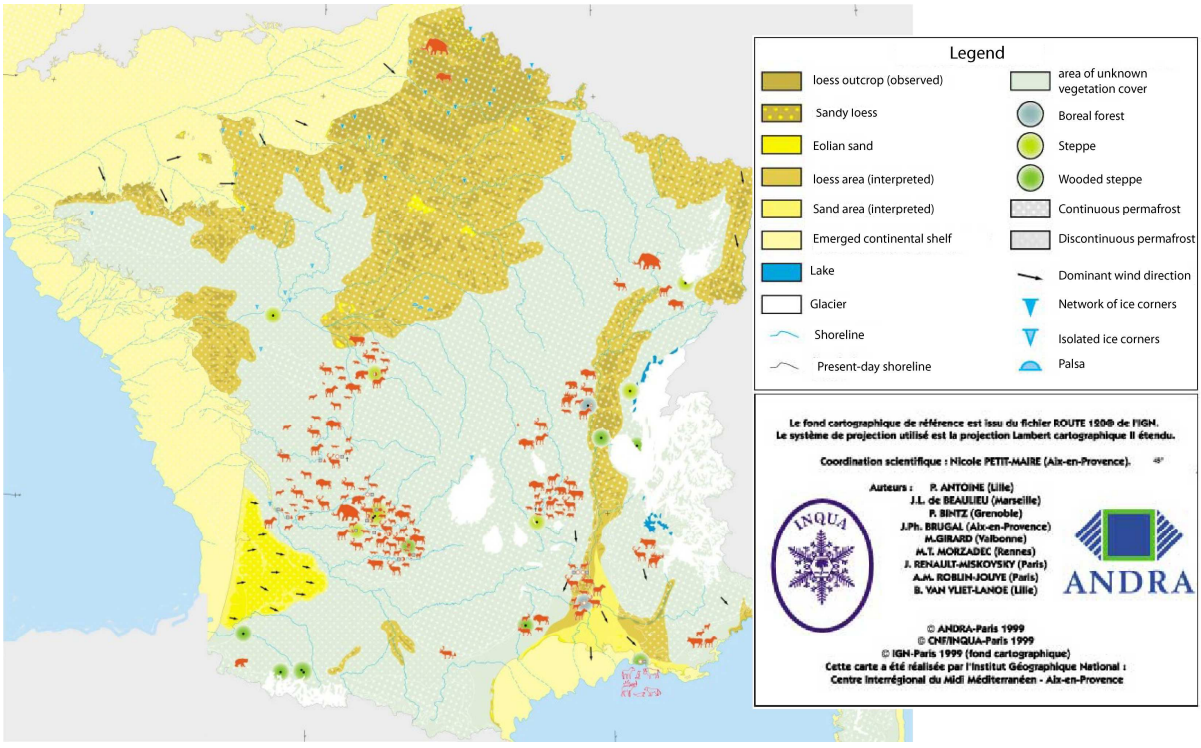

Fig. 34 : Soil composition at 18 ka (ANDRA - CNF-INQUA - IGN).

Three morphological domains were formed by paleo-rivers (Gregoire et al., 2016): T1 is the main channel, where paleo-rivers flowed; T2 is the deepest stage of terraces, above T1 (intermediate domain); T3 corresponds to the shallowest terraces close to the present-day shoreline, often localized in sheltered coves and bays (Fig. 31). The two levels of terraces locate in different configurations: T2 is mostly presents in the central part of the Bay and gets narrow towards the Aulne mouth (Fig. 31), while T3 is mostly present in coves and bays. A network of secondary channels within T2 and T3 connects these domains to the main channel (T1). The inclination of morphological domains calculated by Gregoire et al. (2017) reveals that the terraces are very flat domains (0.5-1°) and the slopes between domains show an inclination of 2 to 4°.

3.1.1 Holocene history

During the Holocene period (11.7 ka to present-day), the sea-level rises by about 50 m (mean worldwide value, Woodroff and Horton, 2005). The global warming happening during the Holocene triggered significant retreat of the North European glaciers compared to the Würm period (115 to 11.7 ka BP) and ice sheets melt. This melting is responsible for the rise in mean sea-level (Goslin et al., 2015). The Holocene flooding of the Bay of Brest started around 10 000 years ago, with a local mean sea-level 35 m lower than the present-day one (Gregoire, 2016). The mean sea-level rise is fast (~1 cm.yr^{-1}) between 10 ka and around 7 - 6 ka (BP), then it slows down until it reaches the present-day level (Fig. 35, Goslin et al., 2015).

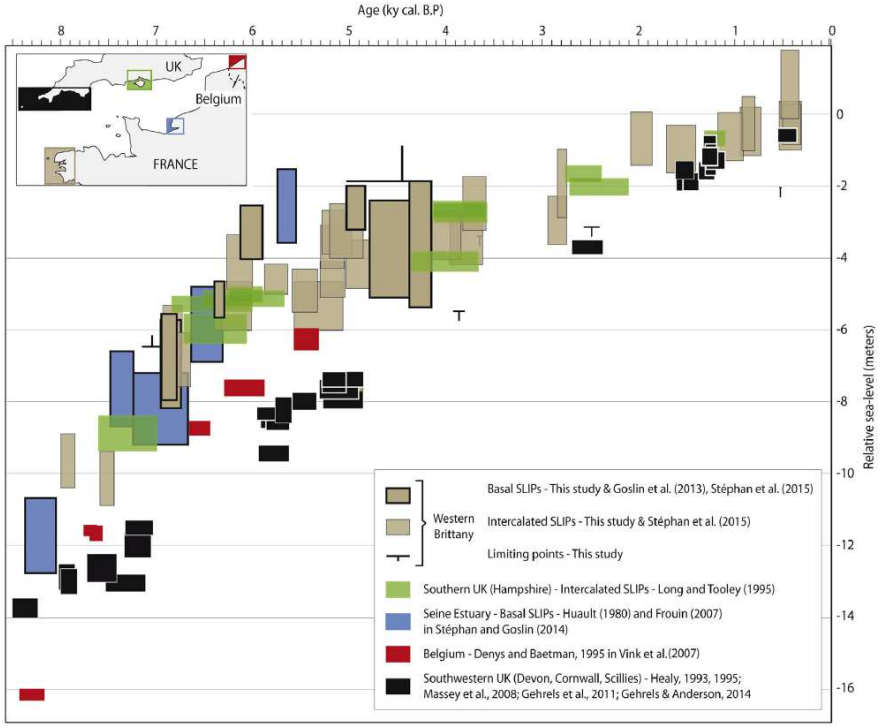

Fig. 35: Inter-regional comparison of RSL records from Western Brittany (brown boxes), South-western UK (Devon, Cornwall e black boxes), Central UK (Hampshire green boxes), Seine estuary (Blue boxes) and Western Belgium (red boxes) during the last 8 ka B.P. Mind that all represented data basal SLIPs (sea-level index points), excepted thin contoured brown boxes and SLIPs from Hampshire. These latter may thus have been lowered by some post-depositional compaction and hence potentially underestimate RSL position (Goslin et al., 2015).

Thus, morphological domains are progressively flooded within the Bay according to sea-level rise and seafloor evolution through sedimentation. At 10 ka (cal. BP), the Bay is almost entirely emerged and only few parts of T1 are flooded. At 9 ka (cal. BP), the sea-level is about 26 m lower than the present-day one (Woodroff and Horton, 2005). In these conditions, T2 terraces are intertidal and T1 is subtidal (Fig. 36). As the rise in sea-level is fast at the beginning of the Holocene, it reaches -10 m at 7.5 ka (cal. BP, Goslin et al., 2015). The intertidal area is then located over T3 terraces and subtidal domain over T2 terraces (Fig. 36). Between 7 and 6 ka (cal. BP), the rise in sea-level slows down (Goslin et al., 2015). Around 7 ka (cal. BP), it reaches 5 m below the present-day one, and leads most of T3 terrasse into subtidal domain. At the present-day, most of the Bay is subtidal due to the steep coastline of the Bay of Brest (Fig. 36)

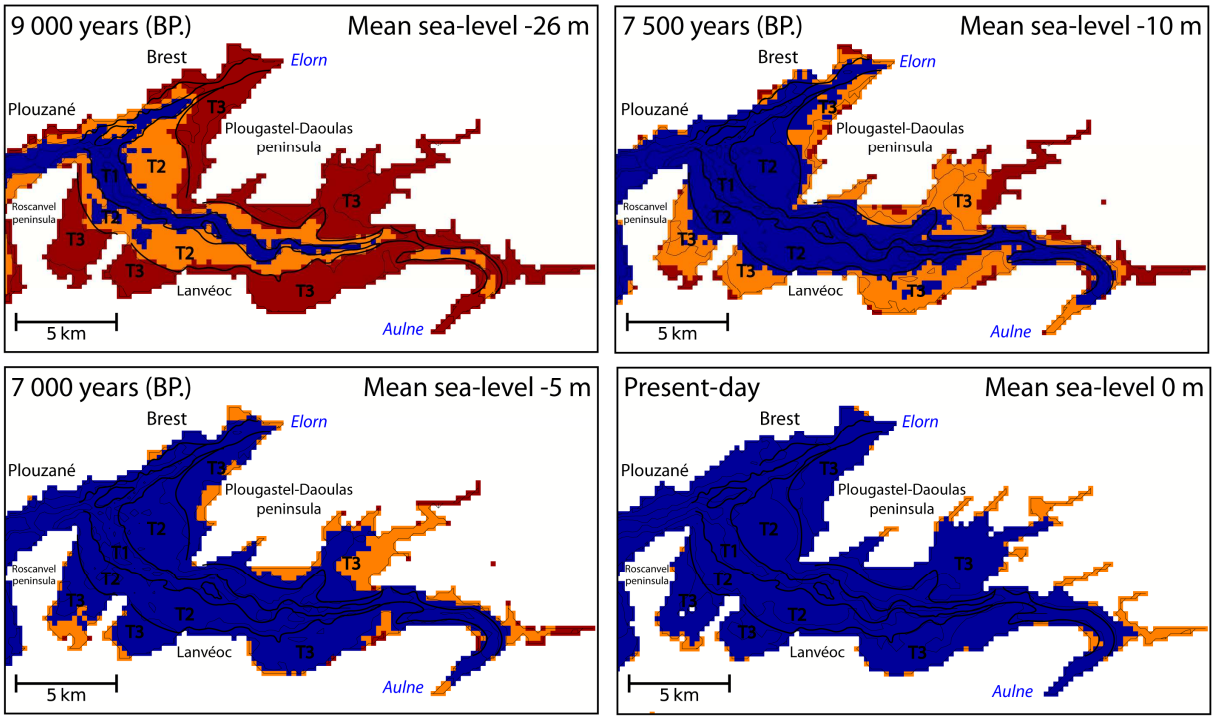

Fig. 36: Key stages of the Bay of Brest flooding, during the Holocene transgression. Subtidal areas are in blue; intertidal areas are in orange; emerged areas are in red. T1: paleo main channel. T2: deepest stage of terraces. T3: shallowest stage of terraces.

During the transgression, four sedimentological units, U0, U1, U2 and U3, are set-up in the Bay of Brest (Gregoire, 2016). These units are identified from seismic interpretations and samples descriptions (from cores, Gregoire et al., 2017). All seismic and sample acquisitions in the Bay (Fig. 37a) are listed in Gregoire (2016). A large seismic dataset (Fig. 37a) is available for the Bay of Brest: more than 1200 km of seismic profiles cover the Bay from rivers mouths to 10 km outside of the Bay (Iroise sea). Seismic data include high resolution seismic profiles acquired with a single-channel streamer and a SPARKER source (campaigns: SAMDISOIR; GEOBREST; GEOLUCAS; SERABEQ 1, Gregoire and Le Roy, 2014) and very high-resolution profiles (sub-bottom profiler) acquired over T3 (SERABEQ 2, Gregoire et al., 2015). Their vertical resolutions are respectively of around 1 m and 30 cm (Gregoire et al., 2017). In this previous work, conversion of seismic two-way travel time to depth used a constant velocity of 1800 $m.s^{-1}$ in sediments. Gravity cores were used for Holocene stratigraphic interpretations and ages

estimates. Note that, as estuaries are areas where sediments are regularly reworked, the age of the grain from shell dating (Gregoire et al., 2017), is potentially different from the age of the preserved deposit. Datings mainly come from cores acquired during SERABEQ-03 campaign (Ehrhold and Gregoire, 2015). Only one core has potentially reached the oldest units, U0, and only about ten reached the second sediment unit, U1 (Fig. 37b). Sediment chronology established in the Bay of Brest by Gregoire et al. (2017) is based on shell dating, correlated to cores description and then to seismic profiles interpretations.

The dataset (cores and seismic) used come from Gregoire (2016). The dataset was resyntetised for the needs of the study (e.g. thickness maps, bathymetric maps, 10 cores descriptions and some local seismic interpretation). The main aim of studying sedimentary records was to obtain an overview of all information available for the set-up of our methodology and modelling approach. In this study, the ten cores reaching the oldest units were described. Tab 1 resumes the cores locations, length and simplified grain-size observations (in four classes, see their position on Fig. 37). Cores were firstly correlated to seismic data (not ages), in order to obtain consistent grain size information within seismic units (between seismic markers interpretation), given the uncertainty of shell dating due to remobilisation inside estuaries. Gregoire et al. (2017) present a summary of data and key observations in order to explain the chronology set up.

Tab. 1: Resume of cores information and simplified observations (cores not presented in this chapter are available in annexes)

from SERABEQ 3 (Ehrhold and Gregoire, 2015)		Ks_27	Ks_34	Ks_35	Ks_38	Ks_39	ks_40	Ks_41	Ks_43	Ks_44	Vz_31
longitude		-4.4774	-4.3637	-4.4078	-4.4804	-4.5168	-4.5229	-4.4655	-4.4703	-4.4626	-4.4708
latitude		48.3032	48.2999	48.3126	48.2996	48.3128	48.3219	48.3662	48.3507	48.3620	48.3518
length (m)		1,68	2,64	3,31	3,52	3,55	3,57	2,14	3,6	3,31	2,64
grain-size classes observed:	U3	FS and S	M and FS	M and FS	M and FS	M and FS	S and G	FS and G	S	FS and S	FS
M: muds; FS: fine sands; S: sands; G: gravels	U2	M	S	M and S	FS	M and S	-	M	-	M and FS	FS
	U1	-	M	M and FS	M	M	M	-	M	M and FS	-

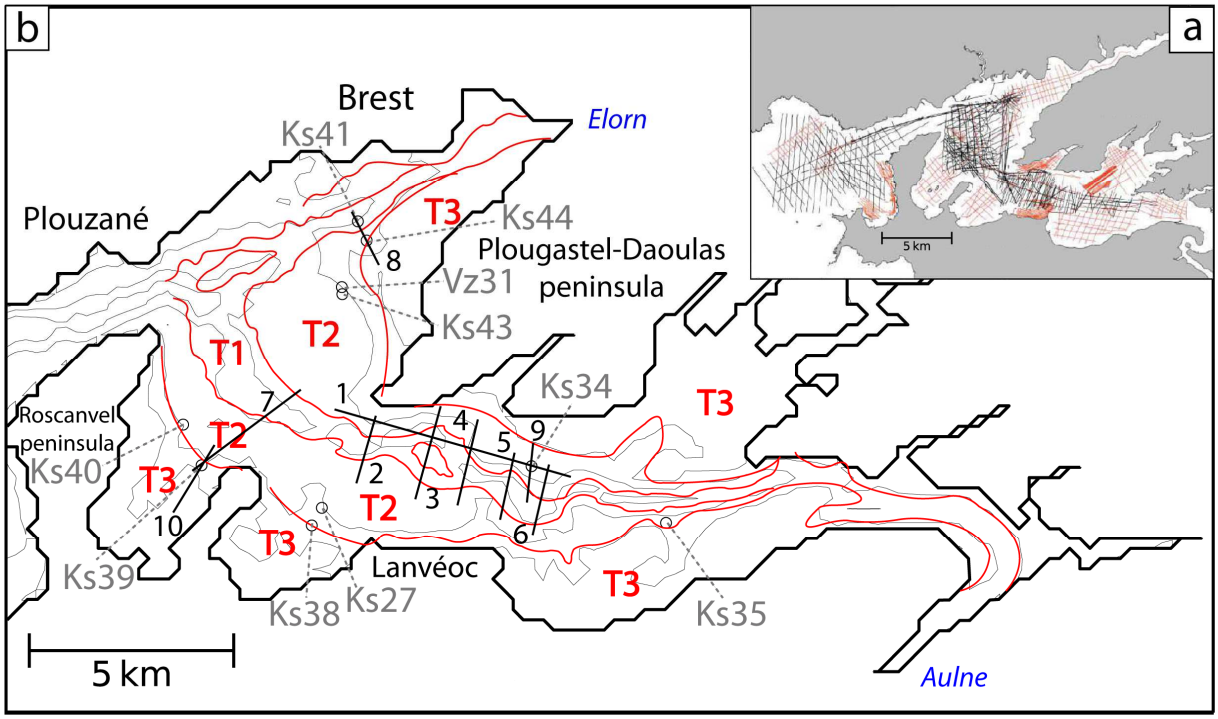

Fig. 37: (a) Location map of all seismic profiles used in this study (Gregoire et al., 2017). (b) Location map of seismic lines and gravity-cores shown in this study.

The Holocene infilling chronology of the Bay of Brest relies on stratigraphic interpretation of Gregoire et al. (2017). The first sediment unit (U0) deposit starts approximatively at ~10 ka (cal. BP) and ends at ~9 ka (cal. BP). The sea-level rises quickly during that period ranging from -35 m to -26 m relative to the present-day sea-level. Then, U1 takes place between ~9 and ~7 ka (cal. BP), with a fast sea-level rise (-26 to -5 m relative to the present-day sea-level, Fig. 38). During U2 deposit, the sea-level rise is much slower than during U1, ranging from -5 m at ~7 ka (cal. BP) to almost the present-day sea-level at ~3-2 ka (cal. BP, Fig. 35, Goslin et al., 2015). After U2 deposit, a sediment hiatus of ~ 1 000 years is observed and interpreted as a MFS (Maximum Flooding Surface, Fig. 38, Gregoire et al., 2017). At ~2 ka (cal. BP), U3 starts to set-up, until present-day (Fig. 38). Unfortunately, cores observations did not allow to establish a correlation between ages and observations within sediment units. The chronology within sediment units remains unknown.

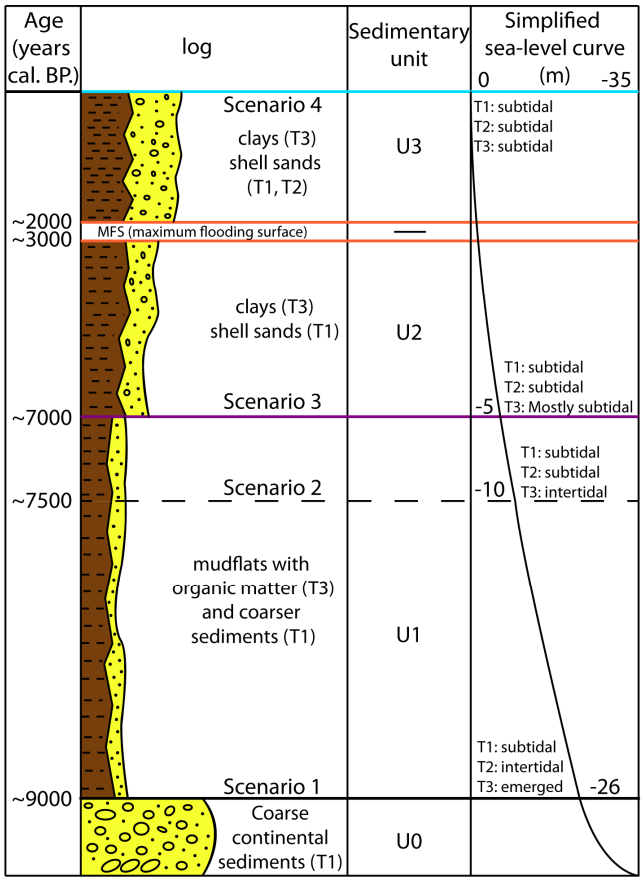

Fig. 38: Stratigraphic log over the Holocene period in the Bay of Brest on top (chronology from Gregoire et al., 2017). The vertical scale displays approximative global unit thicknesses and the horizontal scale represents approximative mean grain size of units (lines are not straight, as mean grain size changes within units). Approximative mud and sand proportions are displayed in brown and yellow.

The sediment units in the Bay of Brest seem to be well preserved. Stratigraphic interpretation over the Holocene, from Gregoire (2016), displays short hiatus and several meters of each sediment unit is preserved over different morphological domains (Gregoire et al., 2017). Moreover, as the tectonic responsible of the semi-enclosed configuration is much older than 10 ka (BP, Hallegouet et al., 1994; Ballèvre et al., 2009), the Bay of Brest is protected from oceanic waves during all its infill period (Monbet and Bassoullet, 1989).

3.1.1.1 U0, 10 - 9 ka (BP)

Before 10 ka (BP) only continental deposits are observed. They constitute the basal pavement of the main channel, as well as the infill of secondary channels and terraces, (Gregoire, 2016). Due to glacial erosion, a lot of continental sediment are supposed to reach the Bay mostly by fluvial discharge.

The oldest sediment unit encountered in the Bay of Brest is U0. Its deposition take place between 10 and 9 ka (cal. BP, Gregoire et al., 2017), with a sea-level ranging from -35 m and -26 m relative to the present-day sea-level (Woodroff and Horton, 2005). During this period, only some parts of T1 (the main channel) are subtidal, the others are in the intertidal area. Within the Bay, only rivers channels are invaded by the tide: it is therefore a ria system. Unfortunately, no sediment sample is available in this morphological domain (T1) and U0 interpretation relies on seismic only. Although it was not recovered

by coring, its chaotic geometry and discontinuous reflectors are interpreted as a signature of heterogeneous and coarse continental deposits (Gregoire et al., 2017). U0 deposits display mainly architectures characterized by many toplaps and downlaps (Figs. 39, 41), or bedrock depression filling patterns characterized by onlap over the bedrock (Fig. 39). U0 deposit are mostly observed within the main channel and in some secondary channels over T2 in the central part (Fig. 40).

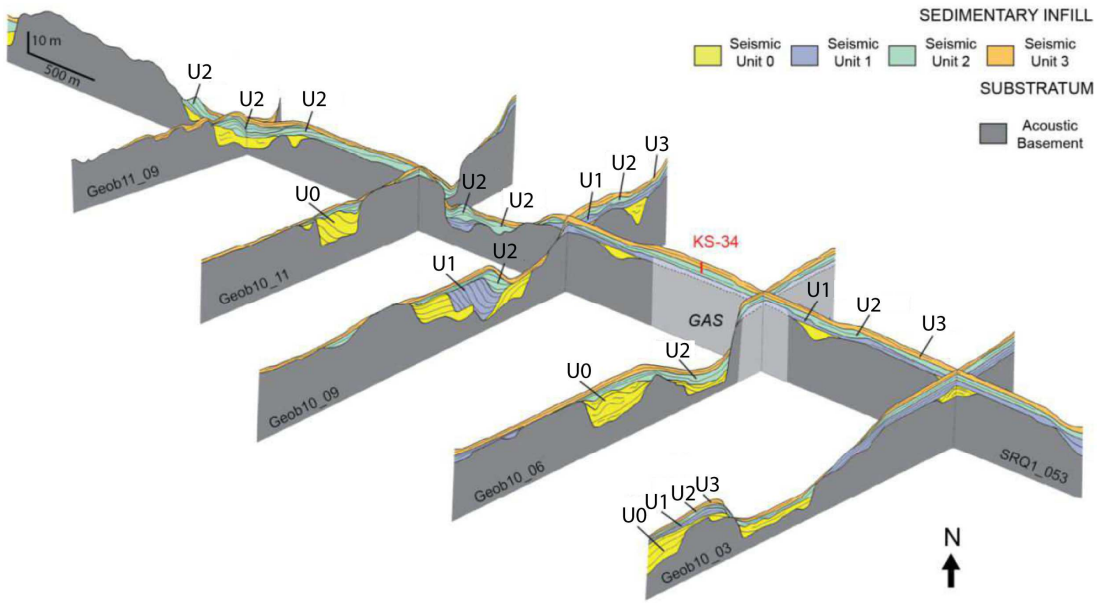

Fig. 39: Fence diagram of seismic profiles showing the internal architecture of the main Aulne axis and its secondary network (location on Fig. 37b, profiles 1 to 6). Dashed lines were used where the acoustics masks (gas) can hide the reflectors architecture (Gregoire et al., 2017).

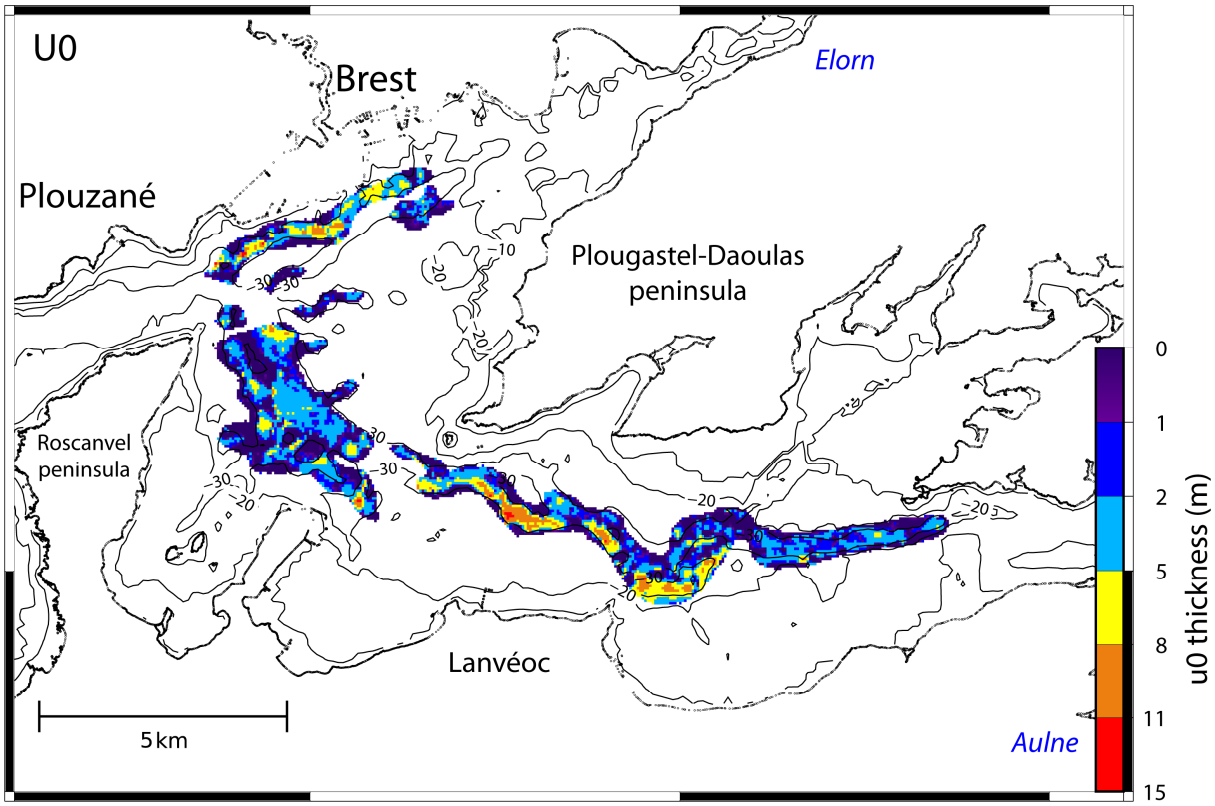

Fig. 40: Thickness maps of sediment unit U0, reconstructed with from seismic interpretations of Gregoire (2016).

At the beginning of the Holocene infill (10 to 9 ka), the sediment infill is still mainly continental and only some sand bars in the central part are probably influenced by the tide (Figs. 39 and 41). Previous continental sediments and U0 deposits display irregular reflectors and deposits localised mainly over T1 and secondary channels, it is therefore very difficult to distinguish them. They are interpreted as low sea-level deposits (LST, Gregoire et al., 2017).

3.1.1.2 U1, 9 ka - 7 ka (BP)

U1 deposition takes place during the interval 9 - 7 ka (cal. BP, Gregoire et al., 2017). U1 overlays either U0 or the bed rock. U1 overlays U0 only within the channels (the main and the secondary ones). When superimposed, these units are separated by a discontinuity, which is visible thanks to truncations of U0 reflectors located in some parts of paleo-channels (Fig. 39) with U1 discordant overlying deposits (Figs. 39 and 41). In the deepest part of the Bay (T1), U1 deposits display typical shape of sand bars with locally high thickness (about 11 m maximum, Fig. 43) and terminations of reflectors with top- and down-laps (Fig. 41).

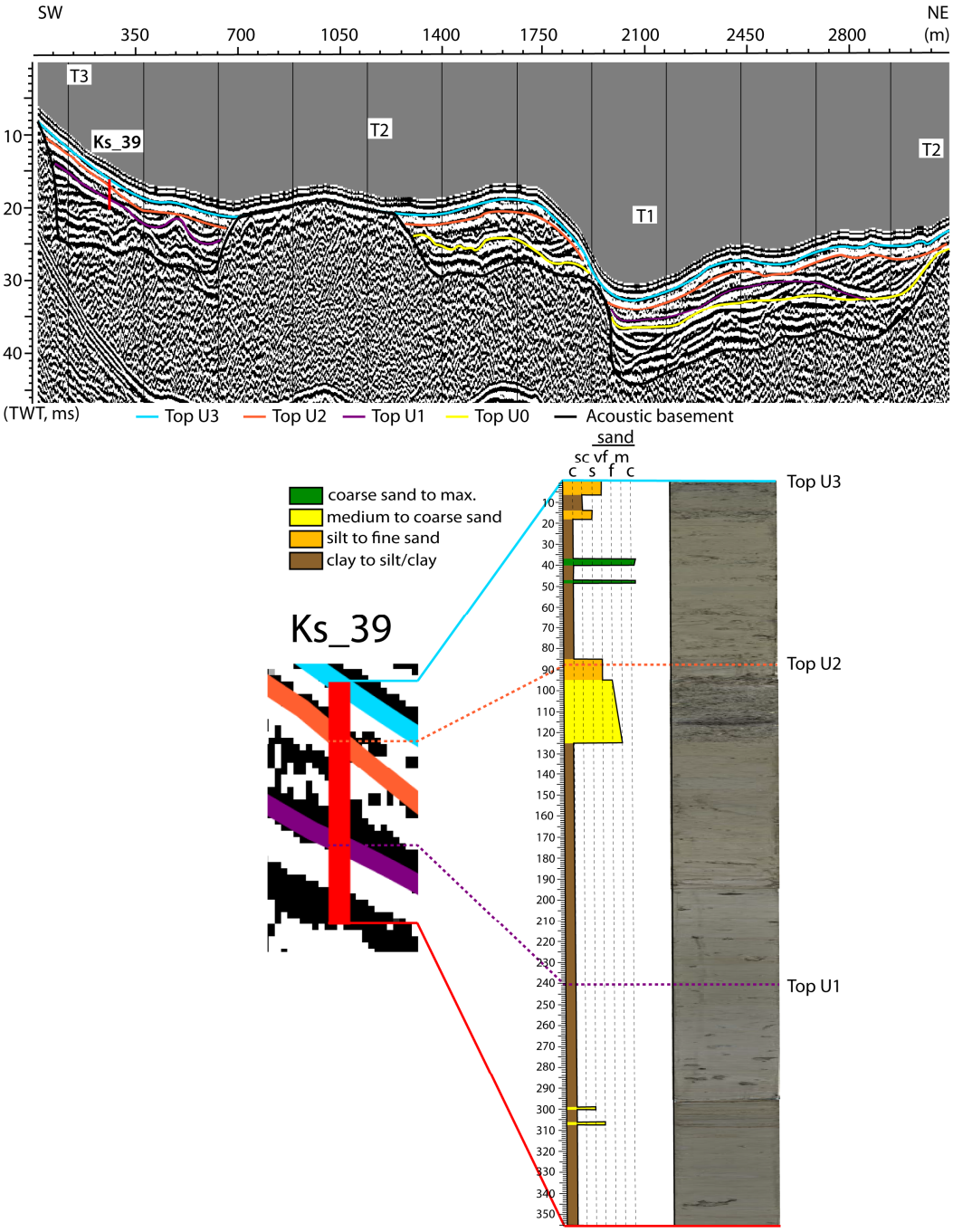

Fig. 41: (On top) Interpreted seismic profile (location on Fig. 37b, profile 7). (on bottom) Photographies and lithologic log for cores Ks_39.

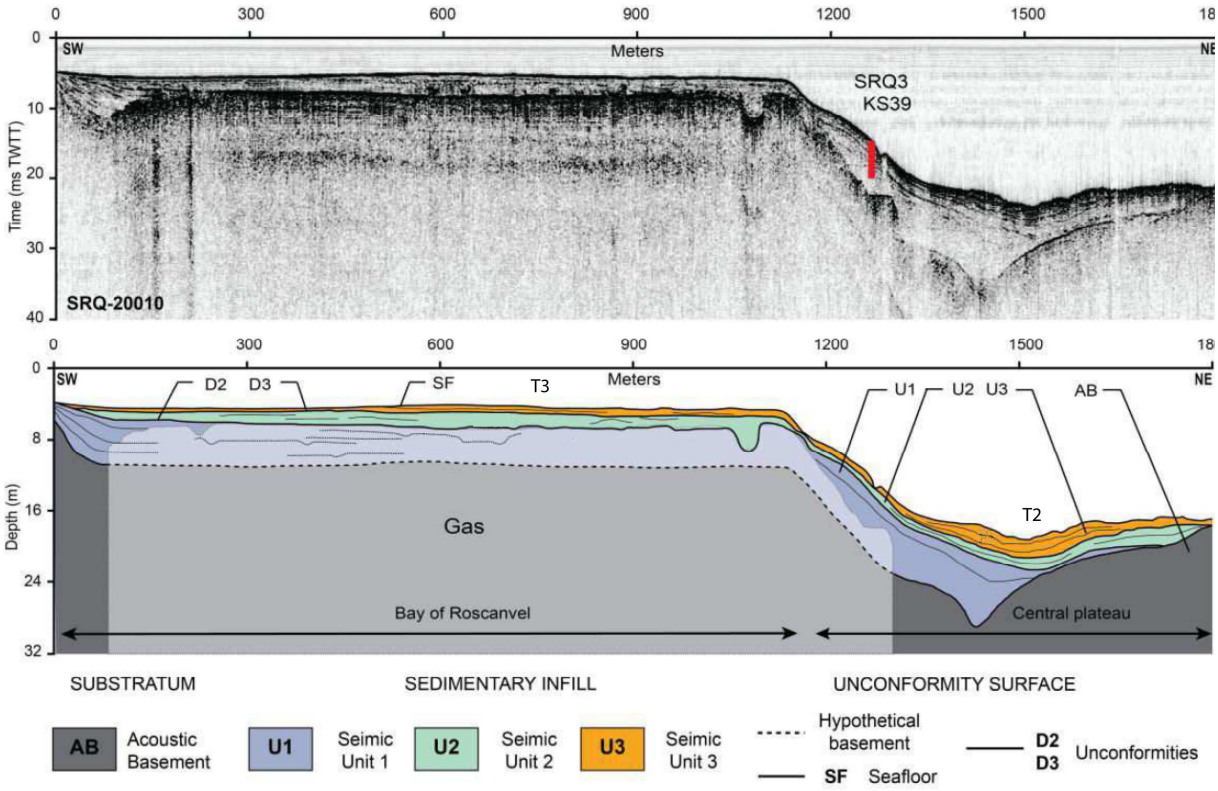

Fig. 42: Seismic SRQ 20010 profile (on top) and its interpretation (on bottom, location on Fig. 37b, profile 10). The vertical scale is in ms two-way travel time for the seismic line and in meters for the interpretative profile. Horizontal scale is in meters (Gregoire et al., 2017).

Over the shallowest terraces (T3) we mostly observe aggradation patterns (Figs. 42, 44, 46), with some onlaps ending reflectors over bed rock irregularities (Fig. 42). Over T3 some cut and fill facies were observed by Gregoire et al. (2017). U1 deposits are mostly present over T3 and on slopes between T2 and T3 domains (thickness average around 5 m, Fig. 43). Three thick accumulations (about 10 to 15 m maximum, Fig. 43) are located inside the main channel. Core samples are available only on slopes between T3 and T2, and over T3. Cores samples show only muddy sediment over T3 (e.g. Figs. 41, 44, 46 and Tab. 1) and muddy sediment mixed with some very fine sands on slopes (Tab. 1). Over T1 they are interpreted through seismic facies as sands or coarser sediments by Gregoire et al., 2017. These three different types of deposits are assumed to correspond to two deposition regimes by Gregoire et al. (2017): they respectively correspond to supratidal and intertidal flat deposits in shallow parts (T3) and slope (T2-T3). In contrast, geometries observed in the deeper part of T1, suggest a relatively high hydrodynamic regime allowing formation of sand-dominated point bars and spit bars along subtidal sinuous channels. Cut and fill facies observed over T3 (Gregoire et al., 2017) also highlight a strong hydrodynamic in secondary channels.

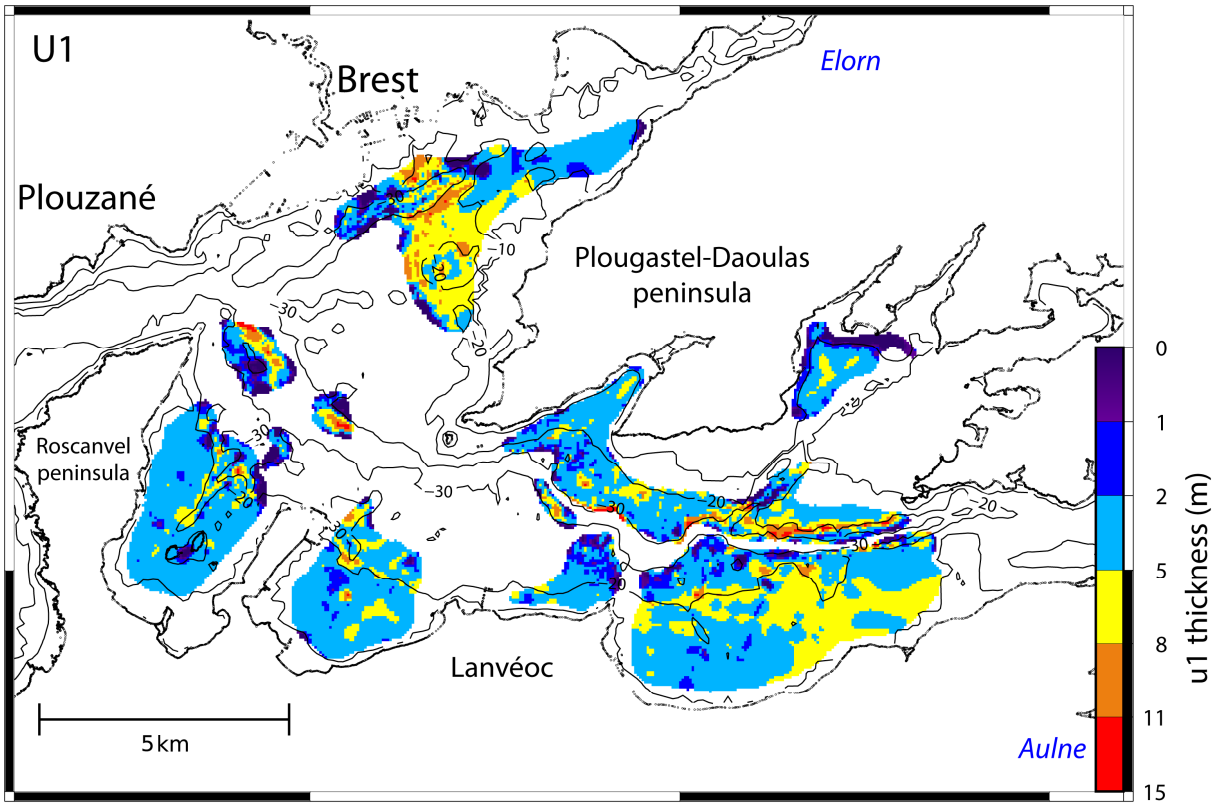

Fig. 43: Thickness maps of sediment unit U1, reconstructed from seismic interpretations of Gregoire (2016).

U1 deposits are interpreted as transgressive deposits (TST, Gregoire et al., 2017), but the chronology within the sediment unit remains unknown due to the lack of samples and probable reworking of sediments. During U1 time-span, the tidal dynamic is visible through deposition patterns: tidal (mainly muddy) flats deposits close to the intertidal zone and sand bars in the main channel. This interpretation is in agreement with the conceptual scheme of Dalrymple et al. (2012). However, the absence of deposition over T2 terraces, which are intertidal at the beginning of the 9 - 7 ka (BP) period, remains unexplained.

3.1.1.3 U2, 7 ka - 3 ka (BP)

After a quick sediment hiatus of about 200 years the deposition of the sediment unit U2 occurs over about 4 ka (Gregoire et al., 2017). U2 displays similar seismic facies as U1: over shallowest parts (T3 and slopes between T2 and T3) reflectors are continuous and form aggrading patterns (Figs. 44 and 46); over deepest parts (T1) they end in toplaps and downlaps and form sand bar patterns (Fig. 41). U1 and U2 are separated by a discontinuity, easily visible in the paleo-network, U2 lying in discordance over U1 (Fig. 41). The U1-U2 transition is much more difficult to highlight over T3 terraces, as deposition patterns are similar between U1 and U2. U2 deposits are supposed to seal some ebb channel over T3 (Gregoire et al., 2017). Some U2 reflectors dowlaps ending highlight the discontinuity (e.g. Fig. 44) and it can be follow thanks to continuous reflectors.

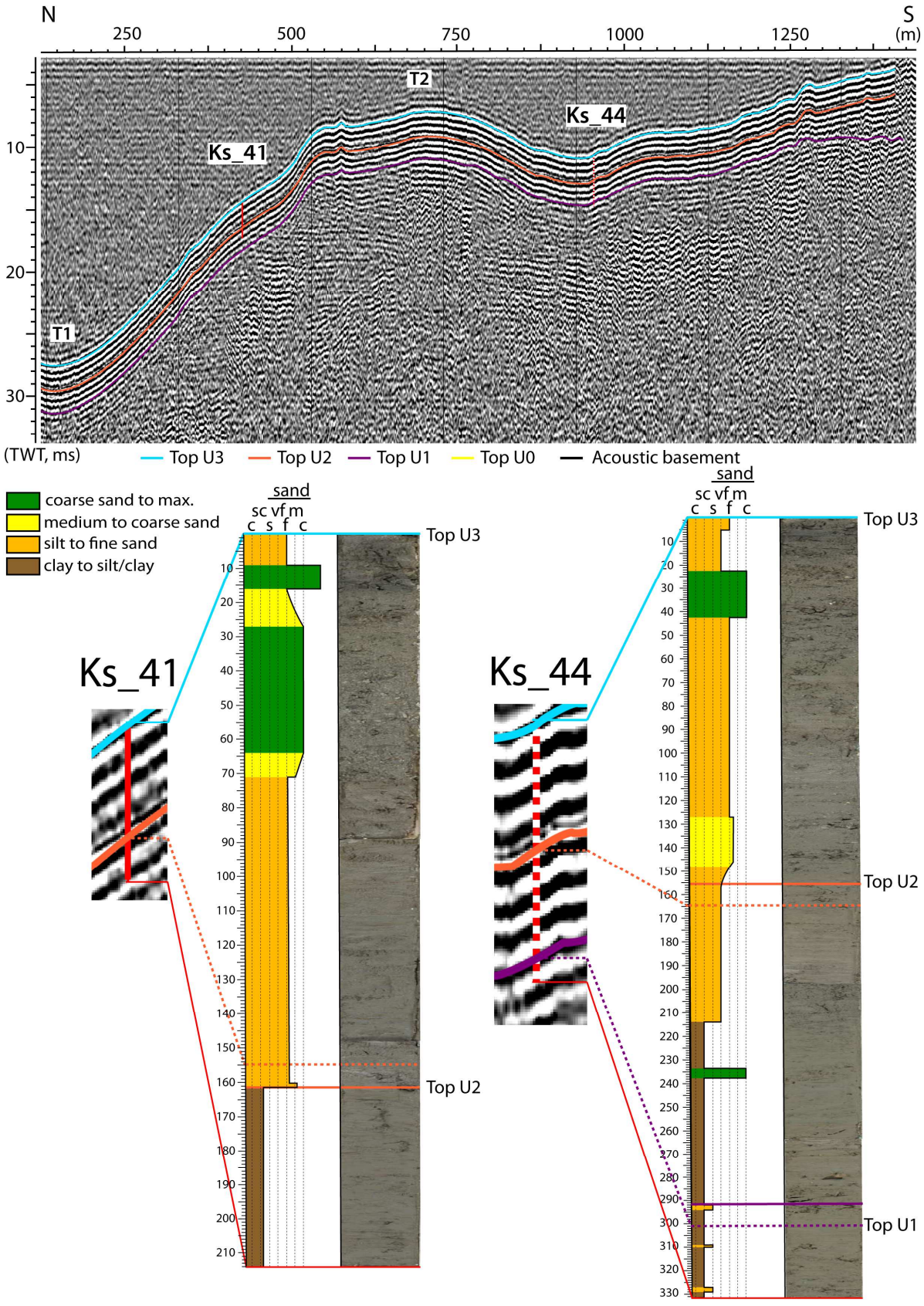

Fig. 44: (on top) Interpreted seismic profile (location on Fig. 37b, profile 8). (on bottom) Photographies and lithologic logs for cores Ks_41 and Ks_44. Dashed purple and orange lines are markers from seismic interpretation and full purple and orange lines represent the interpreted top of U1 and U2 (made to compensate the difference of resolution between cores and seismic profile).

U2 strongest thicknesses (between 5 to more than 11 m) are located in the central area over T1 and only small deposits are located over T2 at the south of the main channel (Fig. 45). They are assumed to be sandy sediments thanks to seismic pattern interpretation of Gregoire et al. (2017). On the slopes between T2 and T3 and over T3, several meters of sediments are preserved (less than 1 to 5 m, Fig. 45). Core samples show that U2 is mainly composed of fine to medium sands and mud in those locations (Figs. 37b, 41, 44, 46 and Tab. 1). In the centre, the global grain size observed inside cores (located at the edges of T2 terraces) is coarser than during U1 (Figs. 41 and 44). In the upper area all morphological domains are covered by U2 sediments (T3, T2, T1, Fig. 44). Only two cores are present in the upper area and both present medium sands (Ks_34, Fig. 46, Ks_35, Tab. 1) and Ks_35 displays also mud.

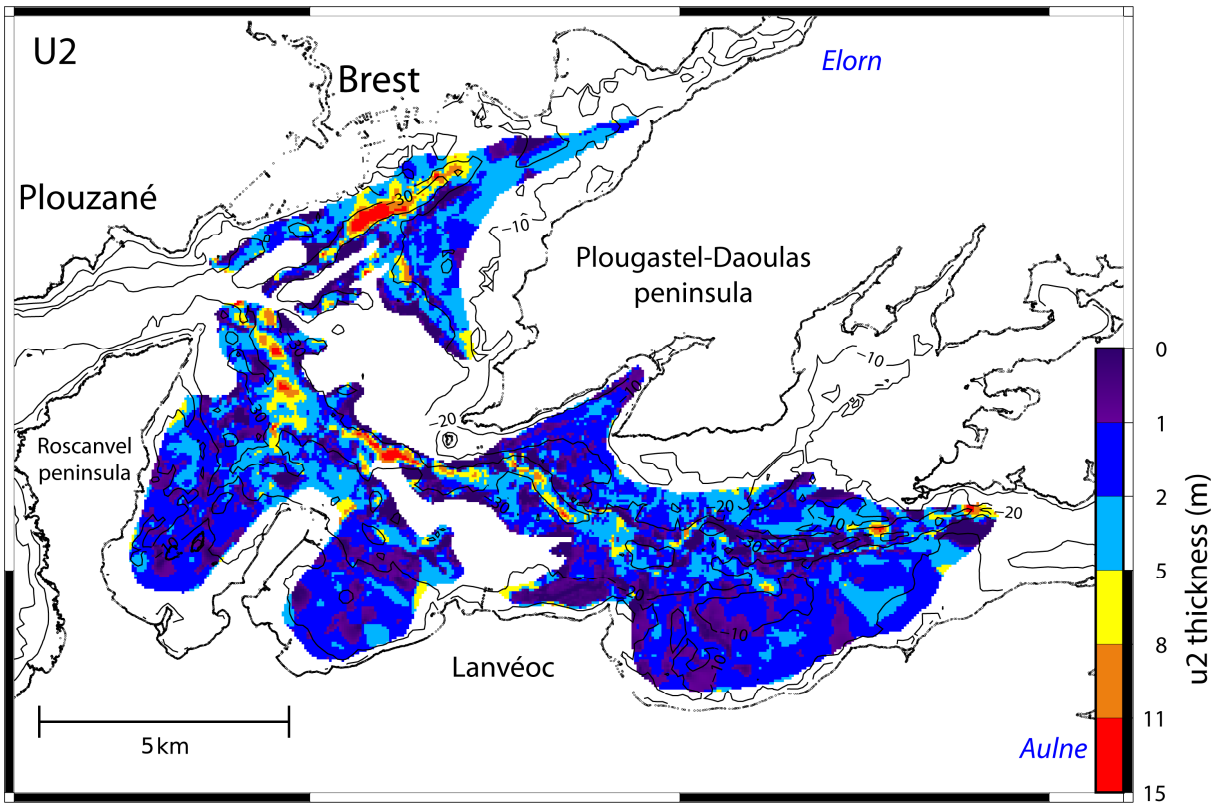

Fig. 45: Thickness maps of sediment unit U2, reconstructed from seismic interpretations of Gregoire (2016).

Global seismic patterns of U2 display many similarities with U1 in the centre: thickness distribution (mainly over T1 and T3) and geometries (high energic patterns over T1 and aggradation over T3). Most of U2 deposits are located over T1 and are interpreted as sands (Gregoire et al., 2017). This unit is therefore associated to a greater input of shelly marine sand than the previous one (Figs. 41, 44, 46; Gregoire et al., 2017), which can be linked with wide accumulations located over T1 in the centre. U2 is interpreted as the second part of the transgressive system track (TST, Gregoire et al., 2017). However, U1 and U2 display important differences: in the centre, main preserved deposits are located over T1 during U2 (while they were over T3 during U1) ; U2 deposits cover the upper area, while none are recorded for U1 over T1 (Figs. 43 and 45). Gregoire et al. (2017) observed sand bars inside seismic patterns of U2 near the mouth of the Aulne and the Elorn rivers. These figures would be the result of

the establishment of different flow direction of ebb and flood tides over those areas around 7-6 ka (cal. BP, Gregoire et al., 2017); i.e. tidal currents are no longer bidirectional, ebb and flood tides induced currents are not taking place over the same locations.

3.1.1.4 U3, 2 ka (BP) - present-day

The last sediment unit, U3, settles since 2 ka (cal. BP) and is still active at present-day (Gregoire et al., 2017). U3 overlays U2, after a hiatus of about 1 000 years, corresponding to a MFS (Maximum Flooding Surface, Gregoire et al., 2017). U3 displays mainly aggrading parallel reflectors, draping the Bay (Figs. 41, 42, 44, 46). The surface between U2 and U3 is easily visible inside T1, as U3 deposits are in discordance over U2 (Fig. 41). Over T3, and on slopes between T3 and T2, the top of U2 is marked by an erosive surface, with an irregular morphology (Figs. 44 and 46). This marker is visible only on the very high resolution of subbottom profiler data (Figs. 44 and 46). This surface is likely linked to the induration of U2 top during the hiatus between U2 and U3 (MFS), which is associated to an erosive period according to Gregoire et al. (2017). Thin reflectors overlying the bed rock over T2 in the centre are also interpreted as U3 deposits (Gregoire et al., 2017).

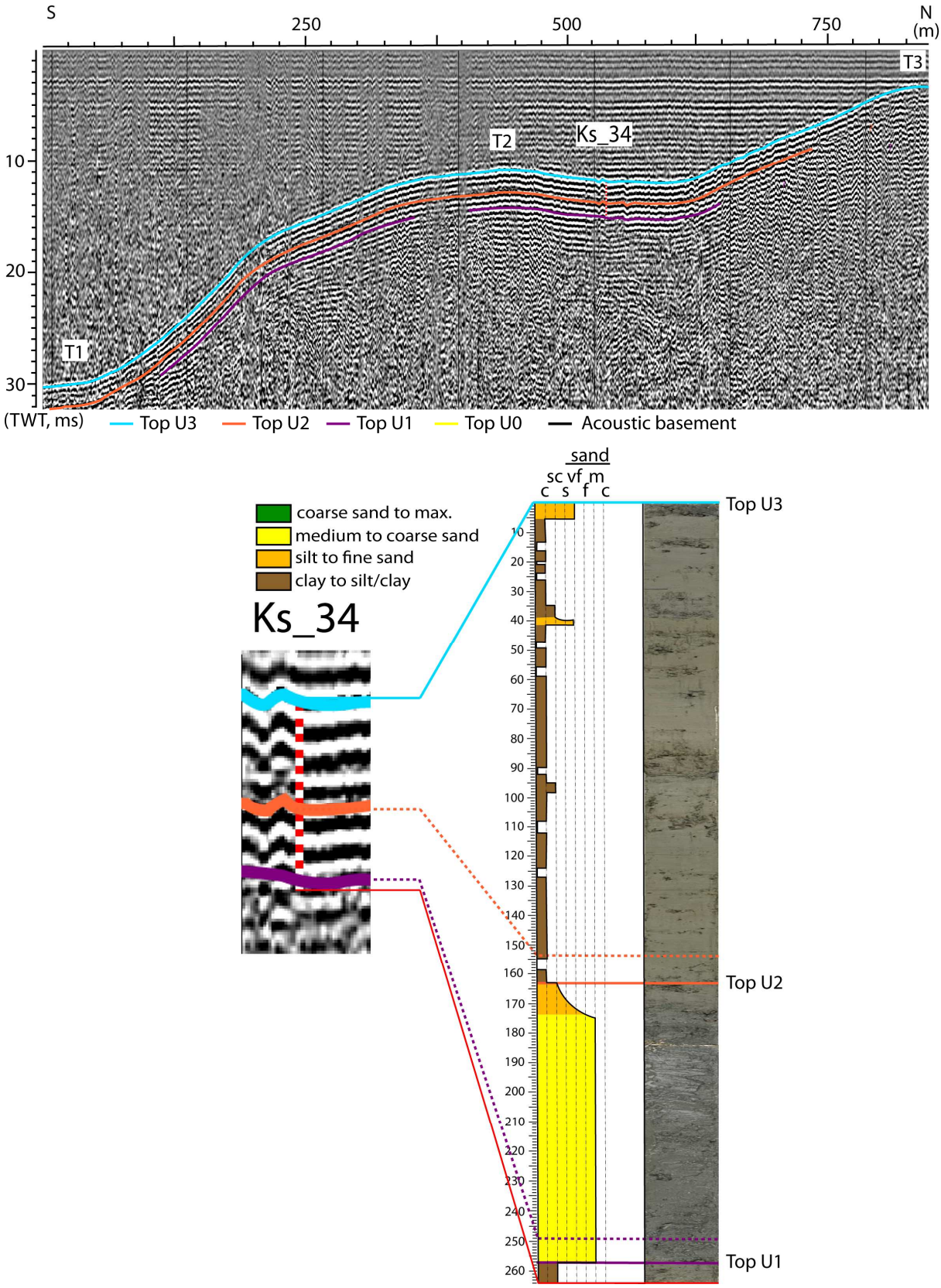

Fig. 46: (on top) Interpreted seismic profile (location on Fig. 37b, profile 9). (on bottom) Photographies and lithologic logs for cores Ks_41 and Ks_44. Dashed purple and orange lines are markers from seismic interpretation and full purple and orange lines represent the interpreted top of U1 and U2 (made to compensate the difference of resolution between cores and seismic profile).

The thickness map of U3, calculated from seismic interpretation of Gregoire et al. (2017), reveals that U3 covers the entire estuary (Fig. 47). It drapes previous sediment units and appears as a thin shelly sand layer on the top of tidal banks, organized in dunes or ripples (Fig. 48, Gregoire et al., 2017). All the cores studied on slopes between T2 and T3 (central area) display a global granulometric increase compared to previous units (e.g. Figs. 41, 44 and Tab. 1). Mud, fine to medium sands are observed with some intercalations of gravels (Figs. 41, 44, 46 and Tab. 1). During U3, muddy sediments are more proximal (over T3 only) than during U2. The grain size distribution at the present-day was studied by Gregoire (2016) thanks to seafloor sampling all over the Bay. It led to a map of grain size distribution over the Bay (Fig. 48). As U3 is still active at the present-day, the top of this unit corresponds to the present-day seafloor. T2 terraces in the centre are mostly covered with coarse sediments. U3 is composed of sands of different grain sizes over T1 while it covers T3 terraces with mostly muddy sediments. In the upper area, muds dominate and are mixed with sands of variable grain sizes. T1 displays the coarsest deposits of the upper domain (more sandy sediment) compared to the other morphological domains (Fig. 48).

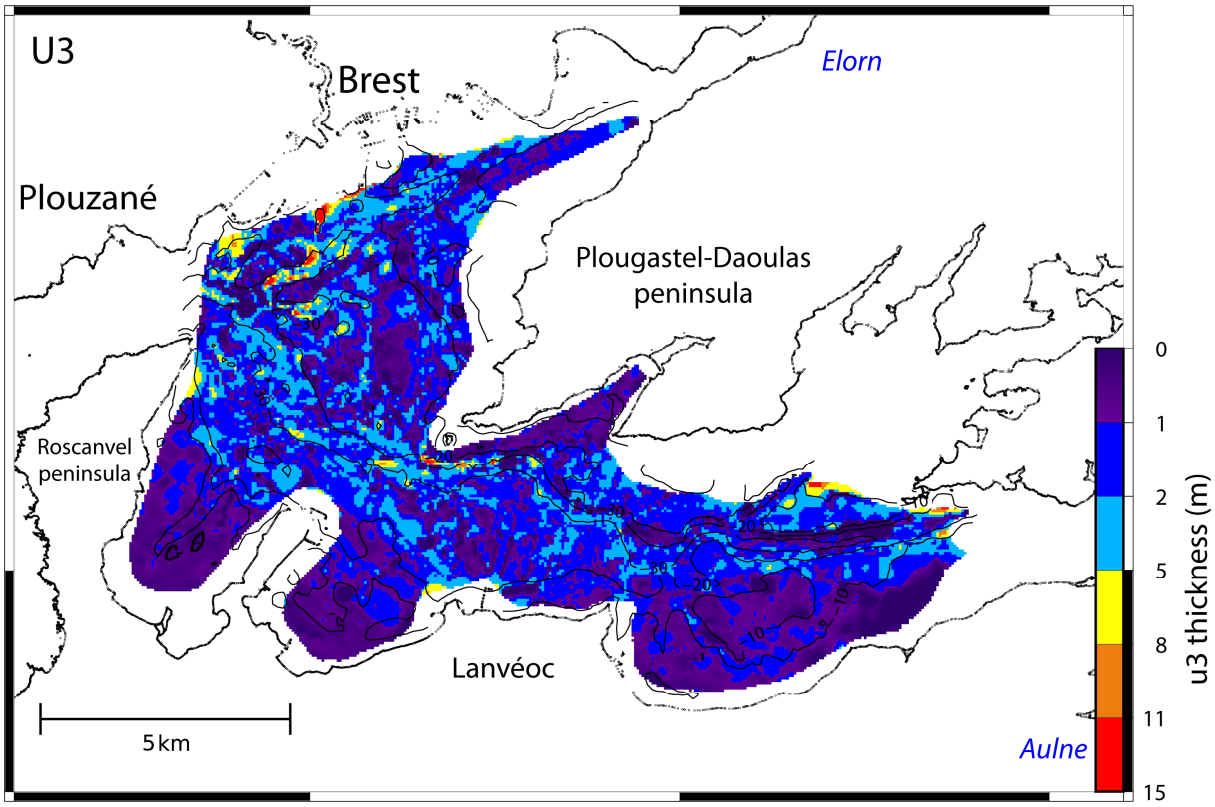

Fig. 47: Thickness maps of sediment unit U3, reconstructed from seismic interpretations of Gregoire (2016).

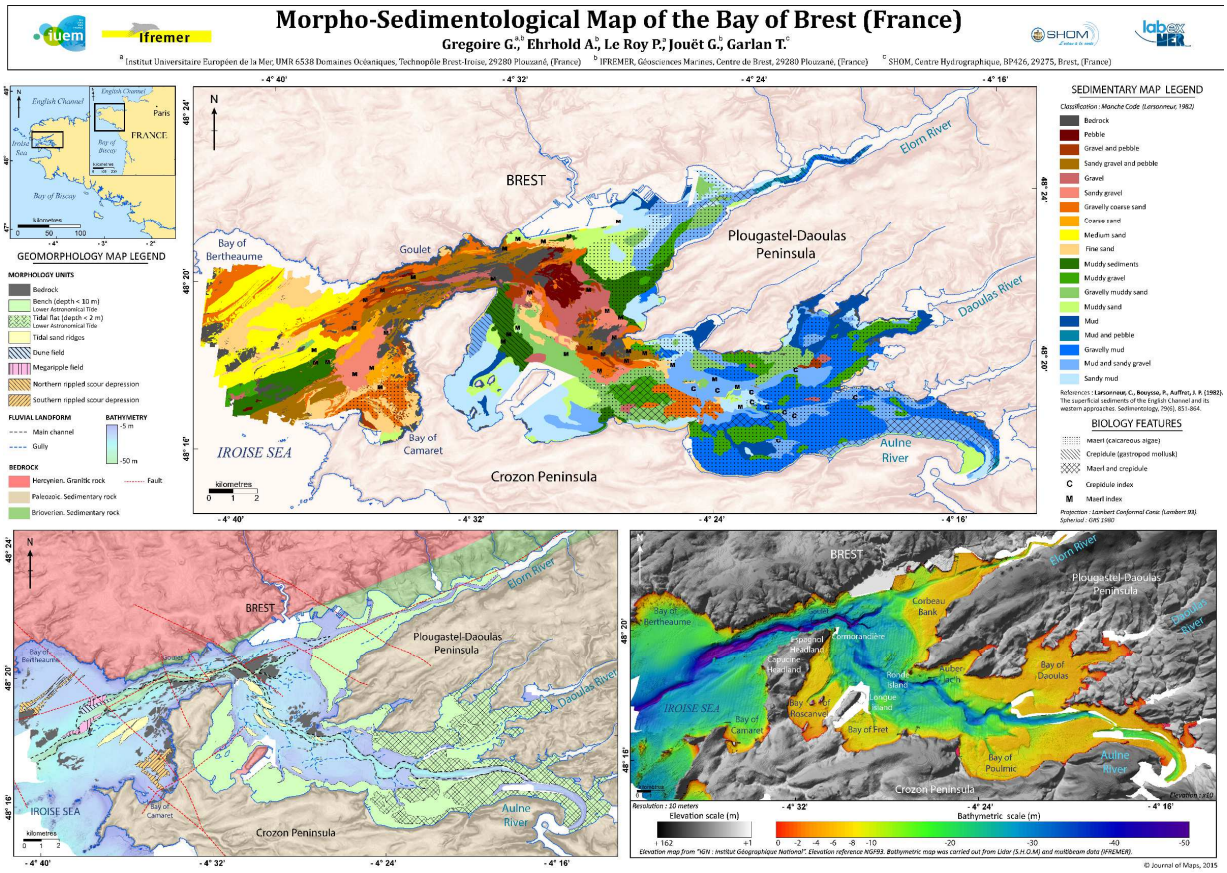

Fig. 48: (on top) Grain size distribution of the present-day seafloor of the Bay of Brest. (On bottom left) Sediment figures observed over the seafloor. (On bottom right) The present-day bathymetry (Gregoire, 2016).

U3 deposits are interpreted as high sea-level deposits (HST) and drape the entire bay (Gregoire et al., 2017). At ~2 ka, the present-day hydrodynamic is installed and the centre of the Bay is affected by strong tidal currents, which prevent fine sediment deposition (accumulated in the shallowest parts, Gregoire et al., 2017). U3 displays the thinnest global thicknesses compared to the other units (Fig. 43, 44, 46), but it is the only unit that is significantly preserved over T2 in the centre (Fig. 47). According to Gregoire et al. (2017), most of the U3 deposition occurs in the embayment and in the estuaries, as well as on the top of tidal banks where the sand-gravel shelly sediments are organized in dunes. It means that fine deposits of U3 accumulate in quiet parts of the Bay and coarser deposits of U3 accumulate inside dunes and ripple marks in areas of likely strong tidal currents (centre of the Bay of Brest, over T2 and T1).

3.1.2 Hydrodynamics Forcings

The Bay of Brest is a macrotidal estuary. It is fed by many rivers (Aulne, Elorn, Mignonne, Douffine, Penfeld, river of the Faou, Camfrout and others). The region is affected by strong waves, especially during winter. Numerous storms hit the Breton coast every year mostly during autumn and winter. However, the Bay of Brest displays a special configuration, that separates the Bay from the Iroise sea by a strait between Plouzané and Roscanvel peninsula (1.8 km wide). The oceanic swell is attenuated at the passage of the strait by the refraction on the edges and it is diffracted at its exit; it therefore induces a very weak swell climate compared to the energy regime outside the Bay. Thus,

while the mean annual wave height is 2.4 m further offshore in the Iroise Sea, in the Bay of Brest, the mean annual significant wave height value is about 0.25 m (Monbet and Bassoullet, 1989). This statement is also supported by the example during Bella storm (2020) strongly attenuated in the Bay (see details in the next chapter). The Bay of Brest is therefore protected by its semi-enclosed configuration, which is formed since the end of the Oligocene (Fig. 32, Hallegouet et al., 1994). Even if oceanic waves hardly affect the Bay of Brest, local wind could significantly influence the hydrodynamics. However, the Bay (~180 km²) has a very particular shape with an irregular coastline forming straits and coves (Fig. 31), inducing a short fetch (~25 km max, Stéphan et al., 2012). At present-day, local wind generates waves not higher than 0.8 m except at specific locations (north of the central area, Beudin, 2014). In the past, the fetch should have been even shorter as the flooded surface was lower than at present-day.

The main forcings that can significantly influence the hydrodynamics within the Bay of Brest during the Holocene appear to be tide and rivers. The evolution of those two forcings is thus important to study hydrodynamics evolution over the Holocene. The two following sections describes these two forcings during the Holocene in the Bay of Brest.

3.1.2.1 Rivers

The Bay of Brest is fed by several small rivers, separated in six watershed domains: the Aulne, the Elorn, the Mignonne, the Penfeld, Faou rivier, Crozon river and Plougastel-Daoulas river (Fig. 49). Rainwater is drained by a watershed with a total surface area of 2645 km^2.The Aulne, located in the south-east and the Elorn, located in the north-east, are the two main rivers (Fig. 49) whose catchments respectively extend over 1820 km^2 and 380 km^2 (Troadec and Le Goff, 1997). Water flow of all rivers is relatively small. Annual means of river water discharges vary within years between 22 and 30 $m^3.s^{-1}$ for the Aulne river, between 6 and 10 $m^3.s^{-1}$ for the Elorn river, and between 0.5 to 1.5 $m^3.s^{-1}$, for the Mignonne river (http://www.hydro.eaufrance.fr/). The concentrations of suspended matter for the same rivers are approximatively known (from the same source) with respective annual mean values around 0.2 $g.l^{-1}$, 0.1 $g.l^{-1}$, 0.08 $g.l^{-1}$. Note also that sediment concentrations (suspended matters) coming from the open sea are unknown over the whole period (present-day included). Those values correspond to present-day values after many human modifications since the nineteenth century. The Aulne was particularly anthropized when it was incorporated into the Nantes-Brest canal and many modifications (dams) were done for navigation needs (Acolas et al., 2006). These values thus need to be carefully used and changed for pre-industrialisation times.

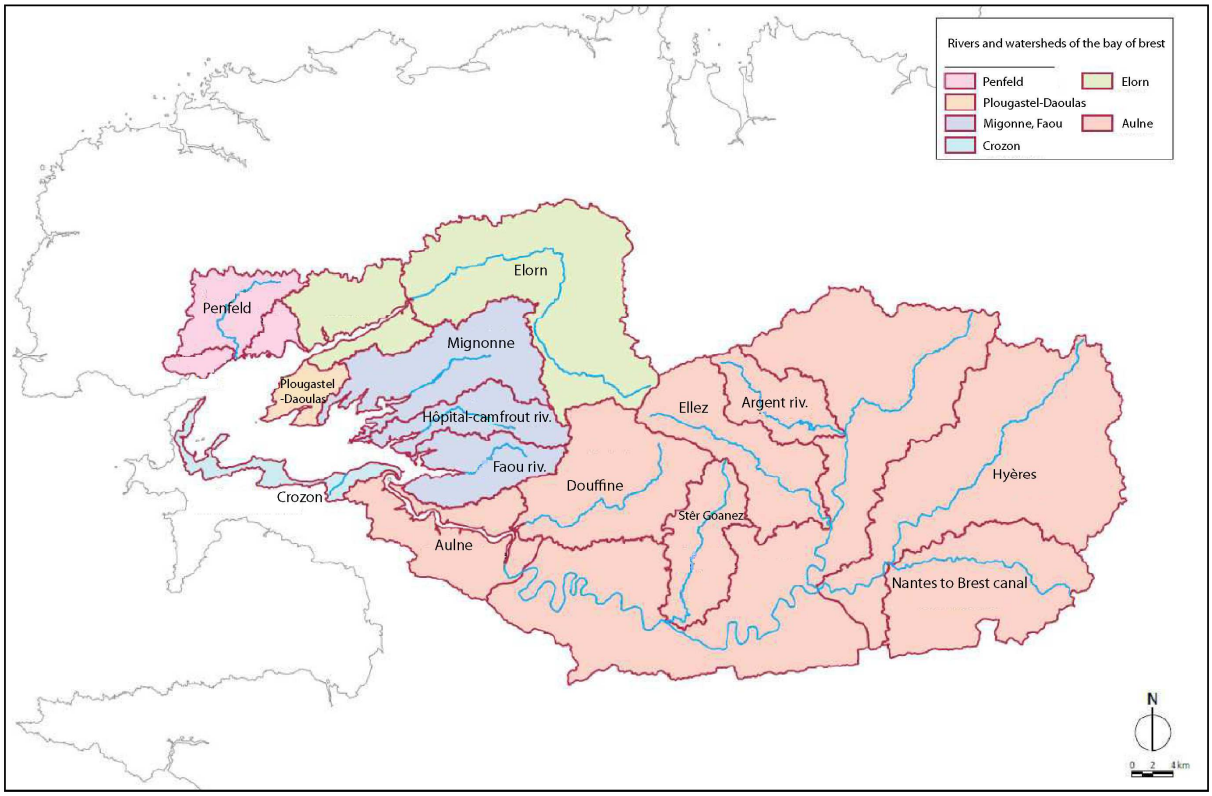

Fig. 49: Delimitation of the sub-watersheds of the Bay of Brest (Gregoire, 2016).

For the past, only proxies can give information on the evolution of rivers. In the Bay of Brest, palynological studies give information about climatic evolution and induced rivers evolution over the Holocene (Fernane, 2014; Lambert, 2017). These studies gave qualitative clues about the climatic evolution around the Bay of Brest and highlight three main climatic periods.

The Lower Holocene (11.7 to 8.2 ka BP) is characterised by high summer insolation values and is still strongly impacted by the presence of continental ice-sheet that developed during the last ice age (Lambert, 2017). At the beginning of the Holocene (10 ka, BP), the climate was colder than at the present-day and the runoff was strong due to a weak vegetation (Lambert, 2017). Within that period the Bay of Brest is a periglacial environment.

The vegetation then gradually grew around the Bay of Brest in connection with a climate warming during the Holocene climate optimum (between 8.2 to 4.2 ka BP, Koshkarova and Koshkarov, 2004). That period is associated to an increase of precipitations in Northern Europe (Seppä and Birks, 2001; Bjune et al., 2005), especially at the beginning of the period (Berger and Guilaine, 2009) and in the interval 6 - 5 ka (BP, Mojtahid et al., 2013). Penaud et al. (2020) suggest that the stronger humidity is linked to the North Atlantic Current, which may have amplified seasonal continental humidity in Western France during the Holocene climatic optimum.

After this climatic optimum, temperatures globally decrease (Berger and Loutre, 1991). This period also saw an important expansion of agriculture in the region, even if older traces could have been found (Lambert, 2017). The deforestation due to human activity (agriculture mainly) is getting more and more important. By replacing forest by fields for agriculture, humans increase the runoff from the land towards rivers (Lambert, 2017). Precipitation slightly decreases in comparison with the previous period in Northern Europe (Seppä and Birks, 2001; Bjune et al., 2005).

Another important parameter for rivers sediment discharge is the rivers profile, which is mostly linked to sea-level variations. When the sea-level is low, rivers profile are steeper and the potential energy increases between rivers and the Bay. Thus, we can suppose that rivers display higher sediment discharge than during high stages.

3.1.2.2 The tide

Tide is the main forcing of the Bay of Brest hydrodynamics at present-day and probably during all the sediment infilling of the estuary: sea surface variation are due at 99% to tide and hydrodynamic currents are due at 96% to the tide, at the present-day (Beudin, 2014). The tide is very well described around Brittany at present-day (atlas of 143 components, SHOM CST-France, Le Roy, R., Simon, B., 2003). Only few studies explored the variation of the tidal range in response to sea-level evolution around Brittany. Previous works explored the possible effects on some tidal components of a higher sea-level (M2, S2, N2, M4, MS4 and MN4, Idier et al., 2017) and of a lower sea-level (M2, Uehara et al., 2006; Ward et al., 2016, M2+S2, Goslin et al., 2015). Simulations at large time-scale of Uehara et al. (2006) and Ward et al. (2016) explore the evolution of the M2 component of the tidal spectrum over the last 16 and 21 ka in the northwest European shelf seas (previous chapter, Figs. 11 and 12). M2 is usually the main component of the tidal spectrum in strong semi-diurnal regime. The M2 component dominates largely in the Bay of Brest, accounting for 63% of the reconstructed water level signal and 47% of the current velocity signal (Beudin, 2014). M2 amplitude is around 2 and 2.5 m at the present-day (Beudin, 2014; Ward et al., 2016), with a frequency of 0,0805114 h^{-1} (S2 amplitude is about 0.8 to 1 m and with a frequency of 0,0833333 h^{-1}, Beudin, 2014). The M2 elevation amplitudes calculated in Ward et al. (2016) at 8 ka are equal to present-day M2 elevation amplitudes, and are about 0.5 m higher at 10 ka than at present-day, at the NE point of Brittany (about 15 km from the entrance of the Bay, Fig. 11). In Goslin et al. (2015) the tidal range is modelled for several steps of the Holocene transgression around Brittany point (Fig. 10), considering a new local sea-level curve (calculated from sedimentary record, Fig. 29). The tidal range is there calculated from the sum of M2 and S2 components. The results show a comparable tidal range between 6 Ka and the present-day, at the entrance of the Bay of Brest (Porsmilin). Between 8 and 6 ka (BP) Goslin et al. (2015) showed a decrease of about 0.5 m in the tidal range at the closest mesh from the entrance of the Bay. Those two studies display antagonist results, with a tide amplitude (M2 or M2+S2) higher or lower of about 50 cm within 8 - 10 ka (BP) than at the present-day. We therefore assume a constant amplitude of the tide over the last 9 thousand years.

From previous sections, we have seen that the Bay of Brest displays several metres of Holocene preserved sediment mean thickness. Sedimentary records cover almost the entire period of the study (10 ka to the present-day, Gregoire et al., 2017). These sediments are deposited in a macrotidal environment protected from waves during the whole depositional period (Monbet and Bassoullet, 1989; Hallegouet et al., 1994). Moreover, the Bay of Brest is fed by small rivers and its shape does not allow the formation of significant wave by local winds (Stéphan et al., 2012; Beudin, 2014). The estuary is therefore supposed to be largely dominated by tide, which presents a high (and assumed constant) amplitude over the Holocene (Goslin et al., 2015; Ward et al., 2016). Thus, the study area seems to be the ideal place to observe and model the evolution of the impact of tidal currents on sediments over a long period.

3.2 The modelling strategy

The aim of this study is to explore the impact of tide on sediment deposits in an estuary over a transgression (10 000 years). Along the coast many forcings drive sediment deposits: wind, waves, tide and others. The Bay of Brest is chosen for our study because it is macrotidal and naturally protected from ocean swells throughout its Holocene infill (Monbet and Bassoullet, 1989; Hallegouet et al., 1994). All rivers flowing into this estuary show a low mean annual water discharge at present-day (30 $m^3.s^{-1}$ max) and the tidal influence was observed in all sediment units (Gregoire et al., 2017). Over the long-term (~10 000 years) only partial records are available in estuaries and many questions remain concerning their sediment infilling under the action of tidal currents: How do tidal currents evolve according to long-term parameters, such as sea-level and seafloor variations? What are the consequences of hydrodynamical evolution on sediment dynamics, in terms of erosion and deposition patterns, and sediment grain-sizes classes distribution?

The use of numerical modelling is the only way to study the impact of tide on sediment transport and geomorphology in an estuary over long time-scales if not enough sediment data are available. Unfortunately, none model is able to reproduce the tide over such a long period of time (~10 000 years). Stratigraphic models, which are mainly diffusive, are not able to take into account such a quick oscillating phenomenon as the tide without simplification. Too large calculation steps are considered. Moreover, the effect of 10 000 or 100 000 tides on sediment deposits is unknown. Hydro-sediment models are the only ones able to reproduce accurately tidal processes and induced sediment dynamics, but over short time scales (from event to hundreds of years). To overcome this limitation, this study proposes a methodology to combine sedimentary records and hydro-sedimentary modelling. But, in order to reach the time-scale of the Holocene transgression (10 ka), the idea is to use hydro-sediment modelling over key paleoenvironments of a tide-dominated estuary infill, in order to simulate all main hydro-sediment dynamics variations observed from sedimentary records. It is not possible to run a continuous hydro-sediment modelling over the entire Holocene. Thus, we propose to identify (with sedimentary records), generate (with paleoenvironmental reconstruction) and model (with pure hydrodynamic or hydro-sediment modelling) successive scenarios that will represent the major trends of the observed sediment dynamics (Fig. 50, see results in Chapters 4 and 5) over the entire Holocene.

Using this approach, our second objective will be to determine if a simplification of the tidal process is possible; i.e can we define (and how) one or several (synthetic) tides (representative of the most significant morphological evolution over the estuary), which can be used for long-term numerical (stratigraphic) modelling (Fig. 50)? (This will be developed in chapter 6).

This work is organised in seven major steps presented in Fig. 50, which are: (1) the interpretation of sedimentary records (from data and bibliography); (2) the identification of key steps of the estuary infilling; (3) reconstruction of paleoenvironments corresponding to these key-steps (respective sea-level heights and seafloor morphologies); (4) tide modelling in function of those paleoenvironments (i.e. scenarios); (5) sediment transport modelling in function of these scenarios; (6) interpretation of the tidal impact evolution, by comparing simulations results; (7) determination of main sediment volume evolution time intervals, and reflexion about how the observed tidal impact into one or several morphogen(s) tide(s).

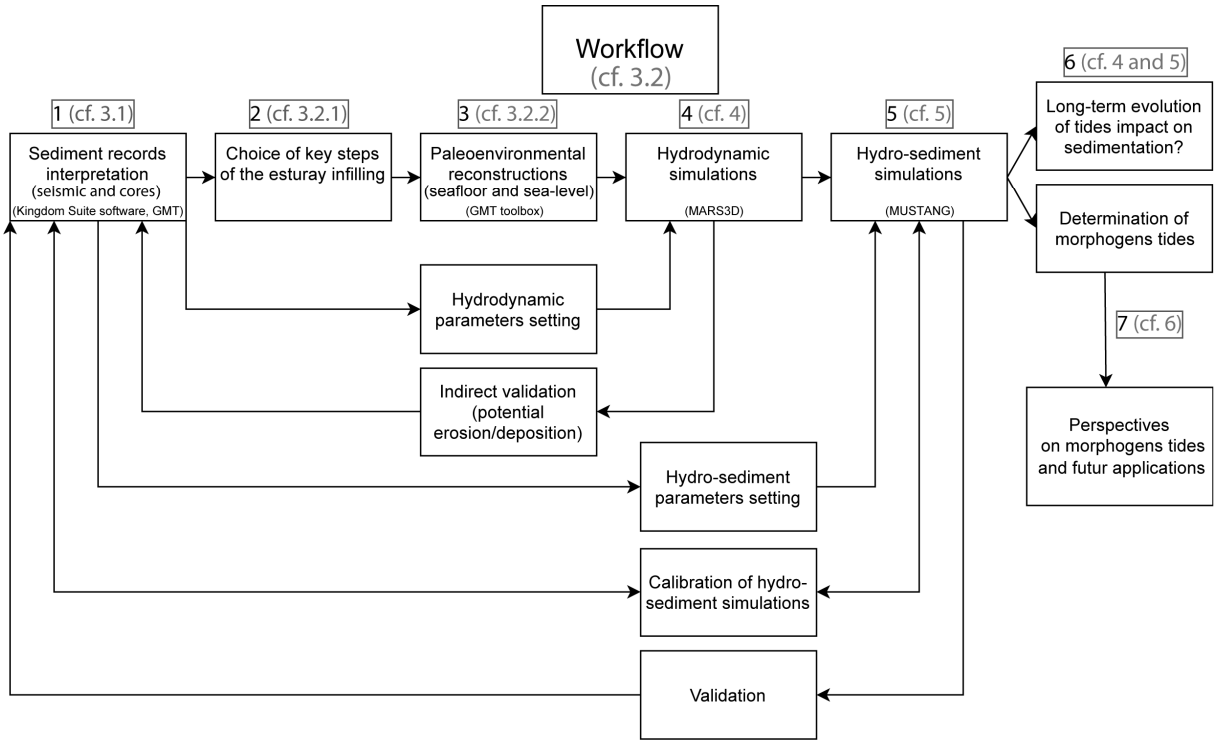

Fig. 50: Workflow describing the main steps realised in our study

3.2.1 Modelling scenarios choice

The first step is to establish paleoenvironmental reconstructions, which includes two key steps: (i) the choice of the Bay of Brest infill steps (at a specific age) that needs to be simulated and (ii) their reconstructions. Paleoenvironments are defined as seafloor bathymetry and sea-level at a specific time. A paleoenvironment needs to be defined for each main significant coastline movements (e.g. the flooding of a morphological domain) and major (hydro) sediment deposition dynamic changes (observed from stratigraphic interpretation). The choice of modelling scenarios is very important, as we will carry out short-term simulations (years) which are supposed to be representative of hydrodynamic and hydro-sediment trends during periods of the order of thousand years. This assumption can be made only because a new paleoenvironment is generated for each observed and assumed change in sediment dynamics. In this way, it is possible to compare simulations results and sedimentary records. It also allows to discuss triggers of the main hydrodynamic variations and their implications for stratigraphic interpretation of tide-dominated estuaries.

3.2.1.1 Modelling scenarios choice for the Bay of Brest

The chosen scenarios cover the period 9 ka (BP) to the present-day. The first unit U0 (10-9 ka cal. BP) is not analysed in this study, because during its deposition the Bay is supposed to be a ria system. As this study aims to observe the impact of tide on sediment, the study starts at 9 ka, with the deposition of U1, when the Bay is supposed to be a tide-dominated estuary. Four scenarios are built to represent major paleoenvironmental changes during U1 (2 scenarios), U2 (1 scenario) and U3 (1 scenario) deposition (Fig. 38). As the three sediment units show different deposition patterns in terms of thicknesses and grain-size classes distribution, at least 1 scenario is set for each sediment unit.

During the deposition of the first sediment unit analysed (U1), the rise in sea-level is quick, ranging from -26 m to -5 m (compared to present-day sea-level). Within that period of time, T2 and then T3 terraces are flooded (Figs. 36 and 51). Two scenarios are set to represent the hydro-sediment dynamics during U1 deposition. The first scenario aims at reproducing the tidal dynamics at the beginning of U1 deposition. At this time (9 000 years BP), the sea-level was 26 m below the present-day level and the seafloor correspond to the top of U0 (Figs. 38 and 52). In those conditions, the intertidal area is over T2 terraces and T1 is a subtidal area (Figs. 36 and 51).

The objective of the second scenario is to model the final phase of U1 deposits, around 7 500 years BP (Fig. 38). At that time, the sea-level is 10 m lower than at the present-day, the intertidal area is over T3 and T2 is in subtidal area (Figs. 36 and 51). As this scenario aims to represent the last deposits of U1 and the chronology of the deposits is unknown within 9 ka and 7 ka BP (U1 deposition time interval), the input bathymetry chosen is the top of this same unit (Figs. 51 and 52). Due to these large sea-level variations, the Bay of Brest configuration was very different between the beginning and the end of U1 deposition period. Through scenarios 1 and 2, simulations will represent the flooding of T2 and T3 terraces.

During the deposition of U2, the rise in sea-level slows down (-5 m to almost the present-day level, Fig. 35, Goslin et al., 2015). T3 terraces correspond mostly to a subtidal area and few intertidal areas are present along the coast and towards the rivers mouth (Figs. 36). In addition, no major change is observed on the seismic data. The goal of the third simulation is to represent hydro-sediment dynamics inducing U2 deposits. Scenario 3 is set at around 7 000 years cal BP, with a sea-level at -5 m under the present-day sea-level (Fig. 38). Seafloor morphology corresponds to the top of U1 (Figs. 51 and 52).

The last sediment unit, U3, is also represented by only one scenario. During U3 deposition preserved sediment thickness is small (mean thickness around 2 m) and the sea-level remains close to the present-day one (Fig. 38). The basin shape is almost the same within the entire time interval of U3 deposit. Scenario 4 is set at the present-day and aims to represent U3 hydro-sediment dynamic (Fig. 51 and 52). The whole bay is submerged and mostly characterized by subtidal areas (Fig. 36). This scenario also allows to carry out the validation of the hydrodynamic simulations with comparison to in-situ measurements.

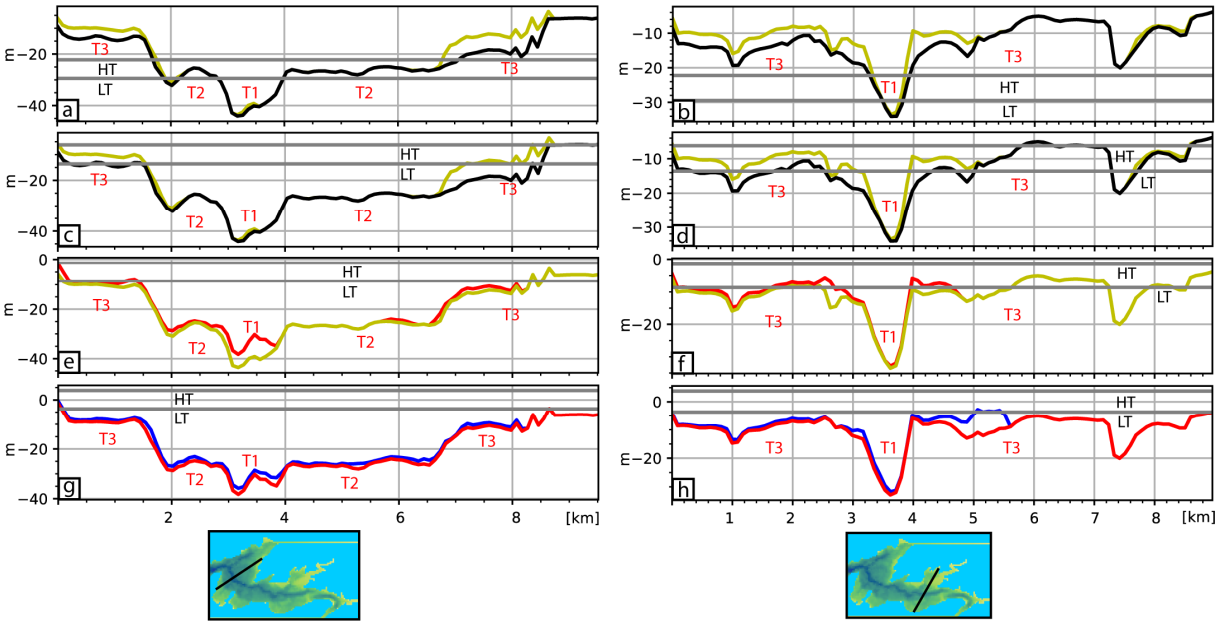

Fig. 51: Cross-sections of sediment unit thicknesses (in meters): black lines represent the top of U0, yellow lines the top of U1, red lines the top of U2 and blue lines the top of U3. Inset maps show the locations of cross-sections in the upper area (a, c, e, g) and in the central area (b, d, f, h). Grey lines represent the highest free surface level (HT: Highest Tide) and the lowest free surface level (LT: Lowest Tide) of the corresponding scenario (a and b: scenario 1; b and c: scenario 2; e and f: scenario 3; g and h: scenario 4).

3.2.1.2 Paleoenvironmental reconstructions

To obtain a bathymetric map for each scenario, the first step is to determine the basement depths and sediment unit thicknesses over the Bay. Then bathymetric map of each scenario is successively calculated by adding sediment unit thicknesses. For example, in scenario 1 the seafloor corresponds to the top of U0 (basement depth + U0 thickness). Bathymetric maps are reconstructed from the interpretation of seismic data (Gregoire et al., 2017), acquired during several cruises (see the complete list in Gregoire, 2016 and section 3.1.1). Seismic markers depths, recorded in two-way travel time (TWTT, seconds), are converted to depth (meters) using the velocity law set by Gregoire et al. (2017). The present-day depth of each seismic marker is calculated using a constant velocity law within the sediment (1800 $m.s^{-1}$) and in the water column (1550 $m.s^{-1}$). Those values are chosen to remain consistent and comparable with stratigraphic analysis of the Bay of Brest made by Gregoire et al. (2017). Moreover, thickness maps allow to extract valuable information on sediment units distribution. Bathymetric maps of the basement and thickness maps of each unit were calculated with GMT (Generic Mapping Tool, Wessel et al., 2013), using a 50 m spatial interpolation. These maps are finely meshed (50 m) to prevent over-interpolation of sediment deposits and to have validation data with the best resolution as possible.

Scenario 1 bathymetry (top U0) is rebuilt by adding U0 thickness to the basement map (Fig. 52). U1 thickness is added to the first scenario bathymetric map (Fig. 52, Top U0) and the result is the seafloor morphology for the second and third scenarios (Fig. 52, Top U1). The present-day morphological map is created from SHOM's data (Fig. 52, present-day bathymetry). All the maps refer to the present-day mean sea-level and sea-level variations between simulation are directly implemented into simulations.

Numerical modelling needs bathymetric information at each point of the configuration but seismic data are not available everywhere within the Bay of Brest and (complete seismic data extension is available in Fig. 37a). Most of the no data areas are located in very shallow to intertidal areas, where

no ship was able to perform seismic acquisition. Those shallow areas close to the coast are emerged during all the scenarios except the present-day situation. We then used the present-day bathymetric data from the SHOM (2015b) to complete our reconstructed bathymetric maps. This approximation has therefore no influence on simulations, it is only performed for numerical purposes. Note that, at the south of Plougastel-Daoulas peninsula, a gas area prevents a clear image of the seismic structures and seismic markers could not have been interpreted (Gregoire, 2016). For numerical needs, we also used present-day bathymetric data from the SHOM (2015b) to complete our reconstruction, but the bathymetry is there likely under-estimated (it appears less deep than it should be).

The main uncertainty about these bathymetric reconstructions is linked to the amount of erosion. No information is available about the quantity of sediments remobilised by tidal currents during the deposition of subsequent units, so only the preserved sediments are taken into account here. The amount of recycled sediment for each unit by subsequent hydrodynamics is therefore the main uncertainty for our paleoenvironmental reconstructions.

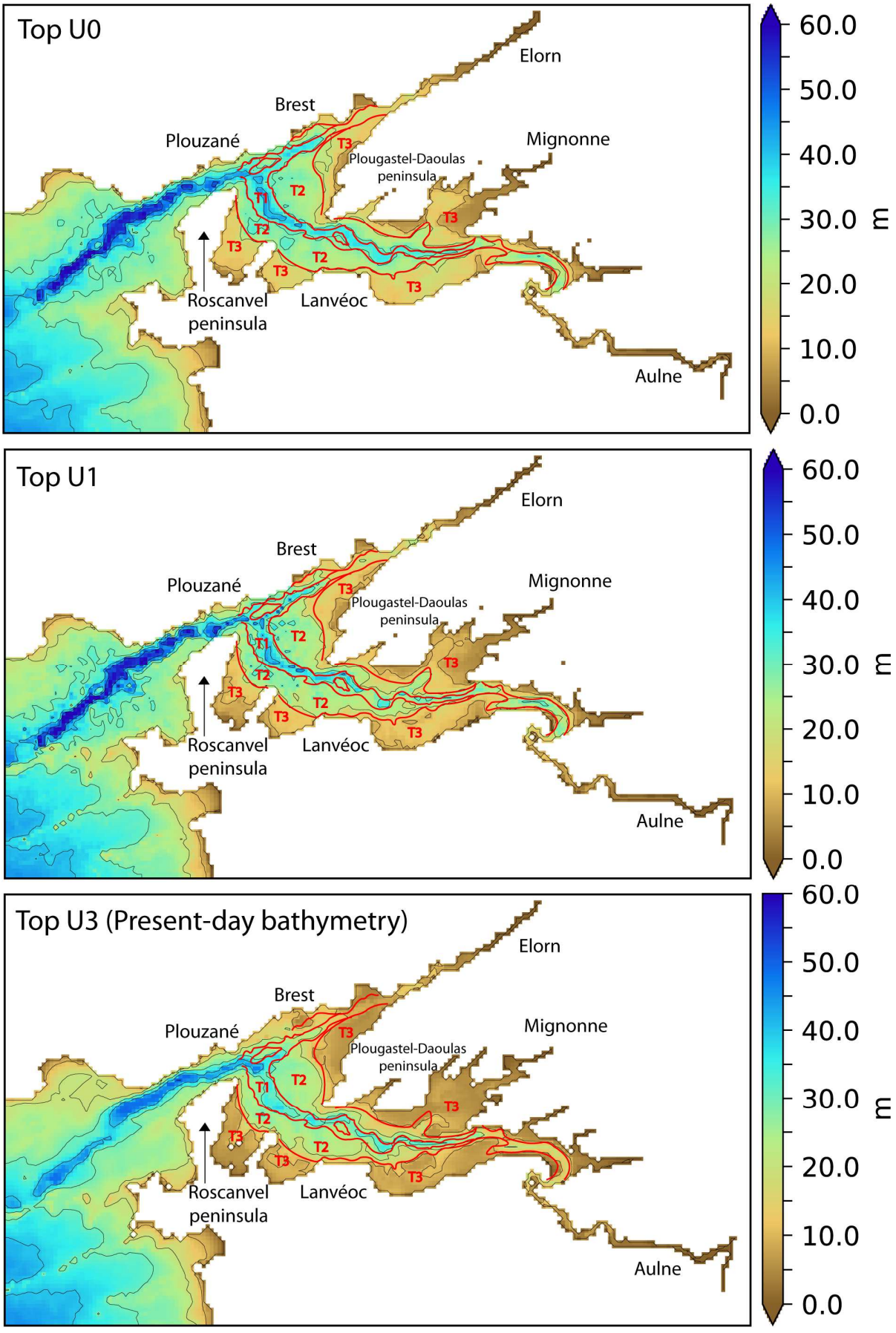

Fig. 52: Paleobathymetric maps of the top of U0, U1 and U3, relative to the present-day sea-level. Red lines represent the superimposed boundaries of the morphological domains (T1, T2, T3).

3.2.3 Numerical modelling

The model used is the coastal hydrodynamic model, MARS3D (Lazure and Dumas, 2008), coupled with the sediment module MUSTANG (MUd and Sand TrAnsport modelliNG, Le Hir et al., 2011; Mengual et al., 2017). The hydrodynamic core (MARS3D) computes the hydrodynamic variables (currents, free surface elevation). It has demonstrated its ability to reproduce the main characteristics of oceanic flows (tidal amplitude and phase, 3D currents) in several estuaries (e.g. Seine: Grasso et al., 2018, Gironde: Diaz et al., 2020, Charente: Toublanc et al., 2014, the Bay of Brest: Petton et al., 2020). The sediment module, MUSTANG, computes sediment transport, erosion and deposition processes and morphological evolution in coastal and estuarine environments. The simulated sediment dynamics from MUSTANG has been validated under various environmental coastal forcings like tides, waves, rivers and (e.g. Diaz et al., 2020; Lemoine and Le Hir, 2021; Mengual et al., 2021). The set-up of hydrodynamic and hydro-sediment modelling for this study are respectively described in the two next chapters.

3.2.4 Validation

Validation is one of the main issues for hydrodynamic and hydro-sediment simulations in the past. Conventional validation is carried out by comparing simulation outputs to in-situ hydrodynamic and sediment measurements/data. The parameters usually analysed for validation are current velocities, sea surface heights variations, temperature and salinity. For hydro-sediment simulations suspended matters concentration fluxes are the most used.

Hydrodynamic simulations (once validated) provide a 3D overview of the hydrodynamics within the study area. The oldest hydrodynamic data in the Bay of Brest are 300 years old and thus, within the four scenarios set-up in our methodology, only scenario 4 can be validated in usual way. The present-day configuration of the Bay of Brest was built by Petton (Pers. Comm). This configuration was used and validated in previous studies by comparison with different dataset of in-situ measurements (temperature/salinity and ADCP, Klouch et al., 2016; Petton et al., 2016; Frère et al., 2017; Chataigner, 2018; Petton et al., 2020; Petton et al., 2021). Moreover, a further validation, linking five ADCP (acoustic Doppler current profiler) is carried out in this PhD (next chapter). All comparisons made between our simulations at present-day and in-situ measurements give confidence in the model ability to reproduce the hydrodynamics in the Bay of Brest.

For the three others scenarios (1, 2, 3) no hydrodynamics data exist and hydrodynamic cannot be directly validated. Simulations outputs are thus compared to sedimentary records for validation. This comparison is direct for hydro-sediment simulations and is done through potential erosion and deposition for hydrodynamic simulations. Once validated, hydro-sedimentary simulations provide us quantitative parameters for past hydrodynamic data. In this study, the global sediment distribution and the grain-size classes distributions, will be compared to sediment data through the thickness maps built from stratigraphic record and the lithologic and stratigraphic logs of cores. The ten cores reaching the oldest units were described. Tab 1 resumes the cores locations, length and simplified grain-size observations (in four classes, see their position on Fig. 37). The objective of this validation is not to simulate the observed grain size at the exact pixel of the core location, but rather to validate the global deposition and erosion trends. We aim to check if simulations can explain sedimentary records. We expect to simulate a realistic distribution of erosion and deposition zones, and a realistic distribution of grain-size classes for each successive steps identified over the Holocene hydro-sedimentary history of the Bay of Brest.

4 Hydrodynamic modelling (article)

“Continental Shelf Research”, Published article, 2021

https://doi.org/10.1016/j.csr.2021.104595

Préface

Cette préface a pour objectif de présenter l'article intitulé : « Numerical Modelling of a Macrotidal Bay over the Last 9,000 Years : An Interdisciplinary Methodology to Understand the Influence of Sea-Level Variations on Tidal Currents in the Bay of Brest. », qui a été publié dans le volume 231 paru en décembre 2021 dans Continental Shelf Research.

La méthodologie imaginée pour explorer l'évolution des courants sur de longues périodes nécessite la mise en place de plusieurs scénarii de modélisation à différentes époques. De longues étapes de calibration et paramétrisation sont nécessaires pour simuler une hydrodynamique cohérente sur chacun d'entre eux. Au moins autant d'étapes sont nécessaires pour y implémenter les interactions avec le sédiment par la suite. Sachant qu'aucune simulation hydro-sédimentaire ne peut être réalisée tant que l'hydrodynamique n'est pas simulée convenablement pour chaque scénario, nous avons donc fait le choix de traiter et publier l'hydrodynamique et la dynamique hydro-sédimentaire en deux parties.

Cet article présente la mise en place des modélisations hydrodynamiques en rade de Brest au cours des 9 000 dernières années. Pour cela il revient notamment sur la méthodologie, la mise en place des scénarii, leurs reconstructions, ainsi que les forçages considérés. Ce papier présente également le modèle hydrodynamique utilisé (MARS3D) et sa paramétrisation. Comme vu précédemment (chapitre 3) la méthodologie repose sur la comparaison des résultats avec les enregistrements sédimentaires. Or, avec uniquement la simulation de l'hydrodynamique, aucune comparaison directe n'est possible. Pour pouvoir réaliser ce point essentiel de la méthodologie, le potentiel d'érosion pour trois classes granulométriques non-cohésives et le potentiel de dépôt des sédiments cohésifs a été calculé.

Les résultats présentent l'hydrodynamique induite par la marée au cours des 4 scenarios. Dans un premier temps l'évolution des courants barotropiques est analysée par l'intermédiaire de moyennes sur un flot et un jusant de vives eaux, ainsi que sur toute l'année avec des percentiles (90). Ensuite, les courants sur le fond sont analysés grâce aux calculs des potentiels d'érosion et de dépôt et comparés aux cartes d'épaisseurs des différentes unités sédimentaires.

La discussion de cet article aborde dans un premier temps les limites des simulations, notamment dues au manque d'information dans le passé. Ensuite, elle s'axe principalement autour d'une reconstruction Holocène de l'hydrodynamique en rade de Brest : (1) flot et jusant sont principalement bidirectionnels et situés sur le chenal principal au début de l'Holocène (9 ka) et se séparent durant le scenario 2 (7.5 ka) au centre et le scénario 3 (7 ka) dans la zone supérieure. Un gyre anticyclonique se forme alors au centre durant le flot et pendant le jusant les courants les plus intenses se situent au sud du chenal principal. Dans la zone supérieure, les courants de flots sont toujours majoritairement sur le chenal et les courants de jusant principalement sur les terrasses les moins profondes. (2) Ces deux changements de circulation sont très fortement influencés par les détroits entre Plouzané et la presqu'île de Roscanvel, ainsi qu'entre Lanvéoc et Plougastel-Daoulas, qui orientent les flux d'eau (entrant et sortant). (3) La propagation des courants de marées semble également liée à la montée du niveau marin par rapport à la surface inondée. Les potentiels d'érosion et dépôts mettent en avant un retrait vers l'aval des forts courants de marée lors du scénario 3 en comparaison du scénario 2 et une avancée prononcée vers l'amont lors du scénario 4 (actuel, par rapport au scénario 3). Il semblerait que les retraits rapides du trait de côte engendrent la migration des dépôts potentiels (issus des vitesses sur le fond) vers l'aval (détroit entre Plouzané et la péninsule de Roscanvel). A l'inverse la montée du niveau marin, sans ou avec peu de recul du trait de côte, engendre une migration vers l'amont (flancs de l'estuaire et embouchures des rivières).

La comparaison, bien qu'indirecte, via les potentiels de dépôt et d'érosion montre la cohérence des simulations au cours de la reconstruction avec les enregistrements sédimentaires et la pertinence de cette méthodologie pour étudier les courants de marée sur de longues périodes. Enfin, les apports de cette méthodologie pour explorer l'évolution hydrodynamique long-terme, en comparaison d'études et techniques précédentes, sont discutés.

Numerical Modelling of a Macrotidal Bay over the Last 9,000 Years: An Interdisciplinary Methodology to Understand the Influence of Sea-Level Variations on Tidal Currents in the Bay of Brest.

Matthieu Guillaume Olivier[a,c,d], Estelle Leroux[a], Marina Rabineau[d], Pierre Le Hir[b], Didier Granjeon[c], Teddy Chataigner[e], Alexis Beudin[f], Héloïse Muller[b]

a IFREMER – LGS laboratory – Pointe du Diable, 29280 Plouzané, France (molivier@ifremer.fr, eleroux@ifremer.fr)

b IFREMER – DYNECO/DHYSED laboratory – Pointe du Diable, 29280, Plouzané, France (hmuller@ifremer.fr, Pierre.Le.Hir@ifremer.fr)

c IFP Énergies nouvelles – 1 et 4, avenue de Bois-Préau, 92500, Rueil-Malmaison, France (didier.granjeon@ifpen.fr)

d Univ Brest, CNRS, Univ. Bretagne-Sud, Laboratoire Géosciences Océan (LGO), UMR6538, IUEM, rue Dumont d'Urville, F-29280, Plouzané, France (marina.rabineau@univ-brest.fr)

e ENPC, Hydraulics Laboratory, Saint-Venant, 6 quai Watier, 78400 Chatou, France (teddy.chataigner@enpc.fr)

f BW-CGC, 53 rue du commandant Groix, 29200 Brest, France (alexis.beudin@bw-cgc.fr)

Abstract

Estuaries play a major role in the transfer of sediments from the continents to the shelves and deep ocean basins. Their position at the interface between land and sea promotes them as a key area for the understanding of ocean sediment supply, but yet long-term evolution remains poorly understood. The main reasons of the lack of knowledge about estuaries filling are the lack of hydrodynamic data in the past and the temporal application of numerical models. Oceanographers and geologists have developed numerical models to simulate currents and sedimentation. On one hand, hydro-sediment models allow a good physical representation of estuarine hydrodynamic processes and their impact on sedimentation, but only over time-scale spanning years to decades. On the other hand, stratigraphic diffusive models aim to study the impact of various geological processes on sedimentary basins over millions of years, but they are unable to describe in detail the tidal hydrodynamic processes that govern estuaries.

In response to this time-scale issue, this study presents a first step attempt to explore the evolution of tidal current distribution in relation with Holocene eustatic variations and seafloor evolution. Here we focus on a macro-tidal estuary, the Bay of Brest, where tidal processes dominate, as the estuary is naturally protected from ocean swells. This paper aims to set up a methodology to simulate the (past) tidal currents over a long time period and correlate them with sedimentary data. Major changes in deposit dynamics are first identified from cores and seismic data, and the corresponding paleo-topographies and paleo-sea-levels are rebuilt. A process-based hydrodynamic model (MARS3D) is then used to test the impacts of these paleo-bathymetries on hydrodynamics over a 1-year time span. Four

scenarios have been considered, representing four key stages of the Holocene transgression in the Bay of Brest.

The simulated barotropic current distributions were analysed and bottom currents impact on the seafloor compared with sedimentary records to understand past hydrodynamic context and associated sediment spatial distribution over geological time scale. Hydrodynamic simulations and sediments records are linked, in order to propose a reconstruction of the tidal influence on sediments over the last 9000 years. The results show changes of the tidal patterns related to the paleoenvironmental evolution (bathymetry and sea-level variations). Even if a hydro-sediment model would be needed to make a direct correlation between simulated currents and sediment records, this successful application in the Bay of Brest shows that discontinuous modelling can help to understand tidal current evolution and their impact on sediment distribution over long periods.

Keywords: Hydrodynamic modelling; Tidal currents; Paleoenvironmental reconstruction; Holocene sedimentation; Erosion and deposition potential indexes

4.1. Introduction

Past estuarine sedimentary systems remain poorly understood, yet they are key areas in the global understanding of sedimentary dynamics. Estuaries are located at the interface between rivers and ocean basins and represent a key link between the source and sink in a source-to-sink approach. As complex and always changing environments, for example regarding their salinity characteristics, they host a specific type of biodiversity. The very heterogeneous petrophysical properties of tidal sedimentary rocks in these environments, the abundance of life, organic matter and specific morphology such as incised valleys can make them excellent petroleum systems (Posamentier and Allen, 1993; Dalrymple, 2010). Besides the resource aspect, within the context of Holocene deglaciation and sea-level rise, the action of tidal currents is expected to change significantly along and over the coastline. Understanding the influence of the sea-level and the bathymetry on tides over a rather long period of time (9 ka) is therefore important in both past and future contexts. It appears that there are mainly two ways to explore changes in tidal circulation: a detailed study of the sedimentary record, which is an indirect approach, or numerical modelling. This last option is vast, as several types of modelling are available to study geomorphological changes in coastal areas.

For geological time-scales (more than 1 ka), stratigraphic models are the most popular. Stratigraphic models use a deterministic approach based on diffusion, which is the only approach allowing the simulation of the filling of sedimentary basins at the time and space scales considered in geology. They aim to simulate the synthetic result of geological processes over millions of years (Granjeon and Joseph, 1999; Bruneau et al., 2017; Crombez et al., 2017). They deal with the results of long-term processes such as subsidence or tectonic movements and, as they are not based on high resolution processes, their computational costs are rather small. Thus, due to the high frequency oscillations of tidal processes, stratigraphic models do not consider explicitly tidal processes and at present-day, they are unable to simulate the residual effect of tides over long time periods.

On another side, oceanographers have developed hydrodynamic and hydro-sediment models based on the resolution of physical processes, which allow to study the hydrodynamic effects on sedimentation at very fine spatial scale (meter), but only over short-time periods (from hours to decades, e.g. Bárcena et al., 2016; Grasso and Le Hir, 2019; Tosic et al., 2019). As they are based on the physical representation of processes that evolve rapidly (wind-induced and tidal currents, wave

regimes, density-induced flows, erosion, deposition, bedload or suspended sediment transport), the calculation steps are very short (∼10 s). The computational time of hydro-sediment models doesn't allow to simulate periods longer than 10 years, unless simplifications of the integration of the time-consuming processes are made. In Cayocca (2000) for example, tidal currents computation is simplified (annual mean) to simulate the last 300 years of the coastal evolution of Arcachon lagoon. The morphological evolutions of nearshore basins are most often approached by the so-called "reduced complexity models". It is an important topic for society but complex for researchers, because it mixes processes in the order of 1 s with others in the order of one hundred years. Many techniques have been developed to simulate this type of environment, a synthesis of these techniques is proposed by Roelvink (2006). The most used technique is to run hydro-sediment models with a morphological factor. The principle is to apply a multiplicative factor for erosion and deposition processes estimated by a hydro-sediment model (Franz et al., 2017; Le Tu et al., 2019; Elmilady et al., 2020). Usually, this technic does not exceed 100 years. However, some studies used much larger factors (400 in Braat et al., 2017) to explore morphological evolution over longer time scales.

Because of the different time and space scales they deal with, these two types of models are not used for the same purposes (Joseph et al., 2016). The upscaling of coastal processes representation is the key to understand many depositional systems, but they are ruled by the interaction of many processes such as waves, river flows, tides and storm events. The predominance of a particular process is linked to the configuration of the coast and many places have been described as tide-dominated coasts (Choi and Dalrymple, 2004; Tessier, 2012; Zhang et al., 2017). Long term deposits in this type of environment are not easily simulated, hydro-sediment models are not able to provide results over geological time scale. On the other hand, stratigraphic models cannot simulate the detailed highly variable tidal hydrodynamic processes. Here, we propose to combine sedimentology, physics, and numerical modelling to explore the influence of the paleoenvironmental evolution (defined as bathymetry and sea-level variations) on the distribution and characteristics of tidal currents. From a geological point of view, we aim to understand how tides impact sediment deposits distribution and how it changes with paleoenvironmental evolution (seafloor morphology, sea-level variations). However, it is a difficult challenge to address, as we have no direct data on hydrodynamic characteristics dating back more than 300 years.

The idea is to rebuild paleoenvironments and model the associated tide oscillations. Wells et al. (2007b; 2007a) used the model ICOM (Imperial College Ocean Modelling) during 30 days in order to study the tidal distribution during a high sea-level period (highstand) and an early stage of a transgression (late Pennsylvanian, 298.9 to 323.2 Ma). Tidal reconstructions at a global scale were also performed for the Aptian (125 Ma to 113 Ma, Wells et al., 2010). Those pioneering works led to many other studies to model the tide in the past with the model ICOM and even to correlate these simulations with sedimentary deposits by calculating the bed shear stress (Cretaceous, Bohemian basin, Mitchell et al., 2010; late Oligocene-Miocene, South China Sea, Collins et al., 2018). All those studies considered only the tide in hydrodynamic calculations. The approach proposed and the reconstructions provided by Imperial College are major advances in the understanding of the paleoenvironment influence on past tides and their subsequent impact on sedimentation at large spatial (sedimentary basin to global) and temporal (about 10–50 Ma) scales.

In this study, four paleoenvironments are generated to represent tidal evolution during Holocene period in the Bay of Brest (France). The paper is structured as follows. After introduction, section 4.2 (Study area context) describes the Bay of Brest, its geological setting, our knowledge of the present-day hydrodynamic context and its Holocene history. Section 4.3 (Methods) describes the model used with its parameterisation, the setting up of the scenarios and potential erosion and deposition indexes.

Hydrodynamics influence on sedimentation evolution linked with the rise of sea-level and seafloor changes is detailed in section 4.4 (Results). These results are then discussed in section 4.5 and the main conclusions and perspectives are drawn up in section 4.6.

4.2. The study area: the Bay of Brest

4.2.1. Geological description

The shape of the Bay of Brest is a consequence of three major orogenic episodes creating the Pentevrian (2 Ga to 750 Ma), Cadomian (600–530 Ma) and Hercynean (380–250 Ma) chains (Ballèvre et al., 2009; 2014). The Hercynian chain was divided into different provinces, separated from each other by faults and grinding zones. The North Armorican Shear crosses the study area and formed the bed of the Elorn river and the strait between Plouzané and the Roscanvel peninsula, named the "Goulet" (Fig. 1).

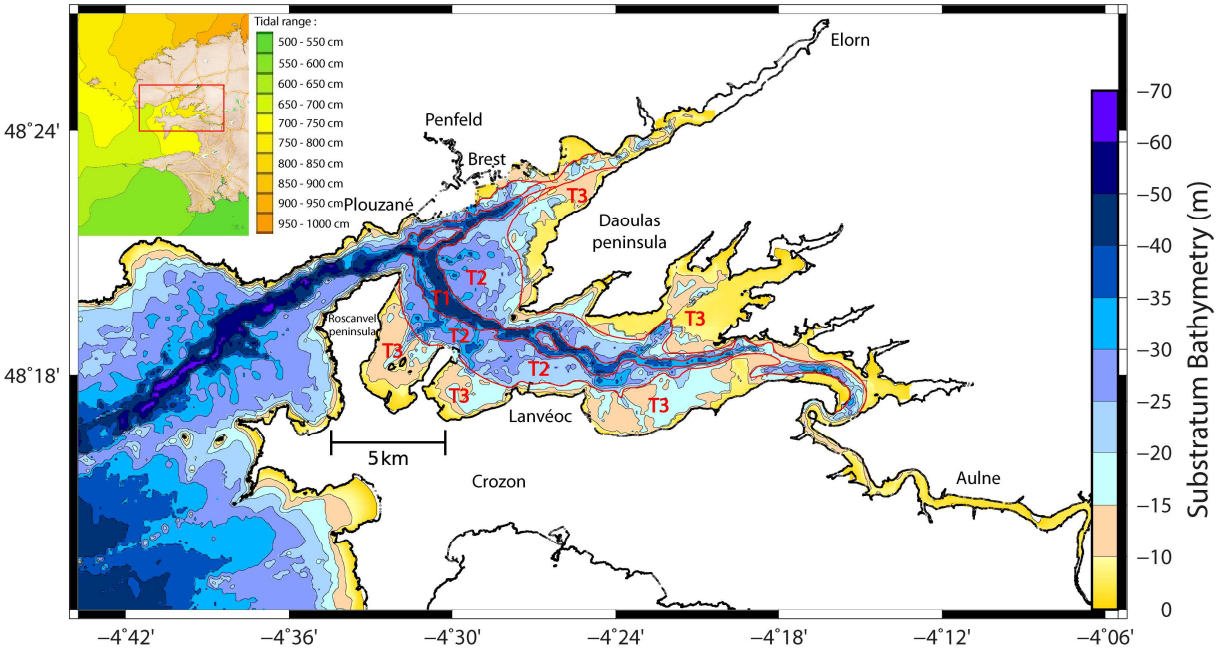

Fig. 53: Bathymetric map of the Bay of Brest basement relative to the present-day mean sea-level. The inset-map, modified from SHOM (2015a), shows the tidal range of an exceptional spring tide (tidal range between 7.5 and 8 m). T1: main channel. T2: first terraces stage. T3: the shallowest terraces.

During the tertiary era the Bay of Brest emerged several times, because of glacio-eustatic movements and the basement was eroded by paleo-rivers during low sea-level stages (Hallegouet et al., 1994). It resulted in three morphological domains (Fig. 53, Fig. 54): T1 is the main channel, where paleo-rivers flowed; T2 consists of the first stage of terraces, above T1; T3 corresponds to the shallowest terraces close to the present-day shoreline, localized in sheltered coves and bays. A network of secondary channels within T2 and T3 connects these domains to the main channel (T1). More details on the geomorphology of the Bay of Brest are provided in Gregoire et al. (2016).

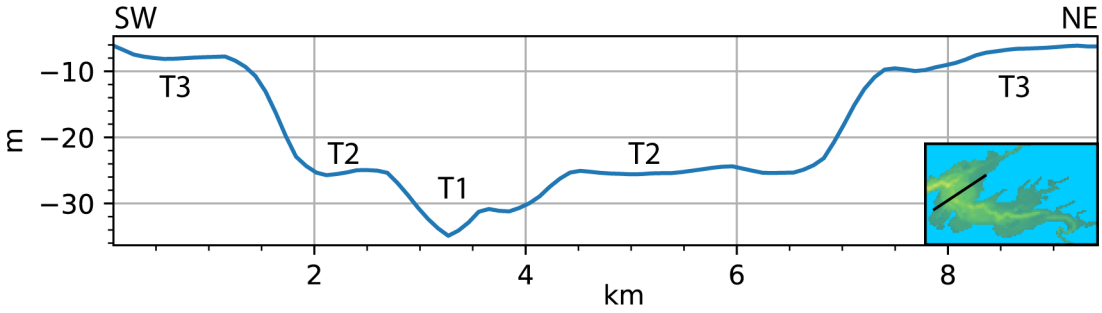

Fig. 54: Present-day bathymetric section relative to the present-day sea-level. T1: main channel. T2: first terraces stage. T3: the shallowest terraces.

The 180 km2 bay can be divided in two parts. The central part has its limits at two straits, the first formed between Plouzane and Roscanvel and the second between Lanveoc and Daoulas peninsula (Fig. 53). The upper part (can be named inner zone too) is at the east of the strait between Lanvéoc and Daoulas peninsula (Fig. 53). The outer zone corresponds to the Iroise sea and is not analysed in this study.

4.2.2. Hydrodynamic characteristic of the Bay of Brest

The Bay of Brest is classified as a macrotidal system (Fig. 53). The mean spring tidal range is 5.9 m and the mean neap tidal range is 2.80 m in Brest harbour (Beudin, 2014). The Bay is protected from oceanic waves thanks to the strait between Plouzané and Roscanvel peninsula. This strait is 1.8 km wide connecting the Iroise sea and the Bay of Brest. The semi-enclosed configuration of the Bay of Brest induces a very weak swell climate compared to the energy regime outside the Bay. Indeed, the swell is attenuated at the passage of the strait by the refraction on the edges and is diffracted at its exit. Thus, while the mean annual wave height is 2.4 m further offshore in the Iroise Sea, in the port of Brest, the mean annual significant wave height value is about 0.25 m (Monbet and Bassoullet, 1989). This statement is supported by the example of the Bella storm, which exposed the Iroise Sea to swells of almost 10 m and at the same time the Bay of Brest suffered waves of less than 1 m (Fig. 55a and 55b). Under classic forcing (waves from WSW, max 3 m in the Iroise Sea and 33 km/h wind from the NE, Fig. 55c) the Bay of Brest experiences waves around 0.22m (mean, Fig. 55d). In the latter case, the wave orientation in the Bay clearly indicates that it is forced by the NE wind. Even if the wind sea takes over the ocean swell inside the Bay, wind remains a minor forcing because of the short fetch of the Bay of Brest (~25 km max, Stéphan et al., 2012). This particular configuration allows us to focus on the tidal dynamic.

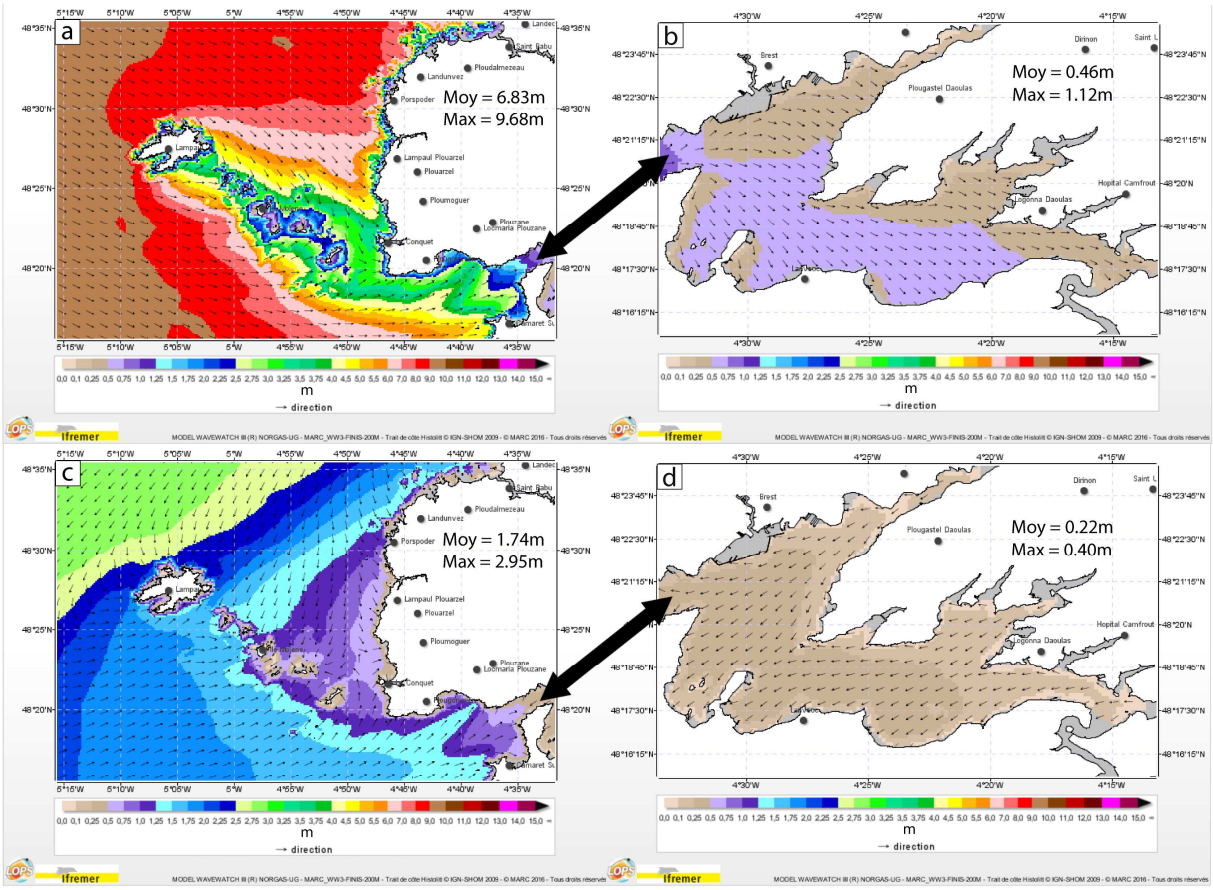

Fig. 55: Significant wave height in the Iroise Sea (a and c) and in the Bay of Brest (b and d). a and b are screen shot at 2 p.m. on 28/12/2020 during the Bella storm (wind: 40 km/h from NW, waves: from WSW). c and d are screen shot at 11 a.m. on 25/04/2021 (wind of 33 km/h from NE, waves from WSW), which represent a usual forcing over French Brittany coast. Data and illustrations from the marc operational forecast system (see website: http://marc.ifremer.fr/).

4.2.3. Holocene history

During the last deglaciation, the sea-level rose quickly at the beginning of the Holocene in Brittany and gradually slowed down until it reaches today's level (Goslin et al., 2015). During the rise of sea-level in the Bay of Brest, four sedimentary units were deposited: U0, U1, U2 and U3 (Gregoire, 2016). The Holocene story of the Bay of Brest started with a mean sea-level 35 m lower than today. At this time (10 000 years ago) only the main channel was submerged (T1). Unit U0 was deposited at this time and was mainly composed of coarse continental sediments. Unfortunately, no samples could have been taken from this unit, so this interpretation relies only on seismic facies (Gregoire et al., 2017).

At 9000 years cal BP, sea-level reached −26 m from the present-day level, resulting in water submersion on T2 terraces (intertidal area, Fig. 57). This age marked the start of U1 deposition (Fig. 56). The sea-level rise was rapid during the deposition of U1 and at 7500 years cal BP, the sea-level exceeded the elevation of most of the T3 terraces, placing them in the intertidal area (Fig. 57). During the interval 9000–7000 years cal BP (Unit 1 deposition), most of deposits were muddy and preserved in the T3 domain. No deposit was preserved on T2 and only three patches were recorded in the main channel, two in the central part and the thinnest between Lanvéoc and Daoulas Peninsula (Gregoire et al., 2017, and Fig. 58 below).

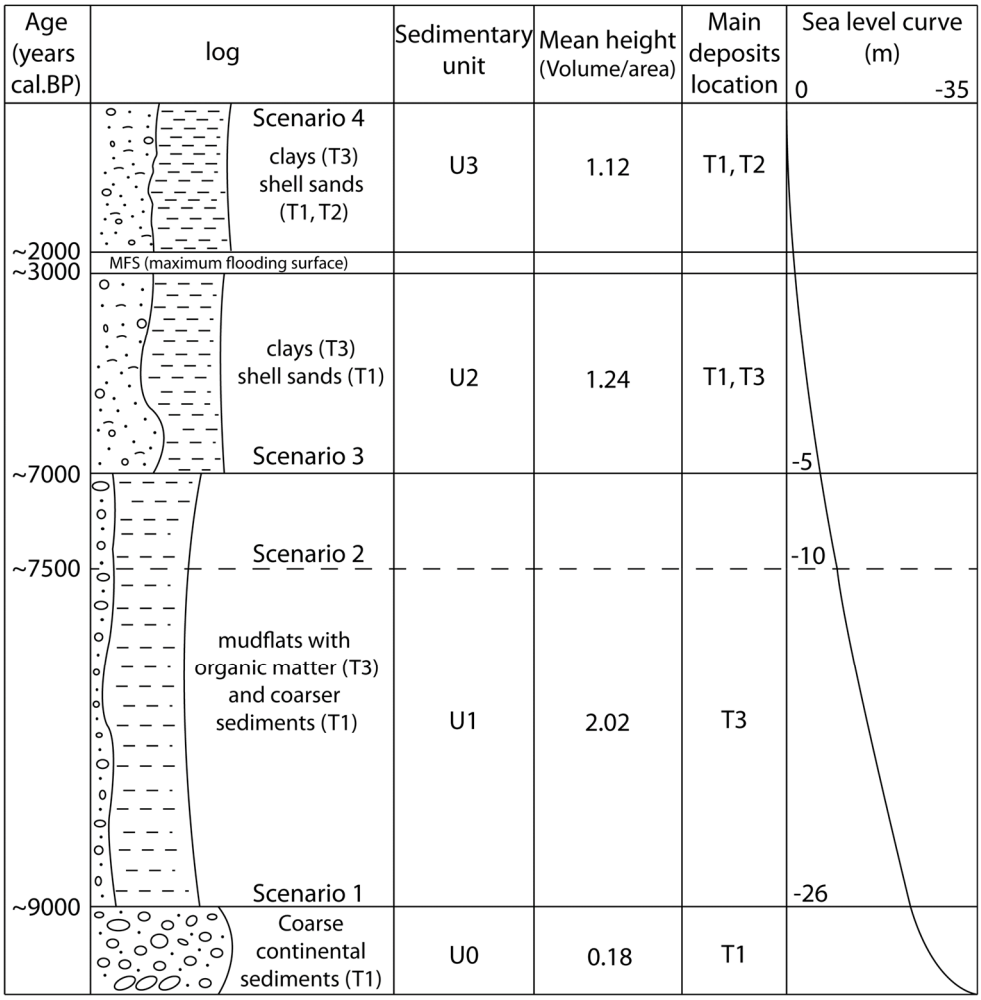

Fig. 56: Stratigraphic log of the Holocene period in the Bay of Brest (modified from Gregoire, 2016). The vertical scale varies with the thickness of the units and the horizontal scale represents the global grain size of the units.

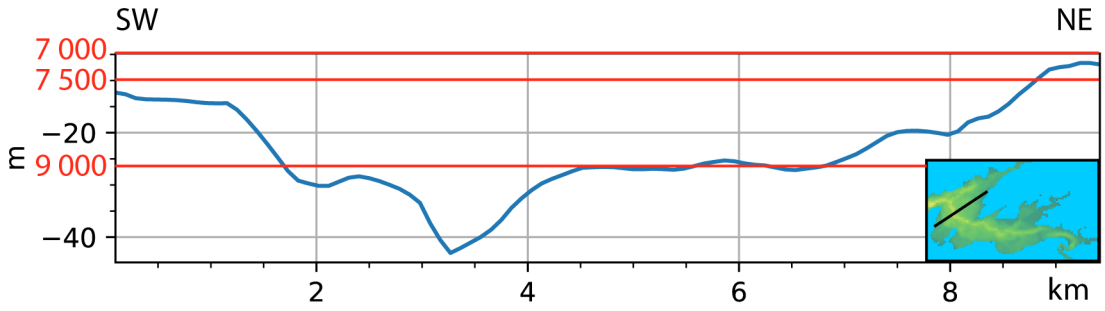

Fig. 57: Top U0 bathymetric section relative to the present-day mean sea-level. Red lines represent the mean sea-level at 9 000, 7 500 and 7 000 years cal BP.

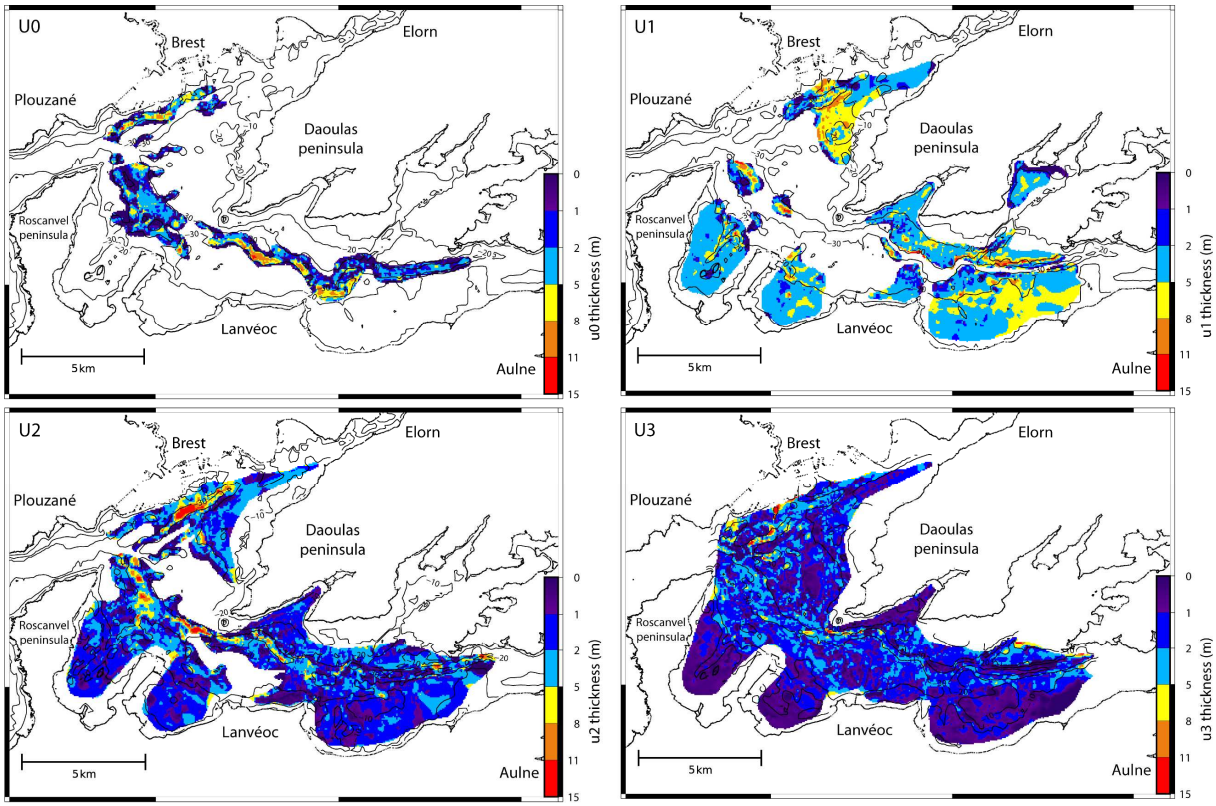

Fig. 58: Thickness maps of sedimentary units U0 to U3 (vertical seismic resolution around 1m) reconstructed with GMT from seismic interpretations of Gregoire (2016).

The beginning of the U2 deposit was estimated at around 7000 years cal. BP with a sea-level of −5 m relative to the present one (Fig. 56, Fig. 57). The water level rose gradually over the interval 7000–3000 years cal. BP until it reached the current sea-level. The MFS (Maximum Flooding Surface), set ~3000 years cal. BP correspond thus to the top of the transgressive U2 (Fig. 58). U2 is interpreted as mainly cohesive sediments on T3 and sandy sediments in the main channel (Gregoire, 2016). No information is available for the sediment's nature present over few areas of T2.

The more recent sedimentary unit, U3, started ~2000 years cal. BP and is still active now (Fig. 56). Deposits related to U3 take place over the MFS surface. They are present over all morphological domains and exceed 5 m in thickness only on rare occasions in the main channel and on T2 terraces (Fig. 58). The map of the present-day sedimentary cover of the Bay of Brest (Gregoire, 2016) shows coarse sands and gravels over T2 at the north of the central area of the Bay and sands at the south. The main channel shows all sizes of sand and the T3 terraces mainly mud. The upper zone is composed of finer sediments, described as a mixture of sand and mud.

4.3. Methodology and tools

The challenge is to rebuild key stages of the paleoenvironmental evolution and run hydrodynamical simulations with the resulting past bathymetries to explore the associated hydrodynamics and its impact on sediment distribution. First, the model and its setup are described in part 3.1. Then, the chosen periods that represent the key steps of the paleoenvironmental Holocene evolution of the study area are presented (part 3.2). The method to rebuild these paleoenvironments

(each defined by their specific bathymetry and sea-level) is explained in part 3.3. Finally, a potential erosion and a potential deposition index are proposed to help correlation between sediment deposits and simulated bottom currents (see 3.4).

4.3.1. The hydrodynamic model (MARS3D)

The code used for this study is the model of coastal hydrodynamics MARS3D (Lazure and Dumas, 2008). It is a finite-difference 3D code that computes tide propagation and associated currents from the resolution of the primitive equations using the hydrostatic equilibrium hypothesis and Boussinesq approximation. It is written in spherical coordinates for the horizontal and sigma coordinates for the vertical.

The Bay of Brest configuration for the present-day is issued by Petton (Pers. Comm). A horizontal Cartesian mesh of 250 m × 250 m is used. We assume some uncertainties in the geological data, in particular linked to sea-level variations, seismic interpretation and seismic covering (Goslin et al., 2015; Gregoire, 2016). A grid finer than 250 m would not be justified compared to our data set and their uncertainties. We look only at major hydrodynamic patterns and finer mesh size is not needed. The water column is vertically discretized into 20 levels to simulate properly the bottom currents (useful in the potential erosion and potential deposition indexes computation, see section 3.4).

The bed roughness distribution is taken uniform over the entire area. Indeed, since the sediment cover is unknown for the past stages in the Bay of Brest, the choice of a uniform roughness length helps not to produce misleading circulation with a badly validated parameterization and facilitate the comparison between the scenarios. It is set constant and equal to 3.35 mm from the Nikuradse formulation using an average grain diameter of 500 µm, which corresponds to the present-day observations and past stage (cores observations from Gregoire, 2016).

The simulations are run with realistic tides over the year 2014 for each selected combination of bathymetry and sea-level. The choice of the year 2014 is motivated by the availability of the validation (tidal gauge, 5 ADCP) and input data (river discharge, tidal spectrum) for that period.

The hydrodynamic circulation model is forced at the western and southern marine boundaries by the entire tidal spectrum (143 components) extracted from the SHOM CST-France (Le Roy and Simon 2003), for each stage simulated. To study tidal currents over paleoenvironments the spectrum could be simplified, however the present-day configuration of the Bay of Brest used in other studies is already validated with the full spectrum only. The tide is very well described around Brittany at present time (atlas of 143 components). However, few data are available for different sea-level around Brittany and especially in the past. Previous works explored the possible effects on some tidal components of a higher sea-level (M2, S2, N2, M4, MS4 and MN4, Idier et al., 2017) and of a lower sea-level (M2, Uehara et al., 2006; Ward et al., 2016 and paleo-tidal ranges, Goslin et al., 2015). The simulations at large scale of Uehara et al. (2006) and Ward et al. (2016) explore the evolution of the M2 component of the tidal spectrum over the last 16 and 21 thousand years in the northwest European shelf seas. The M2 elevation amplitudes calculated in Ward et al. (2016) are equal at 0 ka and at 8 ka (between 2 and 2.5m, Beudin, 2014; Ward et al., 2016). Goslin et al., 2015 also show an equivalent tidal range between the present-day and 6 ka, for the Porsmilin site (7 km from the entrance of the Bay). Ward et al. (2016) reveals that M2 elevation amplitude is about 0.5 m higher at 10 ka than at present-day, at the NE point of Brittany (about 15 km from the entrance of the Bay). A harmonic decomposition is performed for the Bay of Brest and reveals that the M2 component dominates in the Bay of Brest. Its amplitude is about two times higher than S2 (ellipsis available in supplementary material, and Beudin, 2014). Tidal

component analysis is not developed in this study that focuses on the evolution of tidal currents distribution and its impact on the seafloor. Even if the harmonic decomposition analysis is not developed in this study, it allows to consider an equal forcing in all the scenarios (comprise between 9000 years cal BP and the present-day). M2 amplitude is under estimated by 0.25 m at 9000 years cal BP (mean between 8 and 10 ka), this is considered acceptable in comparison to other set-up hypothesis (uniform bed roughness, river discharges) and data uncertainties (seismic Gregoire, 2016, sea-level Goslin et al., 2015). Furthermore, Goslin et al., 2015 show a decrease in the tidal range at the entrance of the Bay of Brest of about 30 to 50 cm between 6 ka and 8 ka. Following those simulations, the tide would be rather underestimated for the oldest scenario in this study.

The model is also forced by daily flows of the main rivers: Aulne, Elorn and Mignonne (mean flow in 2014: 30 m^3/s, 10 m^3/s, 1.5 m^3/s). The real flow for the year 2014 is used thanks to the data of the DREAL Bretagne (Regional Directorate for the Environment, Planning and Housing, http://www.hydro.eaufrance.fr/).

This configuration of the Bay of Brest was validated and used in other studies (Klouch et al., 2016; Frère et al., 2017; Petton et al., 2020) and also compared to various datasets (temperature/salinity and ADCP, Petton et al., 2016; 2021). It has demonstrated its ability to reproduce the main characteristics of oceanic flows (tidal amplitude and phase, 3D currents). A further validation is available in the supplementary material of this paper. It concerns currents velocity compared to 5 ADCP (over October 2014 Petton et al., 2016, and on July 16, 2014) and water height compared to Brest harbour's tidal gauge over the whole year 2014. The comparison to hydrodynamic data is possible only for present-day, because of the lack of hydro dynamical data for the past.

4.3.2. Modelling scenarios

We generate a modelling scenario for each sedimentary unit, but U0 environmental context cannot be represented. We do not have enough information about it (no sample and no indication about the age of the layer base) and the mesh size of the grid (250 m) is often larger than the flooded area during this period. On the other hand, the immersion of the different morphological domains is an important paleoenvironmental change that must be simulated. Therefore, four scenarios are built corresponding to major paleoenvironmental changes between the periods of U1 (2 scenarios), U2 (1 scenario) and U3 (1 scenario) deposits.

The first scenario aims at reproducing the tidal dynamics at the beginning of U1 deposits. At this time (9000 years cal BP), the sea-level was −26 m below the present-day level. The bathymetry corresponds to the top of the U0 unit. T2 was in an intertidal domain and T1 was in a subtidal area (Fig. 57).

The objective of the second scenario is to model the final phase of U1 deposits, around 7500 years cal BP The sea-level rose quickly at the beginning of the Holocene from −26m to −5 m. Due to these large sea-level variations, the context was very different throughout the deposit period of U1. In this second scenario, with a sea-level 10 m lower than the present-day, T3 was located in an intertidal area whereas T2 was in a subtidal area. As this scenario aims to represent the terminal deposits of U1 and the chronology of the deposits is unknown within 9 ka and 7 ka cal. BP (U1 deposit period), the input bathymetry chosen is the top of the same unit (Figs. 56 and 57).

The goal of the third simulation is to represent U2 deposit period. The third scenario was run at around 7000 years cal. BP, with a sea-level at −5 m under the present-day level. Seafloor morphology at this time corresponded also to U1 top morphology. The sea-level rose only by 5 m during U2 period, and

no major change was observed on the seismic data. So, only one scenario was built during the U2 deposit (Figs. 56 and 57).

The purpose of the fourth scenario is to reproduce the present-day context. The whole bay is submerged and mostly characterized by subtidal areas. The aim is to represent U3 dynamics which is still active at present day (Fig. 56).

4.3.3. Paleo-bathymetric reconstructions

The paleo-bathymetric reconstructions are based on seismic data collected during several cruises (see the complete list in Gregoire, 2016). The present-day depth of each seismic marker is calculated from the interpretation of the seismic data (Gregoire et al., 2017). Seismic depths in two-way travel time (seconds) is converted to depth (metres) by applying a constant velocity law in the sediment (1800 m/s) and in the water column (1550 m/s) to be consistent with previous studies (Gregoire et al., 2017). Bathymetric maps of the basement and thickness maps of each unit were calculated with GMT (Generic Mapping Tool), using a 50 m spatial interpolation. The geological maps are finely meshed (50m) to prevent over-interpolation of sedimentary deposits. Wider interpolation would change the depositional boundary and the objective is to keep our validation data at the best possible resolution. These maps are then combined with the seabed present-day bathymetric data from the SHOM (2015b) to complete areas where no seismic data were available (the seismic data extension is available in Gregoire et al., 2017). Most of these areas are located in very shallow to intertidal areas, where no ship was able to perform seismic acquisition. So, they are emerged during all the scenarios except the present-day situation. This approximation has no influence on the simulated circulation in the Bay of Brest, it is only performed for numerical purposes. Only in one place bathymetry is overestimated, because gas prevents a proper seismic acquisition and the sediment deposits could not be interpreted. It is located on T3 terraces at the south of the Daoulas peninsula, close to the mouth of the Mignonne River (Fig. 59).

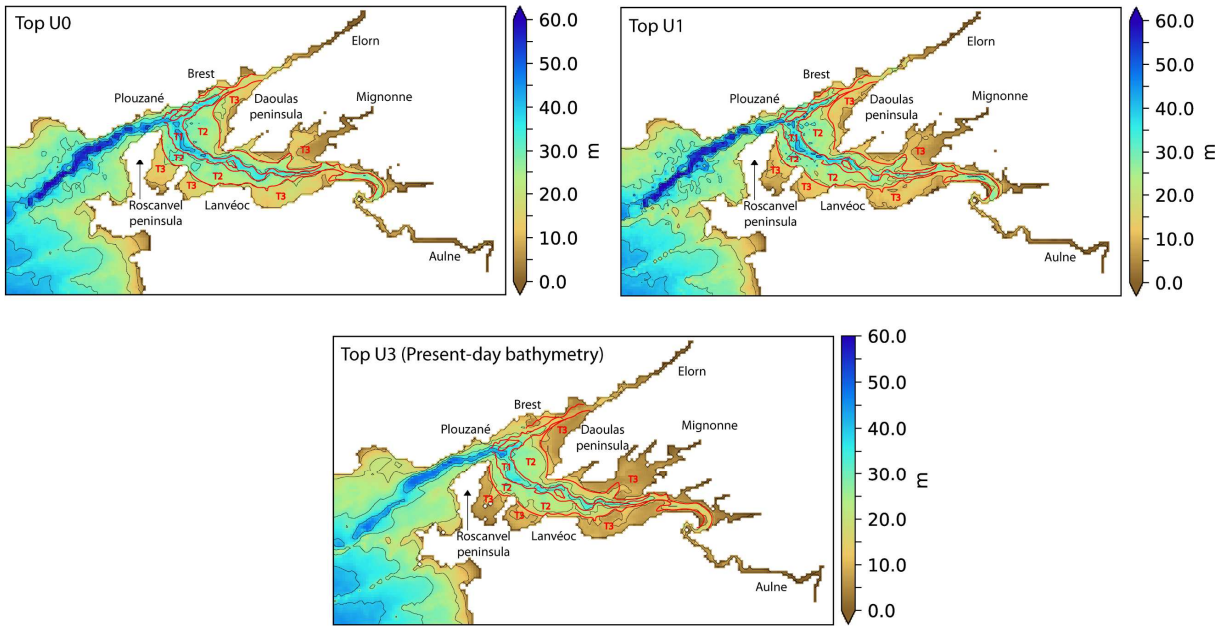

Fig. 59: Bathymetric maps of the top of U0, U1 and U3, relative to the present-day sea-level. Red lines represent the superimposed boundaries of the morphological domains of the basement map (Fig. 53).

U0 thickness is added to the basement map (Fig. 53) to generate seafloor bathymetry for scenario 1 (Fig. 59, Top U0). U1 thickness is added to the first scenario bathymetric map (U0 top, Fig. 59) and the result is the seafloor morphology for the second and third scenarios (Fig. 59, Top U1). The present-day morphological map is created from SHOM's data (Fig. 59, present-day bathymetry). The boundaries of the T1, T2, T3 domains (Fig. 53) are superimposed to each bathymetric map to allow us to see that these domains evolved slightly with sedimentary deposits, during the Holocene transgression.

4.3.4 Potential index calculation

Two different methodologies are used to observe the influence of simulated bottom currents on the seafloor. It seems important to separate sand and mud because of the different behaviour of these two types of sediments. We perform an erosion potential index for non-cohesive sediments (see details below 4.3.4.1). As far as sands are concerned, most of the transport is realised by bedload or saltation (suspension phases are very short), so that no sand can be transported if there is no erosion zone nearby. It is therefore justified to look at potential erosion areas, which reveal the areas where non-cohesive sediments are potentially transported.

Fine particles can be transported in suspension for a long time, and their presence on the bed depends on the probability of deposition, more than on erosion possibility. This is especially true as deposited cohesive sediments are likely to be consolidated and hardly erodible after significant time. Thus, we calculated a potential deposition index (see details below 4.3.4.2) for cohesive sediments.

4.3.4.1. Potential erosion index

Non-cohesive sediments are characterized by a high settling rate and therefore settles right next to the areas where the stress is strong enough to trigger their reworking (depending on the size of the grain). To account for the variability of the stresses likely to displace a given sediment as a function of tidal range, Cognat (2019) proposed to calculate a potential erosion index that is characteristic of this grain size. This index is constructed as the integral over time of the a-dimensional shear excess. The a-dimensional shear excess is expressed as *F*. It stands for the excess of tidal current shear stress (τ_F) relative to the critical bed shear stress linked to the grain-size classes of sediments (τ_c).

Eq. 3: $$F = \int_t^n (f(t)) \quad (1)$$

With $f(t)$= 0 if $\tau_F(t) \leq \tau_c$

$f(t)$= $\left(\frac{\tau_f(t)}{\tau_c}\right) - 1$ if $\tau_F(t) > \tau_c$

To determine the potential erosion index, it is therefore necessary to know the critical shear stress for each particle size class (τ_c) and the shear stress (τ_f) at each time step (Eq. 4).

Eq. 4: $\tau_F(t) = \rho_{wat} * u^{*2}(t)$ (2)

Where ρ_{wat} is the water density, fixed and equal to 1023 $kg.m^3$ and u^* is the friction velocity at t (Eq. 5). The friction velocity is deduced from an assumed logarithmic velocity profile near the bed, and can be computed from the near bottom velocity provided by the numerical model and a skin roughness length *z0.*

Eq. 5: $U^* = \frac{K.U_{bot}(t)}{\ln(\frac{Z(t)}{Z0})}$ (3)

With *K* constant of Karman equal to 0.4, *z0* the skin roughness taken uniform and equal to 0.001 m. *z* represents the elevation where the bottom velocity U_{bot} is simulated, equal to the half of the bottom sigma layer. The critical shear stress (τ_c), needs to be determined for various granulometric classes. The grain-size classes were estimated from previous work (Gregoire, 2016) and the study of about 10 core samples. Four sedimentary classes are selected D = 0,0030 m ; 0,0011 m ; 0,0002 m and 0,000015 m. For non-cohesive sediments, the critical shear stress (τ_c) for erosion is deduced from the Soulsby (1997) expression of the critical mobility parameter introduced by Shields (1936), based on experimental results. The mobility parameter θ represents the ratio between the flow-induced shear stress and the weight of sand particle in water:

Eq. 6: $\theta = \frac{u_*^2}{(s-1)gD} = \frac{\tau}{\rho(s-1)gD}$ (4)

Where *g* is gravity acceleration, *D* is the particle size, *s* the relative density of particles in water $s = \rho_{sediment}/\rho_{wat}$ and the critical mobility parameter of such particles is determined with Soulsby (1997) equation:

Eq. 7: $\theta_c = \frac{0.3}{1+1.2D^*} + 0.055[1 - \exp(-0.02D^*)]$ (5)

where the non-dimensional diameter D***** is deduced from the diameter D:

$$D^* = D[\frac{(s-1)g}{v^2}]^{\frac{1}{3}}$$

Where v is the kinematic viscosity of water.

Using equation (6), the critical shear stress is deduced from θ_c. The process is repeated for the three different particle sizes: D=0,0030 m ; 0,0011 m ; 0,0002 m. τ_c is calculated for each with Eq. 4 and the values obtained are presented in Tab. 2.

Tab. 2: u_c^* and τ_c parameter for each grain-size classes

	Gravel 3 mm	Sand 1.1 mm	Fine sand 200 μm	Mud 15 μm (3.4.2)
u_c^* (m.s^{-1})	0.045	0.023	0.012	-
τ_c (Pa)	2.072	0.541	0.147	0.1

The potential erosion index F stands for the excess of bed shear stress compared to those values (τ_c, Tab. 2) and therefore represents the ability of tidal currents to rework and transport gravel, sand and fine sand from the seafloor.

4.3.4.2 Potential deposition index

The deposition potential index for cohesive sediments is based on a kind of "symmetric" concept. It represents the integral over time of the probability of mud deposition, following the concept introduced by Krone (1962): the (net) deposition rate of a cohesive sediment is proportional to the probability that a depositing sediment is not re-entrained by near-bottom turbulence, represented by the bed shear stress. Krone (1962) suggests a critical shear stress for mud deposition τ_d, above which deposition does not occur. The probability of deposition P(dep) reads:

P(dep) = 1-τ/τ_d, for $\tau < \tau_d$, and =0 for $\tau > \tau_d$.

By this way, the potential deposition index can be computed for each mesh over the simulation (Eq. 8).

Eq. 8: $$F = \sum_{t=0}^{n}(f(t)) \quad (7)$$

With $f(t) = 0$ if $\tau_F(t) \geq \tau_d$

$$f(t) = \left(1 - \frac{\tau_f(t)}{\tau_d}\right) \text{ if } \tau_F(t) < \tau_c$$

According to literature, τ_d is in the order of 0.1 Pa for fresh (depositing) mud.

4.4 Results

All the results presented in this study intend to show the tidal currents distribution during the Holocene transgression. In order to discuss tidal impact on sediment movements, both depth-

averaged velocity (4.1) and potential transport and deposition indices (4.2) are studied. The first subsection (4.1) aims to describe the ebb and flood tide barotropic currents. Currents directions evolution resulting from sea-level rise is analysed first. Then a percentile 90 is also calculated over one year to analyse the shift of the strongest ebb and flood barotropic currents between different scenarios and therefore try to interpret the evolution through time of the main likely sediment transfer zone within the Bay of Brest. The second subsection shows the potential erosion and deposition index calculated over one year. It allows to decipher where and how tidal near-bottom currents play and have played a major influence on the sedimentation/erosion couple (4.2).

4.4.1. Ebb and flood tide evolution

The results presented correspond to a mean over one flood and one ebb of maximum spring tides. We seek to highlight the changes in barotropic current directions between the different scenarios. Other analyses during neap or medium tides revealed similar directions with less intensity and a smaller spatial extension in general. Strongest currents (characterized by the largest spatial extension and the strongest velocities) will likely trigger much more (or of higher amplitudes) erosion or deposition processes. It is therefore more interesting to observe trends of a spring tide cycle.

During the first scenario (9000 years cal BP), ebb and flood tidal currents show the same patterns: they are confined in the deepest part of the Bay in the main channel T1 (Figs. 60a and 61a). Ebb and flood display the same orientation and therefore currents are almost only bidirectional.

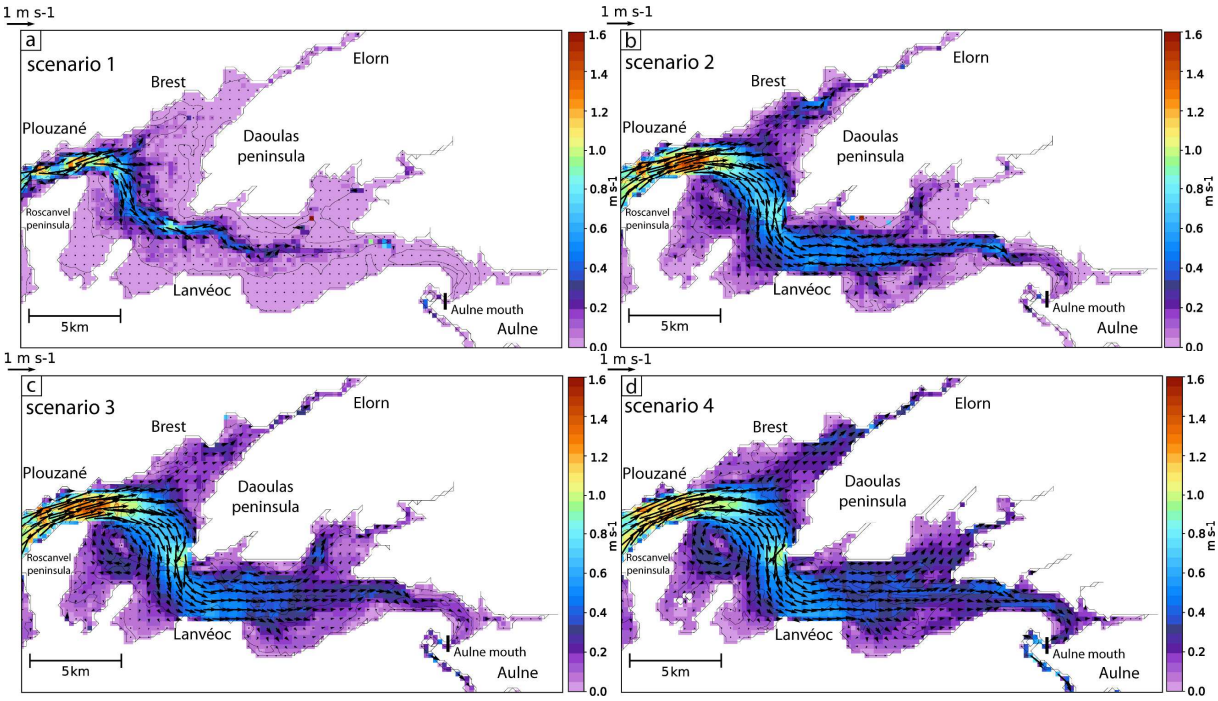

Fig. 60: Mean velocity and direction of tidal currents over one flood of maximum spring tide. a: scenario 1 (beginning of U1 deposits); b: scenario 2 (end of U1 deposits); c: scenario3 (beginning of U2 deposits); d: scenario 4 (top U3, still active).

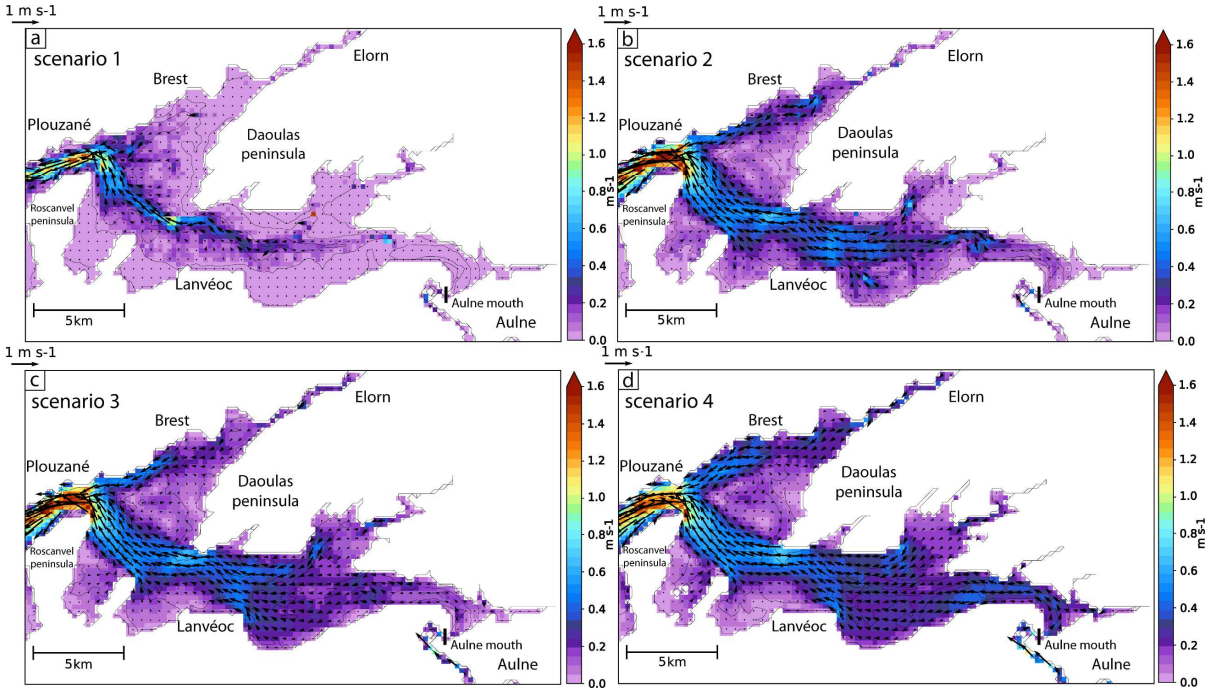

Fig. 61: Mean velocity and direction of tidal currents over one ebb of maximum spring tide. a: scenario 1 (beginning of U1 deposits); b: scenario 2 (end of U1 deposits); c: scenario3 (beginning of U2 deposits); d: scenario 4 (top U3, still active).

1500 years later, the sea-level has risen by 16 m, the flow of the ebb and flood tides is function of the coastline morphology. In the centre of the Bay, straits (between Plouzané and Roscanvel peninsula and between Daoulas Peninsula and Lanvéoc) concentrate tidal energy and force the flood to flow through the north of the main channel and the ebb southwards of the central zone (Figs. 60b and 61b). In both cases, these water flows form an anticyclonic gyre, which is twice faster during flood than during ebb tide (Figs. 60b and 61n: 0.2–0.3 and 0.1 m/s respectively). The ebb and flood currents remain confined within the main channel in the upper zone of the Bay of Brest (upstream of the strait between Daoulas Peninsula and Lanvéoc), which is shallower than in the centre (T1 = 30–40 m in the centre and 20–30 m in the upper area, with a present-day sea-level). As T2 extension is smaller and smaller toward the Aulne mouth, T1 represents most of the subtidal domain in the upper area. The transition from the (very flat) T2 terraces into subtidal domain allows the tidal currents to extend over a much larger area. The new larger extension of T2 terraces permits the ebb and flood currents to propagate over different locations in the central zone (flood tide over T2 at the north and ebb tide over T2 and T1 at south) and form structures like the gyres.

In the third scenario (7000 years cal BP), ebb and flood directions are similar to scenario 2 in the centre of the Bay. The gyre grows in the centre and shows higher velocity during flood tide (0.3 m/s, for the southern part of the gyre, Fig. 60c). The major changes occur in the upper part: water flows are no longer confined within T1 domain after the strait between Daoulas Peninsula and Lanvéoc (Figs. 60c and 61c). Here T3 is located in the subtidal area, which allows ebb tide currents to expand over the entire upper zone. Orientation of the flood is triggered by the strait morphology between Lanvéoc and Daoulas peninsula and keeps a spatial distribution mostly over T1 and T2. Ebb and flood current propagate over different locations in the upper zone: flood tide flows to the East over T1 and T2 and Ebb tide flows to the West all over the area. This is due to the same process as the one observed in the centre of the Bay during the scenario 2: an initial flat and large intertidal domain (around 2 and 3 km for terraces in the Bay of Brest) becomes the shallowest subtidal domain.

In the fourth scenario (present-day), ebb and flood tides directions and distributions are similar to those simulated in scenario 3. The size of the gyre at flood tide and the associated velocity are higher than in the previous context (0.3–0.4 m/s, for the southern part of the gyre, Fig. 60d). The gyre at flood tide becomes progressively wider and faster during the Holocene. Besides, the size of the gyre of ebb tide evolves very little during the same period and remains conversely slow. The increasing depth over the terraces allows to demarcate ebb and flood tide currents distribution. Ebb tide shows similar vectors over the entire upper zone (Fig. 61d) while flood direction remains to the East, mainly localized over T1, oriented by the strait between Daoulas peninsula and Lanvéoc (Figs. 60d and 61d). Even if the water depth has increased by 5 m compared to the previous scenario, the submerged area is almost identical. This leads to greater flooding upstream (higher tidal flow) and stronger tidal currents further upstream towards the Aulne and the Elorn rivers than in the previous scenario (Figs. 60d and 61d).

An analysis of currents direction during the river flooding event in February 2014 is performed to check if rivers flows may have also influenced these patterns. We try to quantify how far the Aulne river flow influenced the oscillating velocity signal corresponding to the tide from the river mouth (Figs. 60 and 61). This flooding occurred during neap and mid-tide cycles. The Aulne water discharge induces a downstream flow during flood tide 9 km downstream of the river mouth in scenario 1 and 11 km upstream during scenario 4 (Figs. 60 and 61). The present-day Aulne river flow is approximately three times stronger than the Elorn one. We thus infer that, as even a mega flood does not seem to compete with tide imprints (a fortiori during neap or middle tide), the rivers influence on the hydrodynamics inside the Bay are weak compared to tidal impacts.

In order to understand the evolution of the areas under the influence of high barotropic ebb and flood tides, the 90 percentile is computed for each of them and for each scenario. The 90 percentile helps to look at the tidal current's maximum extent over the entire simulation and enables to remove potential excessive values. The objective is to identify the major changes in potential sediment transfer zones, with the analyse of the evolution of strongest currents over morphological domains between scenarios.

In scenario 1 (9000 years cal BP), the strongest currents (0.6 to more than 1 m/s) are located over T1. Ebb and food tides currents are located in the same places (Figs. 62a and 62b). Therefore, suspended matter transfer likely occurs mainly over T1.

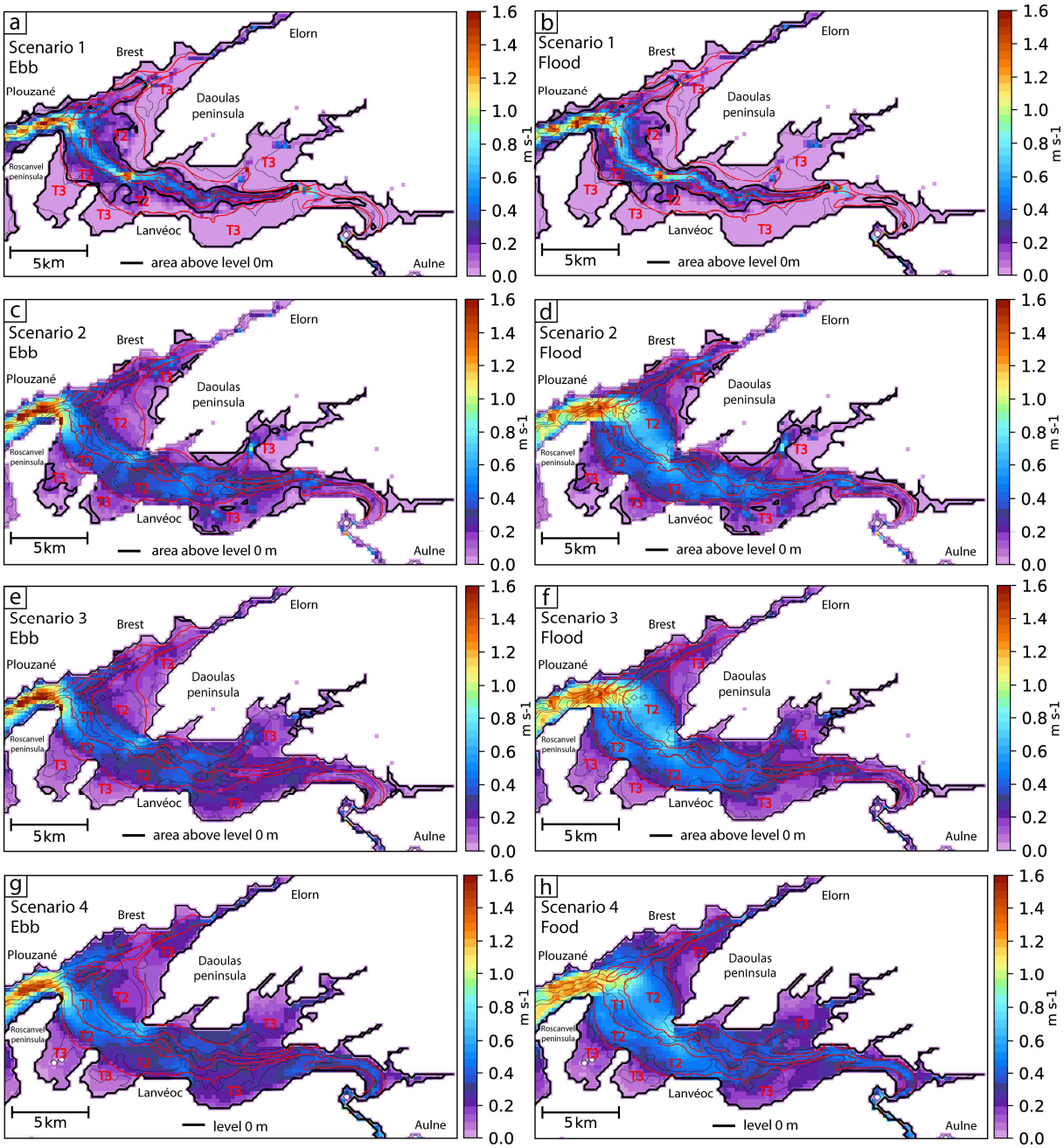

Fig. 62: Percentiles 90 of barotropic currents over one year, for ebb (a, c, e, g) and flood (b, d, f, h) tides during each scenario. The level 0m represents the mean sea-level of the scenario and red lines are the limits of the morphological domains.

In scenario 2 (7 500 years cal. BP), strongest currents (0.4–0.8 m/s, less strong than previously) extend to T2 in the centre of the Bay. Strong flood tide currents are visible over the entire T2 terraces with higher velocity at the north of the main channel (Fig. 62d). Strong ebb tide currents are observed south of the central zone over T1 and T2 (0.4–0.8 m/s, Fig. 62c). Most of the potential suspended sediment transport therefore shifts from T1 in scenario 1 to T2 in scenario 2. Upstream of the strait between Daoulas Peninsula and Lanvéoc, strongest velocities of ebb and flood tides are mainly localized over T1 and in secondary channels that connect T3 and T1 (0.4–0.7 m/s, Figs. 62c and 62d).

In scenario 3 (7000 years cal BP), the locations of high intensity of ebb and flood tides areas are similar to those of the previous scenario (0.4–0.8 m/s, in the centre of the Bay), but their extents are slightly larger (Fig. 62e and 62f). The biggest changes occur in the upper area: the flood velocity decreases on T1 compared to scenario 2 (0.3–0.4 m/s, Fig. 62f) and the ebb tide is faster on T3 than on T1 (0.25 m/s and less than 0.2 m/s, Fig. 62e).

In scenario 4 (present-day), ebb and flood display the same pattern as in the 2 previous scenarios in the central part (0.4–0.8 m/s, Fig. 62). Between Brest and Daoulas peninsula over all the T3 terraces ebb and flood velocity is around 0.2 m/s (Fig. 62g and 62h). In the upper part, T3 terraces are mostly affected by ebb, but with higher currents (0.3 m/s, Fig. 62g). Strong currents are simulated more upstream toward the Aulne river than in scenario 3 (0.4–0.6 m/s, Fig. 62g and 62h). The present-day context presents the highest potential transport for suspended sediments over T3 (Fig. 62). Only the two terraces located at the south of the central zone, between Roscanvel peninsula and Lanvéoc are less impacted by tidal flows, because they are protected by the coastline (Fig. 62).

These percentiles and currents directions reveal an evolution of the location of main tidal currents: (1) They are confined in the main channel (T1) with high velocities during ebb and flood tides and opposite directions. (2) As soon as the area surrounding T1 becomes subtidal (T2 at 7500 years cal. BP in the central zone and T3 at 7000 years cal. BP in the upper zone), velocities decrease within the main channel and strongest currents spread over the domain surrounding T1 (section 4.2.2). The sea-level rise over a terrace strongly increases the submerged area (due to a very flat morphology). This leads to a differentiation between ebb and flood tide current distribution, which is mainly influenced by straits morphology. It is the strait between Lanvéoc and Daoulas that leads the ebb over T1 in the central zone and the flood over T1 in the upper zone. Another effect of the strait influence is that currents are always eastwards at north of the central zone and always westward at the south. (3) The submerged area between scenario 2 (7500 years cal. BP) and 3 (7000 years cal. BP) increases a lot with the passage in subtidal domain of most of the T3 terraces, while sea-level increases by 5 m. Currents spread over a much larger area in the estuary and less intense currents than before reach the upper zone. The submerged area between scenarios 3 (7000 years cal. BP) and 4 (present-day) is almost the same, most of the T3 terraces are already in subtidal domain in scenario 3 and the sea-level increases by 5 m. The inundation upstream increases and strong tidal current spread further upstream into the estuary in scenario 4 than in scenario 3.

Changes in tidal current intensity are mainly related to the increase of the basin width in relation to the water height. Higher velocities are observed in the upper part of the estuary when the sea-level increases and not the submerged surface; and weaker velocities are observed upstream when the submerged surface increases and not the sea-level.

4.4.2. Bottom currents impact on the seafloor

This section aims to explore the influence of tidal bottom currents on the seabed which means on the erosion/deposition patterns via the analysis of a potential erosion index for non-cohesive sediments and a potential deposition index for cohesive sediments (section 4.3.4). Those indexes help to make the link between the simulated currents and the sediment records, by estimating the potential loss or deposition of sediment induced by bottom tidal currents over one year.

In the first scenario (bathymetry at the top of U0 and sea-level at −26 m relative to present-day), all grain-size classes present a high erosion potential in the main channel, except gravels which are only mobilisable in the narrowest parts of the channel (Fig. 63). The intertidal zone (T2 domain) shows a

much lower erosion index (Figs. 63b, 63c, 63d) and the highest potential deposit for mud (Fig. 63a). The T2 terraces may receive most of the cohesive sediment deposits (mud) and some fine sand.

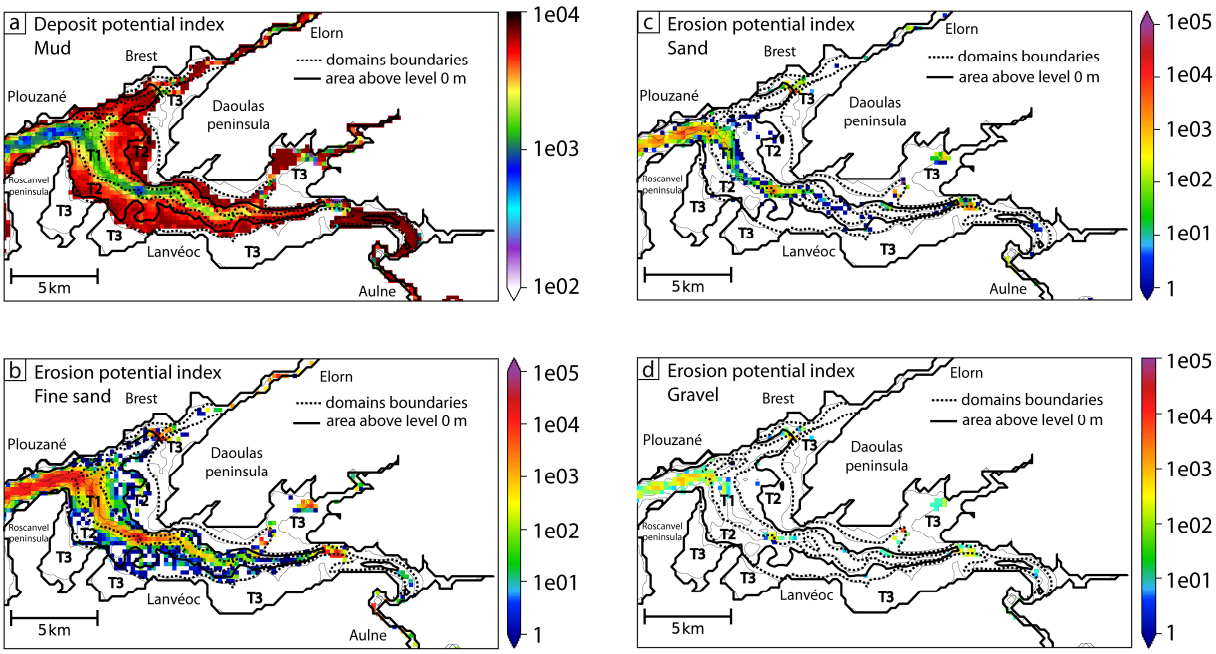

Fig. 63: Deposition potential (a: mud) and erosion potential indexes (b: fine sands, c: sands, d: gravels) calculated for scenario 1 (beginning of U1 deposits). Black lines represent the area above the mean sea-level and white zones are equal to 0.

In the second scenario (bathymetry at the top of U1 and sea-level at −10 m relative to present-day) the erosion potential index is the highest over T2 domain in the centre of the Bay of Brest. The action of the currents on the bottom is less intense in T1 than in the previous scenario (Fig. 63, Fig. 64) and the T2 domain displays currents able to carry sands and fine sands (Fig. 64b and 64c). The deepest part of T1 and on slopes between T2 and T3 become the most favourable areas for the deposition of sands and fine sands. The maximum potential deposit for mud is located over T3 terraces (Fig. 64a). Over T1 in the upper part of the Bay of Brest, fine sands potential erosion is similar as over T2 in the centre and is strong in secondary channels too (Fig. 64b). Fine sands are therefore transported to T2 and T3 in the upper zone.

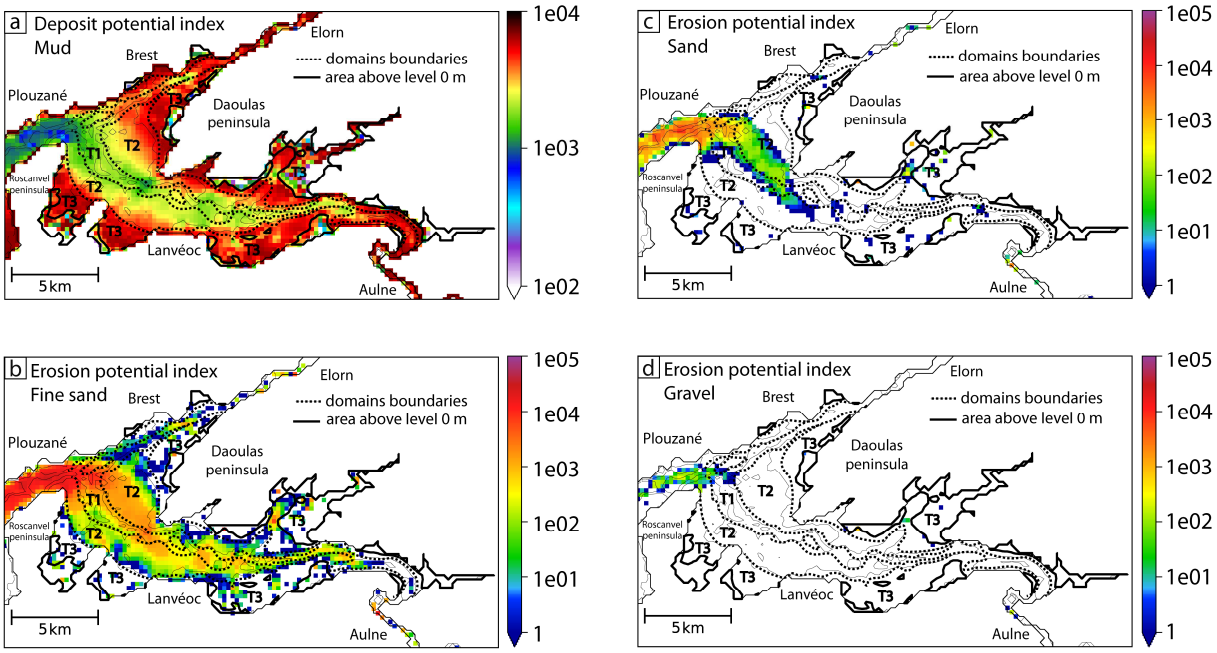

Fig. 64 : Deposition potential (a: mud) and erosion potential indexes (b: fine sands, c: sands, d: gravels) calculated for scenario 2 (end of U1 deposits). Black lines represent the area above the mean sea-level and white zones are equal to 0.

In the third scenario (bathymetry at the top of U1 and sea-level at −5 m relative to present-day), the centre of the Bay of Brest displays a similar potential erosion and deposition as in the second scenario, but the area with highest erosion potential is more extended at the south of the centre of the Bay (Figs. 64 and 65). The potential deposition of mud is the highest over T3 in the central zone (Fig. 65a). In the upper zone, in the main channel (T1) the potential erosion index for fine sands is tenfold lower than in scenario 2 (Figs. 64b and 65b). The distribution of the potential deposition for mud also highlights a decrease in bottom current velocity, which is greater on T1 and more uniform throughout the upper zone than in the previous scenario (Figs. 64a and 65a).

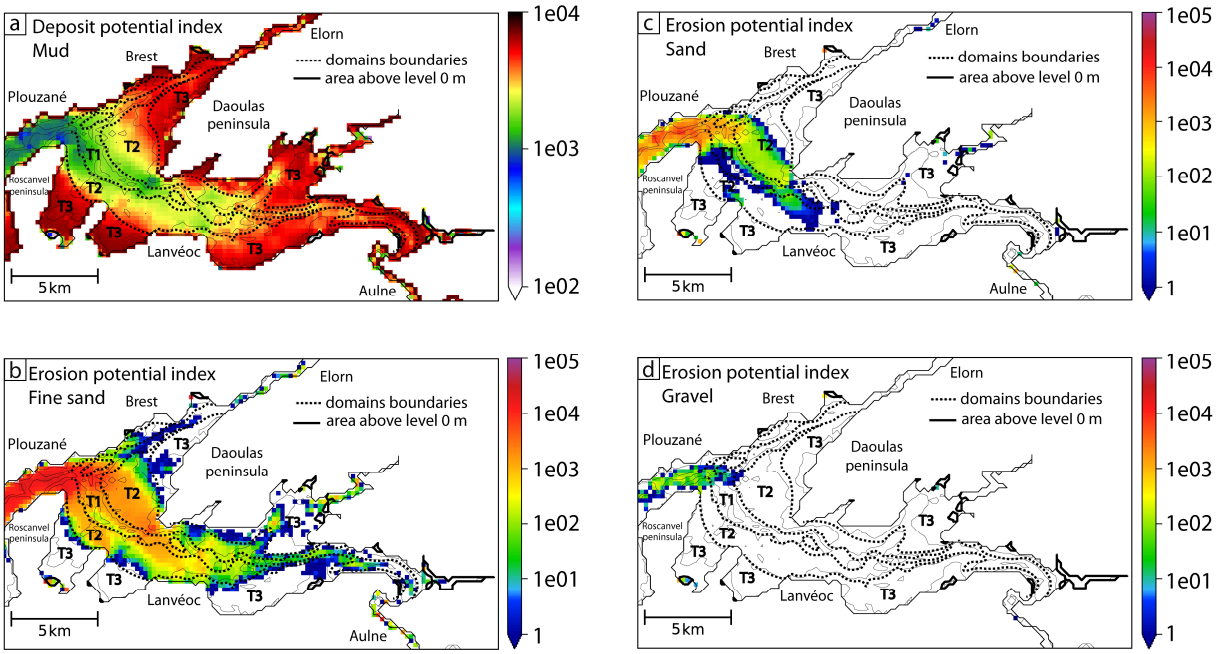

Fig. 65: Deposition potential (a: mud) and erosion potential indexes (b: fine sands, c: sands, d: gravels) calculated for scenario 3 (beginning of U2 deposits). Black lines represent the area above the mean sea-level and white zones are equal to 0.

During the scenario 4 (present-day bathymetry and sea-level), the areas of potential erosion of all grain-size classes cover a larger area and show a similar intensity than the previous scenario (Figs. 65 and 66). The deepest zones (T1) are still less affected by potential erosion than in the T2 terraces in the centre. The potential deposition of mud displays the highest values over T3, but these values decrease over T3 in the upper zone compared to scenario 3 (Figs. 65a and 66a). New areas of strong bottom action appear near the river mouths in this scenario (Aulne and Elorn). In those areas the potential mud deposit is equivalent as in the centre (around, Fig. 66a) and even sands can be mobilized close to the Aulne river mouth (Fig. 66c).

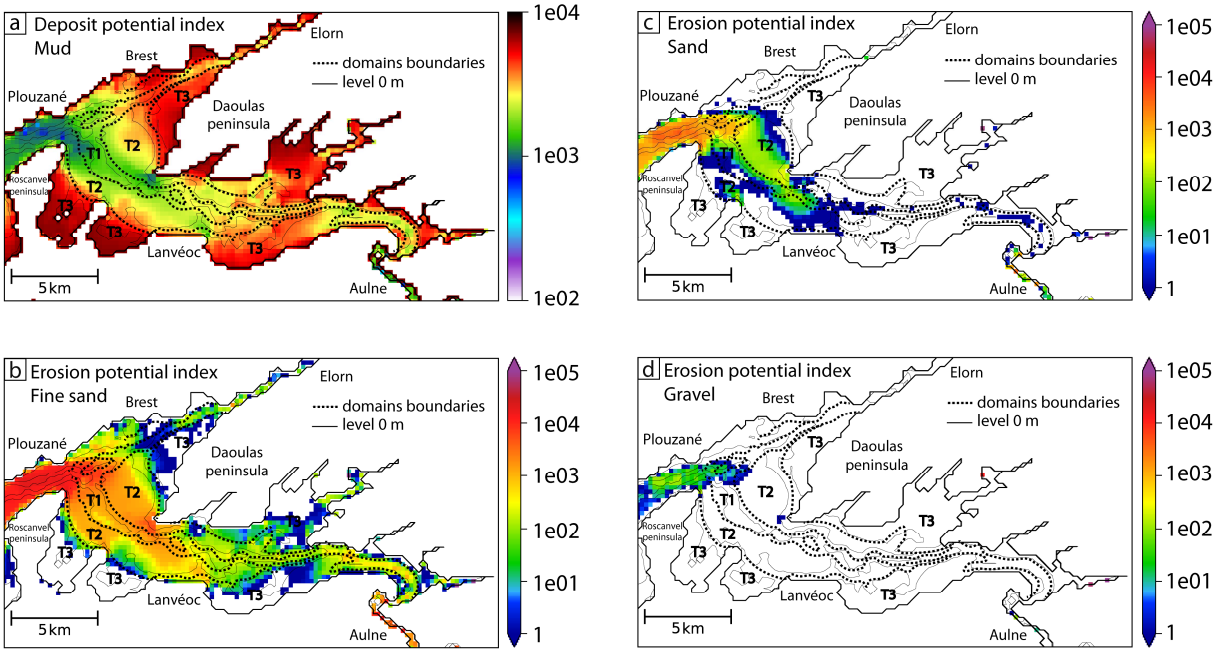

Fig. 66: Deposition potential (a: mud) and erosion potential indexes (b: fine sands, c: sands, d: gravels) calculated for scenario 4 (top of U3 deposits, still active). Black lines represent the mean sea-level and white zones are equal to 0.

The estimates of potential erosion and deposition indexes allow us to correlate major trends between simulated hydrodynamics and sediment records. The erosion potential indexes are first mostly localized in the main channel, then with sea-level rise, the high erosion potential extends to T2 domain in the centre of the Bay (between scenario 1 and 2, Figs. 63 and 64). In the same time strong potential deposition index for mud moves from T2 to T3, when T3 are intertidal terraces (scenario 2). All the muds deposited over T2 in scenario 1, are removed during scenario 2 and settle over T3. This is consistent with the deposition of U1, with only a few accumulations in the main channel in the centre of the Bay and most of the preserved sediments are observed on T3 domain (Fig. 58). Then, during scenario 3 bottom currents display similar patterns in the central zone, with a higher ability to carry non-cohesive sediment at the south (Figs. 65a and 65b). Between scenarios 2 and 3 (Figs. 64 and 65), the values of potential erosion decrease within the main channel in the upper area. Upstream of the strait between Daoulas Peninsula and Lanvéoc, the potential deposition of mud increases over T1 between scenario 2 and 3, and during U2 deposits are observed over all the upper zone. Only T2 at the north of the main channel in the centre and between Daoulas peninsula and Lanvéoc is under erosion (Fig. 58). During scenario 4, potential mud deposition decreases over T3 in the upper zone compared to the previous scenario and potential erosion of fine sands shows that bottom currents are able to transport fine sands to or from the river mouths (Fig. 66b). In the centre of the Bay similar patterns are observed as in scenario 3. U3 thickness map shows the lowest thicknesses over T3 compared to U1 and U2 and important deposits over T1 (Fig. 58). That correspond to the potential erosion and deposition simulated, but several meters of U3 sediments are recorded over T2 in the central zone and remain unexplained (Fig. 58). The sedimentary map of Gregoire (2016) provides more information about the grain-size classes repartitions for the present-day: (i) T2 is mainly covered by very coarse non-cohesive sediments at the north of the main channel, (ii) sands and fine sands predominate at the south and within the main channel (T1), and (iii) muds are predominant over T3. (iiii) The surface coverage of the upper part is made mostly of cohesive sediments with a sandier mixture on T1 and T2 than T3. We simulate a similar repartition in the central part, with sands transport mostly at the north,

fine sands that can be mobilized over T2 and T1 at the south of the central zone and strongest muds potential deposits over T3 (Fig. 66). In the upper area, the sediment map from Gregoire (2016) and the computed indexes show a good match too: potential deposition index for muds is higher over T3 than T1 and T2, and only fine sands are able to be transported by bottom currents in the upper area (mostly over T1 and T2, Figs. 66a and 66b).

In the centre, the hydrodynamic patterns remain similar since the scenario 2, strong currents over T2 transport cohesive sediments towards the shallowest morphological domain (T3, scenario 2, 3 and 4, section 4.1) and towards the remote and quiet zones of the estuary, both are the only places where muds display a strong potential deposition index (Figs. 63a, 64a, 65a, 66a). Potential erosion index indicates that non-cohesive sediments (except gravel) are presumed to be transported mostly over T2 in the centre and deposited in the main channel (T1) and on slopes between T2 and T3 (both located at the edges of T2 terraces, Figs. 64, 65, 66).

4.5. Discussion

In this study, we proposed paleotides reconstructions and discussed their impact on the distribution of the sedimentary units of the Bay of Brest, but some uncertainties need to be taken into account. To extend the bathymetric coverage on T3, at the south of the Daoulas peninsula, present-day bathymetric data were used. We do not know what is the effect of this overestimated bathymetry on the distribution of tidal currents in the upper zone. The ebb tide could have flowed over this part of T3 domain earlier than in scenario 3, depending on U2 and U3 thicknesses. The presence of Brest harbour also prevents a bathymetric reconstruction at the north of the central zone, because no records are available due to human modifications. In this area past hydrodynamics cannot be simulated correctly.

The choice to carry out a second scenario for U1 allows to highlight the influence of a significant coastline movement on the distribution of tidal currents. However, the exact date of this paleoenvironment (T3 intertidal, scenario 2) is unknown, because the chronology of deposition within U1 is unknown too.

The composition of each paleoenvironment seafloor is unknown and for this reason the roughness length is kept uniform. This can change the currents velocities, but it has a very slight influence compared to bathymetric and sea-level evolution.

The rivers discharge evolution is the greatest uncertainty of the study even if the Bay is affected by small rivers. In the absence of records for past stages, a true water discharge cannot be implemented. The use of a hydro-sediment model is the only way to calibrate rivers discharge with a sensitivity analysis, by comparing the sediment rate simulated and the one from each paleoenvironment over the estuary. This methodology can be supported by qualitative information from palynological studies (Fernane, 2014; Lambert, 2017).

The last incertitude is about the tidal amplitude during the first scenario. The amplitude of M2 component could be under estimated of about 0.25 m in our study (Ward et al., 2016), with an M2 amplitude of about 2 m in the Bay of Brest at the present-day (Beudin, 2014). Or conversely the entire tidal range could be overestimated by 0.50 m or more (Goslin et al., 2015) The consideration of the evolution of forcing in the past represent a great difficulty as no data are available. The quantification of their respective influence on hydro-sediment dynamic is a perspective for a future work. A deeper

analysis of forcings (especially rivers discharge and tide) can help to understand past interactions in estuaries and their impact on estuaries filling.

Our reconstructions focused on the distribution of sedimentary units U1, U2 and U3 in the Bay of Brest. At the beginning of U1's deposition (9 000 years cal. BP, sea-level −26m), the main channel (T1) concentrated the strongest currents, which prevented the deposition of cohesive sediments. Muds were directed towards the intertidal domain (T2) whereas sands and fine sands were transported upstream and downstream by the alternating ebb and flood tides, eventually triggering sand bars. The rapid sea-level rise moved T2 terraces into subtidal domain and T3 into intertidal domain at 7 500 years cal. BP (sea-level −10m). The submerged area increased considerably, allowing tidal currents to extend to T2 domain in the central area. The straits (between Plouzané and Roscanvel peninsula, and between Daoulas peninsula and Lanvéoc) oriented ebb tide southward and flood tide northward in the central zone. High flood velocities in the entrance of the Bay of Brest induced an anti-cyclonic gyre in the centre of the Bay, with higher velocities at the North than at the South of the main channel. In this configuration the sediments previously deposited on T2 were eroded and transferred on T3 terraces. Non-cohesive sediments were mainly transported on T2 and deposited at the edge of the T2 terraces (slopes between T2 and T3 and into the main channel T1). This change in currents distribution explained the absence of muddy sediment within U1 over T2 and their records over T3. In the upper zone, strong flood and ebb tide currents in the main channel prevented sediment deposition during all U1 deposit period.

Even if the sea-level rise slowed down during U2 deposits (Goslin et al., 2015), T3 terraces also became subtidal (sea-level -5m) at 7 000 years cal. BP It marked the start of U2 deposits. The currents distribution remained similar to the second scenario in the centre, still influenced by the straits morphologies, but characterized by faster currents and greater extension over T2 than during the previous 7 500–7 000 years cal. BP period. U2 sandy sediments settled within the main channel and on slopes between T2 and T3, whereas muddy sediment settled on T3. Ebb tide flowed over the whole area in the upper zone, while flood tide was orientated towards T1 and T2 by the strait separating the central and the upper part of the Bay of Brest. The T3 flooding considerably increased the area over which the tidal currents flow, while the sea-level raised only by 5 m. Slower currents reached the upper zone and permitted U2 sediments to settle over the whole upper zone. They contained mainly mud mixed with fine sands on T1 and T2.

Then, between 7 000 years cal. BP and the present-day the velocity of the sea-level rise decreased (globally) until it reached the present-day sea-level, while the submerged area did not increase. Currents during U3 were faster than during U2 and the flooding increased upstream in the estuary, towards the river mouths (Aulne and Elorn). Tidal currents were able to transport non-cohesive sediments more upstream in the estuary than the currents during U2 and prevented the deposition of muds close to river mouths (Aulne and Elorn). Muds settled upstream in the rivers and over T3 terraces in smaller quantity than before. The tidal dynamics remained similar as the previous unit during U3 in the central zone, but an important sediment thickness is present over T2 in the centre. U3 is still active at the present-day, so these deposits are potentially still moving such as sand dunes. This hypothesis suggests that non-cohesive sediments were deposited on T2 during the deposition of U1 and U2 but have been constantly recycled for the last 7 500 years. This should be verified with bathymetric acquisition at regular time intervals or high-resolution seismic acquisition.

Our approach focusing on a macrotidal bay (180 km2) over 9 000 years considers much smaller temporal and spatial scales than previous works from the Imperial college (Wells et al., 2007a; Wells et al., 2007b; Wells et al., 2010) and is under the action of less forcings: waves and wind are considered negligible compared to the tide (section 4.2.1.2, Fig. 55) over the entire time-scale. Its

paleoenvironmental evolution over the last 9 000 years (bathymetry, Gregoire et al., 2017 and mean sea-level, Goslin et al., 2015), reveals that the fetch length (25 km today – Stéphan et al., 2012) is shorter at lower sea-levels than the present-day one and that the strait protecting the estuary from the swell is already formed during the Pliocene (5.3 Ma to 2.8 Ma, Hallegouet et al., 1994). In our study the simulated past hydrodynamics can be almost exclusively related to tide propagation. As the hydrodynamic is validated for the present-day stage, we have confidence in the hydrodynamics produced with the other bathymetries. The fact that the hydrodynamic results presented in this study explain the sedimentary distribution observed during the Holocene transgression, shows that the assumptions made in this study are justified.

We use here the same methodology as that proposed by Mitchell et al. (2010) and Collins et al. (2018) : rebuild paleoenvironmental scenarios to study the evolution of tidal currents distribution in the past. In our case, the Bay of Brest over the last 9 000 years is well-known, thanks to sedimentary records. We were able to simulate four distinct and successive contexts (sea-level and associated paleogeography) that are representative of all the major trends/steps of the Holocene history. This hypothesis that the four chosen scenarios (corresponding to four discontinuous steps) are indeed representing continuous hydrodynamic changes is a critical point, but allows us to discuss which factor(s) may trigger the major hydrodynamics changes observed in our simulations over the Holocene.

Simulating tide dynamics over time periods of at least 1 ka remains a challenge for the oceanographic and geological communities that face a scale problem between their respective modelling tools (Joseph et al., 2016). Hydrodynamic models are able to simulate processes over time periods ranging from few-days to around 10 years. With a simplified integration of the processes, or the use of a morphological multiplicative factor this type of model can simulate over hundreds of years. For stratigraphic modelling the problem is to downscale calculation steps. Stratigraphic model consider only the resultant effect of all the processes using diffusive equations that apply at basins scale and allow simulations over much longer time period (hundreds of Ma) with longer time steps (1 ka to 10 Ma, Ku Shafie and Madon, 2008, Burgess in Roberts, 2012). This kind of model does not allow to take into account a process oscillating as quickly as the tide. It would need to upscale the tidal calculation (no general or global effect is known over long periods) or to downscale the calculation of the other processes, which is not the objective of stratigraphic model.

The scenarios are for now the only way to reach time scales of geological interest (at least 1 ka to 10 ka) in the study of the impact of tidal currents on sediment distribution. Discussing the hydrodynamic evolution during the entire transgression in the Bay of Brest is a first step towards upscaling of the tidal impact on sediment. In the future, we plan to use these four scenarios, representing all sedimentary units and major coastline changes, to explore possible simplification for tidal currents calculations. The aim is to use representatives simplified tides as inputs for a stratigraphic model and thus simulate the whole period (9 000 years cal. BP). Potential deposition and erosion indexes are an interesting approach, as they allow to integrate in the simulations the impact of bottom tidal currents on sediments, without smoothing the extreme events (e.g. spring and neap tides). This appears as a good way to bring together fine (hydrodynamic) and long (stratigraphic) time scales.

4.6. Conclusion

This study explored the responses of the Mars3D hydrodynamic model to four paleoenvironmental contexts chosen and rebuild during the Holocene transgression in the Bay of Brest (9 000 years cal. BP to present). These four scenarios represent all the units defined from sediment

records (Gregoire, 2016) and extrema of the paleoenvironmental changes defined as bathymetric and sea-level variations. Our use of hydro-sediment models of a well-known estuary over well constrained time period (9 ka, Holocene) is a rather new attempt to better understand the changes and behaviour of tidal processes through changing environments. It permits to link tidal currents evolution to paleoenvironmental changes between scenarios and therefore discuss what triggers the observed evolution. This new approach simulates the evolution of tidal dynamics over the last 9 000 years and highlights the impact of morphology and water depth on the tidal currents, as well as probable influence of bottom currents on deposition of cohesive sediments and erosion/transport of non-cohesive sediments. Based on these correlations between sedimentary archive and simulated tidal currents, the study proposes a reconstruction of the sedimentary filling during the entire Holocene transgression in the Bay of Brest.

This study succeeded to correlate the results of hydrodynamic simulations and sediment records in a qualitative way. Further modelling would be required using the hydro-sediment module e.g. MUSTANG (MUd and Sand TrAnsport modelliNG, Le Hir et al., 2011) coupled to MARS3D to simulate sediment dynamics correlate simulated scenarios and data in a quantitative way. This would provide further evidence of the relevance and effectiveness/weaknesses of the method presented here.

Acknowledgements: This work was funded by IFREMER (Institut Français de Recherche pour l'Exploitation de la Mer) and IFPEN (Institut Français du Pétrole et Energies Nouvelles), through a PHD grant awarded to M. Olivier and prepared at EDSML Doctoral School at UBO (University of Brest) We would like to thank Romaric Verney, Francois Dufois, Benedicte Thouvenin, for their numerous advices and help (all from DYNECO/DHYSED laboratory – IFREMER). We would like to thank also Sébastien Petton (LPI laboratory - IFREMER) for all the work he carried out with the present-day configuration of the Bay of Brest. We would like to thank Bernadette Tessier (M2C laboratory – Caen University), Laure Simplet (LGS laboratory – IFREMER) and Nicolas Le Dantec (LGO laboratory – IUEM) for their follow-up on my PhD committee. The authors acknowledge the fruitful and constructive English editing advice and corrections by Alison Chalm. Special thanks to Pascal Le Roy (LGO laboratory – IUEM), Axel Ehrhold (LGS laboratory – IFREMER), Gwenael Jouet (LGS laboratory – IFREMER) for their long-term work in the Bay of Brest and the numerous cruises they carried out and the data set they made available to us. This work was more particularly based on Gwendoline Grégoire's PHD (now at Intechmer). We would like to thank the Beicip-Franlab for providing us with a free license to OpenFlow suite, that allowed us to explore the possibilities of stratigraphic models and their requirements to take into account the tide impact on sedimentation.

5 Hydro-sedimentary modelling (article)

Prepared article

Préface

Cette préface a pour objectif de présenter l'article intitulé : « Numerical Modelling of Tidal Sediment Dynamics in the Bay of Brest over the Holocene : How the Use of a Process-Based Model over Paleoenvironmental Reconstitutions can Help to Understand Long-Term Tidal Deposits ? », qui a été préparé en vue d'une publication.

Par conséquent le contexte, les scénarios, ainsi que la méthodologie utilisée sont de nouveau présentés. Cependant, la partie méthodologie de cet article se concentre sur la mise en place des modélisations hydro-sédimentaires. Le modèle utilisé (MARS3D/MUSTANG), ainsi que les choix de paramétrisation y sont détaillés. Des simulations morpho-dynamiques sont réalisées avec 4 classes granulométriques et une couche initiale de 50 cm sur deux ans (avec une année de spin-up, pour initialiser la dynamique sédimentaire de surface de chaque scénario). Une étape de calibration des apports sédimentaires a été réalisée avec une méthode d'essais et erreurs, en modifiant le débit des rivières jusqu'à obtenir un taux de sédimentation comparable entre les simulations et les unités sédimentaires correspondantes, tandis que la quantité de sédiment disponible aux bordures marines est gardée constante entre les scénarios (concentration inversement proportionnelle à l'évolution de la section, liée aux variations du niveau marin). Cet article détaille également la méthodologie de comparaison entre les simulations et les enregistrements sédimentaires ; i.e., les variations bathymétriques simulées (érosion/dépôts) sont comparées aux cartes d'épaisseurs sédimentaires et la répartition simulée des classes granulométriques est comparée aux observations (simplifiées) issues des carottes sédimentaires.

Les résultats sont divisés en quatre parties, une pour chaque scénario. Pour chacune d'entre elles, une carte de l'évolution bathymétrique après 1 an est décrite et comparée à la carte d'épaisseur de l'unité sédimentaire correspondante. Ensuite, l'évolution de la masse des différentes classes granulométriques en chaque point de la rade de Brest est présentée et comparée aux enregistrements sédimentaires issus des carottes.

Dans un premier temps, la discussion de cet article propose une reconstitution de la dynamique hydro-sédimentaire induite par la marée en rade de Brest. La corrélation avec les enregistrements sédimentaires y est discutée et les résultats de simulations sont résumés sous la forme deux coupes par scénario, une dans la zone centrale et une dans la zone supérieure de la rade de Brest. La comparaison entre la reconstruction et les enregistrements sédimentaires a mis en avant une excellente corrélation, avec seulement quatre observations issues des carottes qui restent inexpliquées par les simulations. Ensuite la calibration des apports sédimentaires est discutée en fonction des conclusions de précédentes études (palynologiques principalement). Bien que ces études donnent des informations qualitatives sur l'évolution climatique et environnementale, elles vont dans le sens de l'évolution des débits déterminée entre les scénarios (calibration). Ce qui nous a permis d'étudier l'impact des apports marins et fluviatiles au cours des quatre scénarii. Les simulations avec uniquement les apports marins représentent environ 82% des apports sédimentaires des simulations avec les apports marins et fluviatiles durant les 9 000 dernières années (moyenne pondérée avec les périodes de dépôts des unités sédimentaires), contre moins de 6% pour les simulations avec uniquement les apports des rivières. Enfin, la dernière partie discute de l'implication des résultats obtenus pour l'interprétation stratigraphique des estuaires dominés par la marée. Les résultats de la rade de Brest sont d'abord simplifiés, pour ne représenter que les limites de dépôts des sédiments cohésifs et non-cohésifs, ainsi que des logs schématiques du remplissage des différents domaines morphologiques. Il apparaît que les limites érosion/dépôt et sédiments cohésifs/non-cohésifs ne se déplacent pas nécessairement vers l'amont de l'estuaire pendant une transgression. Ces limites

bougent vers l'amont et les flancs de l'estuaire quand le niveau marin remonte et la section d'écoulement reste d'une largeur similaire. Et à l'inverse quand la largeur de la section d'écoulement augmente brutalement (passage en domaine subtidale des terrasses) ces limites bougent vers l'aval et le chenal principal (pour une configuration similaire à la rade de Brest, avec un ennoiement progressif en amont liée aux berges abruptes des rivières). Dans cet article nous proposons un schéma conceptuel représentant l'évolution de ces limites en relation avec la morphologie du fond et le niveau marin.

Numerical Modelling of Tidal Sediment Dynamics in the Bay of Brest over the Holocene: How the Use of a Process-Based Model over Paleoenvironmental Reconstitutions can Help Understand Long-term Tidal Deposits?

Matthieu Guillaume Olivier[a,c], Estelle Leroux[d], Didier Granjeon[c], Pierre Le Hir[b], Marina Rabineau[a], Pascal Le Roy[a], Laure Simplet[d], Axel Ehrhold[a], Héloïse Muller[b]

a IFREMER/IUEM – ASTRE laboratory – UMR Geo-Ocean – Pointe du Diable, 29280 Plouzané, France

b IFREMER – DYNECO/DHYSED laboratory – Pointe du Diable, 29280, Plouzané, France

c IFP Énergies nouvelles – 1 et 4, avenue de Bois-Préau, 92500, Rueil-Malmaison, France

d IFREMER/IUEM – GIPS laboratory – UMR Geo-Ocean – Pointe du Diable, 29280 Plouzané, France

d IFREMER/IUEM – ODYSC laboratory – UMR Geo-Ocean – Pointe du Diable, 29280 Plouzané, France

Abstract

Long-term sedimentary infill of tide-dominated estuaries remains poorly understood. The main issue is the time-scale gap between the tidal process (hourly variations) and sedimentary layer formation (hundreds to thousands of years). Hydrodynamics induced by tides are responsible for intense remobilization of sedimentary layers inside estuaries and thus only partial sedimentary records are available. This consequently complicates understanding and interpreting the influence of hydrodynamic forcings via the preserved sedimentary deposits, as well as their chronology. Numerical modelling would appear to be the most-appropriate solution to overcome the lack of sediment deposit preservation. Hydro-sediment modelling is the only way to explicitly simulate the impact of the tidal process on sediments. However, simulations time-span of these models are currently limited to decades, without simplification or schematization of the tide impact on sediments. Even when simplified, simulated time intervals hardly exceed hundreds of years. This study (and Olivier et al., 2021) exposes a methodology exploring the evolution of hydro-sediment dynamics induced by tide over large time-scales (e.g. a transgression, ~10 ka). The aim is to use sedimentary records to identify and rebuild each key paleoenvironments of the sediment infilling in a tide-dominated estuary (defined as seafloor morphology and sea-level), in order to run them through hydro-sedimentary simulations (MARS3D/MUSTANG). The Bay of Brest is the area selected to test the methodology. Four paleoenvironments made up of four grain-size classes and defined by four distinct sea-level and seafloor scenarios are used to study the evolution of tidal-current impact on the erosion/deposition patterns over the last 9000 years. To overcome the lack of hydrodynamic data in the past, simulation results were compared with sedimentary records in terms of: amount of sediment deposited (sedimentation rates), distribution of erosion/deposition patterns (thickness maps) and distribution of grain-size classes (cores). Simulation results allowed: (I) to explain most of the sediment distribution for each sedimentary unit; (II) to reconstruct tide influence on the Holocene infilling of the Bay of Brest; (III) to discuss the evolution of the influence of sediment supply sources; (IV) and therefore to

demonstrate that the methodology is relevant to study sediment dynamic over a long time interval (9 ka). (V) The reconstruction highlights the longitudinal evolution of erosion/deposition and cohesive/non-cohesive deposit boundaries, which evolve with sea-level rise in relation to the active-flow section width in the Bay of Brest: fast and significant expansion of the active-flow section width (passage into subtidal domain of terraces) induces a downward movement of those boundaries inside the estuary and when sea-level rises and the active-flow section width remains similar, those limits move upward of the estuary.

5.1. Introduction

Tides are a key process in the understanding of sediment dynamic in many coastal areas throughout the world, particularly in bays and estuaries. Although they cover a relatively small percentage of all sedimentary environments, as they are located at the interface between rivers and continental shelves, bays and estuaries are key actors that control sediment trapping and sediment supply to ocean basins (with deltas). They are consequently a key area in the transfer of sediment from source to sink. How and how much do estuaries trap sediments during transgression, or regression cycles (about ten thousand years each) is therefore an important question to answer in order to understand estuaries and ocean basin stratigraphy. Yet tide-dominated estuary infill remains poorly understood because sedimentary records are the only data available, but are often only partially preserved. Processes acting on sediment transport in tide-dominated estuaries are very complex, as they are influenced by numerous hydrodynamic and sedimentological factors over a wide range of temporal and spatial scales (Wang, 2012). Tidal sedimentary rocks are the result of hundreds to thousands of years of a short temporal scale forcing, as tidal currents vary on an hourly scale. Water flow patterns evolve with sea-level variation and sediments are thus reworked repeatedly during the long-term infilling of an estuary. It is therefore very complicated to discretize the different events and understand the evolution of the system (Tessier et al., 2012). The stratigraphic response of estuaries to sea-level variation is even more complicated to understand, as it varies according to the combination of sea-level variation rates, sediment supply, bedrock morphology, and hydrodynamics (Tessier, 2012). The stratigraphic interpretation of tidal deposits is carried out by analogy with present-day observations (e.g. Reynaud et al., 2006; Shanmugam et al., 2009; Flemming, 2012; Olariu et al., 2012; Reynaud and James, 2012; Lee et al., 2022), which are summarized in conceptual models (e.g. Dalrymple and Choi, 2007; Dalrymple et al., 2012). The interpreted depositional environments are assembled to determine the depth and influence of hydrodynamics by analogy. They are then associated with transgressive and regressive cycles: LST (Lowstand System Tract), TST (Transgressive System Tract) and HST (Highstand System Tract). In estuary sequence stratigraphy, transgressive and regressive movements are linked to the interpreted evolution of shoreline, which comes from depositional environment interpretation of the sedimentary record (e.g. the intertidal mud/sand limit, sand bars, salt marsh). Due to poor preservation, it is unusual to observe longitudinal variation of facies deposits, even in the presence of a large dataset (e.g. cores, seismic, outcrops, Tessier, 2012). Moreover, designation of the transgressive surface (and thus the LST) is particularly difficult as many of the prominent surfaces in the estuary fill are diachronous facies boundaries (Dalrymple and Zaitlin, 1994). The combination of diachronous facies boundaries, poor preservation of deposits, the great variability of facies and hydro-sediment processes in estuaries, substantially complicates establishing common patterns for different stages of sea-level rise (LST, TST, HST). This was demonstrated in a synthesis of tide-dominated estuary Holocene infill, made by Tessier (2012). The distribution of preserved sediment deposits is not sufficient to explain hydrodynamic evolution in estuaries over large time scales. The hydro-sediment response of estuaries to long-term parameters (hundreds to

thousands of years), such as sea-level or seafloor evolution between sedimentary units, often remains unknown.

In the absence of sedimentary records (or only partial), numerical modelling is the only way to study the effect of tides on sediments over an estuary. Hydro-sedimentological modelling is designed to resolve physical processes acting along the coast (e.g. tide, wave, wind, river discharge), which provides the representation of the tide and its effects on the seafloor. Hydro-sediment models are used to complete in-situ measurements (e.g. current velocities, sea surface variations) and accurately represent the impact of hydrodynamics on sediments throughout the estuary. However, the time step imposed by hydrodynamic processes acting in estuaries implies to simulate only short time intervals (from hours to decades, e.g. Bárcena et al., 2016; Grasso and Le Hir, 2019; Tosic et al., 2019). The temporal scale limit of hydro-sediment modelling is an important scientific lock, because transgressions last about ten thousand years and the formation of sedimentary units around hundreds to thousands of years (Dalrymple et al., 1992; Tessier et al., 2012). To overcome this time scale issue, many techniques have been developed to simulate longer time intervals (around thousand years maximum). A synthesis of these techniques is proposed by Roelvink (2006). The most used technique is to apply a multiplicative factor (n) for erosion and deposition fluxes, or the net erosion/deposition, estimated by a hydro-sediment model (e.g. Franz et al., 2017; Le Tu et al., 2019; Elmilady et al., 2020). Volumes deposited are therefore the expression of present-day forcing (1 to 10 years) multiplied by n at each time step. This technique has the advantage of simulating deposit thicknesses comparable to sedimentary records. In the case of the tide, it means that the tidal forcing impact simulated (water height, current velocities) is repeated n times, before the simulation passes to the next one. Some studies have used a very high morphological factor to approach time intervals in the order of a thousand years. Mainly conceptual estuaries were simulated and they all led to estuary equilibrium configuration (Lanzoni and Seminara, 2002; Bolla Pittaluga et al., 2015; Guo et al., 2015; Braat et al., 2017). Simulations of Bolla Pittaluga et al. (2015) indicated that the investigated system always moves toward an equilibrium configuration in which the net sediment flux in a tidal cycle remains constant throughout the estuary and equal to the constant sediment flux delivered by the river. The majority of sediment features, such as tidal channels, dunes and tidal flats, are the result of a system seeking to reach its dynamic equilibrium (Coco et al., 2013). However, eustatism or subsidence processes keep changing the conditions to reach this dynamic equilibrium and that is why almost no natural estuary has reached it yet.

The influence of hydrodynamic processes on estuary infilling (erosion and deposition) over a transgression or regression remains an important question. This study exposes a methodology to explore the influence of paleoenvironmental evolution (seafloor and sea level) on the sediment dynamics of tide-dominated estuaries. It proposes to use hydro-sediment modelling to complement in-situ measurements, but at several stages of a transgression. The main difference with studies at the present-day is that in-situ measurements are not sea-surface height or current velocities, as the oldest hydrodynamic data are only 300 years old (Brest tidal gauge), but are sedimentary records (the only data available for the past). Studies from Imperial college have already analyzed past tide influences on sediments at large spatial (sedimentary basin to global) and temporal scales (about 10-50 Ma, e.g. Wells et al., 2007a; Mitchell et al., 2010; Wells et al., 2010). By using the hydrodynamical ICOM model (Imperial College Ocean Modelling) for short time intervals (days to months), hydrodynamic simulations were linked to sedimentary records with bed shear stress calculation over paleoenvironmental reconstructions (e.g. Cretaceous, Bohemian basin, Mitchell et al., 2010; late Oligocene-Miocene, South China Sea, Collins et al., 2018; late Pennsylvanian Seaway of NW Eurasia, Wells et al., 2007a; 2007b). Other studies have explored recent and old paleoenvironmental impact on tides, such as Reynaud and Dalrymple (2012, Holocene and Lower Cretaceous, and Zuchuat et al., 2022,

lower Oxfordian). The innovative aspect of our study is that the reconstructed scenarios represent all the key stages of estuary infilling and therefore allow to discuss the evolution of the hydro-sediment dynamics between the scenarios and their triggers (Olivier et al., 2021). The objective of this study is to observe the hydro-sediment response of an estuary to geological parameters, such as seafloor morphology and sea-level evolution (section 5.2.1). Comparable methodologies were used to study other estuaries on a century time scale (e.g. Marennes-Oléron bay, 1826 to 2004, Bertin et al., 2005; Seine estuary, 1960 to 2010 Grasso and Le Hir, 2019). The methodology here is applied to the Bay of Brest Holocene time interval (section 5.2.2). It is a macrotidal estuary naturally protected from oceanic waves (Monbet and Bassoullet, 1989; Beudin, 2014), with a sediment infilling starting 10 000 years ago and several meters of those sediments preserved (Gregoire et al., 2017). Four scenarios are defined according to its infilling history (section 5.2.3). Then the hydro-sediment dynamic is simulated for each of them with MARS3D-MUSTANG (5.2.4, Lazure and Dumas, 2008; Le Hir et al., 2011) and the sediment supply is calibrated for each scenario by comparing the sediment rate of preserved sedimentary records and simulation over one year (5.2.5). Simulations are not expected to be an exact representation of past stages, but to present the same global patterns of erosion and deposition as sediment thickness maps of units, and the same global grain-size class distribution as observed in cores (5.2.6). Simulation results, for each scenario, are compared with global sedimentary unit trends recorded by cores and seismic (5.3). The results are used to propose a reconstruction of the Bay of Brest infilling (5.4.1). Then, the discussion focuses on the calibration and impact of sediment supply sources used in simulations (marine and river, 5.4.2). The last point discusses the influence of paleoenvironmental evolution on hydro-sediment dynamics and the implications for the stratigraphic analysis of estuaries (5.4.3).

5.2 Methodology and tools

5.2.1 The modelling strategy

This paper aims to explore the evolution of long-term (a transgression, i.e. about 10 000 years) tide-induced deposits in response to sea-level rise and seafloor evolution in a tide-dominated estuary. With only partial sedimentary records and no hydrodynamic data in the past, the idea is to use numerical modelling to complement in-situ observations. Building successive scenarios is the only option to simulate the tide and reach the temporal scale of a transgression. The scenarios are thus expected to be representative of larger time intervals than the ones simulated. For this reason, a new scenario is generated for each paleoenvironmental and sediment dynamic change identified. Sedimentary records are then used to rebuild past seafloor morphologies (using thickness maps of seismic units) and sea-level curves (Goslin et al., 2015; García-Artola et al., 2018). Hydro-sediment modelling is used to simulate the response of tidal-induced sediment dynamics to seafloor and sea-level evolution. Hydro-sediment modelling in this study is expected to show the evolution of erosion and deposition areas, and grain-size distribution induced by tidal currents. This can provide information on deposit preservation, longitudinal evolution of grain-size classes and triggers of main hydro-sediment dynamic changes. This study is not expected to be an exact representation of past estuary dynamics, but seeks to upscale the consideration of tide impact on sediments, by providing the hydro-sediment dynamic evolution link to key paleoenvironments (scenarios) of an estuary infilling. The first step is to compare sedimentary records and simulations in order to calibrate sediment supply and validate global trends, which is possible only because the scenarios are representative of larger time intervals than the ones simulated. The second main goal is to identify factors triggering main hydro-sediment dynamic changes and their implication for estuarine

stratigraphic interpretations. The methodology is applied to the Bay of Brest, where four scenarios are reconstructed from 9 000 years ago to present-day (sea-level -26 m to 0 m, Goslin et al., 2015; García-Artola et al., 2018). This work follows a previous paper (Olivier et al., 2021) dedicated to hydrodynamic changes, where four scenarios were established and described. The present paper focuses on the application of a hydro-sedimentary model (MARS3D-MUSTANG) to these four scenarios.

5.2.2 The Bay of Brest

The Bay of Brest is a semi-enclosed macrotidal bay located at the western end of Brittany, France (Fig. 67). The mean spring tidal range is 5.9 m and the mean neap tidal range is 2.8 m in Brest harbour (Beudin, 2014). The Bay is protected from ocean waves by the strait between Plouzané and the Roscanvel peninsula (1.8 km wide, connecting the Bay and the continental shelf, Ballèvre et al., 2009; 2014). This configuration induces a very weak swell climate compared to the wave energy regime outside the Bay (Iroise Sea, Monbet and Bassoullet, 1989; Olivier et al., 2021). The study area also displays a short fetch (~25 km, Stéphan et al., 2012), protecting it from significant wind-induced waves.

During the Tertiary era, glacio-eustatic movements generated transgressions and regressions around the Brittany region. The Bay of Brest emerged several times during low sea-level stages and the basement is eroded by paleo-rivers since the Oligocene (Hallegouet et al., 1994). Past fluvial systems generated three morphological domains (Gregoire et al., 2016, Fig. 67): T1 is the main paleo channel; T2 is the first stage of terraces, above T1; T3 corresponds to the shallowest terraces localized in sheltered coves and bays. A network of secondary channels within T2 and T3 connects these domains to the main channel (T1, Fig. 67).

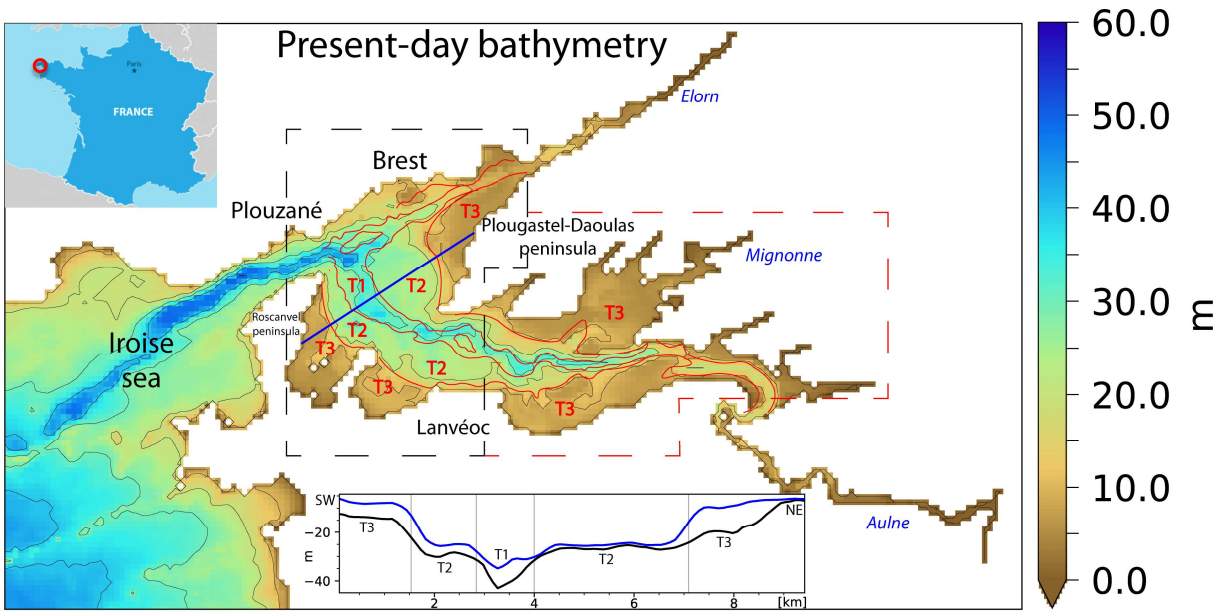

Fig. 67: Present-day bathymetric map of the Bay of Brest, generated from SHOM data (2015). The inset-bathymetric section is indicated by a blue line on the map. On this section, the blue line corresponds to present-day bathymetry and the black line to the beginning of the Holocene infilling of the Bay of Brest (9 ka BP). T1: paleo main channel. T2: deepest stage of terraces. T3: shallowest stage of terraces (delimited by grey lines). Black dotted box represents the limits of the central area and red dotted box shows the limits of the upper area of the Bay.

This estuary is the perfect place to explore tidal impact on hydro-sediment dynamics, because of its specific characteristics: I) it is a macrotidal system, II) it is protected from ocean waves (Monbet and Bassoullet, 1989) and III) it has a specific seafloor morphology (three different morphological domains), providing observation of the influence of several paleoenvironmental configurations. In this study, the estuary is divided into two parts: the upper part, to the east of the strait between Lanvéoc and the Plougastel-Daoulas peninsula (towards the estuary of the Aulne river, Fig. 67), the central part is delimited by the same strait as in the east and the one between Plouzané and Roscanvel peninsula at the west. This strait behaves like a bottleneck in terms of hydro-sediment processes. All areas westward of this strait such as the Iroise Sea, are affected by waves and storms and therefore not analysed in this paper (Fig. 67). The three most important rivers are the Aulne (estuary located to the south-east of the upper part, annual mean water discharge around 30 $m^3.s^{-1}$ and suspended matter concentration around 0.2 $g.l^{-1}$), the Elorn (estuary located to the north-east of the central part, annual mean water discharge around 10 $m^3.s^{-1}$ and suspended matter concentration around 0.1 $g.l^{-1}$) and the Mignonne (estuary located to the north of the upper part, annual mean water discharge around 1.5 $m^3.s^{-1}$ and suspended matter concentration around 0.08 $g.l^{-1}$).

Over the Holocene, the evolution of river sediment supply is unknown and only proxies can give clues on regional climate evolution. The Lower Holocene (11.7 to 8.2 ka BP) is characterized by high summer insolation values and is still strongly impacted by the remanent presence of continental ice-sheet that developed during the last ice age (Lambert, 2017). The vegetation then gradually grew around the Bay of Brest (Lambert, 2017) and precipitations increased in northern Europe (Seppä and Birks, 2001; Bjune et al., 2005), in connection with a climate warming during the Holocene climate optimum between 8.2 to 4.2 ka (BP, Koshkarova and Koshkarov, 2004). After this climatic optimum, temperatures globally decreased (Berger and Loutre, 1991) and precipitations slightly decreased in northern Europe (Seppä and Birks, 2001; Bjune et al., 2005). This time interval also saw an important expansion of agriculture in the region (Lambert, 2017) inducing deforestation and therefore a greater runoff from the land towards rivers (Lambert, 2017). Another important parameter of river sediment discharge is the river profile, which is linked to sea-level variations. When sea-level falls, river profiles are steeper and the potential energy increases between rivers and the Bay and the opposite occurs when sea-level rises (i.e. a greater velocity is expected inside rivers during low stage than during high stage).

5.2.3 Modelling scenarios

Four scenarios were defined to represent the main steps of hydro-sediment evolution over the Holocene transgression in the Bay of Brest. The scenarios represent different paleoenvironments at a specific age and are defined by a bathymetric map (Olivier et al., 2021). The aim is to represent key paleoenvironments of the Bay of Brest at different stages of sediment infilling. A scenario is therefore reconstructed after each major change in stratigraphic patterns (deposit dynamics) and after each important retreat of the coastline, such as the flooding of a new morphological domain. The choice of simulated time intervals is based on the work of Gregoire (2016; Gregoire et al., 2017), which defined four sedimentary units for the Holocene period: U0 (~10-9 ka cal. BP, LST), U1(~9-7 ka cal. BP, TST), U2(~7-3 ka cal. BP, TST) and U3 (~2-0 ka cal. BP, HST, Fig. 68).

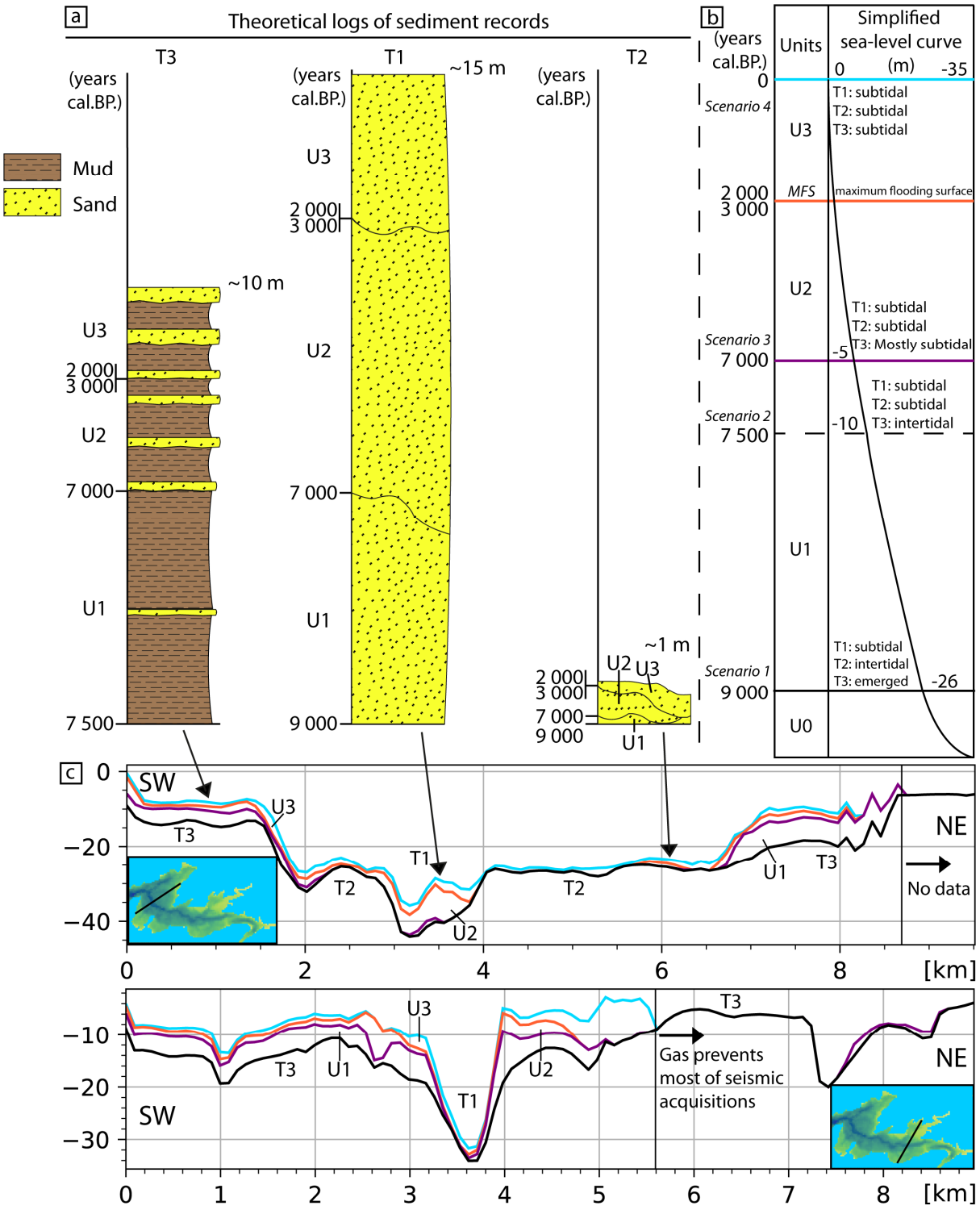

Fig. 68 : a: theorical logs for each morphological domain over the Holocene time interval in the Bay of Brest (from the interpretation of 10 cores and previous study of Gregoire, 2016). Muds are displayed in brown and sands in yellow. c: Sedimentary units chronology (from Grégoire, 2016) and simplified sea-level curve over the Holocene. c: two sections present the depth of each sedimentary unit top, relative to the present-day mean sea level: black line for the top of U0, purple for the top of U1, orange for the top of U2 and light blue for the top of U3 (top corresponding to remarkable stratigraphic surfaces, see Gregoire et al., 2017).

For the period before 10 ka (BP), the Bay of Brest is characterised by a fluvial sediment dynamic and during U0 (10 to 9 ka BP), sediment deposition is typical of a ria system. This study focuses on tide-

dominated stages of the Holocene transgression within the Bay of Brest over the last 9 000 years. The four scenarios represent major paleoenvironmental evolutions during the deposition of U1, U2 and U3. U1 is characterised by a wide range of sea-level variations during its deposition from -26 to -5 m (Fig. 68) and therefore two scenarios are generated for this sedimentary unit. Scenario 1 is set at the beginning of this time interval at 9 ka (BP), with a seafloor corresponding to the top of U0. During this scenario the intertidal area is located over T2 terraces. Scenario 2 is set at 7.5 ka (BP) and aims to represent the end of U1. The chronology inside sedimentary units is poorly known and thus the selected seafloor for scenario 2 is the top of U1, as the aim is to explore hydro-sediment dynamics conditions at the beginning of U1 with scenario 1 (9 - 7.5 ka BP) and the end of U1 with scenario 2 (7.5 - 7 ka BP). The intertidal area is over T3 during scenario 2. Then, during U2 deposition the rise in sea-level slows down (-5 to 0 m). The configuration (seafloor and sea level) remains similar during this time interval (7 - 3 ka BP) and thus scenario 3 aims to represent the entire deposition time interval of U2. Scenario 3 is set at 7 ka (BP), with the top of U1 as the seafloor. During scenario 3 almost all T3 terraces are subtidal. During U3, sea-level remains close to that of the present-day (Fig. 68) and thus only one paleoenvironment is generated to represent U3. Scenario 4 is set at the present day and aims to represent the entire deposition time interval of U3 (2 - 0 ka BP), which is still active at the present day. Present-day seafloor (top of U3) and sea-level are used for this scenario. During the Holocene, preserved mud deposits are mainly localised over T3 and most of the preserved sand deposits are localised over T1 (Fig. 68). All details on sediment data and bathymetric maps generation (Tab. 3) used for the construction of these 4 paleoenvironments, are provided in Olivier et al. (2021).

Tab. 3: Summary of scenario settings

Scenario and simulation aim	Scenario 1 (Beginning of U1)	Scenario 2 (End of U1)	Scenario 3 (U2)	Scenario 4 (U3)
Age	9 000 years BP	7 500 years BP	7 000 years BP	Present day
Mean sea-level (compared to present day)	-26 m	-10 m	-5 m	0 m
Seafloor	Top U0	Top U1	Top U1	Top U3 (present-day seafloor)

5.2.4. The hydro-morpho-sediment model MARS3D-MUSTANG

The sediment module, MUSTANG, is coupled with the hydrodynamic model MARS3D. The hydrodynamic code MARS3D computes the hydrodynamic variables (currents, free-surface elevation) and MUSTANG computes sediment transport, erosion and deposition processes and morphological evolutions in coastal and estuarine environments (Le Hir et al., 2011; Mengual et al., 2017). The hydrodynamic code and its settings are described in Olivier et al. (2021).

The horizontal computation grid is Cartesian, with mesh-size of 250 m x 250 m and the water column is composed of 20 levels. This very fine vertical resolution results from previous applications of the 3D model in the Bay of Brest (Klouch et al., 2016; Frère et al., 2017; Petton et al., 2020). Given the time dedicated to the implementation of the grid and the validation of hydrodynamics, a similar configuration is used in this study. In the water column, the model resolves advection/diffusion equations for different classes of particle (in a 3-D framework for mud and in a 2D framework for sands). Although coarse non-cohesive sediments are transported as bedload, the ability of the model to simulate their dynamics by considering transport in suspension was previously demonstrated using

a fitted erosion law (Le Hir et al., 2011; Dufois and Le Hir, 2015). The settling velocity of each particle class is constant and depends on grain size (Chataigner, 2018). The model accounts for the transport of four sediment classes: gravels 3 mm; sands 1.1 mm; fine sands 200 μm and muds 15 μm. The selection of these representative grain-size classes is based on previous work (Gregoire, 2016) and on study of 10 sediment cores. For each class, grain density is 2600 kg/m^3 (quartz density).

In the Bay of Brest configuration, the sediment model has the same horizontal resolution as the hydro-dynamic model and manages up to 100 layers, with variable thicknesses between 1 μm and 1 cm (excluding the deepest layer, which can be thicker), according to deposition and erosion events. When the maximum number of layers is exceeded, the two deeper ones are merged. The initial sediment bed has a uniform thickness of 0.5 m inside the Bay (no erodible sediment outside the Bay), and is composed of 10% gravel, 20% sand, 30% fine sand and 40% mud (approximation from Gregoire, 2016). The basement is located below this initial sediment layer and is not erodible. The basement is presumed to be coarse continental sediment at the beginning of sediment infilling in the Bay of Brest 9 000 years ago (Gregoire, 2016). The skin roughness is assumed to be uniform and constant for all simulations, and equal to 1 mm, corresponding to a seafloor of coarse sediment. The choice of a uniform roughness length helps not to produce misleading flow patterns with a poorly validated parameterisation and facilitates the comparison between scenarios. The erosion flux (E) for sands and mud is expressed in a "Partheniades-Ariathurai" form (Nielsen, 1992):

$$\text{Eq. 9: } E_{sands} = E0_s \left(\frac{\tau}{\tau c_i} - 1\right)^n$$

$$\text{Eq. 10: } E_{mud} = E0_m \left(\frac{\tau}{\tau c_i} - 1\right)$$

with E0 the erodibility for mud ($E0_m$) or sands ($E0_s$), τ the bottom shear stress, τc_i the critical shear stress for erosion (Tab. 4) and n a power coefficient applied to excess erosion (= 1.5, according to van Rijn, 1994). A linear interpolation between sand and mud behaviour is used, depending on proportions of the mixture. Net sedimentation is driven by the excess of shear stress induced by the water flow on the seafloor, according to Krone's law:

$$\text{Eq. 11: } D_i = Ws_i C_i \left(1 - \frac{\tau}{\tau d_i}\right)$$

With, for each sediment class i, D_i, sedimentation rate, Ws_i settling velocity (mud=5*10^{-3} $m.s^{-1}$, sand values are calculated from Soulsby, 1997), C_i concentration in suspension (g.l^{-1}) and τd_i critical shear stress for deposition ($N.m^{-2}$).

The value of τd_i is set very high for sands (1000 Pa) to allow full deposition, and rather high for mud to prevent its deposition when the bottom layer is very turbulent, as consolidation processes are not explicitly accounted for (Tab. 4). The primary consolidation of sediments is then disabled for the sake of computing costs, and secondary consolidation is neglected, in agreement with the short duration of simulations, which is much shorter than diagenetic processes duration, responsible for the long-term consolidation of sediment. Simulations are morphodynamic, which means that seafloor elevation is recomputed according to the erosion and deposition fluxes calculated. Simulations are carried out for a two-year period, but only the second one is analyzed. One year of spin-up is set to initialize the surface sediment dynamic and avoid the recording of artificial movements. Initializing hydrodynamics

takes a few days, but tidal currents need months to redistribute sediments which were initially uniformly distributed. The year of spin-up allows to initialize the surficial grain-size distribution, in agreement with the hydrodynamics of the time (for each scenario), in a context where the shape and nature of the bottom surface layer is uncertain.

Tab. 4: Hydro-sediment model parameter settings

Hydro-sediment model parameters	τc_i (Pa) Olivier et al., 2021				$E0_i$		τd_i (Pa)	
Values	mud	fine sand	sand	gravel	mud	sands	mud	sands
	0,1	0,147	0,541	2,072	0,003	0,01	1	1000

5.2.5 Sediment supply calibration

To calibrate sediment supply, the only quantitative information available for the Bay is the volume of preserved deposits for each sedimentary unit, which is calculated from thickness maps. For each sedimentary unit, the positive balance between deposition and erosion for each grain-size class is recorded, i.e. when the quantity deposited is greater than the quantity eroded (preserved deposits). For example, sand deposits can be recorded where there is mostly mud erosion. However, the evolution of hydrodynamic conditions can erode the sedimentary units a long time after their deposition. The amount of deposit eroded by subsequent hydro-sedimentary dynamics cannot be quantified and constitutes the greatest uncertainty in the study of past sediment systems. The calculated volume only accounts for the preserved part of sediment deposits, as the reworked fraction within sedimentary units is unknown.

For comparison with simulations over one year, the volumes of sedimentary units are converted into mean sedimentation rates over the Bay, depending on each sedimentary unit time span (Eq. 12, Tab. 5). Sedimentation rates therefore rely on the sediment volume calculated from the thickness map of each unit, based on the seismic interpretation, and filling chronology of the Bay (Gregoire, 2016, Fig. 68).

$$\text{Eq. 12: } Ux = \frac{\text{volume } (m^3)}{\text{deposit time-interval (years)}} = \text{sediment rate } (m^3/\text{years})$$

Tab. 5 : Preserved sedimentation rate calculated from seismic unit volumes and ages.

U1 (9 to 7 ka BP)	U2 (7 to 3 ka BP)	U3 (2 ka BP to present-day)
$136.2 * 10^3\ m^3/\text{y}$	$44.1 * 10^3\ m^3/\text{y}$	$75.6 * 10^3\ m^3/\text{y}$

For each scenario, the calibration of sediment supply is based on the comparison between the sum of positive balances (quantity of sediment gained minus quantity lost) of each sediment class in the model and the preserved sedimentation rates calculated from the sedimentary record (see above, Tab. 5). If the modelled balance is negative for a given size class (erosion larger than deposition), it does not

contribute to net sedimentation, and consequently is not accounted for in the calibration of sediment supply.

In the model, sediment inputs from rivers and at oceanic borders were considered. However, only the present-day, and so human-influenced, fluxes of fine suspended sediments in upstream rivers (Aulne, Elorn and Mignonne) are approximately known (section 2.2, Tab. 6, scenario 4). Other studies have highlighted the potential climate-change impact on river discharge over the last 9 000 years (Fernane, 2014; Lambert, 2017; Penaud et al., 2020), but mainly qualitative information is available (section 2.2). Hardly any information is available for oceanic inputs, even at the present day. To overcome these uncertainties, oceanic border supply was calibrated with the present-day context (scenario 4), when the mean river discharges and concentrations of suspended matter are approximately known. In fact, in the modelling frame, the sediment concentration for each class was set only when water entered the computational domain, while water exchanges at the open sea boundary were computed by the model. Simulated sediment fluxes at the open sea boundary result from these "calibrated" concentrations and computed water fluxes. The calibration procedure was as follows. First, a mass balance was made between the beginning and the end of the second year, for each grain-size class (area similar to the available seismic coverage, Fig. 69, Tab. 7). Then all positive values were summed and the result was converted to volume using the classic medium sediment density 1600 kg/m^3 (before any compaction or diagenesis processes, Tab. 7), and compared with the sedimentation rate calculated from sedimentary records (Tab. 5). To calibrate the suspended sediment concentration at the sea boundary, a trial and error method was used, meaning that several two-year simulations were run until the annual simulated net deposition rate was close to the annual rate deduced from the preserved sedimentary unit volume.

For the other three scenarios (1, 2 and 3), sediment availability is assumed to be constant at oceanic boundaries during the Holocene. During this long interval, the whole section of the sea boundary varied considerably, particularly in relation to sea-level changes. Tidal currents were likely to vary simultaneously. The hydrodynamic model is expected to predict these changes, assuming that topo-bathymetry remained constant in the area throughout this period. The availability of sediment is assimilated to the mass in suspension within the sea boundary, which constitutes a strong assumption. For each scenario, the suspended sediment concentration of each sediment class at the oceanic boundary was deduced from the corresponding calibrated value for the present-day scenario, inversely proportional to the average section of the boundary (Tab. 6).

Then, past scenarios were calibrated by modifying river water discharge to obtain similar annual sedimentation rates for simulations and seismic units, using the same calculation as in scenario 4. To avoid poorly parameterized annual variations for past river regimes, suspended matter and river water discharge were set as constant over the simulations. Mean values based on present-day data from DREAL Bretagne, were considered for all scenarios (Tab. 6, scenario 4). For scenarios 1, 2 and 3, a multiplicative factor was applied to the present-day mean water discharge of the rivers to obtain the same sedimentation rate as that calculated from sedimentary records (Tabs. 8 and 9). For each simulation, the global volume of simulated deposits is therefore equivalent to the annual deposited (and preserved) volume of the corresponding sedimentary units: U1 (scenarios 1: 9 to 7.5 ka BP and 2: 7.5 to 7 ka BP), U2 (scenario 3: 7 to 3 ka BP), U3 (scenario 4: 3 ka BP to present-day, Tabs. 7 and 9). However, scenarios 1 and 2 are calibrated together as they represent the same sedimentary unit (U1), assuming a stronger river discharge during scenario 1 than in scenario 2 (see section 2.2). Their calibration (scenarios 1 and 2) results in the weighted average of both simulations, based on deposition chronology, compared to U1 annual sedimentation rate (Tabs. 7 and 9). The four calibrated simulations are presented in section 3.

Tab. 6: Hydro-sediment model forcing settings.

Scenario (Sc), river water discharge multiplicative factor (*x)	River water discharge ($m^3.s^{-1}$)			River suspended matter (g. l^{-1})			Oceanic border concentration (g. l^{-1})			
	Aulne	Elorn	Mignonne	Aulne	Elorn	Mignonne	mud	fine sand	sand	gravel
Sc 1*10.9	327	109	16,35	0,2	0,1	0,08	1,07E-02	6,89E-04	3,44E-04	3,44E-04
Sc 2*4	120	40	9	0,2	0,1	0,08	4,31E-03	2,78E-04	1,39E-04	1,39E-04
Sc 3*2	60	20	3	0,2	0,1	0,08	3,58E-03	2,31E-04	1,16E-04	1,16E-04
Sc 4*1	30	10	1,5	0,2	0,1	0,08	3,10E-03	2,00E-04	1,00E-04	1,00E-04

Note Tab. 4: Water fine sediment concentration = 500 (g.l^{-1})

Tab. 7: Mass balance of gains and losses over 1 year of the four granulometric classes and the four scenarios (Sc). The balance is computed over an area of extension similar to seismic records (see Fig. 69).

Scenario (Sc)	mud (kg/y)	fine sand (kg/y)	sand (kg/y)	gravel (kg/y)	total (kg/y)	Volume simulated (m^3/y)	Volume recorded (m^3/y)
Sc 1	$1.30*10^8$	$1.40*10^8$	$8.63*10^6$	$3.49*10^6$	$2.83*10^8$	$176.6 * 10^3$	-
Sc 2	$5.48*10^7$	$-7.74*10^6$	$-2.81*10^6$	$-1.65*10^6$	$5.48*10^7$	$34.2 * 10^3$	-
Sc 1 + Sc 2 (U1)	-	-	-	-	-	$141.0 * 10^3$	$136.2 * 10^3$
Sc 3 (U2)	$7.18*10^7$	$-2.96*10^7$	$-7.12*10^6$	$-3.17*10^6$	$7.18*10^7$	$44.9 * 10^3$	$44.1 * 10^3$
Sc 4 (U3)	$8.90*10^7$	$3.27*10^7$	$-5.56*10^5$	$-3.41*10^4$	$1.22*10^8$	$76.1 * 10^3$	$75.6 * 10^3$

*Note Tab. 7: sc 1 + sc 2 = Weighted average between scenario 1 (beginning of U1) and scenario 2 (end of U1) = (176.6$*$ 10^3 *1500/2000) + (34.2$*$ 10^3 *500/2000). Ponderation based on deposition chronology, i.e. beginning of U1 deposition: 9 ka to 7.5 ka (BP) and end of U1 deposition: 7.5 ka to 7 ka (BP).*

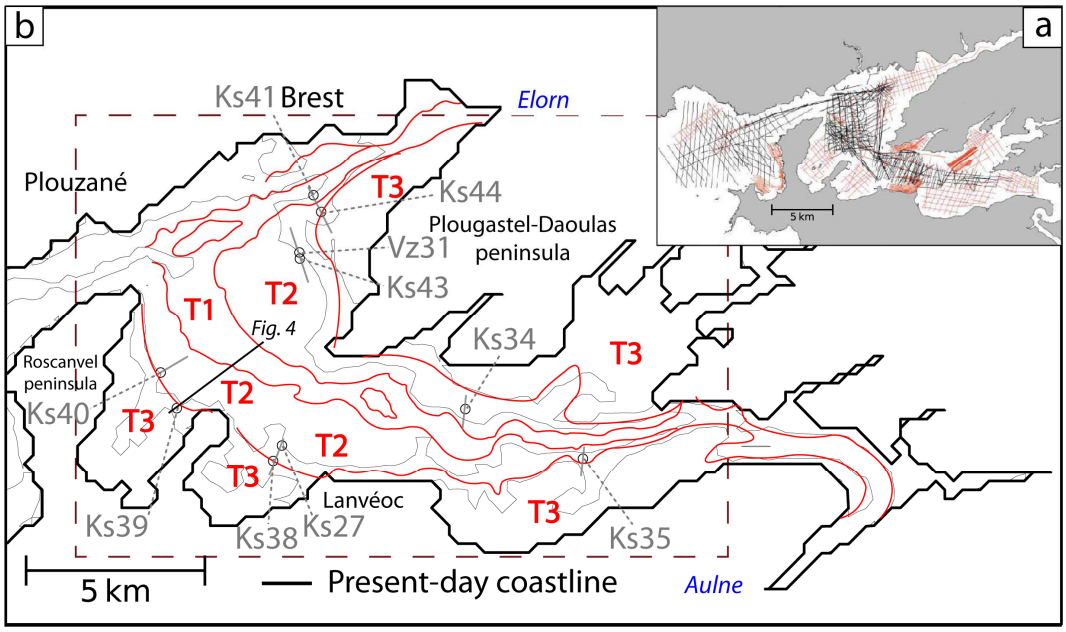

Fig. 69: (a) Location map of all seismic profiles used in this study (from Gregoire et al., 2017). (b) Location map of gravity-cores used in this study (sections 2.6. and 3.). Black line represents the seismic profile presented in section 2.6 and grey lines

the seismic profiles available in supplementary material. The brown dashed rectangle is the area considered by mass balance calculation (Tab. 7).

5.2.6 Comparison between simulations and sediment data

No hydrodynamic data is available for past stages of the bay of Brest infilling in order to validate the simulated hydrodynamics. To overcome this lack of validation for past scenarios, simulation results were compared to observations from sedimentary cores and thickness maps. Thickness maps provide the global distribution of preserved sediment deposits of each sedimentary unit and core observations provide the deposit composition (grain size). For each scenario, a comparison was made between the simulated bathymetric evolution and the thickness map of the corresponding sedimentary unit (section 3 and section 4). This allows to compare global trends of erosion and deposition simulated with in-situ measurements, which are the preserved deposits of each sedimentary unit (global seismic interpretation made by Gregoire, 2016). To compare the simulated grain-size distribution with our data, 10 cores obtained during the SERABEQ-03 campaign (Ehrhold and Gregoire, 2015) are described in this study (Fig. 69 and Tab. 8).

Tab. 8: Summary of core information and observations

from SERABEQ 3 (Ehrhold and Gregoire, 2015)		Ks_27	Ks_34	Ks_35	Ks_38	Ks_39	ks_40	Ks_41	Ks_43	Ks_44	Vz_31
longitude		-4.4774	-4.3637	-4.4078	-4.4804	-4.5168	-4.5229	-4.4655	-4.4703	-4.4626	-4.4708
latitude		48.3032	48.2999	48.3126	48.2996	48.3128	48.3219	48.3662	48.3507	48.3620	48.3518
length (m)		1,68	2,64	3,31	3,52	3,55	3,57	2,14	3,6	3,31	2,64
Grain-size classes observed:	U3	FS and S	M and FS	M and FS	M and FS	M and FS	S and G	FS and G	S	FS and S	FS
M: muds; FS: fine sands; S: sands; G: gravels	U2	M	S	M and S	FS	M and S	-	M	-	M and FS	FS
	U1	-	M	M and FS	M	M	M	-	M	M and FS	-

These cores reached the oldest sedimentary units possible. The correlation between cores and sedimentary units is based on seismic and facies interpretation rather than shell dating, which is uncertain in estuaries because of the intense recycling induced by tide. However, the resolution difference is significant: seismic resolution is around 0.3 to 1 m and core resolution is centimetric. Limits between sedimentary units were set more precisely thanks to facies interpretation (e.g. Fig. 70 and all cores available in supplementary material). Observations are simplified to correspond to the same grain-size classes as used in the simulations: “mud” is for clay to silt and clay, “fine sand” is for silt to fine sand “sand” is for medium to coarse sands and larger grain size corresponds to “gravel” (Fig. 70 and Tab. 8). As our simulations aim to be representative of the main sediment dynamics over large time intervals, only preponderant grain-size classes are considered and not isolated variations (e.g. a small local gravel record). Even if some energetic events (such as storms) can have local effects, observable in the sediment (Ehrhold et al., 2021), they are not representative of main hydro-sediment

dynamics induced by tide and are not simulated here. This is why only the dominant and homogeneous part of the deposits was considered. Cores can testify to the presence of one or two grain-size classes for each sediment unit. For example in core Ks_39, U1 consists mainly of mud and two small fine sand layers (Fig. 70). These two layers are not representative of U1 at this location and were therefore not taken into account for validation (Fig. 70 and Tab. 8). For U2, the main components are mud and sand (Fig. 70 and Tab. 8). For U3, the two fine gravels layers were not taken into account and only mud and fine sands were selected (Fig. 70 and Tab. 8).

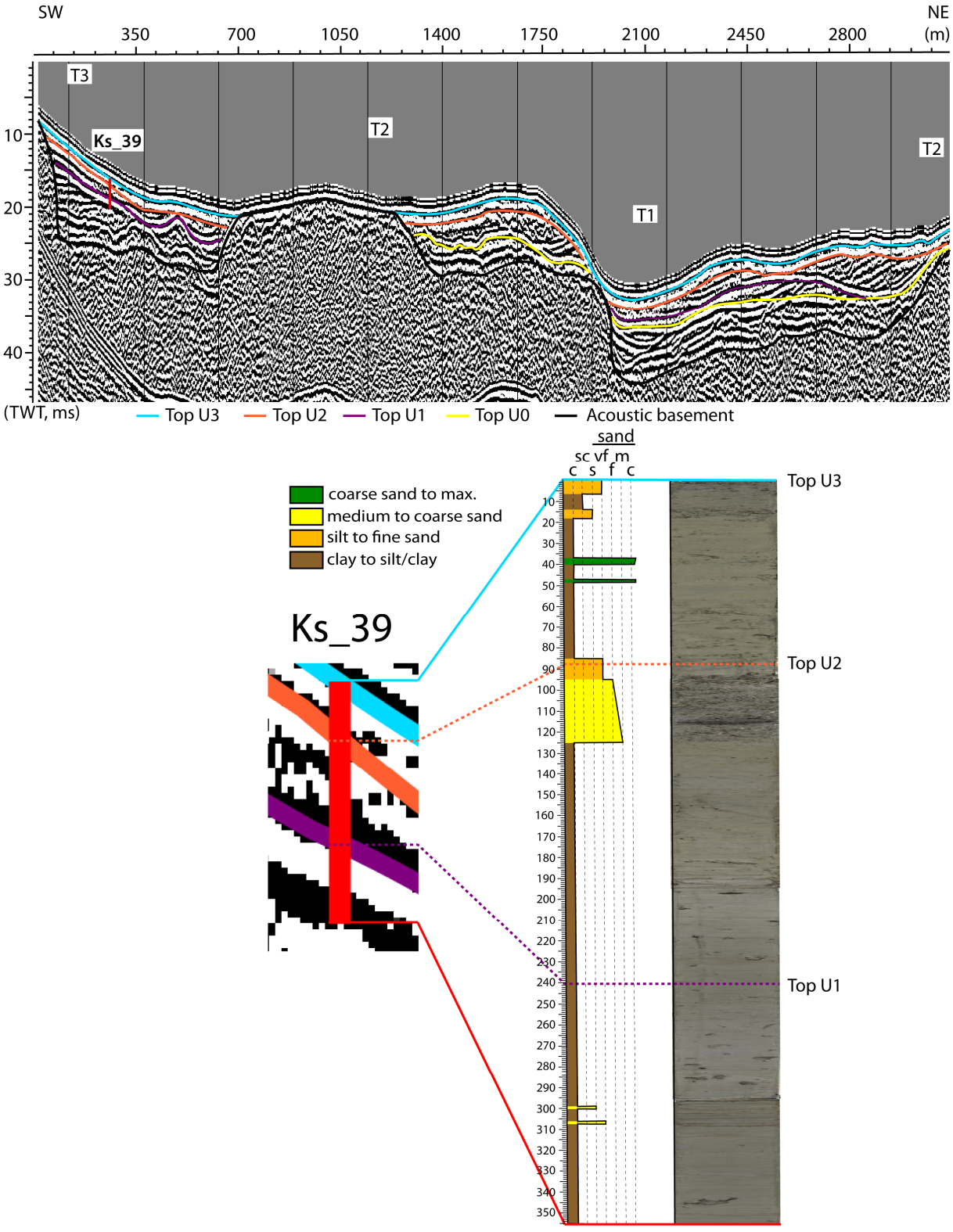

Fig. 70: (Top) Interpreted seismic profile (location on Fig. 69, profile 7). (Bottom) Photography and lithologic log for core Ks_39. c: clay, sc: silt and clay, s: silt, vf: very fine sand, f: fine sand, m: medium sand, c: coarse sand.

The validation of scenarios 1 (beginning of U1) and 2 (end of U1) differ slightly from the two other scenarios. Both represent the same sedimentary unit, but the chronology inside sedimentary units is unknown. Observed deposition of U1 may happen during scenarios 1, or 2, or both (e.g. Fig. 70). The

same core observations are used for these two scenarios and are therefore validated together. This means that scenario 2 must explain the deposition observed in cores or must not show erosion if the corresponding grain-size classes were already deposited in scenario 1 (or less erosion than the quantity previously deposited).

Core observations were compared to the distribution of grain-size classes simulated after one year. The objective is to verify the global distribution of grain-size classes. The aim of these comparisons is to verify the global simulated trends, and not the local details of deposition variations that could be linked factors other than tidal hydrodynamics (e.g. gravity flow, bioclastic accumulation, a meteorological event).

5.3 Results

Part 3 presents simulation results by showing the bathymetric evolution and distribution of grain-size classes after one year for each scenario. They are respectively compared to thickness maps and core observations. Scenarios are presented in chronological order (the oldest to the youngest). Note that a percentile 90 of bottom current velocity over one year (displayed with main flow directions for ebb and flood tides) is available in supplementary material for each scenario (full hydrodynamic analysis and model set-up is available in Olivier et al. 2021).

5.3.1 Scenario 1: start of U1 (9 000-7 500 years BP)

As the sea-level rises quickly during deposition of U1, this unit is represented by two different scenarios. The sedimentary records should therefore result from the succession of scenario 1 and scenario 2 hydro-sediment dynamics. The bathymetric evolution after one year of scenario 1 shows that most of the deposits are located over T2, over the widest parts of the main channel (T1) and, towards the Elorn river, T1 entirely undergoes sedimentation (maximum around 0.05m, Fig. 71). Areas suffering erosion are only the narrowest parts of the main channel and rare locations of T2. The simulated bathymetric evolution and the thickness map of U1 only fit over T1 (Fig. 71). T3 is still continental during this first scenario and there is therefore no tidal deposition there. A significant thickness is simulated over T2 during the beginning of U1, but none are preserved in sedimentary records (inset map of Fig. 71).

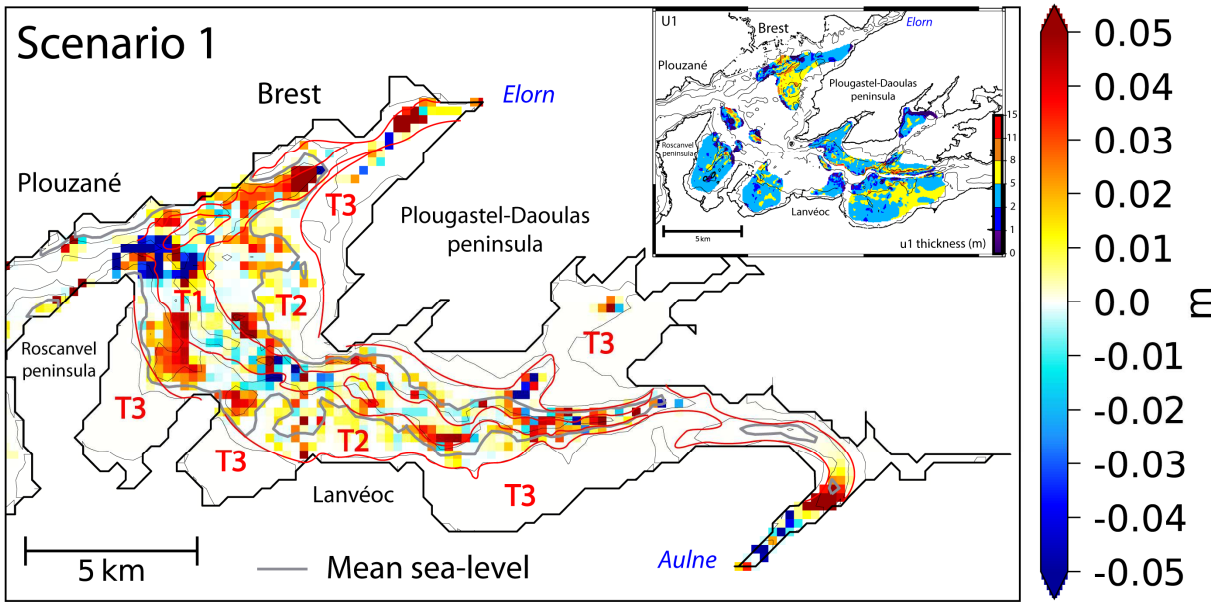

Fig. 71: Bathymetric evolution after 1 year for scenario 1 (9 k. BP). Red lines are morphological domain limits (T1, T2 T3) and the black line is the present-day coastline. Grey lines represent the mean sea-level (-26 m). The inset map is the thickness map of U1 modified from Olivier et al. (2021).

The erosion/deposition patterns are very different between grain-size classes in scenario 1: mud is eroded in the entire subtidal zone (T1) and deposited on T2 terraces (intertidal, maximum around 30 kg/m², Fig. 72a). At each core location or very close (one cell of the computation grid) where muds are observed, mud deposits are simulated (Fig. 72a, Tab. 8, Ks_34, Ks_35, Ks_38, Ks_39, Ks_40, Ks_43 and Ks_44). Core observations are in agreement with mud deposits simulated on slopes between T2 and T3. All non-cohesive sediment classes (fine sand, sand and gravel) are mostly present over T1, only some fine sands are present in secondary channels and reach some areas of T2 (Figs. 72b, 72c, 72d). Unfortunately, cores are available mostly at the interface between T2 and T3. However, two cores present fine sand accumulations (Ks_35 and Ks_44) and no fine sand deposit is simulated at the beginning of U1 at these locations (Fig. 72b).

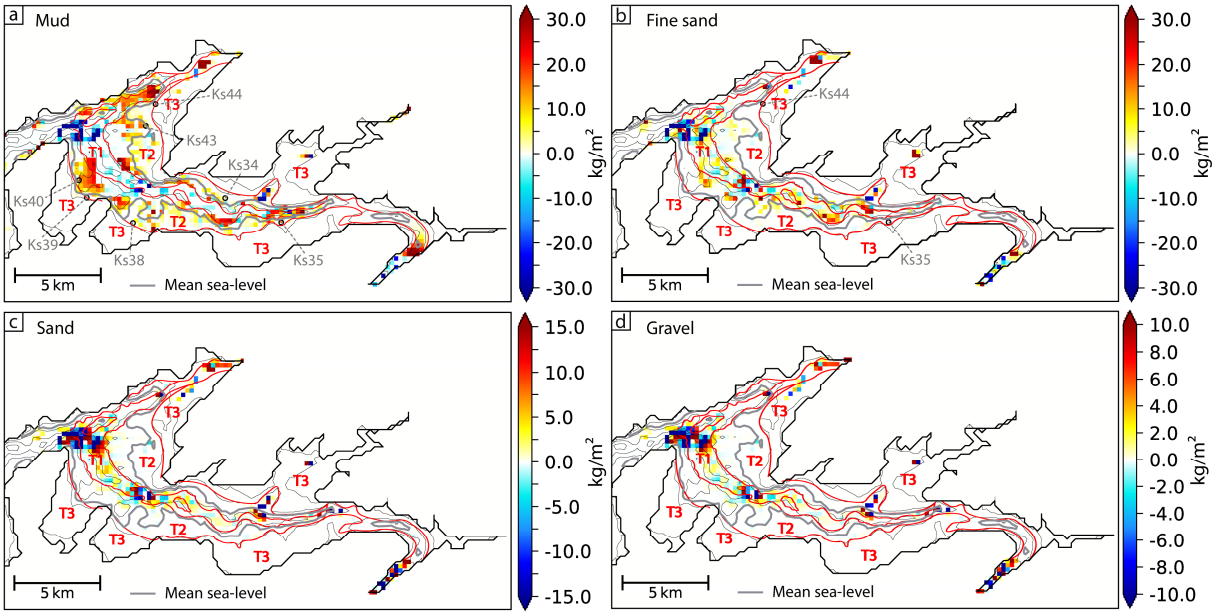

Fig. 72: Grain-size class evolution after 1 year for scenario 1 (9 ka BP): a mud, b fine sand, c sand, d gravel. Black circles indicate locations where the corresponding grain-size class were recorded by cores. Core names are available in grey. Grey lines represent the mean sea-level and red lines are morphological domain limits.

5.3.2 Scenario 2: end of U1 (7 500 – 7 000 years BP)

During scenario 2, the bathymetric evolution simulated is coherent with the thickness map of U1 (Fig. 73), with most of the deposits over T3, on slopes between T3 and T2 (maximum around 0.04m, Fig. 73) and some accumulations located in the deepest parts of T1 (in the centre and to the north of the central area,). Most of T2 domain and T1 in the upper part do suffer erosion (maximum around -0.02m over T2, Fig. 73).

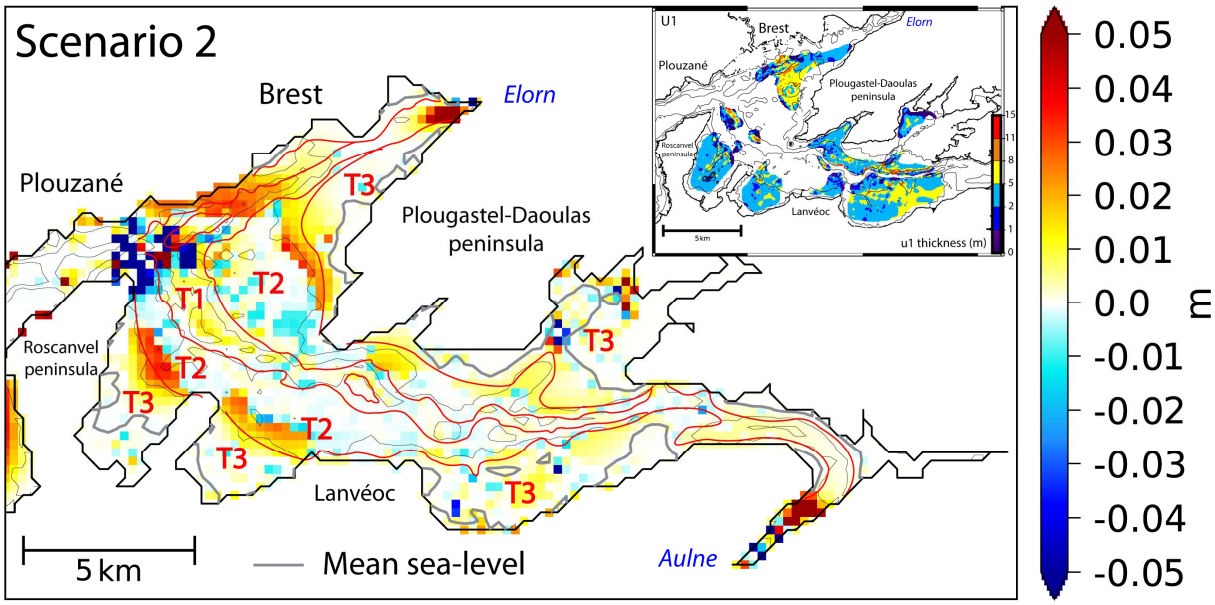

Fig. 73: Bathymetric evolution after 1 year for scenario 2 (7.5 ka BP). Red lines are morphological domains limits (T1, T2 T3) and black line is the present-day coastline. Grey lines represent the mean sea-level (-10 m). The inset-map is the thickness of U1 modified from Olivier et al. (2021).

During scenario 2 (end of U1), mud deposits are simulated only over T3 and on slopes between T2 and T3 (between 5 and 20 kg/m², Fig. 74a). All the cores presenting mud records (Fig. 74a, Ks_38, Ks_39, Ks_40, Ks_43 and Ks_44) are located where mud deposits are simulated, except for Ks_34 and Ks_35. At Ks_34 and Ks_35 locations, the balance between erosion and deposition is close to 0 (Fig. 74a), but mud deposits are simulated during scenario 1 (Fig. 74a). If no erosion is simulated during scenario 2 (end of U1), deposits from the beginning of U1 (scenario 1) should be preserved and are indeed observed inside cores (Ks_34 and Ks_35). In the centre of the bay, non-cohesive sediments are remobilised mostly from T2 towards T1 and for fine sands also towards T3 (Figs. 74b, 74c, 74d). Cores on slopes between T2 and T3, do corroborate this simulation result as they display only mud and fine sand. Fine sand deposit is observed in Ks_44 and is simulated close to the ks_44 location. In the upper area, slight movements of sand and gravel are simulated over T1 and secondary channels, but over these areas, only fine sands are deposited in significant quantity (around 5 kg/m², Figs. 74b, 74c, 74d). Fine sands are observed inside core Ks35, which is located in a secondary channel in the upper area (Fig. 74b). Deposits simulated in T1 are impossible to confirm by field data as no cores are available in this morphological domain. However, the seismic facies were interpreted as coarse sediments (Gregoire, 2016) and would therefore corroborate the simulation results.

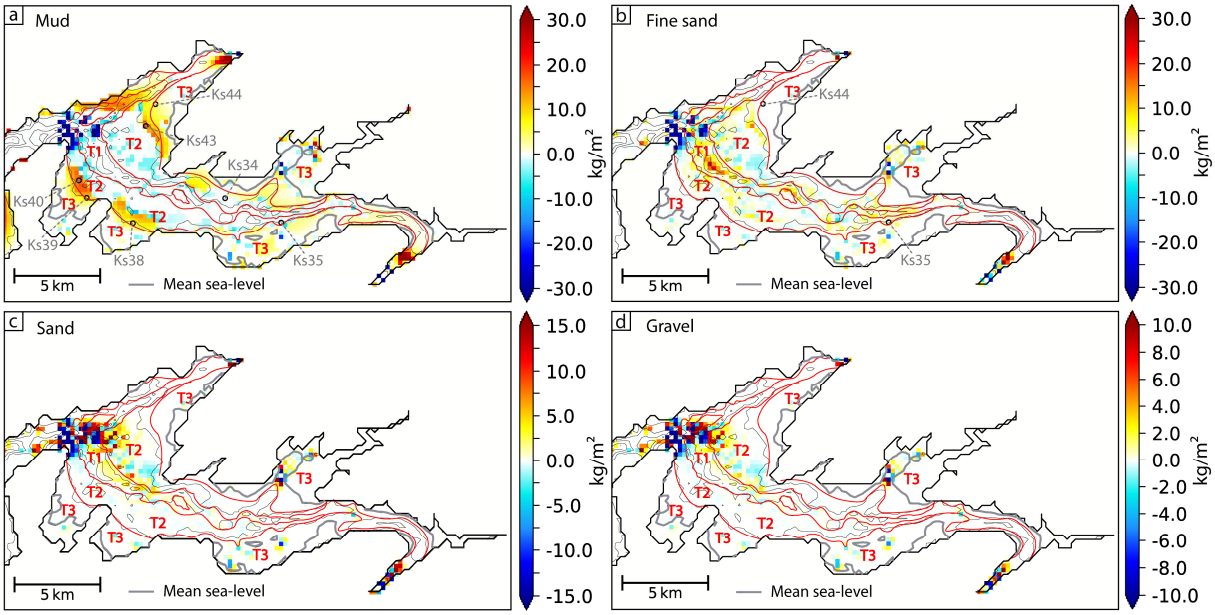

Fig. 74: Grain-size class evolution after 1 year for scenario 2 (7.5 ka BP): a mud, b fine sand, c sand, d gravel. Black circles show where the corresponding grain-size class were recorded by cores. Core names are available in grey. Grey lines represent the mean sea-level and red lines are morphological domain limits.

5.3.3 Scenario 3: U2 (7 000 – 3 000 years BP)

At this stage, erosion is mainly located over T2 in the central part and in the strait between Plougastel-Daoulas and Lanvéoc (maximum -0.03m, Fig. 75). Simulated deposits are located over: T3, the slopes between T2 and T3 in the central area (maximum 0.04m), and most of the upper area (T1 to T3, around 0.01m, Fig. 75). The thickness map of U2 displays the same patterns: no deposit is preserved over T2 in the north of the main channel and the north of Lanvéoc, and accumulations are recorded over the rest of the Bay (inset map, Fig. 75).

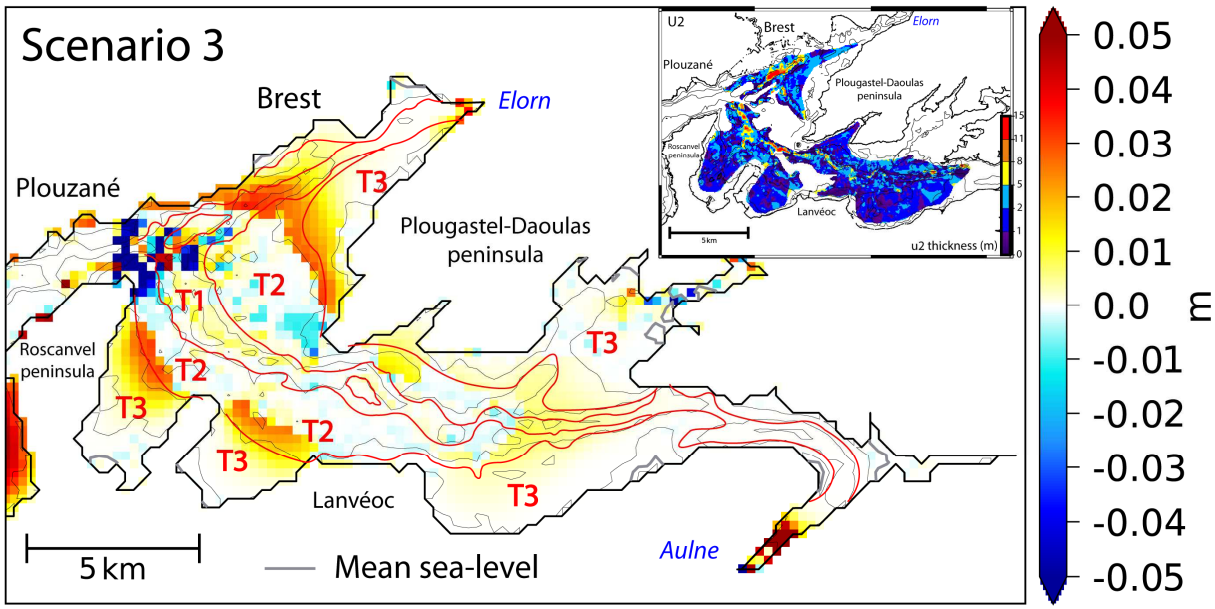

Fig. 75: Bathymetric evolution after 1 year for scenario 3 (7 ka BP). Red lines are morphological domain limits (T1, T2 T3) and the black line is the present-day coastline. Grey lines represent the mean sea-level (-5 m). The inset map is the thickness of U2 modified from Olivier et al. (2021).

At 7 000 years (BP), mud deposits are simulated over T3, on slopes between T2 and T3, and over most of the upper area (Fig. 76a). Mud deposits are recorded in Ks_35, but the two cores available in the upper part also display sands (Ks_34 and Ks_35, Fig. 76c). Mud deposits are also observed in cores Ks_27, Ks_39, Ks_41 and Ks_44 in the centre (Fig. 76a), where mud deposits are simulated. Non-cohesive sediment erosion (and thus transport) is simulated mostly over T2 and deposition is simulated at the edges of the same morphological domain: on slopes between T2 and T3 (mostly fine sands, 5 to 10 kg/m², Fig. 76b) and T1 (maximum 15 kg/m² for fine sands, Fig. 76b). Observations of cores Ks_38, Ks_44 and Vz_31 also show fine sands on slopes between T2 and T3 and fine-sand deposits are simulated close to the three core locations (Fig. 76b). Ks_39 reveals the presence of some sand on the slope between T2 and T3, but very few deposits of sand are simulated close to core Ks_39 (Fig. 76c, less than 1 kg/m²).

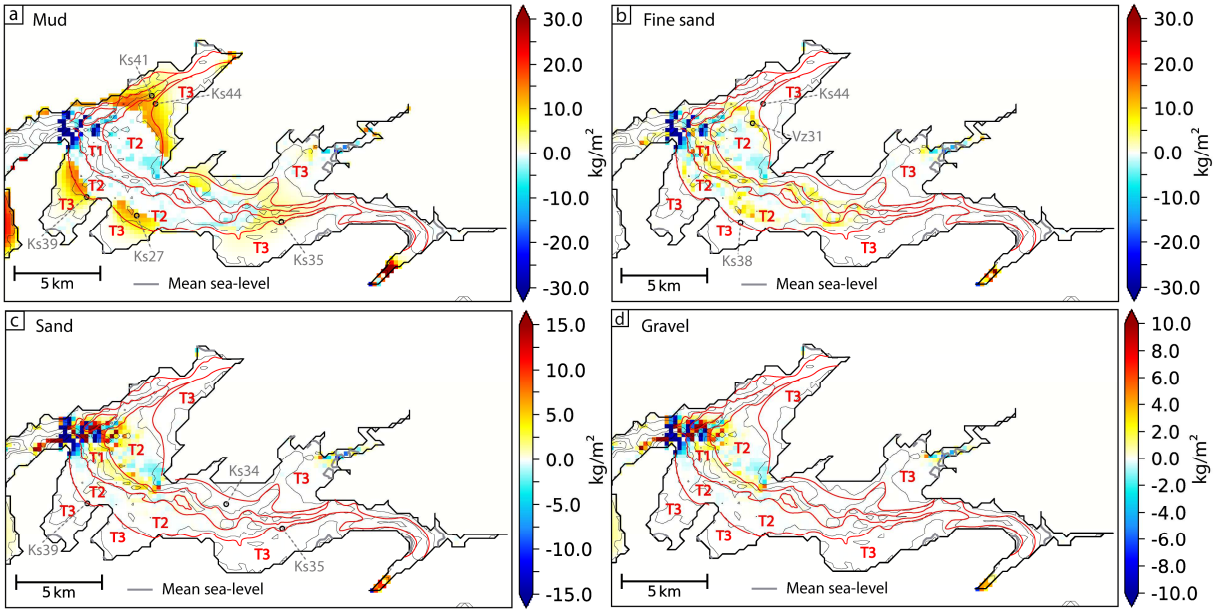

Fig. 76: Grain-size class evolution after 1 year for scenario 3 (7 ka BP): a mud, b fine sand, c sand, d gravel. Black circles show where the corresponding grain-size classes were recorded by cores. Core names are available in grey. Grey lines represent the mean sea-level and red lines are morphological domain limits.

5.3.4 Scenario 4: U3 (2 000 years BP - Present-day)

During scenario 4, erosion patterns are mainly located over T2 (maximum -0.04 m, Fig. 77), over T1 in the upper part and towards the mouth of the Aulne river (<-0.01 m). Depositional areas are over T3 (maximum 0.04 m, Fig. 77) and T1 in the centre (maximum 0.05 m, Fig. 77). Important deposits are also simulated on slopes between T3 and T2 east of Lanvéoc (maximum 0.03 m, Fig. 77). There is one major difference between the bathymetric evolution simulated and the thickness map of U3: simulated deposits are located mostly over T1 and T3 in the centre (Fig. 77) whereas seismic data interpretation describes some deposits also over T2 (inset map, Fig. 77).

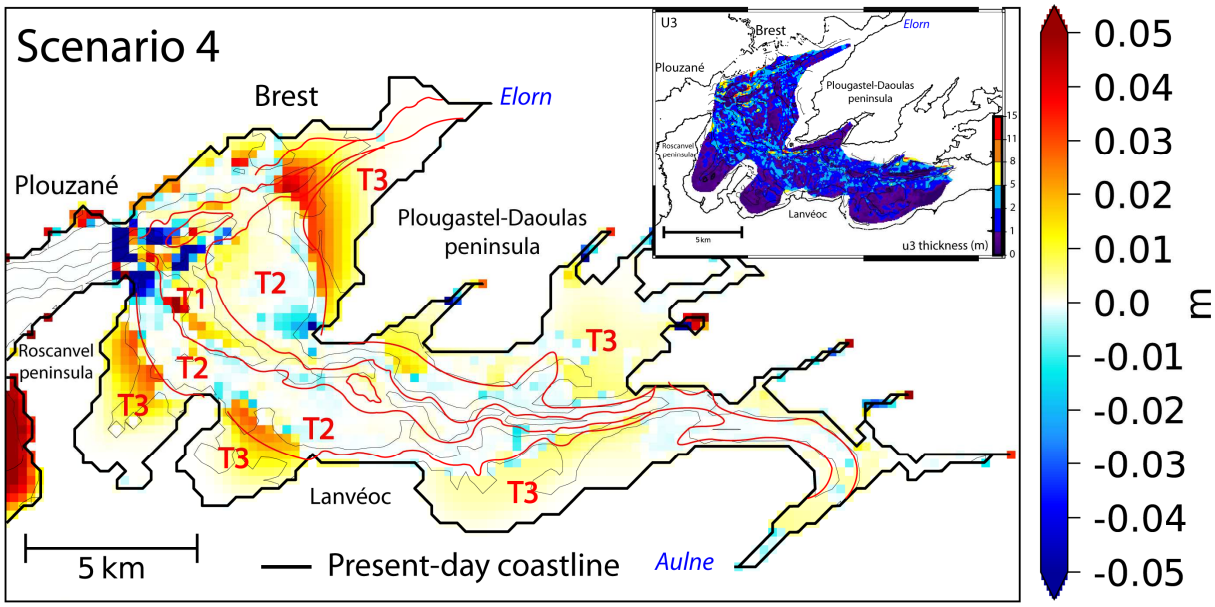

Fig. 77: Bathymetric evolution after 1 year for scenario 4 (present-day). Red lines are morphological domain limits (T1, T2 T3) and the black line is the present-day coastline. The inset map is the thickness of U3 modified from Olivier et al. (2021).

During U3, cohesive sediments settle mostly over T3 (around 1 to 15 kg/m², Fig. 78a) and non-cohesive sediments at the edges of T2 domains (T1 mostly and slopes between T2 and T3, fine sands: maximum > 30 kg/m², sands: maximum 5 kg/m², gravels: maximum 2 kg/m², Figs. 78b, 78c, 78d). Muds are observed only in Ks_35, Ks_38, Ks_39 (T3) and Ks_34 (T2), but at the Ks34 location, no mud deposit is simulated. Fine-sand deposits are simulated close to cores that also show fine-sand grain size (Fig. 78b, Ks_27, Ks_34, Ks_35, Ks_38, Ks_39, Ks_41, Ks_44, Vz_31). Sands simulated and observed in cores (Ks_27, Ks_40, Ks_43, Ks_44) also make a good match, even if small quantities are simulated at these core locations (around 1 kg/m², Fig. 78c). Also note that two cores (Ks_40 and Ks_41) show gravel deposit that is not simulated, close to T1 in the north of the central part and on slopes between T2 and T3 in the south (Fig. 78d). The presence of consequent gravel deposits in two cores is unexplained by the tidal process and should be discussed.

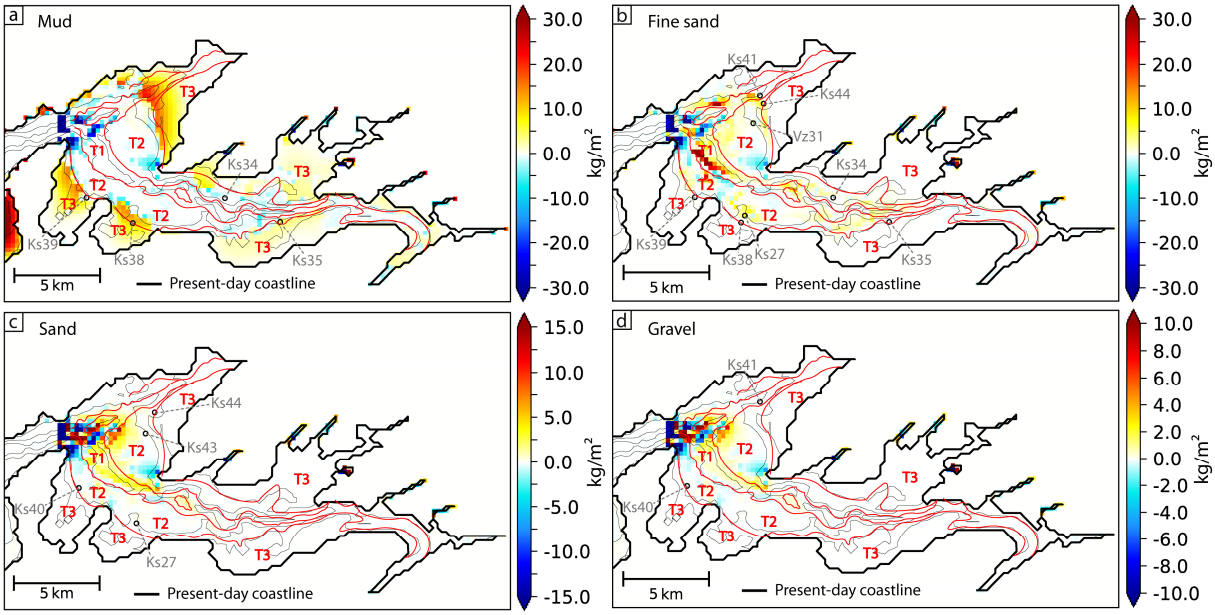

Fig. 78: Grain-size class evolution after 1 year for scenario 4 (present-day): a mud, b fine sand, c sand, d gravel. Black circles show where the corresponding grain-size classes were recorded by cores. Core names are available in grey and red lines are morphological domain limits.

5.4 Discussion

5.4.1 Holocene reconstruction

The numerical simulations of the four scenarios allow to make a reconstruction of hydro-sediment pattern evolution for the three sedimentary units U1 to U3 over the last 9 ka. At the beginning of U1 deposit (9 ka BP) sea-level is 26 metres lower than present-day level (intertidal area over T2 terraces). Main deposition takes place over T2 and within the main channel in the upper zone (Figs. 79a and 79b). Then, at the end of U1 deposition (7.5 ka BP), sea-level reaches 10 metres below present-day level, shifting the intertidal area from T2 (scenario 1) to T3 (scenario 2). Bottom current velocities over T1 decrease with increasing depth and the highest velocities are then observed over T2 (Olivier et al., 2021 and supplementary materials). Tidal currents no longer follow the shape of the main channel in the central area. The distribution of main currents is largely influenced by strait morphology in the east (ebb) and west (flood) of the central area, that orientates water fluxes (Olivier et al., 2021). This results in the formation of a clockwise gyre in the centre of the bay. Tidal currents induce strong erosion of the initial sediment layer (especially mud): most of the sediment deposited during scenario 1 is reworked (over T2 and T1 towards the Aulne mouth, Figs. 79a to 79d). The sediment dynamic simulated for scenario 2 explains the absence of most of scenario 1 deposits from sedimentary records. The beginning of U1 (scenario 1: 9 to 7.5 ka BP) is almost not preserved, except over T1 and mud deposits over slopes between T2 and T3 in the centre of the Bay. Sedimentation during scenario 2 mainly occurs over T3 (mud), in the centre of the bay over the slopes between T2 and T3 (mud and fine sand) and over T1 (fine sand and sand, Figs. 72, 79c and 79d). The simulated bathymetric evolutions of scenarios 1 and 2 are consistent with U1 thickness map, in the same way as the distribution of grain-size classes with core observations. This demonstrates that sedimentary records of U1 mainly testify to the end of U1 hydro-sediment dynamic (scenario 2: 7.5 to 7 ka BP). The beginning (scenario 1: 9 to 7.5 ka BP) is almost unpreserved (Fig. 79a to 79d).

U2 deposition takes place between 7 ka and 3 ka (BP, scenario 3) with sea-level five meters below the present-day level. Most of the T3 terraces are then located in a subtidal domain and ebb and flood tide distributions are different in the upper area (ebb T3 and flood T1, Olivier et al., 2021). Simulation outputs and sedimentary records (thickness map and cores) display the same trends throughout the Bay: main sedimentation over T3, the slopes between T2 and T3, T1 in the centre (Fig. 79e), and over most of the upper area (Fig. 79f). Between U1 and U2 the hydro-sediment patterns are similar in the centre, but very different in the upper zone (Fig. 79d and 79f). Between scenarios 2 and 3 sea-level rises by only five metres, while most T3 terraces become subtidal. The subtidal area increases substantially in comparison to the amplitude of sea-level rise (Fig. 81e). The active flow section width (i.e. the section on which incoming and outgoing water to/from upstream areas flow) increases greatly, (only T1 and T2 in scenario 2, and T1, T2 and T3 in scenario 3). This results in weaker currents in the upper area than in the previous scenario (end of U1, Olivier et al., 2021) and it allows the deposition of mud in all morphological domains in the upper area (Figs. 79a and 79f). However, we observe a difference of maximum sediment rate between simulations and sedimentary records over T1 and T3 in the centre: the largest sediment thicknesses observed are located over T1 (Fig. 79e), but the largest thicknesses simulated are over T3 and over the slopes between T2 and T3 (Fig. 79e). In the centre (T1 and T2), deposits are made mostly of sands and fine sands (without mud), while over T3, deposits are mainly mud (Fig. 76). This suggests that during U2 deposition, larger volumes of fine sands and sands, and a smaller volume of mud were available than during U1 deposition (scenarios 1 and 2). Sediment supply probably changed between U1 and U2. This hypothesis is supported by the good correlation between erosion/deposition patterns simulated and sedimentary records (Figs. 75 and 76), but further simulations would be needed to confirm sediment supply evolution.

During deposition of the last sedimentary unit U3 (scenario 4), sea-level remained close to present-day level. In this configuration, T3 terraces are subtidal and only a few intertidal areas are observed within the Bay of Brest. Between scenario 3 and 4, sea-level rises by five metres, while the subtidal area in the Bay remains similar (there are few new subtidal areas close to the rivers mouths, especially the Aulne one). The active flow section width remains similar and the water volume transported by the tide through the active flow section increases. More intense currents characterise the upper area compared to scenario 3 (Olivier et al., 2021). During scenario 4, currents prevent mud deposits over T1 domain in the upper area, which was covered by mud during scenario 3 (Figs. 76a and 78a). The bathymetric evolution of scenario 4 and the thickness map of U3 are consistent over the upper area and over T1 and T3 in the centre (Figs. 79g and 79h). However, the thickness map displays U3 deposits over T2 in the centre (Figs. 77 and 79g). As no core is available over T2, observations only rely on seismic interpretation. The hydro-sediment dynamic simulated over T2 remains unchanged from scenario 2 to 4 in the centre (7 500 years BP, gyre formation): muds are removed from T2 and T1 towards T3 and non-cohesive grain-size classes are mostly transported over T2. This suggests that the sediment deposits interpreted for U3 over T2, could be non-cohesive sediments frequently reworked over the last 7 500 years. This hypothesis is supported by present-day grain-size classes and sediment structure distribution maps (Gregoire et al., 2016), which reveal that T2 terraces in the centre are either mostly covered with coarse sediments, or not covered, and many active sediment structures have been identified over the same area (e.g. sand ridges, comet tails). Taking into account the simulated dynamics (scenarios 2, 3 and 4) and observations from Gregoire (2016), sediment thickness (ranging from 1 to 5 m) over T2 terraces (U3, Figs. 77 and 79g) probably correspond to non-cohesive sediments reworked over the last 7 500 years.

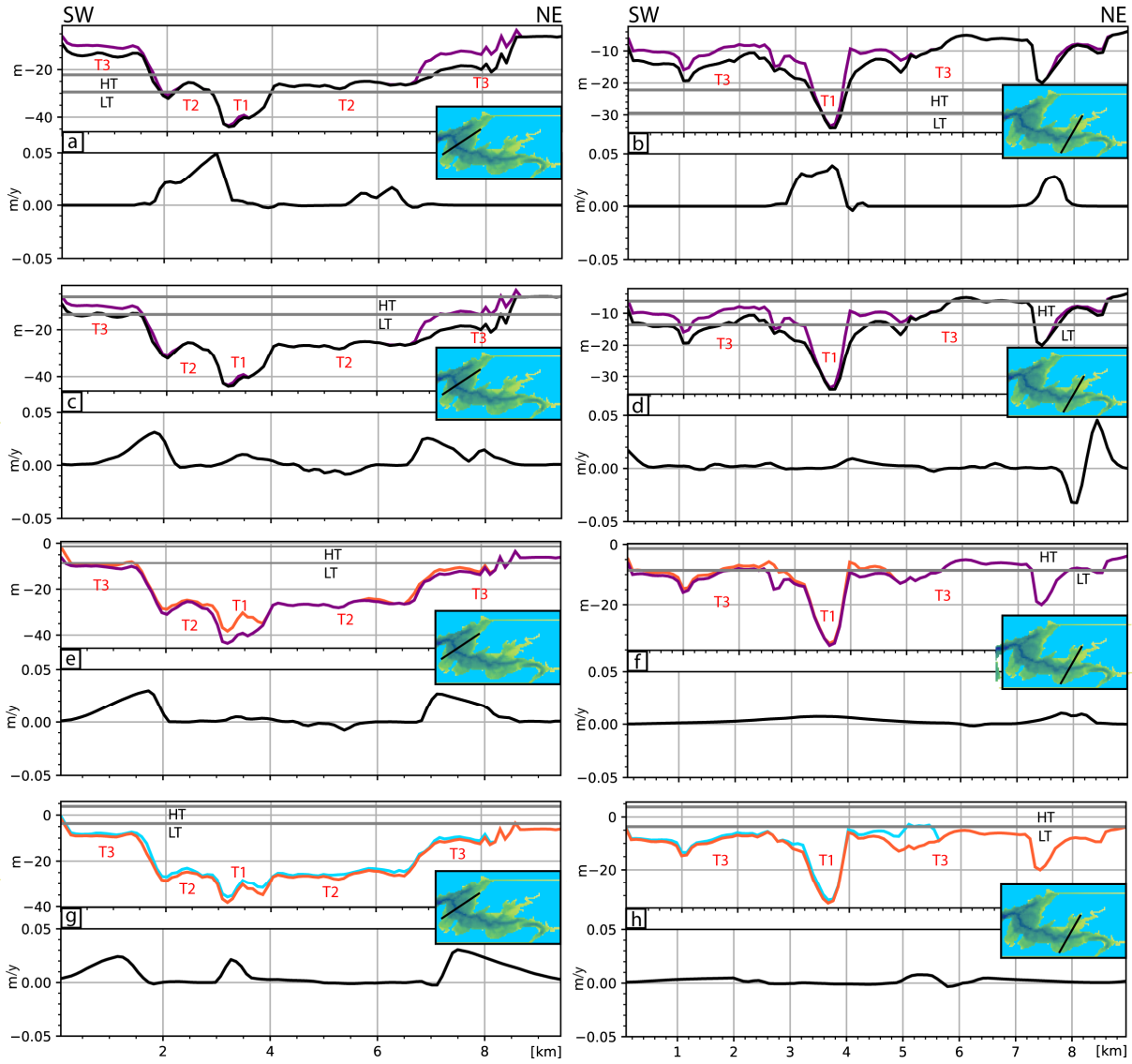

Fig. 79: Cross-section of sedimentary unit thicknesses (black line top of U0, purple line top of U1, orange line top of U2 and blue line top of U3) compared to simulated bathymetric evolution over 1 year, in the central area (a: scenario 1, c: scenario 2, e: scenario 3, and g: scenario 4) and in the upper area (b: scenario 1, d: scenario 2, f: scenario 3, and h: scenario 4). Inset maps show the locations of cross-sections. Grey lines represent the highest free surface level (HT: Highest Tide) and the lowest free surface level (LT: Lowest Tide).

Global trends of erosion/deposition patterns between simulation and data fit well. However, punctually simulation outputs and geological data mismatch: sand observations (Ks_34 and Ks_35) in the upper zone during scenario 3 (Fig. 76) and gravels (Ks_40 and Ks_41) in the centre during scenario 4 (Fig. 78) remain unexplained by simulations. Simulated tidal currents are not able to transport sands and gravels at these core locations, and therefore it is impossible to link the deposits to tide-induced hydrodynamics (Olivier et al., 2021, Figs. 76 and 78). They are potentially due to non-simulated extreme events, such as river flooding, storm winds, or gravity movement. Such energetic events should be able to transport coarse sediments into the Bay, without later remobilisation by too weak tide-induced currents. They should therefore be recorded in the cores (unless they reach T2 in the centre, which is the only morphological domain where tidal currents can transport sands and gravels during scenarios 2, 3 and 4). Ehrhold et al. (2021) observed storm patterns within some sedimentary facies of units U2 and U3 that may correspond to the coarsest deposits we also observed. Such deposits

cannot be simulated in our scenarios, as river flooding or storm winds (unknown for past stages) are not parameterized in our simulations. However, the presence of these coarse sediments underlines the importance of climatic variations on sediment supply in estuaries. Even anthropic variations, such as infrastructure constructions (dams, harbour…), or dredging, can influence sediment deposits and potentially the deposits of U3 (2 000 years BP to the present-day, Ehrhold et al., 2016; Gregoire et al., 2016).

5.4.2 Sediment supply

5.4.2.1 Holocene river evolution

Previous studies have explored the Holocene climatic evolution within the Bay of Brest and on a larger scale over northern and western Europe, mainly relying on pollen data (e.g. Fernane, 2014; Lambert, 2017). We will discuss here the main conclusions of these studies combined with our own, which are mainly qualitative observations on the evolution of climatic parameters (e.g. temperatures, vegetal covering, precipitations, humidity…). Three main climatic time intervals are highlighted by previous studies at the temporal scale of our scenarios: 11.7 to 8.2 (ka BP, scenario 1); 8.2 to 4.2 (ka BP, scenarios 2 and 3); 4.2 (ka BP) to the present-day (scenario 4):

-From 11.7 to 8.2 ka BP, the climate was colder than at present-day and a strong land runoff is inferred, due to poor vegetation (periglacial environment, Lambert, 2017).

-From 8.2 to 4.2 ka BP, the Holocene climatic optimum occurred and was characterised by a warm time interval (Koshkarova and Koshkarov, 2004), during which vegetation in the watershed of the Bay of Brest significantly expanded (Lambert, 2017). The time interval is also associated with an increase in precipitations in northern Europe (Seppä and Birks, 2001; Bjune et al., 2005), particularly at the beginning of the time interval (Berger and Guilaine, 2009) and within the interval 6-5 ka (BP, Mojtahid et al., 2013). Penaud et al. (2020) suggest that the stronger humidity is linked to the North Atlantic Current, which may have amplified seasonal continental humidity in western France during the Holocene climatic optimum.

-From 4.2 ka BP to the present-day, the climate has become colder than the previous time interval (Berger and Loutre, 1991), but warmer than the first one. Due to human activity (mainly agriculture), deforestation is increasing runoff from the land (Lambert, 2017; David et al., 2022) and, consequently, sediment concentration in rivers. Precipitation slightly decreases in comparison with the previous time interval in northern Europe (Seppä and Birks, 2001; Bjune et al., 2005). Moreover, during the time interval 3.3 to 2.4 ka (BP), the Loire River transport capacity (a major river in western France) declines (David et al., 2022).

Note that evolutions of these parameters were highlighted at shorter time scales than the ones discussed here and cannot be compared with the time intervals studied here. For example, cyclicity between a dry and wet period of ~1500 years is highlighted in western Europe by Smith et al. (2016) during the Holocene; or David et al. (2022) noticed an increase in the Loire River transport capacity within the deposition time interval of U3 (2 ka to present-day), but it cannot be linked to our simulation of scenario 4, as it is supposed to be representative of the whole of deposition of U3.

To summarize environmental and climatic evolution at the time scale of our scenarios, the Bay of Brest undergoes: more precipitation during scenarios 2 (7.5 - 7 ka BP) and 3 (7 - 3 ka BP) and less land runoff than during scenario 1 (9 - 7.5 ka BP); less precipitation in scenario 4 (2 ka - present-day) and more

land runoff than during the two previous scenarios. Each time that precipitation increased, the land run runoff decreased and conversely. In a qualitative way, we could imagine that these two components would compensate each other and finally trigger no variations in sediment supply. We know that river profiles decreased significantly during the Holocene transgression (-26 to 0 m), which, in turn, means a decrease in potential energy (i.e. difference in elevation) between the top of rivers and the Bay and thus a decrease in river current velocities. This implies that river sediment supply should decrease from scenario 1 to 4. It is consistent with simulations, where a trial and error method was applied to determine boundary conditions and sediment fluxes from the rivers. The multiplicative factors (scenario 1 to 4: 10.9, 4, 2, 1) obtained on river water discharge through time are almost a ratio of sea-level variations between scenarios (scenario 1 to 4: -26, -10, -5, 0 m) and show a general decrease. The obtained river water discharge (in order to simulate a realistic volume for each scenario) led to river discharge in agreement with the idea of a sediment flux reduction linked to the slope reduction of rivers.

The evolution of river sediment supplies in the Bay of Brest is linked to the evolution of river profiles at first order (linked to the evolution of sea level). However, at a finer temporal scale, other parameters (e.g. precipitations, vegetal covering) could be key factors in sediment supply evolution.

5.4.2.2 Impact of sediment sources (boundary condition)

The parameterisation of past sediment supply is a challenge, given the number of unknown parameters. However, the impact of different sediment sources is one of the most important issues in understanding coastal basins. To assess the influence of sediment sources in the Bay of Brest, three additional simulations were performed for each scenario. All have the same parameterisation as simulations presented in section 2, but without the initial sediment layer. The four scenarios are simulated without river input (Fig. 80a1 and 80b1), or without input from the oceanic border (Figs. 80a2 and 80b2), or with both sediment sources. The aim is to explore the impact of continental and oceanic sources, in terms of amount and distribution of sediment supply within the Bay.

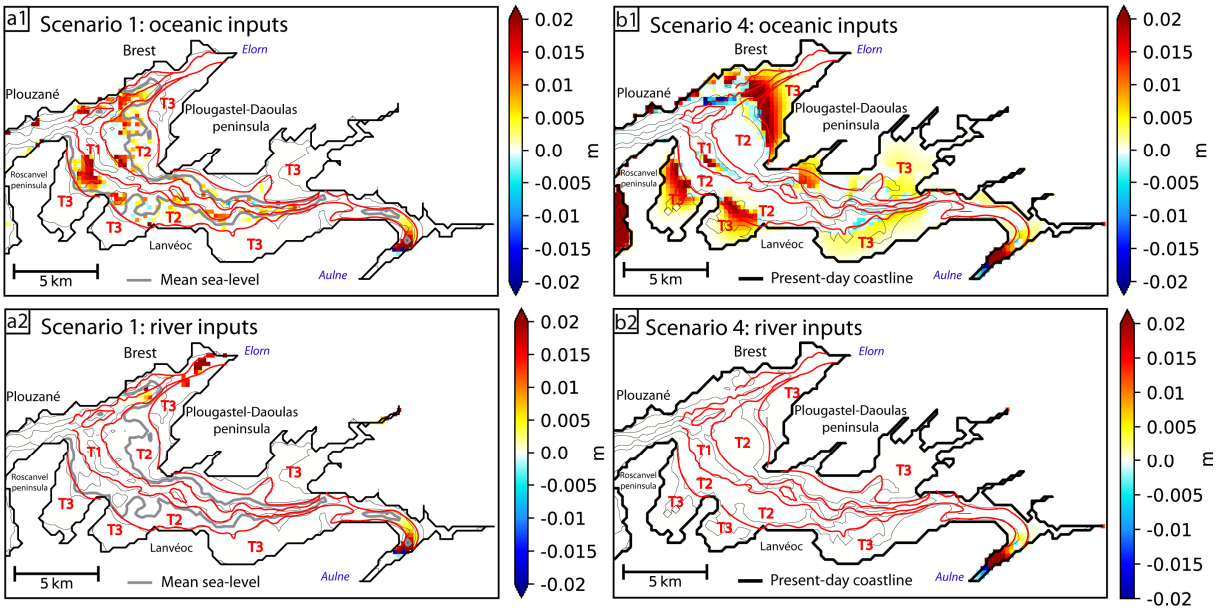

Fig. 80: Simulated bathymetric evolution of the Bay of Brest after one year. a1: Scenario 1 without initial sediment and without river water discharge. b1: Scenario 4 without initial sediment and without river water discharge. a2: Scenario 1

without initial sediment and without oceanic border input. b2: Scenario 4 without initial sediment and without oceanic border input.

The sedimentation induced by river sediment inputs is mainly concentrated over T1 and close to the Elorn and Aulne mouths (Figs. 80a2 and 80b2), while the sedimentation induced by oceanic sediment inputs are more largely distributed throughout the Bay (Figs. 80a1 and 80b1) and in greater quantities for scenarios 1 and 4. The same observations are made for scenarios 2 and 3 and thus only scenarios 1 and 4 are displayed (Fig. 80). Simulations with only oceanic inputs display the same global deposition pattern as the genuine scenarios, with an initial sediment layer in the Bay and river inputs (section 5.3, Figs. 71 and 77, to compare with Figs. 80a1, 80b1).

Simulations without river or oceanic inputs, are compared to those with both sediment sources to quantify the respective influences of sources on simulations (see computational limits Fig. 69). Oceanic inputs represent 55%, and rivers inputs 26% of the quantity deposited in the simulation with both sediment sources during scenario 1, 62% and 9% during scenario 2, 89% and less than 1% during scenario 3, 94% and less than 1% during scenario 4. The river influence on the amount of sediment supply decreases during the Holocene, because of the evolution of the multiplicative factor used on river fluxes between scenarios. The weighted average along the deposition time interval of the three units (Fig. 68) shows that oceanic inputs represent 82% of sediment supply during the Holocene (9 ka BP - present-day), against less than 6% for river inputs.

The methodology applied to calibrate sediment inputs presents three weaknesses. (i) In this study only river water discharges are modified, but suspended matter concentration can be modified too. In theory, the decrease in potential energy should lead to a decrease in river current velocities, which induces a decrease in the amount of suspended matter, but not of river water discharge. This choice was made for numerical reasons, as a too high concentration cannot be transported to the Bay by the present-day river water discharge and most it settles inside rivers. However, changes in river water fluxes had very limited impact on hydrodynamic patterns in the Bay (see supplementary material and Olivier et al., 2021). The most important is thus to have a realistic amount of river sediment supply, as this study focuses on the evolution of sediment dynamics within the bay. (ii) The mixture (grain-size proportions) at boundaries as well as the amount of sediment available at oceanic boundaries, may have changed over the last 9000 years. (iii) The calibration of river discharge relies on the preserved sediment rate calculated from sedimentary units: it corresponds to minimum estimates of sediment budget (not including the possible remobilization and non-preservation of sediment).

5.4.3 Implications for estuarine stratigraphic interpretation

Thanks to hydro-sediment modelling over four scenarios, the impact of mean sea-level variations on hydro-sediment dynamics and the distribution of associated sediment deposits were analysed. At the time scale of the transgression, boundaries between erosion and deposition, as well as the sand/mud transition, are progressively pushed upstream of the estuary (i.e. flanks and in the direction of the river mouth) because of tidal asymmetry in the Bay of Brest (see supplementary material); this is also visible through the grain-size increase in deposits observed from cores located on the slopes between T2 and T3 domains (Tab. 8). However, the progression of these boundaries upwards of the estuary does not correspond to sea-level rise. Tidal dynamic is closely dependent on the underlying morphology and therefore changes through time (Olivier et al., 2021). In the Bay of Brest, large and fast coastline retreats are mainly perpendicular to the main channel, generating a

strong increase in the active flow section width when the terraces (T2 and T3) pass into subtidal domain. The main channel (T1) displays a decreasing cross-section (width) and decreasing bathymetry from the strait between Plouzané and Roscanvel peninsula to the Aulne mouth (~60 to ~20 m depth), which is progressively flooded over the Holocene. Upstream areas of the Bay are rivers with steep banks.

At 9 ka (cal. BP, -26 m), most of non-cohesive sediment are transported over T1 and cohesive sediments settle in intertidal areas (T2 terraces) and over T1 towards river mouths (Fig. 81a).

At 7.5 ka (cal. BP, -10 m), bottom current velocities over T1 decrease with the increasing depth and the highest velocities are then observed over T2 in the centre (Olivier et al., 2021). Most sand movements take place over T2 and they settle at the edges of T2 terraces (over T1 or on slopes between T2 and T3, Fig. 81b and 81e). In the upper area, T1 remains the only subtidal domain (as T2 is small at this spot). Thus, the upstream tidal prism increases substantially (water volume transported by the tide through the upper area), while the active flow section remains of similar width (only T1). Intense tidal currents are observed over T1 and fine sands are transported over the same morphological domain and secondary channels (Fig. 81b). Previous muddy deposits (9 ka cal. BP) are removed from T2 in the centre and from T1 in the upper area towards T3 terraces (Fig. 81b).

At 7 Ka (cal. BP, -5m), patterns similar to the previous scenario are observed in the centre. In the upper area, the active flow section width increases substantially (T3 subtidal, Fig. 81e). This fast and important increase in the active flow section width induces less intense currents in the upper area than during the previous scenario (Olivier et al., 2021), as a slightly greater volume of water is transported by the tide and that volume passes through a much larger section. This phenomenon is amplified by the shallow depth and flat shape of T3, which induces strong friction all over this morphological domain at 7 (Ka cal. BP). This allows the deposition of mud over all the morphological domains and only a few fine sands are transported by tidal currents into the upper area (Fig. 81c).

At the present-day, the limit between mud and sand deposits is located further towards T3 than during the two previous scenarios in the centre, but general patterns are the same since 7.5 ka (cal. BP, Fig. 81). The active flow section in the upper area remains of similar width, while the upstream tidal prism still increases. Thus, higher currents characterize the upper area of the estuary than at 7 ka (cal. BP, Olivier et al., 2021). The augmentation of tidal current velocity is amplified by the reduction of friction over T3 with the increasing depth (Fig. 81e). Non-cohesive sediments are transported more upward over the main channel than during the previous period and muds settle only over T3 (Figs. 81c and 81d).

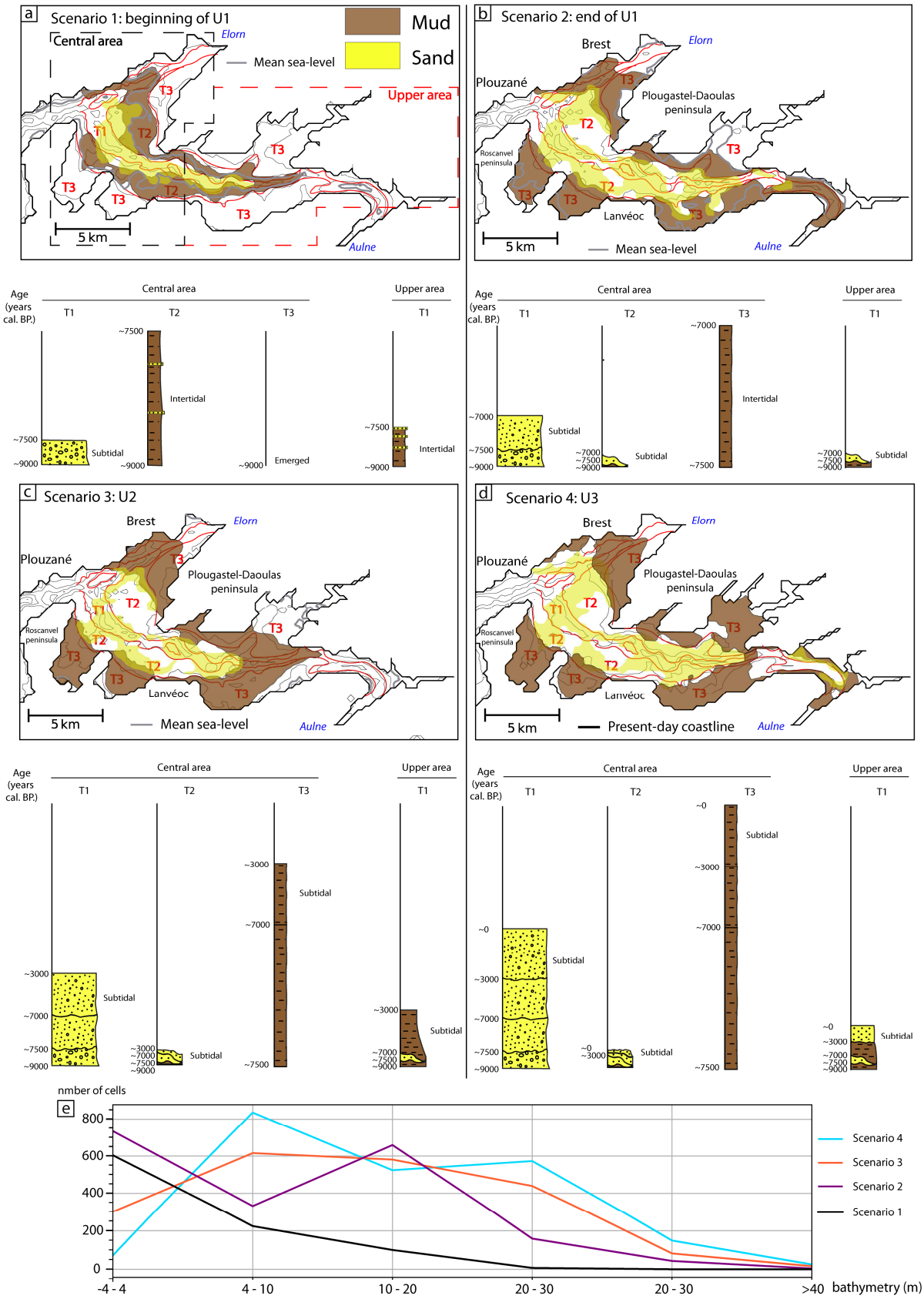

Fig. 81: Maps representing the evolution of depositional areas for mud (brown) and fine sands (yellow), with four synthetic logs displaying the theoretical stratigraphic stacking of each morphological domain after each scenario (vertical scale represents the approximative representative thickness over morphological domains). a: scenario 1, b: scenario 2, c: scenario 3, d: scenario 4 and e: the hypsometry of each scenario (computational limits on Fig. 3). This figure aims to display the evolution of depositional areas and the interpreted preservation of deposits, in relation to paleoenvironmental changes.

These qualitative observations are represented over the simplified upper zone of the Bay of Brest, to highlight the main mechanisms and triggers of hydro-sediment changes (Fig. 82). They demonstrate that movements of the erosion/deposition boundary and of the cohesive/non-cohesive sediment deposition boundary, do not necessarily move upward of the estuary during transgression cycles (as classical sequence stratigraphic interpretations suggest). For estuaries displaying seafloor morphology with a main channel(s) surrounded by different levels of terraces (e.g. morphology inherited from a fluvial paleo-system), those boundaries move upward or downward of the estuary depending on the active flow section width in relation to the volume of water transported by the tide (upstream tidal prism, Fig. 82). If sea-level rises and the active flow section remains of similar width, a greater water volume pass through a similar section and tidal current velocities increase (Figs. 81 and 82, steps 2 and 4). Thus, erosion/deposition and cohesive/non-cohesive sediment deposition boundaries move upward of the estuary (Figs. 81 and 82). When the active flow section width increases, it is over flat and large terraces, which induce an important and fast modification of the active flow section width. A slightly greater water volume passes through a much larger section and it results in a decrease in tidal current velocities. Therefore, the mud/sand boundary moves downward of the estuary (Figs. 81 and 82, step 3). The downward movement of mud/sand and erosion/deposition limits is amplified by the strong friction over terraces when the active flow section width increases (flat and shallow, e.g. Fig. 82, step 3). In the opposite case, when only upstream areas pass into the subtidal domain, the friction decreases over terraces with the increasing depth, which amplified the upward movement (e.g. Fig. 82, step 4).

The main factors controlling the location of mud and sand deposits over the long time scale are therefore the upstream tidal prism (volume of water transported by the tide) and the active flow section width. The relationship between these two parameters can be applied only to estuaries with an upstream morphology similar to the Bay of Brest, as the evolution of the upstream tidal prism plays a major role. Upstream areas of the Bay are only rivers with steep banks and so the evolution of the tidal prism is almost proportional to the rise in sea-level in those areas. This is not always the case as in other areas the tidal prism can increase substantially with only a small rise in sea level, which induces a different evolution of the velocity gradient.

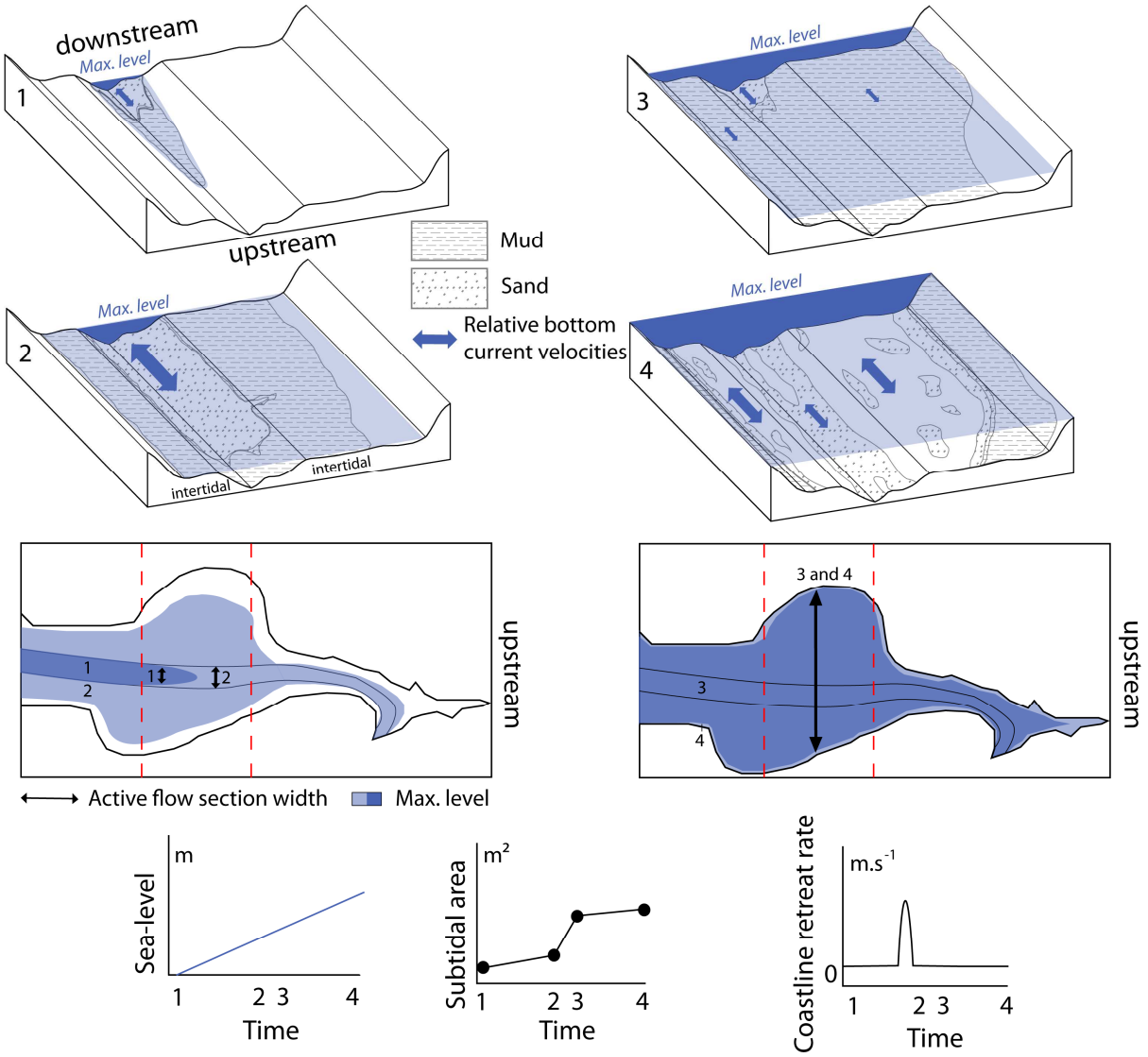

Fig. 82: Conceptual 3D diagrams of the evolution of mud and sand distributions over the simplified upper area of the Bay of Brest (two morphological domains: one channel and one level of terrace), during a transgression with a constant rate of sea-level rise. The blue area represents the maximum sea-level elevation and blue arrows represent the relative main velocities of ebb and flood tides bottom currents between steps. The active flow section width is represented by black arrows. The main channel displays an increase from downstream to upstream areas, whereas bathymetry does not change over terraces. This figure schematically explains the evolution of the sand/mud boundary as a function of sea-level rise and the active section width. Main retreats of sand/mud limit are due to fast and important increase in the active flow section width (passage to subtidal domain of a flat morphological domain) in the case of rising sea level.

We are thus able to propose a schematic conceptual model of the impact of flooding of terraces on the evolution of depositional areas within an estuary (Fig. 82). Simulation results are in line with the global sediment and grain-size distribution of Davis and Dalrymple (2012): the most energetic zone is composed of non-cohesive sediments, that form sediment structures (e.g. sand ridges, comet tails); towards shallower parts of the estuary (flanks and river mouths) deposits are finer (mix of mud and fine sand); and towards the shallowest area to the coastline, deposits are only muddy (Fig. 81). This study also demonstrates that erosion/deposition and the cohesive/non-cohesive boundaries are not equal to a depth threshold, but vary with the distribution of tidal currents. The distribution of tidal currents is primarily function of the shape of the basin (seafloor morphology and sea-level height), but locally the shape of the coastline may be the most significant parameter. For example, straits can

expose some morphological domains to strong tidal currents (e.g. T2, in the centre, Olivier et al., 2021). Conversely coves and bays can protect others from strong currents, such as T3 terraces within the Bay of Brest, which are favourable to mud accumulation from +3 m to -15 m (depth relative to present-day mean sea level, scenarios 2 to 4, Fig. 81).

5.5 Conclusion

The aim of this paper is to explore the tidal impact on sediment dynamic evolution over the Holocene in the Bay of Brest. The methodology is based on sedimentology and hydro-sediment modelling (MARS3D/MUSTANG). The aim is to rebuild each key paleoenvironment (seafloor and sea level) and simulate the hydro-sedimentary response of the estuary to long-term paleoenvironmental evolution. Simulation results have led to several conclusion on tide-dominated estuary infill:

- The simulated deposits are consistent with the hydrodynamical conclusions made in (Olivier et al., 2021) and with sedimentary records based on seismic and core data (only data available from the past). They led to propose a reconstitution of the hydro-sediment dynamic evolution during the Holocene in the Bay of Brest. This explains the sediment infill, and its preservation, observed in sedimentary records. This study demonstrates that the use of hydro-sediment modelling compared to sedimentary records is relevant to study sediment dynamics over a long time interval (9 ka).

- the influence of sediment sources (boundary conditions) was analysed and reveals that marine sediment represents 82% of the simulated sediment supply (inside the Bay) during the Holocene, with a decrease in river influence from 26% (9 ka) to less than 1% (present-day). The sediment supply sources studied and the calibration assume similar availability of offshore sediments and changes in river discharge during the Holocene. River water discharge was adjusted to obtain a simulated net sedimentation rate consistent with the estimated volumes of the sedimentary units. The resulting evolution of river discharge agrees with the conclusions of paleoclimatic studies conducted in the region and is mainly affected by the evolution of river slope profiles.

- Simulated hydro-sediment patterns highlight the longitudinal evolution of erosion/deposition and cohesive/non-cohesive deposit boundaries (and main triggers) over the Holocene infilling of a macrotidal estuary. Limits move upward or downward of the estuary depending on the volume of water transported by the tide in relation to the active flow section width. Considering the same tidal amplitude, if sea-level rises and the active flow section width remains similar, the limits move upward of the estuary and downward in the opposite case. However, this relation is applicable only to estuaries displaying morphological domains made of perpendicular terrace(s) to main channel(s). When the active flow section width increases it is over flat and large terraces and so the increase is fast (small rise in sea-level required) and important. Seafloor morphology is thus of uppermost importance for the evolution of tidal current distribution over long time intervals.

The time interval considered (9 ka) is simulated in a discontinuous way (scenarios). The major limitation of the proposed methodology is that scenarios (two years) are representative of long time intervals (500 to 4000 years). To overcome this assumption, the only way is to reduce the calculation cost of simulations and thus simplify the tide consideration in a model able to consider geological parameters (e.g. subsidence, uplift, sea level…). A perspective of this work is to determine if morphogen(s) tide(s) in the Bay of Brest can be determined for each scenario or the entire Holocene, in order to schematize tidal input. This would allow to upscale the tidal consideration and carry out simulations over the same duration as the deposition of sedimentary units.

6 Search for the definition of morphogen tides in the Bay of Brest

6.1 Introduction

The methodology set up for this PhD allowed us to run hydrodynamic and hydro-sedimentary simulations for reconstructing and studying tidal processes through four key stages within the Bay of Brest. These four stages have been validated by comparison with sedimentary records (chapters 4 and 5) and the succession of these four simulations resume the Holocene evolution of the Bay of Brest. Configurations established for the four scenarios provide thus a precious and wonderful numerical laboratory that can be now analysed in details for answering many scientific problematics dedicated to environment, biology, sedimentology, or hydrodynamics. We can easily and straight away extract a large number of parameters and analyse their evolution through the outputs of the successive scenarios already simulated (and thus over the last 9000 years) such as salinity and temperature gradients, other aspects of hydrodynamic or hydro-sediment processes (e.g. suspended matter dynamic within morphologic domains) and more for four time intervals.

This can obviously interest the communities of hydrodynamicists and sedimentologists/geologists, but also of biologists that are interested in the impacts of hydrodynamics on planktonic and benthic populations for example. New simulations can easily be run as well, to test new parameterisations (e.g. thickness of the initial sediment layer, boundary conditions, sediment supply mixture, i.e. different proportion of grain-size classes…). Change the parameterisation would allow us to test the sensibility of the model to different key parameters and quantify the associated range of uncertainties.

In this chapter we aim to use this numerical laboratory to define and determine the morphogen tide(s) of the Bay of Brest over the Holocene. We consider the morphogen tide(s) as the resume of all tides inducing significant morphological changes within the Bay of Brest.

Main problems in the understanding of long-term tidal impact on sedimentation are linked to the time-scale of the hydro-sedimentary processes induced by tides that varies hourly. The only way to reach larger simulations time scales than classic hydro-sedimentary modelling (or reduced complexity models) is the use of simplified tidal forcing. The definition of a drastically simplified tidal input (morphogen(s) tide(s)) could be the key to understand long-term estuaries infill, the formation of sediment structures and layers. The numerical laboratory is an opportunity to search for morphogen(s) tide(s) in short-term simulations (2 year), that are representative of key infilling periods over the last 9 000 years. It is thus possible to look for morphogen(s) tide(s) in relation to paleoenvironmental evolution (linked to seafloor and sea-level evolutions).

At this step, we can ask ourselves many questions: How should we proceed to identify the tides influencing significantly the sediment volume evolution? Is the long-term sediment deposition controlled by one particular tide, several, or the succession of all ones? Can we (and how) summarise the significant tide(s) into one or more morphogen(s) tide(s)? Do significant tidal impacts evolve with long-term parameters (e.g. seafloor or sea-level), and therefore the corresponding simplified input also?

Answering these questions implies two steps: (i) the determination of tidal clusters with similar (and significant) impact on sediment volume variations and, (ii) the statistical definition of simplified tide(s), corresponding to morphogen(s) tide(s) (representative of each cluster).

For this purpose, outputs of hydro-sedimentary simulations previously performed with MARS3D/MUSTANG are analysed. Although each simulation was run over a time interval of two years, we consider that the first year was dominated by transitory evolution leading progressively to the establishment of a realistic sediment dynamic. Therefore, the evolution of the morphology and sediment volume within the Bay of Brest will only be analysed over the second year.

In this chapter the aim is to define the tidal conditions for which the variations of the amount of sediment are significant and separate significant tides into cluster displaying similar patterns (in term of erosion and deposition). Scenario 4 (at present-day) is first analysed (6.2.1), and then compared to the three others (6.2.2), in order to observe potential changes over the Holocene. Finally, perspective and future work are exposed (6.2.3).

6.2 Present-day influence of tides on sediments

Based on the present-day configuration, this section aims to explore when and how the tide triggers main sediment volume variations within the Bay of Brest. We rely on the simulation of scenario 4 described in the previous chapter. Timeseries of the total sediment volumes (without suspended matters) are analysed within the Bay (area extend on which sediment volumes are calculated, is represented by a red dashed rectangle on Fig. 83) and over 1 year (Fig. 84a).

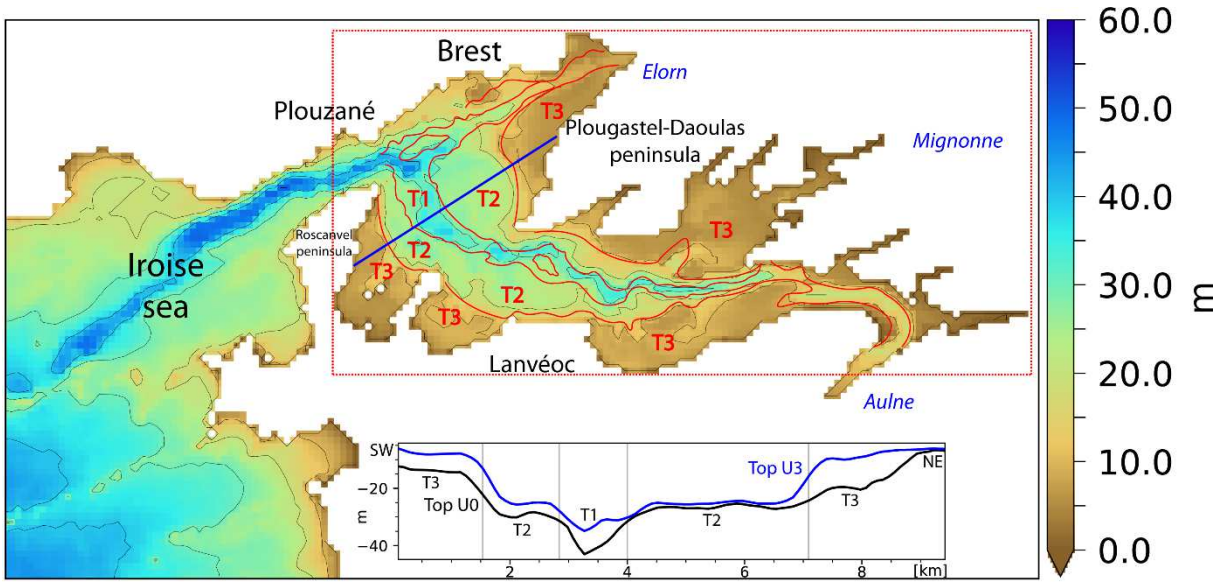

Fig. 83: Present-day bathymetry of the Bay of Brest. Sediment volume is calculated within the area delimited by a red dashed rectangle. The blue straight-line corresponds to the location of the cross-section that will be recurrently displayed all along this chapter to illustrate calculation limits of our analyses. Inset blue and black depth sections represent respectively the elevation of the tops of U3 and U0 along the blue straight line.

Fig. 84a, presents the variation of sediment volume in the Bay during one year, with a zoom over one month. A linear regression is calculated on the sediment volume evolution over one year in the Bay (Fig. 84a). This trend is then removed in order to highlight higher frequency variations (Fig. 84b). Fig. 84b thus displays high-frequency (i.e. daily) sediment volume variations over one year. Fig. 84c displays the evolution of the sediment volume in suspension in the water column over the full bay and one year. Sediment volume variations, high-frequency sediment volume variations and sediment volume in suspension are finally compared to sea surface variations over one year (Fig. 84d).

Over one year, the estuary overall accumulates sediments (mainly coming from oceanic borders, see chap. 5), and this trend is almost linear at year scale, following the linear regression carried out (Fig. 84a). However, in details, sediment volume variations occur during smaller time intervals, and the Bay infill takes place in step rather than all along the year (Fig. 84a and inset zoom). Daily tide variations

induce significant sediment volume variations (of the order of 10^3 m^3, Fig. 84a) only during specific time intervals (Fig. 84a inset zoom): significant variations occur during short time interval of about 7 days and a maximum of the sediment volume variations is found each ~15 days (Fig. 84a and inset zoom). Between those time intervals the sediment volume displays unsignificant variations (Fig. 84a and zoom). Different patterns are observed each ~15 days characterized with a first period (~7 days, M for moderate in Fig. 84) displaying global deposition (up to ~$20*10^3$ m^3) and the second one (~7 days, S for strong in Fig. 84) displaying global erosion (up to ~$40*10^3$ m^3) followed by deposition (up to ~$30*10^3$ m^3, Fig. 84a). The same patterns are observed each month approximatively (Fig. 84a). Those patterns are also observed inside sediment volume in suspension (Fig. 84c), which displays over one year important volume variations each ~15 days with an alternance of strong variations (up to $75*10^3$ m^3) and smaller ones (up to $15*10^3$ m^3). Similar patterns are also repeated each month (Fig. 84c). Between those short-time intervals sediment volume in suspension is close to 0 (Fig. 84c). However, sediment volume deposited or remobilized by those two patterns (occurring each month) are very unequal over the simulation (Fig. 84a). During spring and autumn, sediment volume variations seem to be much more important than during winter and summer (Figs. 84a, 84c). Within time intervals of ~3 months (Fig. 84, red dashed lines, spring and autumn): the tides globally mobilize more sediment than during the next ~3 months (Fig. 84, red dashed lines, summer and winter), during the short time intervals (~7 days) identified each ~15 days above (Fig. 84b, M and S). The maximum sediment volume in suspension is about $75*10^3$ (m^3) in spring and autumn, and $30*10^3$ (m^3) in summer and winter (Fig. 84c).

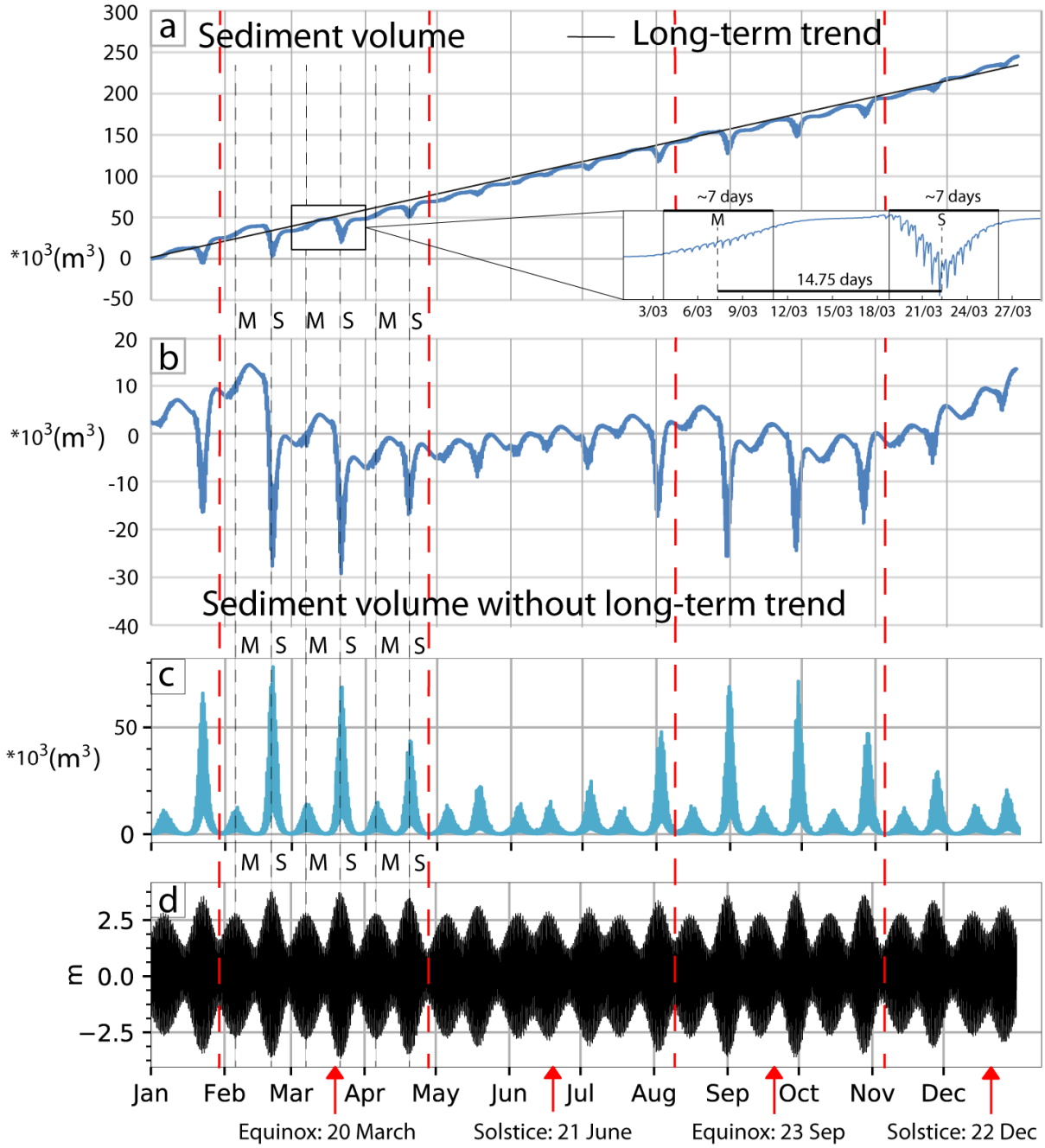

Fig. 84: Evolution over one year of (with the present-day physiography, scenario 4): a, the sediment volume (over the Bay, Fig. 52) and its global annual trend (or long-term trend); b, the sediment volume without the global annual trend; c, the sediment volume in suspension; d, sea surface elevation. Black dashed lines represent moderate (M) and strong (S) spring tides. Red dashed lines display equinox and solstice time intervals identified from sediment volume variations.

The time intervals (~7 days) inducing the main sediment volume variations display three cyclicities that are related to tide frequencies: (i) 14.75 days; (ii) 29.5 days; (iii) 3 months. In non-idealised contexts, the evolution of suspended matter is primarily related to variations of the amount of suspended matter at the boundaries. These observations are possible thanks to the constant availability of sediment at the boundaries over these simulations, which allows to focus on the tidal impact on sediment volume evolution.

(i) The smallest period observed coincides with the first and second full Moon apparitions, which induces spring tides every 14.75 days (Fig. 84). They are called Syzygies and correspond to the moment when the meridian planes of the Moon and the Sun are merged (Fig. 85). Syzygies corresponds to New Moon or Full Moon (Fig. 85). The difference between these New Moon and Full Moon is due to the Moon relative position from the Earth and the Sun (Fig. 85). Significant sediment volume variations time intervals of ~7 days, observed each ~15 days, display the same frequency as lunar cycles (Figs. 84b, 84d, M and S).

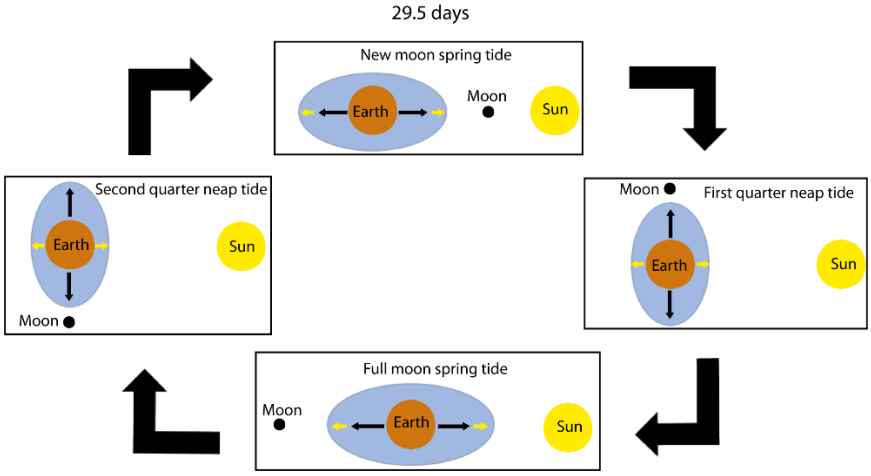

Fig. 85: Schematic lunar cycle

(ii) Both, strong and moderate spring tides, are visible through the evolution of the sediment volume each ~29.5 days (Fig. 84, except in July-August). (iii) Their respective influences display important variations during the simulation (Fig. 84b). Within time intervals of ~3 months, the sediment volume variations induced by the tides (each ~15 days) change a lot. During spring and autumn amplitude of sediment variations are more important than during summer and winter (Fig. 84, red dashed lines). These time intervals correspond to equinoxes and solstices (Figs. 84 and 86). The equinoxes correspond to moments when the declination of the Sun with respect to the equator is zero. Conversely, the solstices correspond to the maximum declination of the Sun with respect to the equator. Equinoctial spring tide (close to the equinoxes) induce the maximum amplitude of the semi-diurnal tide (Figs. 84d and 86). Approximately 173.3 days separate two equinoxes or solstices and thus two equinox (spring and autumn) and two solstice (summer and winter) time intervals occur during one year (~3 months, Figs, 84 and 86).

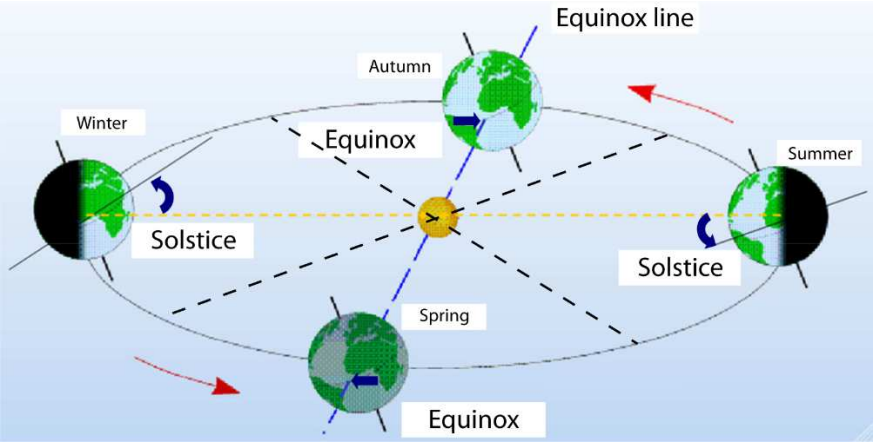

Fig. 86: Schematic representation of equinox and solstices time intervals (modified from SHOM)

At year scale only spring tides (strong and moderate) are visible through the sediment volume evolution and neap tide induce unsignificant variations (Figs. 84a zoom and 84c). However, spring tides respective influences change a lot between equinox and solstice time intervals. During equinox time intervals, strong spring tides are responsible of main erosion patterns, while moderate spring tides induce deposition (Fig. 84). Sediment losses during equinoctial strong spring tides are less important than gains induced by equinoctial moderate spring tides and thus equinox time intervals globally promote deposition (less than the global annual trend, Figs. 84a and 84b). During solstice time-interval both spring tides promote sedimentation over the Bay and globally solstice time intervals induce more deposition than equinox ones and the global annual trend (Fig. 84).

In order to observe ebb and flood tides impacts during spring tides, Fig. 87a displays the sediment volume in suspension during three days and Fig. 87b displays sea surface variations within the same time interval. Within these spring tides the effects of flood and ebb tides are unequal in the Bay of Brest. During ebb and flood an alternation between remobilization and deposition is observed (Fig. 87a and 87b), but suspended matter volume induced by ebb tides are two to three times lower than the one induced by flood tides (Fig. 87). It highlights an asymmetry between the impact of ebb and flood tides on sediment remobilization.

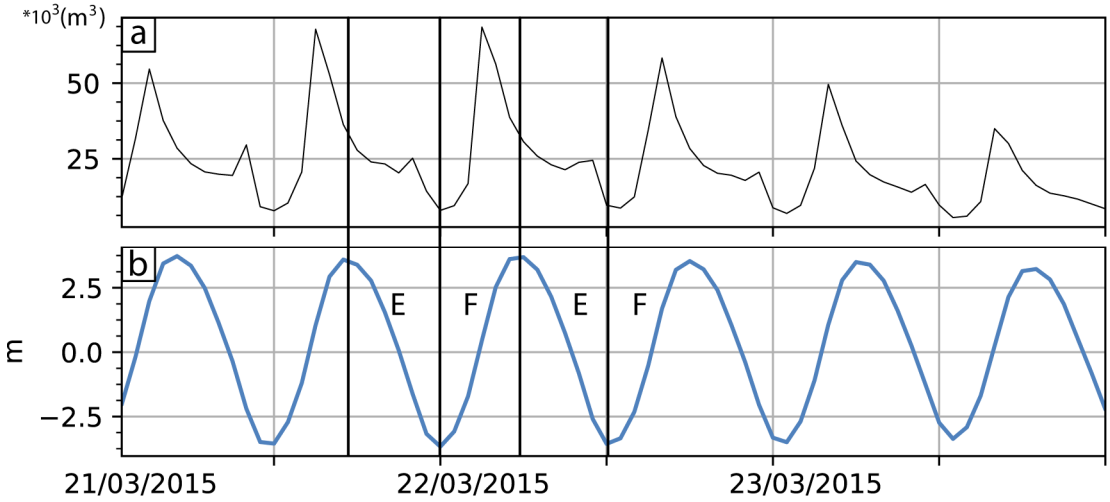

Fig. 87: (a) Evolution of suspended matter volume through time over spring tides for the present-day configuration (scenario 4). (b) Evolution of sea surface variations at the entrance of the Bay (central area). F: Flood tide; E: Ebb tide.

To better understand the infill of the estuary, the sediment volume is calculated by depth range (referring to the lowest limit of the intertidal zone, maximum low tide). They are chosen to fit morphological domains of the Bay of Brest and refer to depth related to the lowest sea-level (Fig. 88 on top). Fig. 88 therefore represents the sediment volume evolution over one year by bathymetric range and displays the sediment volume variations minus the global annual trend.

The long-term sediment volume evolutions are very different between morphological domains: the deepest domain (T1) globally undergoes erosion over the year ($-100*10^3$ m^3, Fig. 88 sediment volume), the intermediate domain (T2) undergoes erosion during equinox time intervals and sedimentation during solstice time intervals ($+45*10^3$ m^3 over one year, Fig. 88 sediment volume), and the shallowest domain (T3) undergoes sedimentation over the year ($+300*10^3$ m^3, Fig. 88 sediment volume). The topographic difference between morphological domains is increasing: the depth of channels and troughs decreases, whereas depth of shallowest terraces increases (referring to a constant sea-level). Moreover, the shallowest domain (T3) accumulates more sediments than the total erosion within the Bay (T1), which suggest that the shallowest parts of the Bay stock a significative part of sediment supply.

The sediment volume over the deepest domain, T1, is always decreasing or stationary (Fig. 88 sediment volume). Most of the erosion happens during strong spring tides within equinox time intervals (up to $\sim15*10^3$ m^3, Fig. 88 sediment volume) and other time intervals hardly induce variations (Fig. 88 sediment volume without annual global trend). Note that the evolution over T1 is strongly affected by the initial conditions (initial layer of 0.5 m containing 40% of muds, see chapter 5), which is not realistic in high energy areas, such as T1 close to the strait between Plouzané and Roscanvel peninsula. T1 erosion is therefore probably over estimated.

Over the intermediate domain (T2 terraces), global trends of sediment volume variations are mainly influenced by strong spring tides: during equinox time intervals they induce erosion (up to $\sim15*10^3$ m^3), and during solstice time intervals they induce accumulation (up to $\sim8*10^3$ m^3, Fig. 88 sediment volume). Moderate spring tides induce in both cases sedimentation over T2 (up to $\sim5*10^3$ m^3, Fig. 88 sediment volume), but in smaller proportion during solstice than equinox time intervals (Fig. 88).

Over the shallowest domain (T3 terraces), both spring tides always induce deposition (Fig. 88 sediment volume), but in smaller proportion during solstice than during equinox time intervals (up to ~30*10^3 m^3, Fig. 88).

The tides impact significantly the sediment volume during the same time interval in each morphological domain, as observed for the entire estuary (Figs. 84 and 88): significant variations occur each ~15 days (strong and moderate spring tides, during ~7 days), with the greatest variations during equinox time intervals (~3 months, Fig. 88). Over each morphological domain neap tides have a negligible influence compared to spring tides on sediment volume variations (Fig. 88).

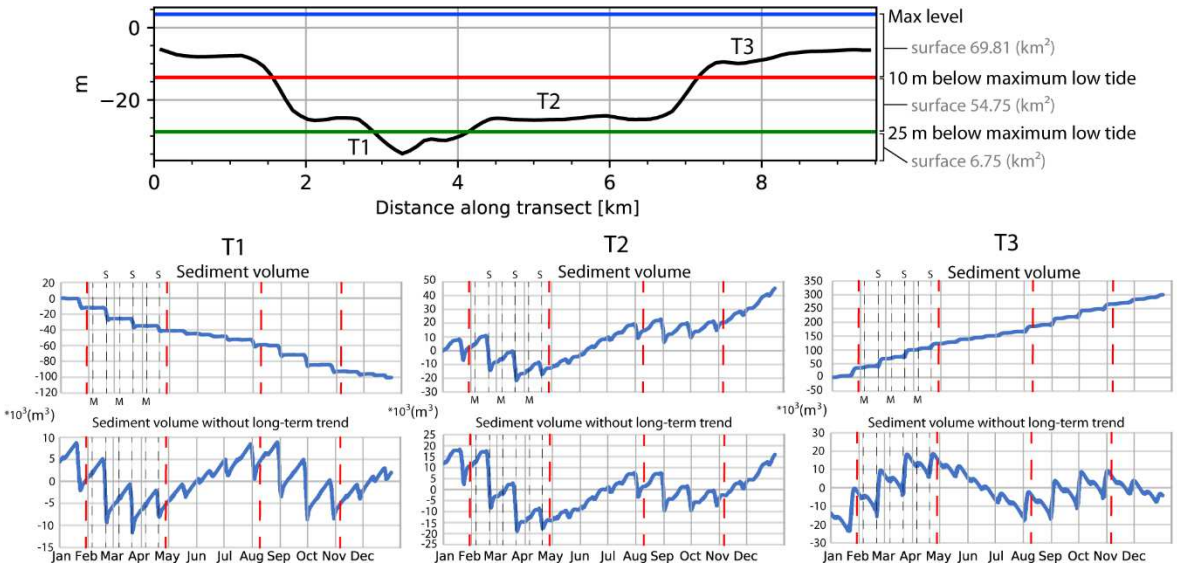

Fig. 88: On top: Bathymetric cross section at present-day (scenario 4, centre of the Bay of Brest), on which the bathymetric limits chosen to represent morphological domains are displayed. On bottom: Evolution over one year of the sediment volume and the sediment volume without annual global trend, for each morphological domain (T1 to T3, from left to right). S: strong spring tide; M: moderate spring tide. Red dashed lines display equinox and solstice time intervals identified from sediment volume variations.

The Bay of Brest suffers significant erosion only during equinoctial strong spring tides over T1 and T2 (Fig. 88, T1: up to 15*10^3 m^3, T2: up to 15*10^3 m^3). In the same time, an important volume of sediment settles over T3 (Fig. 88, up to 30*10^3 m^3). During all other time intervals pointed out (equinoctial strong spring tides and, equinoctial moderate and both solstitial spring tides) the tides induce deposition over T2 and T3 (Fig. 88). During scenario 4, the deepest domain (T1) loses sediments and main accumulations are located in the shallowest part (T3), and in smaller proportion over the intermediate domain (T2). Furthermore, sedimentation increases over T3 when erosion increases over underlying domains (Fig. 88). It suggests that a part of accumulations over shallowest parts should come from the erosion of deeper domains.

6.3 Holocene evolution

6.3.1 Sediment volume

Thanks to the four scenarios modelled in the previous chapter, we can explore the evolution of the tidal impact on sediment volume in the Bay of Brest over the Holocene transgression (9 ka BP

to the present-day). In this chapter, we choose to analyse outputs of simulations with constant oceanic boundary parameterisation as in chapter 5, and with identical river discharges for the four scenarios. The objective is to focus our analysis on the impact of topography and sea-level variations on sediment volume variations in relation to tides only.

The evolutions over one year of the sediment volume, and the sediment volume without the global annual trend are presented on Fig. 89. The change of vertical scales for the sediment volume variations between scenario, is mainly related to the estuary size evolution (more extended is the estuary, greater are the sediment volume variations, Fig. 89).

In all scenario, the Bay of Brest accumulates sediment in a similar global annual trend (Figs. 89 and 84a). The sediment volume displays significant variations during the same time intervals with similar magnitude between time intervals in each scenario (Figs 84 and 89): equinoctial strong spring tides induce the greatest variations (up to ~$10*10^3$ m^3 in scenario 1, ~$15*10^3$ m^3 in scenario 2, ~$15*10^3$ m^3 in scenario3) of the sediment volume (Fig. 89); equinoctial moderate spring tides induce also significant variations, but in lesser proportions (~less than $5*10^3$ m^3 in scenario 1, up to ~$5*10^3$ m^3 in scenario 2, ~$10*10^3$ m^3 in scenario 3, Fig. 89); during solstice time intervals significant variations are observed during both spring tides, but in lesser proportions (~1 to 5 $*10^3$ m^3) than during equinox time intervals (Fig. 89); and neap tides induce unsignificant variations (Fig. 89). Equinoctial moderate and both solstitial spring tides induce sedimentation in every scenario, while equinoctial strong spring tides induce deposition in scenarios 1 and 3, and erosion in scenario 2 and 4 (Fig. 89). During scenarios 1 and 3 the deposition induced by equinox time intervals (respectively ~60 and ~50 $*10^3$ m^3) is thus greater than the one induced by solstitial time intervals (respectively ~30 and ~40 $*10^3$ m^3) and the opposite during scenarios 2 and 4 (Fig. 89). Note that in scenario 2, equinox time interval (~3 months) does not induce any residual deposits (equivalent volume at the beginning and at the end of the equinoxes time intervals). It means that the deposition during equinoctial moderate is equivalent to the erosion induced by equinoctial strong spring tides.

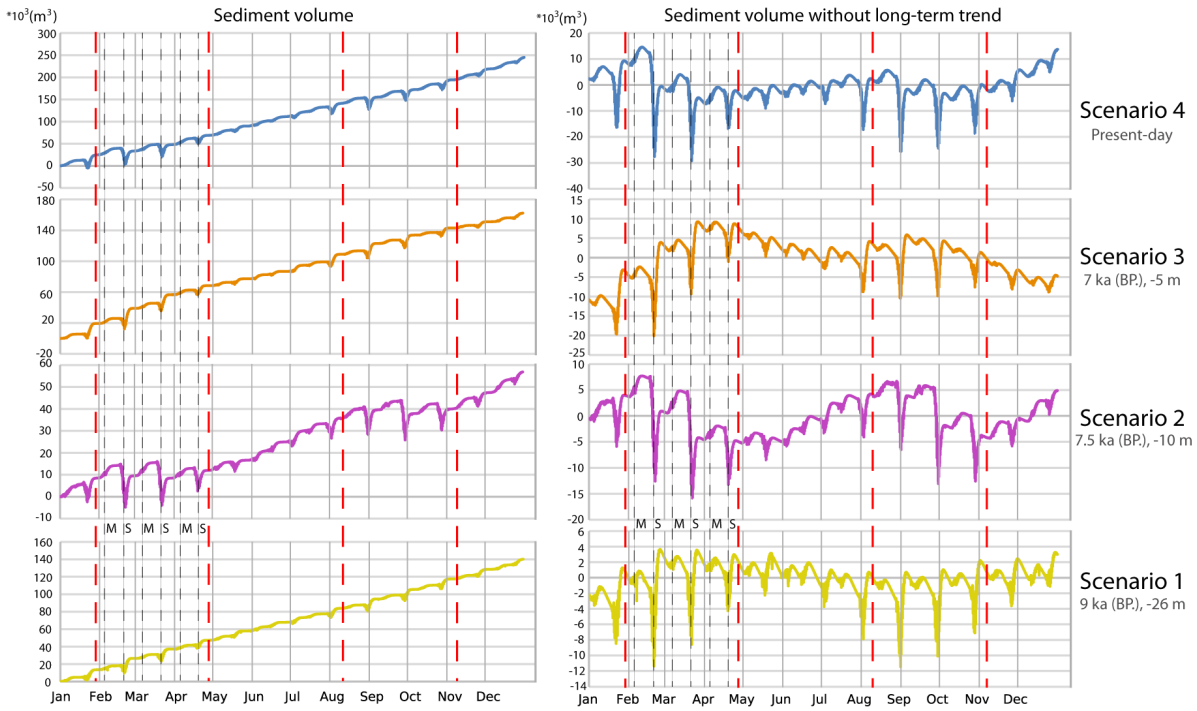

Fig. 89: Sediment volume evolution over one year for each scenario (over the Bay, Fig. 83) and, sediment volume evolution without the global annual trend (respectively left and right). S: strong spring tide; M: moderate spring tide. Red dashed lines display equinox and solstice time intervals identified from sediment volume variations.

In all scenarios the same time intervals characterized by strong and moderate spring tides (with different impact during equinox and solstice) are responsible of the most important changes in sediment volume variations. However, we can wonder why equinoctial strong spring tides induce erosion in some scenario, or deposition in others (or stability)?

To answer that question, the evolution of sediment volume is calculated for each scenario by depth range (Fig. 90). Bathymetric limits are chosen to frame the morphological domains and are thus slightly different for each scenario (referring to the maximum low tide of the corresponding scenario, Fig. 90). Note again the different vertical scales for each scenario and over each morphological domain (surface of depth range available in Fig. 90). As Fig. 88, Fig. 90 displays sediment volume evolution over one year and sediment volume minus the global annual trend, for each morphological domain (a: scenario 3, b: scenario 2; c: scenario 1).

- During scenario 1, T3 is emerged, T2 is the shallowest domain and undergoes sedimentation (+200*10 m^3), while T1 undergoes erosion (-65*10 m^3). Sedimentation over T2 is greater than erosion of T1 (volume deposited of T2 greater than volume eroded over the Bay). Equinoctial strong spring tides induce the main morphological variations (sedimentation up to ~20*10^3 m^3), and moderate equinoctial, and strong and moderate spring tides during solstice also induce sedimentation in lesser proportion (up to ~10*10^3 m^3, Fig. 90c). Over T1 equinoctial strong spring tides induce the main sediment volume variations (erosion, up to ~10*10^3 m^3), and in comparison, moderate equinoctial, and strong and moderate spring tides during solstice induce very few erosion (~3*10^3 m^3, Fig. 90c).
- During scenario 2, T1 undergoes erosion (-30*10^3 m^3, Fig. 90b), T2 undergoes erosion (-50*10^3 m^3, Fig. 90b), T3 undergoes sedimentation (130*10^3 m^3, Fig. 90b). The sedimentation over T3 is greater than the cumulative erosion over T1 and T2 during the simulation. The observed

impact of moderate and strong spring tides during equinox and solstice time intervals is the same over T1 and T3 as scenario 4 (Figs. 88, 90b). Over T2, the erosion induced by equinoctial strong spring tides is much more intense than the sedimentation occurring during solstitial spring tides and moderate equinoctial spring tides. Over the simulation, the tides induce greater erosion (-50*10^3 m^3, Fig. 90) over T2 compared to T1 (-30*10 m^3 Fig. 90).

- During scenario 3, the deepest domain (T1) globally undergoes erosion over the year (-30*10^3 m^3, Fig. 90a sediment volume), the intermediate domain (T2) losses sediment over the simulation (-5*10^3 m^3, Fig. 90a sediment volume), and the shallowest domain (T3) undergoes sedimentation over the year (+200*10^3 m^3, Fig. 90a sediment volume). The sediment volume over the simulation is greater over T3 than the cumulative erosion over T1 and T2 (+200 and -35*10 m^3). Equinoctial strong spring tides are responsible of most of the erosion, which is located over T1 and T2, and main sedimentation over T3 (Fig. 90a sediment volume). Equinoctial moderate spring tides induce a slighter erosion inside T1 and slighter accumulation over T2 and T3 than equinoctial strong spring tides (Fig. 90a). During solstices, both spring tides induce sedimentation over T2 and T3 (Fig. 90a). Globally the tides induce only erosion over T1, erosion during equinox and deposition during solstice time intervals over T2, and only sedimentation over T3 (Fig. 90a). A much lower erosion is observed compared to scenario 2 over T2 (-50 and -5*10^3 m^3, Figs. 90a, 90b). Scenario 3 displays very similar patterns as scenario 4 (Figs. 88 and 90a), except for T2, where erosion during equinoctial strong spring tides is greater than deposition during all over time interval combined (not the case in scenario 4).

Thus, for each scenario the shallowest domain stocks a significant part of sediment inputs (supply). Common patterns are observed over morphological domains throughout the Holocene (Fig. 90): (I) equinoctial strong spring tides always induce main sediment volume variations (II) they always induce deposition over the shallowest morphological domain, and erosion over deeper terraces (than the shallowest domain) and within the main channel; (III) equinoctial moderate, strong and moderate spring tides during solstice time intervals always induce significant sediment volume variations, even if in lesser proportion than equinoctial strong spring tides; (IV) they always induce deposition over the two levels of terraces (T2 and T3 if flooded); (VI) sedimentation over the shallowest terraces is always greater than erosion over T1 and T2, or only T1.

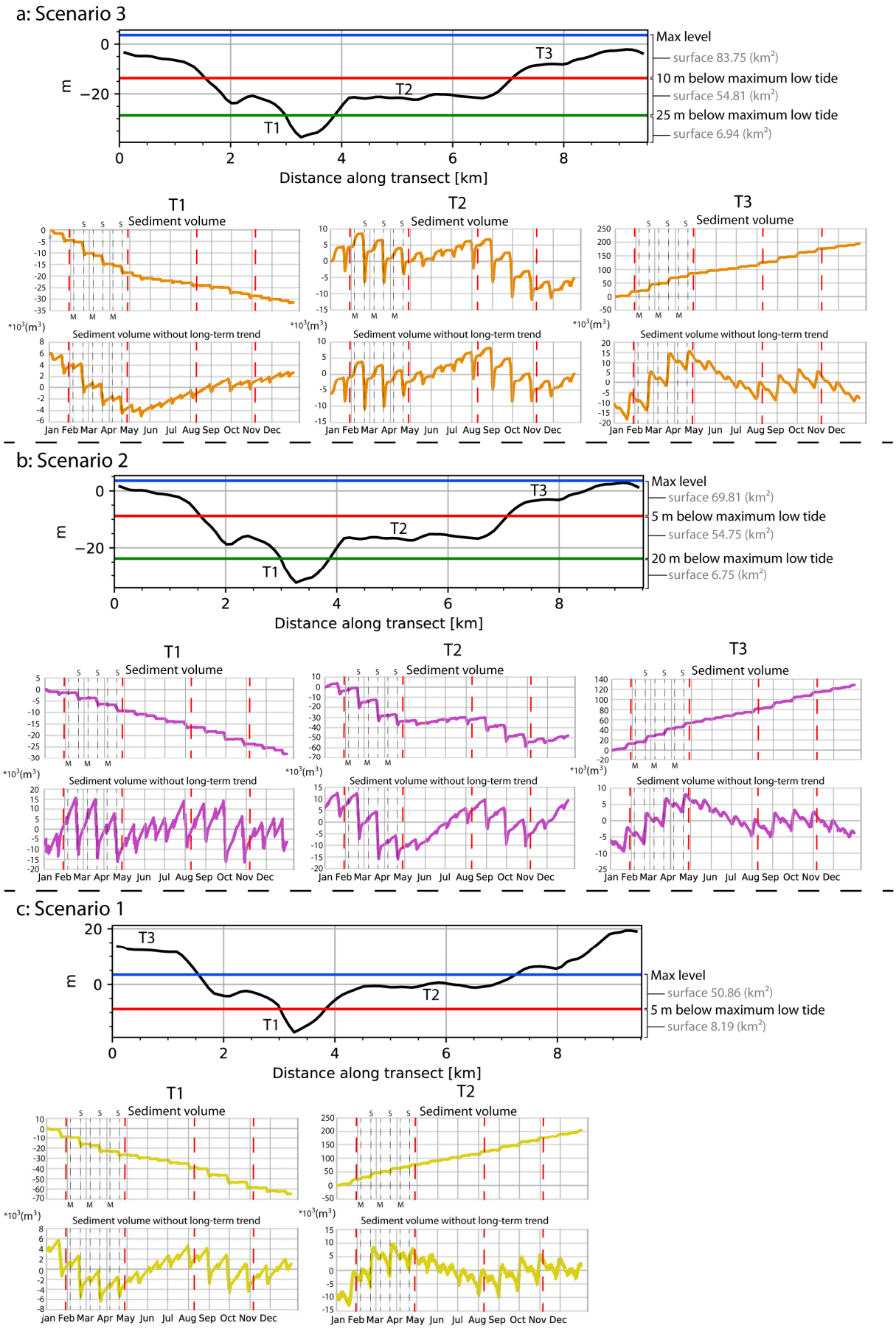
a: Scenario 3
m
Max level
surface 83.75 (km²)
10 m below maximum low tide
surface 54.81 (km²)
25 m below maximum low tide
surface 6.94 (km²)
T1
T2
T3
Distance along transect [km]
Sediment volume
Sediment volume without long-term trend
*10³(m³)
Jan Feb Mar Apr May Jun Jul Aug Sep Oct Nov Dec
b: Scenario 2
Max level
surface 69.81 (km²)
5 m below maximum low tide
surface 54.75 (km²)
20 m below maximum low tide
surface 6.75 (km²)
c: Scenario 1
Max level
surface 50.86 (km²)
5 m below maximum low tide
surface 8.19 (km²)

Fig. 90: For scenarios 3 (a), 2 (b) and 1 (c): (On top) Bathymetric cross section in the centre of the Bay of Brest, on which the bathymetric limits chosen to represent morphological domains are displayed. (On bottom) Sediment volume evolution over one year and sediment volume evolution without the global annual trend, for each morphological domain (T1 to T3, from left to right). S: strong spring tide; M: moderate spring tide. Red dashed lines display equinox and solstice time intervals identified from sediment volume variations.

Looking at the Holocene sediment volume evolution (Figs. 88 and 90), the main channel always undergoes erosion while the shallowest terrasses always undergo sedimentation during the transgression. While potential deposition over intermediate terraces (T2 except in scenario 1) increases as the sea-level rises (scenario 2 negative, i.e. erosion, to scenario 4 positive, i.e. deposition, Figs, 88 and 90). T1 and T2 display different patterns and thus, although sea-level variations (water height) play a major role in tide-induced sediment volume variations over morphological domains, the shapes of the latter seem to also influence those patterns. Potential deposition over T2 and T1 should increase with the increasing depth over the transgression (see chapter 4). However, it is only the case over T2 and not over T1. The setting of initial sediment layer (0.5 m, containing 40% of mud) probably generates a significant and not realistic erosion in the most energetic parts of T1. Further analysis, with different initial conditions, should be carried out to quantify T1 erosion.

Equinoctial strong spring tides always induce deposition over the shallowest domain and erosion over deeper domains. During scenario 1, the shallowest terraces (T2) are much more extended than the deeper domain (T1, Fig. 90c), and thus equinoctial strong spring tides induce sedimentation (Fig. 89). During other scenarios that trend changes thanks to the flooding of T2 terraces and the shallowest terraces (T3) are no longer much more extended than deeper domains (T1 and T2, Fig. 88, 90a, 90b). Strong spring tides during equinox time intervals thus induce erosion globally over the estuary (Fig. 89). However, as seen in chapter 5, during scenario 3 the flooding of T3 terraces induces a large shoreline retreat compared to the sea-level rise and less intense current reach the upper area. Many areas are affected by less intense currents of equinoctial strong spring tides in scenario 3 than in scenarios 2 and 4 (e.g. upper area). That is why strong spring tides during equinox time intervals induce globally sedimentation over the estuary in scenario 3 (Figs. 89 and 90a). Main differences identified in sediment volume variations between scenarios (Fig. 89), which are linked to equinoctial strong spring tides, are due to the configuration of the Bay (relief of seafloor and sea-level height).

6.4 Threshold

The objective now is to quantify the threshold above which the ebb and flood cycles have a significant impact on the sediment volume variations. For each scenario the evolution over one year of the maximum and minimum sediment volume was plotted (Fig. 91a and 91b). They are directly compared to the evolution of the sea surface variation rate ($m.h^{-1}$). Peaks of sea-surface variation rates correspond to mid-tides when tide induced currents are usually the strongest.

This comparison confirms the weak action of neap tides induced currents, which induce unsignificant sediment volume variations (minimum and maximum curves of sediment volumes are superimposed on Fig. 91a and 91b). The minimum and maximum of sediments volume present significant differences during spring tides (Fig. 91a and 91b). To quantify the threshold over which sediment volume variations are significant, a cross plot is made between the maximum and minimum sediment volume and the sea surface variations rate (Fig. 91c). It appears that significant remobilization and deposition begin when sea surface variations rate reaches 1.25 $m.h^{-1}$ (Fig. 91c). Above this threshold, variations of sediment volume increase exponentially.

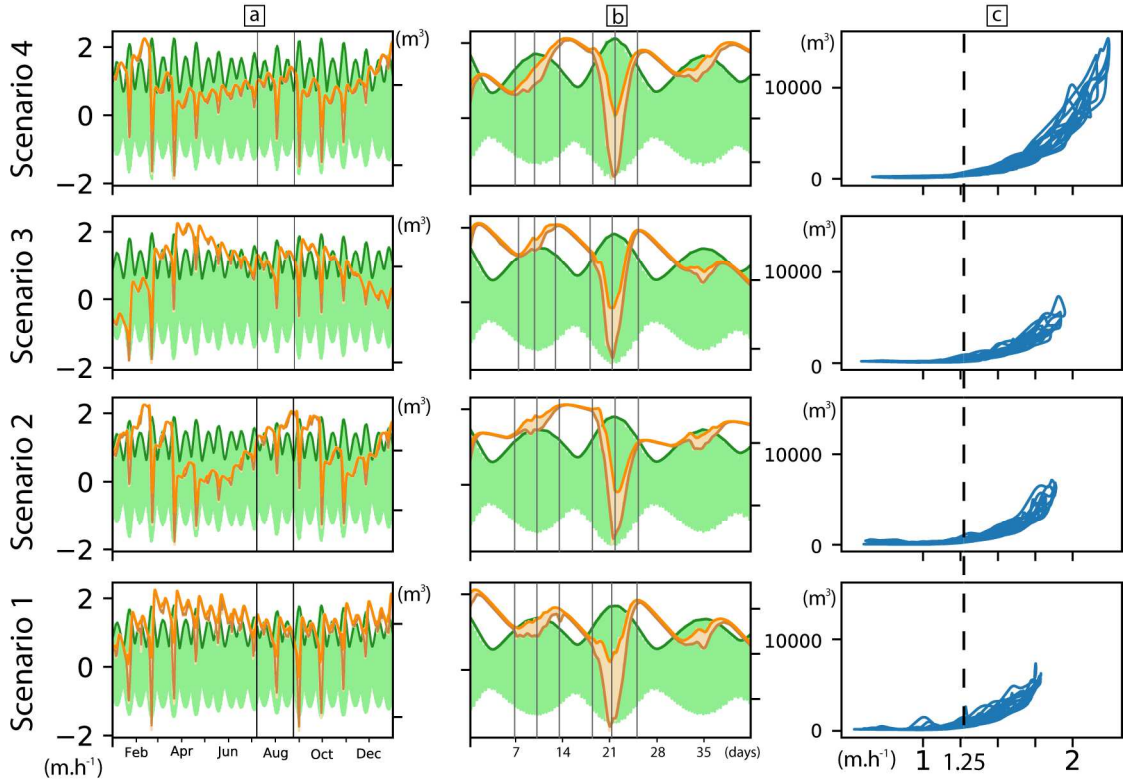

Fig. 91: (a) Envelope of the free surface variation rate over one year in light green (m.h^{-1}), maximum in dark-green), smoothed maximum sediment volume in orange, and smoothed minimum sediment volume in brown (both smoothed over 12 h and without the global annual trend, over the Bay of Brest). (b) Zoom over 1 000 hours. (c) Cross plot between (x) the smoothed maximum sea surface variation rate (over 12 h), and (Y) the maximum difference of sediment volume during a tide (smoothed maximum volume – smoothed minimum volume).

The tide starts to induce significant variations in sediment volume when maximum sea surface variation rate, during a tidal cycle (ebb and flood), reaches 1.25 m.h^{-1} (Fig. 91b). Increasing erosion patterns are promoted by tides until the sea surface variations rate reaches its highest value within the half lunar cycle (14.75 days, Fig. 91b). Then, tides promote deposition until the sea surface variations rate reaches again the same threshold (Fig. 91b grey lines). It is therefore the balance between (1) sediment losses before the highest sea surface variation rate, and (2) gains after it, that determines if the half lunar cycle induces erosion or deposition (Figs. 91b and 91c).

When the sea surface rate variations reach 1.25 m.h^{-1} tidal currents start to induce mud erosion (lowest critical shear stress of all grain-size classes, see chapter 4) in most energetic parts. Then, when currents increase, coarser sediments are mobilized too (in the Bay of Brest). We can also infer that the threshold value is also linked with parameterisation choices, such as the composition of the initial bed layer, the critical shear stress set for each sediment classes, the skin roughness length, the management of mixture (cohesive and non-cohesive) erosion and deposition behaviour. Given the strong velocity gradients present in the Bay of Brest (linked to its morphology), signifiant sediment volume variations are linked to tides with a threshold based on sea surface variation rate rather than bottom current velocities.

6.5 Sediment unit preservation in tide-dominated estuaries

The high-frequency variations of the sediment volume of each morphological domain suggests that a significant fraction of sediments accumulated over the shallowest terraces come from the erosion of deeper domains (Figs. 88 and 90). However, the sediment volume deposited over T3 is greater than the ones eroded from others domains: therefore, T3 stocks an important part of the sediment supply (probably most of fine sediments, Figs. 88 and 90).

Over the entire Holocene the Bay displays the same patterns: the main sedimentation occurs over the shallowest terraces and the deepest domain always undergoes erosion in simulations. The topography of the Bay of Brest is increasing: the channels and troughs depths increase, and the shallowest domains depths decrease (for a constant sea-level, Fig. 92b). This simulation result is in agreement with the present-day seafloor evolution but should not be applied anywhere without a detailed analysis of tidal cycles. For example, the Bay of Douarnenez is an incised valley, located a few kilometers south of the study area. In this bay the deepest domain is also a paleochannel but it is filled by sediments (see Jouet et al., 2003; Augris, 2005). This difference between channel erosion in the Bay of Brest, and channel infill in the Bay of Douarnenez is due to the topographic control which induces a stronger action of tidal currents in the Bay of Brest than in the Bay of Douarnenez. It is important to note that the initial condition of the simulations, placing mud in the main channel, induces a stronger erosion than in reality on this morphological domain. Nevertheless, the main channel is still not filled at present-day in the Bay of Brest, contrary to other incised valleys in French Brittany (e.g. Douarnenez, Concarneau, Saint-Brieuc...).

This study of the evolution of the Bay of Brest also highlights an important sediment reworking by tidal flows during the Holocene transgression. Unless a great coastline retreat occurs (scenario 3), fine sediment deposits (fine sand and mud) are pushed upward towards the shallowest terraces during the transgression and thus previous deposits are remobilized and feed the younger sedimentary unit (chapter 5). Only the shallowest domain never undergoes erosion and always displays the greatest sedimentation rate (Fig. 92). However, if a shallower domain is flooded during the transgression, new hydrodynamics will remove those deposits (e.g. scenario 1 deposits over T2, Fig. 92). It means that transgressive deposits are hardly preserved except over the shallowest morphological domain of all the transgression (T3 in the Bay of Brest).

In those conditions we can expect to find the oldest sedimentary records over the shallowest terraces, as no new current is able to remove the deposits taking place during the transgression. Thus, the shallowest morphological domain should display records as old as the moment when it became intertidal. In the Bay of Brest, T3 terraces are the shallowest morphological domain (of the Holocene transgression) that is submerged from 7.5 ka (BP) to the present-day: the end of U1 (TST) and U2 (TST, Fig. 92a) are thus well preserved there (Fig. 92).

More generally, hydrodynamics promotes a better preservation of HST (Highstand System Tract) than TST (Transgressive System Tract) in tide-dominated estuaries. The HST cannot be removed by new hydrodynamics on the shallowest domains, as it represents the highest sea-level stage (Fig. 92). Moreover, T3 displays the strongest sedimentation rate during scenario 4 (HST, Fig. 92). In the Bay of Brest, potential deposition increases over T2 with its increasing depth, with a maximum sediment volume and sedimentation rate over the intermediate domain during U3 (Figs. 88 and 92). Conditions are the most favourable for deposition over the intermediate domain also during the HST (T2, Figs, 92b). Even if currents are generally faster in channel bottom than over its flanks (less friction), an

increasing sedimentation rate is expected within the channel during transgression. An increasing deposition were simulated in chapter 5 over T1 and is observed through sediment records (chapter 5) over the Holocene. This observation probably not result from real older sediment remobilisation, but from the erosion of the initial sediment layer (0.5 m thick, 40 % muddy), which is not realistic in energetic areas. This observation is thus likely an artefact from initial parameterisation which avoid the observation of realistic processes (such as an increasing potential deposition of fine sands and sands throughout the Holocene).

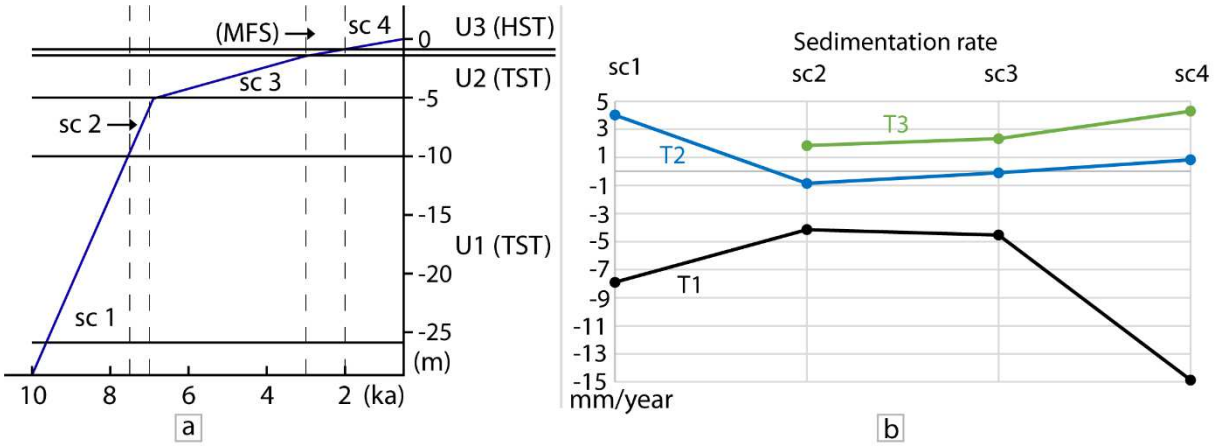

Fig. 92: a: Schematic representation of sea-level rise during the Holocene and associated sedimentary units, in the Bay of Brest (system tract interpreted by Gregoire et al., 2017). b: Sedimentation rate calculated over 1 year for each morphological domain (see Figs. 57 and 59).

Those observation supports previous conclusion of Tessier et al., 2012, which observed in Mont Saint-Michel and Seine estuaries that TST building during rapid rise of sea-level are poorly preserved and HST represent main sedimentary records. And also that, “the relative shallowness of the incision and deepness of the tidal scour, together with the sediment-starved context of the studied estuaries, account for the poor development and preservation of the TST” (Tessier et al., 2012). Taking into account similarities between those three estuaries (incised valley, macrotidal, weak sediment fluvial supply), the patterns observed by Tessier et al. (2012) are probably due to similar action of tidal currents in those estuaries compared to the Bay of Brest. Moreover, the preservation of TST should be better in the Bay of Brest than in those estuaries, as they do not present a shallowest domain sheltered from waves (by the coastline) and flat, such as T3 (see Tessier et al., 2012).

6.6 Perspectives and future works on morphogen tides

Thanks to the previous observations we were able to:

- rank the different tidal cycles. The most important are the equinoctial strong spring tides, followed by the equinoctial moderate, solstitial strong and moderate spring tides and neap tides are neglectable.
- observe that during all the scenarios the estuary is accumulating sediments and filling. The global annual trend for each scenario is not continuous but rather takes place in steps, during most energetic events. This observation is in agreement with conclusions of Winter et al. 2006.

- relate the different impact of the tides on sediment volume to paleoenvironmental, seafloor and sea-level evolution.
- determine that flood currents induce two to three times more resuspension than ebb currents.
- define the threshold of the free sea surface variations rate above which the Bay globally undergoes (and exponentially) erosion and resuspension of sediments.
- show that over the estuary spring tide time intervals promote erosion until the tide displays the quickest sea surface variations rate (of the half lunar cycle) and then they promote deposition.

However, these results are only the first step toward the definition of a drastically simplified tidal forcing able to reproduce over year the morphological evolution, i.e. resume significant tides (for sediment volume variations) into a few morphogen tides. As seen previously, two major behaviour clusters are observed in the Bay of Brest: (1) during equinoctial strong spring tides, and (2) during equinoctial moderate and solstitial moderate and strong spring tides. We determined the minimum threshold of sea surface variation rate necessary to generate significant sediment volume variation. The next step will be to calculate the value of sea surface variation rate limit between the two tidal behaviour clusters, which is the only one missing. The aim is to define boundaries of sea surface variation rate for both clusters. Then, we will be able to study occurrence frequency of the two tidal behaviour clusters, i.e. how many times tides, corresponding to each cluster, occur during one year. It will allow us to use a statistical approach, and define two morphogen tides and their respective impact on sediment volume evolution.

However, one main question remains about the statistical definition of each morphogen tide, which is: Do all tides of each cluster have the same impact on sediment volume evolution? We exposed that the tides inside the two clusters display similar patterns, but do they impact the same locations (inside morphological domains) and in similar quantity? Future investigations must focus on the difference of tidal cycles (ebb and flood) impact on the sediment volume, inside the same cluster. For that purpose, a differential analysis needs to be done for the morphological evolution of the seafloor between tidal cycles of the same cluster. In order to give a range of variations, the differences of sediment volume variations (if any) between the weakest and the strongest tide of each cluster must be carried out firstly. Those results are critical for the statistical definition of morphogen tides: if all the observed tides in each cluster are identical, then morphogen tides will correspond to the average tide of the cluster; if not, it will be necessary to carry out a weighted average depending on the occurrence and the quantity of the sediment volume variations inside the two clusters to obtain the two expected morphogen tides.

We hope to obtain two morphogen tides, for (1) equinoctial strong spring tides and, (2) equinoctial moderate and solstice moderate and strong spring tides. Then, the final goal will be to determine how many occurrences of each cluster are needed to simulate the morphological evolution over one year, and to verify if two morphogen tides are able to reproduce the morphological evolution over one year.

Several perspectives have also to be considered in order to obtain more reliable conclusions about the sediment volume evolution during both clusters. Only after, the tidal impact on 3D sediment morphologies (e.g. sediment structures or layers formation) could be explore, by using simplified inputs based on these clusters (future work). Thanks to our numerical laboratory, other parameterisations can be carried out, which will allow to refined some observations:

- The realisation of simulations without initial sediments (or smaller) would allow us to better understand deposition dynamics linked to each morphological domain and to each

palaeoenvironment. The presence of an initial sediment layer allows us to observe the remobilization dynamics induced by tide. However, in areas that undergo strong currents, the presence of muddy sediment is not realistic and the dynamics of mud erosion can mask deposition dynamics of coarser sediments, such as in some part of T1.

- As pointed-out by Winter et al., (2006), the quantification of sediment river inflow is important to reproduce realistic morphological evolution. The numerical laboratory of the Bay of Brest allows us to study the impact of various sediment supply on sediment dynamics. Firstly, the analyses presented in this chapter should be carried out again from new simulation parameterisation including non-constant river discharges calibrated for each scenario (such as in chapter 5), in order to discuss the contributions of sediment sources to hydro-sedimentary dynamics. Simulations with only river supply and only oceanic supply will contribute also to the understanding of the influence of sediment supply sources on hydro-sedimentary dynamics.

Moreover, one additional post-treatment should be carried out for each scenario to analyse the influence of the two clusters defined in this chapter: full sediment volume evolution including the sediment cover and the resuspended matters in the water column. The aim is to better understand the full sediment dynamics in the Bay of Brest. Fig. 93 is a preliminary attempt for scenario 4. This figure shows that sediments are evacuated from the Bay of Brest only during equinoctial strong spring tides whereas sediments are brought into the Bay during equinoctial moderate and both solstitial spring tides (Fig. 93). During neap tides the sediment volume with suspended matter seems stable.

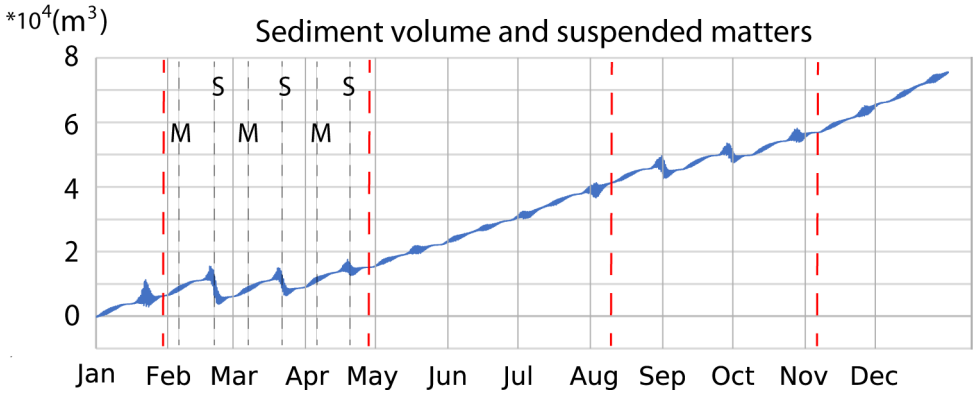

Fig. 93: Total volume evolution (suspended matter and sediment volume) over one year, for scenario 4. S: strong spring tide; M: moderate spring tide. Red dashed lines display equinox and solstice time intervals identified from sediment volume variations.

7 Conclusions and perspectives

7.1 Conclusions

This PhD work had two main objectives: to understand and model the long-term impact of tides on the sediment erosion, transport and deposition in estuaries. The main contributions of this work are:

(I) The definition of a methodology to study tidal currents and induced sediment flows over thousands of years, based on the definition of a few scenarios from geological and seismic data, and the computation of hydrodynamic and hydro-sedimentary simulations for each scenario.

(II) The reconstruction of the hydrodynamics and hydro-sedimentary evolution over the Holocene transgression in the Bay of Brest. These results allowed us also to discuss in particular the influence of paleo-topography and sediment supply on the sediment flows and the preservation or erosion of sedimentary units within the Bay of Brest.

(III) The analysis of the Holocene evolution of tidal hydro-sedimentary dynamics. This analysis allows us to propose a few implications for sequence stratigraphy interpretation in tide-dominated estuaries. A schematic conceptual model is proposed to explain the evolution of erosion/deposition, and non-cohesive/cohesive sediment boundaries, according to paleoenvironmental changes. Furthermore, hypothesis on the link between hydrodynamics and preservation of deposits in tide-dominated estuaries is proposed: hydrodynamics seems to promote a better preservation of tidal deposits during highstand system tract (HST) than transgressive system tract (TST).

(IV) A first step towards the definition of long-term morphogen tides. We defined the time intervals inducing significant sediment volume variations (morphogen tides), and the minimum sea surface variations rate during a tidal cycle that triggered significant sediment volume variations. These promising results allow us to propose a workflow to characterize morphogens tides, which are responsible of the main morphodynamics evolution of the Bay.

About the methodology

From the analysis of previous work and geological data, we reconstructed the Holocene evolution of palaeoenvironments of the Bay of Brest. Four scenarios corresponding to key time intervals were defined by a bathymetric map (estimation of the sediment cover thickness over the basement, and reconstruction of elevation of the seafloor) and a sea-level. First, the water mass movements induced by tides were simulated using the numerical hydrodynamic model MARS3D, then the tidal impacts on sediment erosion, transport in suspension, and deposition were simulated using the numerical hydro-sedimentary model MUSTANG. For each scenario sediment supply were calibrated to fit the sedimentation rate calculated from thickness map and deposition chronology. Secondly, the bathymetric evolution (sedimentation and erosion rate at each point of the simulated domain), and the grain-size distribution (fraction of gravel, sand, fine sand and mud in each cell) were compared to sedimentary records (thickness map from seismic data, grain-size observations from cores) to validate the simulations. For hydrodynamic simulations the comparison was made through the calculation of potential deposition and erosion indexes. The good correlation between sedimentary records, and hydrodynamic and hydro-sedimentary simulation results demonstrates the relevance of the methodology, which made it possible to build a virtual digital model quantifying the Holocene hydro-sedimentary evolution of the Bay of Brest, and therefore to study the tidal impact on sediment flows over long time periods.

About the hydrodynamic and hydro-sediment dynamic evolution in the Bay of Brest

The simulations carried-out in this study allowed us to propose a reconstruction of the hydrodynamic and the hydro-sedimentary dynamic evolution over the Holocene.

Scenario 1, 9 – 7.5 ka BP:

During this period strong bidirectional currents induced by flood and ebb tides take place in the centre of the Bay over T1, which is the only subtidal domain. Most of the sediments are deposited over the intertidal area T2, and T1 in the upper area of the Bay, and are composed mostly of mud, and some fine sands. Most of the non-cohesive sediment transport is located over the main channel in the centre. Some local sediment accumulations are simulated and are consistent with sediment records, but globally T1 deepened over this time interval (corresponding to the beginning of U1 deposition).

Scenario 2, 7.5 – 7 ka BP:

During this period, tidal current gyre forms in the centre of the Bay, and previous fine sediments deposited over T2 are reworked by strong ebb and flood tide currents. Locations of main currents in the Bay are influenced by the strait between Plouzané and Roscanvel peninsula, which drives the incoming water (flood tide) toward the North of the central area, and the strait between Lanvéoc and Plougastel-Daoulas, which drives ebb currents towards the South in the central area. Most of the non-cohesive transport take place over T2 and sediments are deposited at the edges of T2 (slopes over T2 and T3, and T1). In the upper area of the Bay, T1 is still the only subtidal domain and undergoes strong bidirectional ebb of flood tide currents. Over the estuary, mud settles mostly over T3 and slopes between T2 and T3. Most of the sediments deposited during the previous time interval are remobilized. Preserved sedimentary records of U1 testify mostly of the hydrodynamics at the end of U1 deposit. Globally T1 and T2 become deeper, and T3 terrasses get shallower over this period (due to erosion and sedimentation).

Scenario 3, 7 – 3 ka BP:

At the beginning of U2 almost all T3 terrasses pass into subtidal area and, given the morphology of the Bay, the subtidal area increases a lot. In the upper area of the Bay, locations of flood and ebb tide currents are no longer the same, and no longer bidirectional. Main flood currents are driven by the strait between Lanvéoc and Plougastel-Daoulas over T1, while ebb currents are mainly over T3. The currents observed all over the upper area of the Bay are less intense than those during scenario 2, and mud settles over all morphological domains. In this condition, the quantity of non-cohesive sediments reaching the upper area decreases, compared to scenario 2. In the centre, the hydro-sediment dynamic remains similar as during the time interval 7.5 to 7 ka. However, the erosion rate induced by tides (with the same quantity of sediment supply) decreases compared to 7.5 - 7 (ka) over T2 and the sedimentation rate increases over T3. However, T2 and T1 are globally still losing sediments.

Scenario 4, 2 ka BP – present-day:

During the final scenario, more intense currents take place in the upper area of the Bay than during the previous scenarios. Non-cohesive sediments are transported further upstream towards the river mouths, and mud settles only over T3. During this time interval, mud deposits are observed only over T3 also in centre.

The analysis of these four scenarios allows us to understand the evolution of the water and sediment flows in the Bay during the full Holocene. The gyre induced by flood and ebb tide currents (at the south

of the central area of the Bay) gets quicker and quicker from scenario 2 to 4, especially between scenario 3 and scenario 4. Fine sediments deposits (mud mostly and some fine-sands) are progressively pushed towards T3 terrasses from scenario 1 to 4, and are no longer able to settle on slopes between T2 and T3 during the final scenario (except in one place at the East of Lanvéoc). Most of non-cohesive sediments transport take place over T2 since 7.5 ka (scenario 2); it increases through the Holocene and reach its maximum during the final scenario 4. The sedimentation rate (with the same quantity of sediment supply) increases again over T3 compared to scenario 3 and for the first time T2 accumulates sediments.

Simulation results explains most of the sedimentary record observed in the Bay of Brest. The distribution of depositional zones is consistent with the sediment thickness maps and grain-size classes distribution with cores. Three points could be noted:

(1) the simulated thickness map does not fit well with sedimentary records over T2 for the last scenario 4. The simulations of scenarios 2, 3 and 4 suggest that the presence of non-cohesive sediments frequently remobilized during the last 7 500 years. This simulation result is consistent with the recent analysis of present-day sedimentary structures, and the seafloor sediment map, which displays energetic sediment structures, mainly sand ridges, bars and comet tails. The small thickness of 1 to maximum 5 m over T2 is certainly the result of the last 7 500 years (scenarios 2, 3 and 4) and not only scenario 4 hydrodynamic.

(2) a greater sedimentation rate is simulated over T3 compared to T1 in the central part in scenario 3, while sedimentary records display the opposite. However, simulations results and cores suggest that the difference is mainly link with the sediment supply grain-size fractions (mud, fine sand, sand and gravels proportions), which was probably sandier (and containing less mud) than the sediment supply set up for scenario 3 simulation.

(3) Two cores in scenario 3 and in scenario 4 display coarse grain-size classes unexplained by simulations. Those coarse sediments are potentially supplied by exceptional events, such as storm winds or rivers floods. The core observations differ from the simulations in only two points for these two scenarios, which represents a very good correlation.

Further simulations were run to evaluate the influence of sediment sources (boundary conditions) on the infilling of the Bay of Brest: oceanic inputs represent around 55%, against 26% for rivers, of the sediment supplied in the Bay during scenario 1, 62% and 9% during scenario 2, 89% and less than 1% during scenarios 3, 94% and less than 1% in scenario 4. The weighted average along the deposition period of the three units (Fig. 68) shows that oceanic inputs represent 82% of sediments supply during the Holocene (9 Ka BP - present-day), against around 6% for river inputs. Moreover, the river water discharge evolution is consistent with climatic and paleoenvironmental evolution of Brittany and North-Western Europe. The decrease found in river water discharges is almost proportional to the evolution of the river profile linked mostly to sea-level variations.

About implications for sequence stratigraphy interpretation in tide-dominated estuaries

The results obtained for the Bay of Brest led to several observations linked to sequence stratigraphy interpretation of tide-dominated estuaries. In each scenario, simulated global sediment and grain-size distribution shows that (1) the most energetic zone is composed of non-cohesive sediments, which are certainly organized in sediment structures (e.g. sand ridges and bars, comet tails); (2) towards the shallowest parts of the estuary (flanks and river mouths) sediment deposits are finer (mix of mud and

fine sand); and (3) further towards the shallowest area and the coastline sediment deposits are only muddy.

We also observed that the boundaries between erosion and deposition zones, and of cohesive and non-cohesive sediment deposition, are not necessarily moving upward the estuary during the Holocene transgression. The evolution of those boundaries is linked to the distribution and intensity of tidal currents, which are closely linked to the sea-level rise and seafloor morphology. Those boundaries move upward or downward the estuary depending on the volume of water transported by the tide in relation to the active flow section width. Considering the same tidal amplitude, if sea-level rises and the active flow section remains of similar width, a greater water volume pass through a similar section and tidal current velocities increase. Thus, erosion/deposition and cohesive/non-cohesive sediment deposition boundaries move upward of the estuary. When the active flow section width increases, it is over flat and large terraces, which induce an important and fast modification of the active flow section width. A slightly greater water volume passes through a much larger section and it results in a decrease in tidal current velocities. Therefore, the mud/sand boundary moves downward of the estuary. The phenomenon is amplified by the evolution of friction over flat morphological domain, which is strong everywhere when its shallow and decreases with the increasing depth.

This relation can be applied only in estuaries with a similar upstream morphology as the Bay of Brest, as the evolution of the upstream tidal prism play a major role. Upstream areas of the Bay are only rivers with steep banks and so the evolution of the tidal prism is almost proportional to the rise in sea-level in those areas.

The evolution of depositional area between scenarios demonstrates also that erosion/deposition and cohesive/non-cohesive boundaries are not equal to a depth threshold, but they vary with the distribution of tidal currents. As seen previously, their distributions are linked to the shape of the basin and the sea-level height, and locally the shape of the coastline can play a strong role. It highlights that seafloor morphology is thus of an uppermost importance for the evolution of tidal currents distribution over long periods (considering eustatic movements).

The detailed analysis of the hydro-sedimentary simulations allowed us also to formulate hypotheses on the preservation of deposits in tide-dominated estuaries. Hydrodynamics promotes a better preservation of HST (Highstand system tract) than TST (Transgressive system tract) in tide-dominated estuaries. Unless an important increase of the active flow section width happens (e.g., during scenario 3), fine sediment deposits (fine sand and mud mostly) are progressively pushed towards the shallowest terrasses during the transgression, and thus previous deposits are remobilized to feed the next sedimentary unit (mainly because of tidal asymmetry in the Bay). During a transgression, fine shallow deposits are thus preserved only over the shallowest domain (T3 in the case of the Bay of Brest). HST fine sediment deposits are hardly removed from the shallowest morphological domain by the tidal process, as it represents the highest sea-level.

Bottom currents decrease with the increase of depth, and thus potential deposition increases over deepest domains. Only the scenario 4, the simulation at the present-day, displays sedimentation over T2. Transgression deposits (from scenarios 2 and 3) are hardly preserved, except over the shallowest domain of the transgression. Coarser non-cohesive sediments deposits are increasingly likely deposited and preserved over deepest domains, as the sea-level rises. Thus, potential sediment preservation during HST is more important over all morphological domains than during TST.

Towards the definition of long-term morphogen tides

We consider the morphogen tides as the resume of all tides inducing significant morphological changes within the Bay of Brest. To characterize these morphogen tides, we analysed the sediment volume evolution for each scenario. Main sediment volume variations occurred during the same specific tide periods throughout the four scenarios: (I) Short periods of about 7 days during equinoctial strong spring tides induce most of sediment volume variations. They always induce deposition over the shallowest terrasses, erosion over intermediate terrasses and in the main channel (which is globally suffering erosion during the entire Holocene). (II) Equinoctial moderate spring tides and solstitial strong and moderate spring tides (~7 days) also induce significant sediment volume variations, but in lesser proportion than equinoctial strong spring tides. They always induce deposition over the shallowest terraces and intermediate terraces (T2, T3).

The evolution of the sediment volume is closely linked to the mean sea surface variation rate over a few tidal cycles. We identified a threshold, about 1.25 $m.h^{-1}$ over which the tides are high enough to induce significant sediment volume variations. Above this threshold, sediment volume variations grow exponentially. Tidal currents globally promote erosion until the sea surface variations rate reaches its highest value within the half lunar cycle (14.75 days). Then, tides promote deposition until the sea surface variations rate reaches again the threshold.

7.2 Perspectives

Several perspectives arise from this PhD for future works on different topics:

Universal sequence stratigraphy principle? Our conclusions are based on the Holocene evolution of the Bay of Brest, a paleo-fluvial bay protected from the waves by a strait. Results clearly demonstrated that the hydro-sediment dynamic and its evolution, are closely connected to seafloor and coastline morphology. To extend these conclusions to over tidal sedimentary systems, similar studies should be carried out in other estuaries and bays with different morphologies and tidal regimes. This would help us to better characterize the link between hydro-sedimentary dynamics and paleoenvironmental evolution, e.g., to better understand the relationship between sea-level and coastline retreat rates, and HST vs. TST sediment preservation.

Uncertainties on boundary conditions? Due to the lack of information in the past for sediment supply, we assume the fine sediment concentrations were constant in rivers for all scenarios. Previous studies give qualitative clues about precipitation and land run-off evolutions. It would be very interesting to intend a trial-error calibration for suspended matter concentration too. The aim will be to explore a more realistic sediment supply, to better fit river sediment supply history, even if they have a very limited impact on hydrodynamics inside the Bay of Brest. Oceanic sediment supply was identified as the dominant sediment source and the grain-size classes proportions were set constant for all scenarios. Intend a new trial-error for grain-size classes proportions of oceanic sediment supply should be carried out to better understand its impact on the Bay infilling.

Upscaling of the tidal impact on sediments? The most important step forward concerns the definition of morphogen tides, which corresponds to the upscaling of the tidal processes, and of their long-term impact on sediments and on the morphology of the Bay. Our four hydro-sedimentary scenarios of the Bay of Brest give us access to four full 4D (x,y,z,t) digital models of the Bay, with a time step of 30 seconds, and a grid cell size of 250 m, calibrated on sedimentary records. These four scenarios are a

numerical laboratory that will make it possible to better characterize morphogen tides, and the evolution of their characteristics (amplitude, frequency), during the Holocene transgression.

Bibliography

A

Acolas, M.L., Véron, V., Jourdan, H., Bégout, M.L., Sabatié, M.R., Baglinière, J.L., 2006. Upstream migration and reproductive patterns of a population of allis shad in a small river (L'Aulne, Brittany, France). ICES Journal of Marine Science 63, 476–484. https://doi.org/10.1016/j.icesjms.2005.05.022.

Ainsworth, R.B., Bosscher, H., Newall, M.J., 2000. Forward stratigraphic modelling of forced regressions: evidence for the genesis of attached and detached lowstand systems. The Geological Society of London, Special Publications 172, 163–176.

Al-Salmi, M., John, C.M., Hawie, N., 2019. Quantitative controls on the regional geometries and heterogeneities of the Rayda to Shu'aiba formations (Northern Oman) using forward stratigraphic modelling. Marine and Petroleum Geology 99, 45–60. https://doi.org/10.1016/j.marpetgeo.2018.09.030.

Aslanian, D., Moulin, M., Olivet, J.-L., Unternehr, P., Matias, L., Bache, F., Rabineau, M., Nouzé, H., Klingelheofer, F., Contrucci, I., Labails, C., 2009. Brazilian and African passive margins of the Central Segment of the South Atlantic Ocean: Kinematic constraints. Tectonophysics 468, 98–112. https://doi.org/10.1016/j.tecto.2008.12.016.

Augris, C., 2005. Atlas Thématique de L'environnement Marin de La Baie de Douarnenez (Finistère). Editions Quae.

B

Ballèvre, M., Bosse, V., Ducassou, C., Pitra, P., 2009. Palaeozoic history of the Armorican Massif: Models for the tectonic evolution of the suture zones. Comptes Rendus Geoscience 341, 174–201. https://doi.org/10.1016/j.crte.2008.11.009.

Ballèvre, M., Martínez Catalán, J.R., López-Carmona, A., Pitra, P., Abati, J., Fernández, R.D., Ducassou, C., Arenas, R., Bosse, V., Castiñeiras, P., Fernández-Suárez, J., Gómez Barreiro, J., Paquette, J.L., Peucat, J.J., Poujol, M., Ruffet, G., Sánchez Martínez, S., 2014. Correlation of the nappe stack in the Ibero-Armorican arc across the Bay of Biscay: a joint French–Spanish project. Geological Society, London, Special Publications 405, 77–113. https://doi.org/10.1144/SP405.13.

Bárcena, J.F., García-Alba, J., García, A., Álvarez, C., 2016. Analysis of stratification patterns in river-influenced mesotidal and macrotidal estuaries using 3D hydrodynamic modelling and K-means clustering. Estuarine, Coastal and Shelf Science 181, 1–13.

Barnard, P., Erikson, L., Rubin, David, M., Dartnell, P., Kvitek, Rikk, G., 2012. Analyzing bedforms mapped using multibeam sonar to determine regional bedload sediment transport patterns in the San Francisco Bay coastal system Assoc. Sedimentol. Spec. Publi., 273–294.

Barrett, S.J., Webster, J.M., 2017. Reef Sedimentary Accretion Model (ReefSAM): Understanding coral reef evolution on Holocene time scales using 3D stratigraphic forward modelling. Marine Geology 391, 108–126. https://doi.org/10.1016/j.margeo.2017.07.007.

Bellucci, M. S., 2021. Relationship between crustal segmentation, nature, thermicity and salt tectonics in the Western Mediterranean Sea, 480 pp. https://tel.archives-ouvertes.fr/tel-03562840

Beudin, A., 2014. Dynamique et échanges sédimentaires en rade de Brest impactés par l'invasion de crépidules, 224 pp.

Beudin, A., Chapalain, G., Guillou, N., 2013. Suspended sediment modelling in the bay of Brest impacted by the slipper limpet crepidula fornicata. Coastal Dynamics.

Berger, A., Loutre, M.F., 1991. Insolation values for the climate of the last 10 million years. Quaternary Science Reviews 10, 297–317. https://doi.org/10.1016/0277-3791(91)90033-Q.

Berger, J.-F., Guilaine, J., 2009. The 8200calBP abrupt environmental change and the Neolithic transition: A Mediterranean perspective. Quaternary International 200, 31–49. https://doi.org/10.1016/j.quaint.2008.05.013.

Bertin, X., Chaumillon, E., Sottolichio, A., Pedreros, R., 2005. Tidal inlet response to sediment infilling of the associated bay and possible implications of human activities: the Marennes-Oléron Bay and the Maumusson Inlet, France. Continental Shelf Research 25, 1115–1131. https://doi.org/10.1016/j.csr.2004.12.004.

Bird, E., 2011. Coastal Geomorphology: An introduction - second edition. John Wiley & Sons.

Bjune, A.E., Bakke, J., Nesje, A., and Birks, H., 2005. Holocene mean July temperature and winter precipitation in western Norvay inferred from palynological and glaciological lake-sediment proxies. The Holocene 15,2, 177–189.

Bolla Pittaluga, M., Tambroni, N., Canestrelli, A., Slingerland, R., Lanzoni, S., Seminara, G., 2015. Where river and tide meet: The morphodynamic equilibrium of alluvial estuaries. J. Geophys. Res. Earth Surf. 120, 75–94. https://doi.org/10.1002/2014JF003233.

Bouma, A., Hampton, M., Wennekens, M., Dygas, J., 1977. Sand waves and other bedforms in lower Cook Inlet, Alaska. Marine Georesources & Geotechnology, 291–308.

Boyd, R., Dalrymple, R., Zaitlin, B.A., 1992. Classification of clastic coastal depositional environments. Sedimentary Geology 80, 139–150. https://doi.org/10.1016/0037-0738(92)90037-R.

Boyd, R., Dalrymple, R.W., Zaitlin, B.A., 2006. Estuarine and Incised-Valley Facies Models. In: Posamentier, H.W., Walker, R.G. (Eds.) Facies Models Revisited. SEPM (Society for Sedimentary Geology), pp. 171–235.

Braat, L., van Kessel, T., Leuven, J.R.F.W., Kleinhans, M.G., 2017. Effects of mud supply on large-scale estuary morphology and development over centuries to millennia. Earth Surf. Dynam. 5, 617–652. https://doi.org/10.5194/esurf-5-617-2017.

Bruneau, B., Chauveau, B., Baudin, F., Moretti, I., 2017. 3D stratigraphic forward numerical modelling approach for prediction of organic-rich deposits and their heterogeneities. Marine and Petroleum Geology 82, 1–20. https://doi.org/10.1016/j.marpetgeo.2017.01.018.

Busson, J., Joseph, P., Mulder, T., Teles, V., Borgomano, J., Granjeon, D., Betzler, C., Poli, E., Wunsch, M., 2019. High-resolution stratigraphic forward modeling of a Quaternary carbonate margin: Controls and dynamic of the progradation. Sedimentary Geology 379, 77–96. https://doi.org/10.1016/j.sedgeo.2018.11.004.

C

Cartwright, D.E., 1999. Tides, a scientific history.

Cartwright, D.E., Tayler, R.J., 1971. New Computations of the Tide-generating Potential. Geophys. J. R. astr. SOC 23, 45–74.

Cayocca, F., 2001. Long-term morphological modeling of a tidal inlet: the Arcachon Basin, France. Coastal Engineering 42, 115–142. https://doi.org/10.1016/S0378-3839(00)00053-3.

Chataigner, T., 2018. Modélisation de la dynamique sédimentaire en rade de Brest, intégrant une résolution spatiale des fonds plus fine que celle de la masse d'eau.: Master report, University of Occidental Brittany, 36p.

Choi, K.S., Dalrymple, R.W., 2004. Recurring tide-dominated sedimentation in Kyonggi Bay (west coast of Korea): similarity of tidal deposits in late Pleistocene and Holocene sequences. Marine Geology 212, 81–96. https://doi.org/10.1016/j.margeo.2004.07.008.

Clifton, H.E., 2006. A Reexamination of Facies Models for Clastic Shorelines. In: Posamentier, H.W., Walker, R.G. (Eds.) Facies Models Revisited. SEPM (Society for Sedimentary Geology), pp. 293–337.

Coco, G., Zhou, Z., van Maanen, B., Olabarrieta, M., Tinoco, R., Townend, I., 2013. Morphodynamics of tidal networks: Advances and challenges. Marine Geology 346, 1–16. https://doi.org/10.1016/j.margeo.2013.08.005.

Cognat, M., 2019. Rôles des facteurs environnementaux et des interactions biomorphodynamiques sur l'évolution spatio-temporelle des herbiers de zostères dans une lagune mésotidale.

Collins, D.S., Avdis, A., Allison, P.A., Johnson, H.D., Hill, J., Piggott, M.D., 2018. Controls on tidal sedimentation and preservation: Insights from numerical tidal modelling in the Late Oligocene-Miocene South China Sea, Southeast Asia. Sedimentology 65, 2468–2505. https://doi.org/10.1111/sed.12474.

Crombez, V., Rohais, S., Baudin, F., Chauveau, B., Euzen, T., Granjeon, D., 2017. Controlling factors on source rock development: implications from 3D stratigraphic modeling of Triassic deposits in the Western Canada Sedimentary Basin. Bulletin de la Société Géologique de France 188, 7. https://doi.org/10.1051/bsgf/2017188.

D

Dalrymple, R., 2010. Tidal depositional systems. In: James, N.P., Dalrymple, R.W. (Eds.), Facies Models 4: St John's. Geological Association of Canada, 201–231.

Dalrymple, R.W., Choi, K., 2007. Morphologic and facies trends through the fluvial–marine transition in tide-dominated depositional systems: A schematic framework for environmental and sequence-stratigraphic interpretation. Earth-Science Reviews 81, 135–174. https://doi.org/10.1016/j.earscirev.2006.10.002.

Dalrymple, R., Mackay, D., Ichaso, A., Choi, K., 2012. Processes, Morphodynamics, and Facies of Tide-Dominated Estuaries. In: Davis, R.A., Dalrymple, R.W. (Eds.) Principles of Tidal Sedimentology. Springer Science+Business Media B.V., Dordrecht.

Dalrymple, R.W., Rhodes, R.N., 1995. Estuarine dunes and bars. Geomorphology and Sedimentology of Estuaries. Developments in sedimentology 53, 359–422. https://doi.org/10.1093/owc/9780199675647.003.0014.

Dalrymple, R., Zaitlin, B.A., 1994. High-resolution sequence stratigraphy of a complex, incised valley succession, Cobequid Bay — Salmon River estuary, Bay of Fundy, Canada. Sedimentology 41, 1069–1091.

Dalrymple, R.W., Zaitlin, B., Boyd, R., 1992. Estuarine facies models: Conceptual basis and stratigraphic implications. Journal of sedimentary petrology VOL. 62, No. 6, 1130–1146.

Dam, G., van der Wegen, M., Labeur, R.J., Roelvink, D., 2016. Modeling centuries of estuarine morphodynamics in the Western Scheldt estuary. Geophys. Res. Lett. 43, 3839–3847. https://doi.org/10.1002/2015GL066725.

Dauble, A.D., Heppell, S.A., Johansson, M.L., 2012. Settlement patterns of young-of-the-year rockfish among six Oregon estuaries experiencing different levels of human development. Mar. Ecol. Prog. Ser. 448, 143–154. https://doi.org/10.3354/meps09504.

David, O., Penaud, A., Vidal, M., Fersi, W., Lambert, C., Goubert, E., Herlédan, M., Stéphan, P., Pailler, Y., Bourillet, J.-F., Baltzer, A., 2022. Sedimentological and palynological records since 10 ka BP along a proximal-distal gradient on the Armorican shelf (NW France). Quaternary Science Reviews 293, 107678. https://doi.org/10.1016/j.quascirev.2022.107678.

Davies, A.G., Robins, P.E., 2017. Residual flow, bedforms and sediment transport in a tidal channel modelled with variable bed roughness. Geomorphology 295, 855–872. https://doi.org/10.1016/j.geomorph.2017.08.029.

Davis, R., 2012. Tidal Signatures and Their Preservation Potential in Stratigraphic Sequences. In: Davis, R.A., Dalrymple, R.W. (Eds.) Principles of Tidal Sedimentology. Springer Science+Business Media B.V., Dordrecht.

Davis, R.A., Dalrymple, R.W. (Eds.), 2012. Principles of Tidal Sedimentology. Springer Science+Business Media B.V., Dordrecht, 622 pp.

Dias, J., Jouanneau, J., Gonzalez, R., Araújo, M., Drago, T., Garcia, C., Oliveira, A., Rodrigues, A., Vitorino, J., Weber, O., 2002. Present day sedimentary processes on the northern Iberian shelf. Progress in Oceanography 52, 249–259. https://doi.org/10.1016/S0079-6611(02)00009-5.

Diaz, M., Grasso, F., Le Hir, P., Sottolichio, A., Caillaud, M., Thouvenin, B., 2020. Modeling Mud and Sand Transfers Between a Macrotidal Estuary and the Continental Shelf: Influence of the Sediment Transport Parameterization. J. Geophys. Res. Oceans 125. https://doi.org/10.1029/2019JC015643.

Doodson, 1921. The harmonic development of the tide-generating potential. royal society publishing.

Douglas, E.J., Lohrer, A.M., Pilditch, C.A., 2019. Biodiversity breakpoints along stress gradients in estuaries and associated shifts in ecosystem interactions. Scientific reports 9, 17567. https://doi.org/10.1038/s41598-019-54192-0.

Dufois, F., Le Hir, P., 2015. Formulating Fine to Medium Sand Erosion for Suspended Sediment Transport Models. JMSE 3, 906–934. https://doi.org/10.3390/jmse3030906.

E

Egbert, G.D., Ray, R.D., Bills, B.G., 2004. Numerical modeling of the global semidiurnal tide in the present day and in the last glacial maximum. J. Geophys. Res. 109. https://doi.org/10.1029/2003JC001973.

Ehlers, J., Gibbard, P.L., 2004. Quaternary glaciations extent and chronology: Part I: Europe. Elsevier.

Ehrhold, A., Jouet, G., Le Roy, P., Jorry, S.J., Grall, J., Reixach, T., Lambert, C., Gregoire, G., Goslin, J., Roubi, A., Penaud, A., Vidal, M., Siano, R., 2021. Fossil maerl beds as coastal indicators of late Holocene palaeo-environmental evolution in the Bay of Brest (Western France). Palaeogeography, Palaeoclimatology, Palaeoecology 577, 110525. https://doi.org/10.1016/j.palaeo.2021.110525.

Ehrhold, A., Gregoire, G., 2015. SERABEQ-03 cruise,Thalia R/V.

Ehrhold, A., Gregoire, G., Schmidt, S., Jouet. Gwenael, Le Roy, P. (Eds.), 2016. Present-day sedimentation rates and evolution since the last maximum flooding surface event in the Bay of Brest (W-N France) .

Elmilady, H., Wegen, M., Roelvink, D., Spek, A., 2020. Morphodynamic Evolution of a Fringing Sandy Shoal: From Tidal Levees to Sea Level Rise. J. Geophys. Res. Earth Surf. 125. https://doi.org/10.1029/2019JF005397.

F

Fauquette, S., Suc, J.-P., Bertini, A., Popescu, S.-M., Warny, S., Bachiri Taoufiq, N., Perez Villa, M.-J., Chikhi, H., Feddi, N., Subally, D., Clauzon, G., Ferrier, J., 2006. How much did climate force the Messinian salinity crisis? Quantified climatic conditions from pollen records in the Mediterranean region. Palaeogeography, Palaeoclimatology, Palaeoecology 238, 281–301. https://doi.org/10.1016/j.palaeo.2006.03.029.

Fernane, A., 2014. Reconstitution des fluctuations holocènes en relation avec les changements climatiques et l'antropisation sur les côtes bretonnes à partir de bio-indicateurs fossiles (chironomidés, pollen et foraminifères benthiques), Brest, 248 pp.

Ferret, Y., Le Bot, S., Tessier, B., Garlan, T., Lafite, R., 2010. Migration and internal architecture of marine dunes in the eastern English Channel over 14 and 56 year intervals: the influence of tides and decennial storms. Earth Surf. Process. Landforms 35, 1480–1493. https://doi.org/10.1002/esp.2051.

FitzGerald, D.M., Buynevich, I.V., Fenster, M.S., McKinlay, P.A., 2000. Sand dynamics at the mouth of a rock-bound, tide-dominated estuary. Sedimentary Geology 131, 25–49.

Flemming, B., 2012. Siliciclastic Back-Barrier Tidal Flats. In: Davis, R.A., Dalrymple, R.W. (Eds.) Principles of Tidal Sedimentology. Springer Science+Business Media B.V., Dordrecht.

Flemming, B.W., 1980. Sand transport and bedform patterns on the continental shelf between Durban and Port Elizabeth (southeast African continental margin). Sedimentary Geology, 179–205.

Franz, G., Delpey, M.T., Brito, D., Pinto, L., Leitão, P., Neves, R., 2017. Modelling of sediment transport and morphological evolution under the combined action of waves and currents. Ocean Sci. 13, 673–690. https://doi.org/10.5194/os-13-673-2017.

French, J., Payo, A., Murray, B., Orford, J., Eliot, M., Cowell, P., 2016. Appropriate complexity for the prediction of coastal and estuarine geomorphic behaviour at decadal to centennial scales. Geomorphology 256, 3–16. https://doi.org/10.1016/j.geomorph.2015.10.005.

Frère, L., Paul-Pont, I., Rinnert, E., Petton, S., Jaffré, J., Bihannic, I., Soudant, P., Lambert, C., Huvet, A., 2017. Influence of environmental and anthropogenic factors on the composition, concentration and spatial distribution of microplastics: A case study of the Bay of Brest (Brittany, France). Environmental pollution (Barking, Essex : 1987) 225, 211–222. https://doi.org/10.1016/j.envpol.2017.03.023.

G

Galloway, W., 1975. Process Framework for Describing the Morphologic and Stratigraphic Evolution of Deltaic Depositional Systems, 87–98.

Ganthy, F., 2011. Rôle des herbiers de zostères (Zostera noltii) sur la dynamique sédimentaire du Bassin d'Arcachon, Bordeaux, 284 pp.

García-Artola, A., Stéphan, P., Cearreta, A., Kopp, R.E., Khan, N.S., Horton, B.P., 2018. Holocene sea-level database from the Atlantic coast of Europe. Quaternary Science Reviews 196, 177–192. https://doi.org/10.1016/j.quascirev.2018.07.031.

Gingras, M., MacEachern, J., 2012. Tidal Ichnology of Shallow-Water Clastic Settings. In: Davis, R.A., Dalrymple, R.W. (Eds.) Principles of Tidal Sedimentology. Springer Science+Business Media B.V., Dordrecht.

Goslin, J., van Vliet Lanoë, B., Spada, G., Bradley, S., Tarasov, L., Neill, S., Suanez, S., 2015. A new Holocene relative sea-level curve for western Brittany (France): Insights on isostatic dynamics along the Atlantic coasts of north-western Europe. Quaternary Science Reviews 129, 341–365. https://doi.org/10.1016/j.quascirev.2015.10.029.

Granjeon, D., 1996. Modélisation stratigraphique déterministe : conception et applications d'un modèle diffusif 3d multilithologique, Rennes.

Granjeon, D., Joseph, P., 1999. Concepts and applications of a 3d multiple lithology diffusive model in stratigraphic modeling. Society for Sedimentary Geology (SEPM) Special Publications N°62.

Granjeon, D., 2014. 3D stratigraphic forward model compared with analogue flume model: insights on the non-linear water-driven sediment transport and on the impact of baselevel cycles on continental margin and incised valleys, In: Martinius, A.W., Ravnas, R., Howell, J.A., Steel, R.J., Wonham, J.P. (eds.), From depositional systems to sedimentary successions on the Norwegian continental margin. IAS, Special Publication 47, pp. 453-472. ISBN-13: 9781118920466

Granjeon, D., 2019. Use of high-performance stratigraphic forward modelling to improve siliciclastic and carbonate reservoir depositional architecture description. Journal of the Japanese Association for Petroleum Technology, 84 (1), pp. 59-70

Grasso, F., Le Hir, P., 2019. Influence of morphological changes on suspended sediment dynamics in a macrotidal estuary: diachronic analysis in the Seine Estuary (France) from 1960 to 2010. Ocean Dynamics 69, 83–100. https://doi.org/10.1007/s10236-018-1233-x.

Grasso, F., Verney, R., Le Hir, P., Thouvenin, B., Schulz, E., Kervella, Y., Khojasteh Pour Fard, I., Lemoine, J.-P., Dumas, F., Garnier, V., 2018. Suspended Sediment Dynamics in the Macrotidal Seine Estuary (France): 1. Numerical Modeling of Turbidity Maximum Dynamics. J. Geophys. Res. Oceans 123, 558–577. https://doi.org/10.1002/2017JC013185.

Green, J.A.M., Huber, M., 2013. Tidal dissipation in the early Eocene and implications for ocean mixing. Geophys. Res. Lett. 40, 2707–2713. https://doi.org/10.1002/grl.50510.

Gregoire, G., 2016. Dynamique sédimentaire et évolution holocène d'un système macrotidal semi-fermé : l'exemple de la rade de Brest, Brest, 294 pp.

Gregoire, G., Ehrhold, A., Le Roy, P., Jouet, G., Garlan, T., 2016. Modern morpho-sedimentological patterns in a tide-dominated estuary system: the Bay of Brest (west Britanny, France). Journal of Maps 12, 1152–1159. https://doi.org/10.1080/17445647.2016.1139514.

Gregoire, G., Le Roy, P., 2014. SERABEQ-01 LEG1 cruise,Albert Lucas R/V.

Gregoire, G., Le Roy, P., Ehrhold, A., 2015. SERABEQ-02 LEG1 cruise,Haliotis R/V.

Gregoire, G., Le Roy, P., Ehrhold, A., Jouet, G., Garlan, T., 2017. Control factors of Holocene sedimentary infilling in a semi-closed tidal estuarine-like system: the bay of Brest (France). Marine Geology 385, 84–100. https://doi.org/10.1016/j.margeo.2016.11.005.

Gumiaux, C., Gapais, D., Brun, J.P., Chantraine, J., Ruffet, G., 2004. Tectonic history of the Hercynian Armorican Shear belt (Brittany, France). Geodinamica Acta 17, 289–307. https://doi.org/10.3166/ga.17.289-307.

Guo, L., van der Wegen, M., Roelvink, D., Wang, Z.B., He, Q., 2015. Long-term, process-based morphodynamic modeling of a fluvio-deltaic system, part I: The role of river discharge. Continental Shelf Research 109, 95–111. https://doi.org/10.1016/j.csr.2015.09.002.

H

Hallegouet, B., Lozac'h, G., Vigouroux, F., 1994. Formation de la Rade de Brest. Atlas permanent de la mer et du littoral n°1, 21.

Hansen, W., 1966. The reproduction of themotion in the sea bymeans of hydrodynamical numerical methods. Mitteilung Inst. Meereskünde, Univ. Hamburg,, 1–57.

Hayes, M., 1980. General Morphology and Sediment Patterns in Tidal Inlets. Sedimentary Geology 26, 139-156.

Hu, Z., Wang, Z.B., Zitman, T.J., Stive, M.J.F., Bouma, T.J., 2015. Predicting long-term and short-term tidal flat morphodynamics using a dynamic equilibrium theory. J. Geophys. Res. Earth Surf. 120, 1803–1823. https://doi.org/10.1002/2015JF003486.

i

Idier, D., Paris, F., Le Cozannet, G., Boulahya, F., Dumas, F., 2017. Sea-level rise impacts on the tides of the European Shelf. Continental Shelf Research 137, 56–71. https://doi.org/10.1016/j.csr.2017.01.007.

Intergovernmental Oceanographic Commission., 1997. Global Sea Level Observing System (GLOSS) Implementation Plan 1997. Intergovernmental Oceanographic Commission Technical Series 50.

J

Ji, Z.-G., Hu, G., Shen, J., Wan, Y., 2007. Three-dimensional modeling of hydrodynamic processes in the St. Lucie Estuary. Estuarine, Coastal and Shelf Science 73, 188–200. https://doi.org/10.1016/j.ecss.2006.12.016.

Joseph, P., Teles, V., Weill, P., 2016. Modelling approaches in sedimentology: Introduction to the thematic issue. Comptes Rendus Geoscience 348, 473–478. https://doi.org/10.1016/j.crte.2016.04.001.

Jouet, G., Augris, C., Hallegouët, B., Le Roy, P., Rolet, J., 2003. La vallée d'Ys : un paléoréseau hydrographique immergé en baie de Douarnenez (Finistère, France). Comptes Rendus Geoscience 335, 487–494. https://doi.org/10.1016/S1631-0713(03)00066-X.

K

Kang, J., Woo, H.J., Lee, Y.-K., Son, Y.B., 2014. Seasonal sedimentary processes of the macrotidal flat in Gomso Bay, Korea. Journal of Coastal Research 70, 157–162. https://doi.org/10.2112/SI70-027.1.

Katz, R., Spiegelman, M., Carbotte, S., 2004. Ridge migration, asthenospheric flow and the origin of magmatic segmentation in the global mid-ocean ridge system. Geophys. Res. Lett. 31.

Klouch, Z.K., Caradec, F., Plus, M., Hernández-Fariñas, T., Pineau-Guillou, L., Chapelle, A., Schmitt, S., Quéré, J., Guillou, L., Siano, R., 2016. Heterogeneous distribution in sediments and dispersal in waters of Alexandrium minutum in a semi-enclosed coastal ecosystem. Harmful algae 60, 81–91. https://doi.org/10.1016/j.hal.2016.11.001.

Koshkarova, V.L., Koshkarov, A.D., 2004. Regional signatures of changing landscape and climate of northern central Siberia in the Holocene. Geologiya I Geofizika 45(6), 717–729.

Krone, R.B., 1962. Flume estudies of the transport of sediment in estuarial shoaling processes. Berkeley: University of California.

Ku Shafie, K.R., Madon, M., 2008. A review of stratigraphic simulation techniques and their applications in sequence stratigraphy and basin analysis. BGSM 54, 81–89. https://doi.org/10.7186/bgsm54200814.

Kvale, E., 2012. Tidal Constituents of Modern and Ancient Tidal Rhythmites: Criteria for Recognition and Analyses. In: Davis, R.A., Dalrymple, R.W. (Eds.) Principles of Tidal Sedimentology. Springer Science+Business Media B.V., Dordrecht.

L

Langouët, L., Daire, M.-Y., 2009. Ancient Maritime Fish-Traps of Brittany (France): A Reappraisal of the Relationship Between Human and Coastal Environment During the Holocene. J Mari Arch 4, 131–148. https://doi.org/10.1007/s11457-009-9053-2.

Lanzoni, S., Seminara, G., 2002. Long-term evolution and morphodynamic equilibrium of tidal channels. J. Geophys. Res. 107. https://doi.org/10.1029/2000JC000468.

Lambert, C., 2017. Signature paléoenvironnementale des séquences holocènes en Rade de Brest : forçages climatiques et anthropiques, Brest, 248 pp.

Laplace, P.S., 1790. Mémoire sur le flux et le reflux de la mer, Mém. de l'Acad. des Sciences, 45-181.

Laplace, P.S., 1799. Traité de mécanique céleste, 2, Livre 4, et 5.

Laplace, P.S., 1825. Traité de mécanique céleste, 2, Livre 13.

Latteux, B., 1995. Techniques for long-term morphological simulation under tidal action. Marine Geology 126, 129–141. https://doi.org/10.1016/0025-3227(95)00069-B.

Lazure, P., Dumas, F., 2008. An external–internal mode coupling for a 3D hydrodynamical model for applications at regional scale (MARS). Advances in Water Resources 31, 233–250. https://doi.org/10.1016/j.advwatres.2007.06.010.

Le Bot, S., 2001. Morphodynamique de dunes sous-marines sous influence des marées et des tempêtes : processus hydro-sédimentaires et enregistrement exemple du Pas de- Calais., Lille.

Le Bot, S., Trentesaux, A., 2004. Types of internal structure and external morphology of submarine dunes under the influence of tide- and wind-driven processes (Dover Strait, northern France). Marine Geology 211, 143–168. https://doi.org/10.1016/j.margeo.2004.07.002.

Le Hir, P., Cayocca, F., Waeles, B., 2011. Dynamics of sand and mud mixtures: A multiprocess-based modelling strategy. Continental Shelf Research 31, 135-149.

Le Hir P., Ficht A., Silva Jacinto, R., Lesueur, P., Dupont, J.P., ROBERT Lafite, R., Brenon, S., Thouvenin, B., Cugier, P., 2001. Fine sediment transport and accumulations at the mouth of the Seine estuary (France). Estuaries 24, 950–963.

Lemoine, J.P., Le Hir, P., 2021. Maintenance dredging in a macrotidal estuary: Modelling and assessment of its variability with hydro-meteorological forcing. Estuarine, Coastal and Shelf Science 258, 107366. https://doi.org/10.1016/j.ecss.2021.107366.

Le Roux, J.P., Rojas, E.M., 2007. Sediment transport patterns determined from grain size parameters: Overview and state of the art. Sedimentary Geology 202, 473–488. https://doi.org/10.1016/j.sedgeo.2007.03.014.

Leroux, E., 2012. Quantification des flux sédimentaires et de la subsidence du bassin Provençal, Brest, 456 pp.

Leroux, E., Aslanian, D., Rabineau, M., Moulin, M., Granjeon, D., Gorini, C., Droz, L., 2015. Sedimentary markers in the Provençal Basin (western Mediterranean): a window into deep geodynamic processes. Terra Nova 27, 122–129.

Le Roy, R., Simon, B., 2003. Réalisation et validation d'un modèle de marée en Manche et dans le Golfe de Gascogne(application à la réalisation d'un nouveau programme de réduction des sondages bathymétrique. Rapport technique Rapport n002/03.

Lettley, C.D., Pemberton, S.G., Gingras, M.K., Ranger, M.J., Blakney, B.J., 2005. Integrating sedimentology and ichnology to shed light on the system dynamics and paleogeogrpahy of an ancient riverine estuary. In: MacEachern, J.A., Bann, K.L., Gingras, M.K., Pemberton, S.G. (Eds.) Applied ichnology, pp. 144–162.

Leuven, J., Kleinhans, M.G., Weisscher, S., van der Vegt, M., 2016. Tidal sand bar dimensions and shapes in estuaries. Earth-Science Reviews 161, 204–223. https://doi.org/10.1016/j.earscirev.2016.08.004.

Lazure, P., Dumas, F., 2008. An external–internal mode coupling for a 3D hydrodynamical model for applications at regional scale (MARS). Advances in Water Resources 31, 233–250. https://doi.org/10.1016/j.advwatres.2007.06.010.

Le Hir, P., Cayocca, F., Waeles, B., 2011. Dynamics of sand and mud mixtures: A multiprocess-based modelling strategy. Continental Shelf Research 31, 135-149. https://doi.org/10.1016/j.csr.2010.12.009.

Le Hir P., Ficht A., Silva Jacinto, R., Lesueur, P., Dupont, J.P., Lafite, R., Brenon, S., Thouvenin, B., Cugier, P., 2001. Fine sediment transport and accumulations at the mouth of the Seine estuary (France). Estuaries 24, 950–963.

Le Roy, R., Simon, B., 2003. Réalisation et validation d'un modèle de marée en Manche et dans le Golfe de Gascogne(application à la réalisation d'un nouveau programme de réduction des sondages bathymétrique. Rapport technique Rapport n002/03.

Le Tu, X., Thanh, V.Q., Reyns, J., Van, S.P., Anh, D.T., Dang, T.D., Roelvink, D., 2019. Sediment transport and morphodynamical modeling on the estuaries and coastal zone of the Vietnamese Mekong Delta. Continental Shelf Research 186, 64–76. https://doi.org/10.1016/j.csr.2019.07.015.

Lee, B.-R., Yoo, D.-G., Lee, G.-S., 2022. High-resolution sequence stratigraphy and evolution of the Jeju Strait shelf, Korea, since the Last Glacial Maximum. Marine and Petroleum Geology 135, 105389. https://doi.org/10.1016/j.marpetgeo.2021.105389.

M

MacEachern, J.A., Pemberton, S.G., Bann, K.L., Gingras, M.K., 2005. Departures from the archetypal ichnofacies: effective recognition of physico-chemical stresses in the rock record. In: MacEachern, J.A., Bann, K.L., Gingras, M.K., Pemberton, S.G. (Eds.) Applied ichnology, pp. 65–93.

Menard, H.W., 1969. Elevation and subsidence of oceanic crust. Earth and Planetary Science Letters 6, Issue 4, 275–284.

Mengual, B., Hir, P., Cayocca, F., Garlan, T., 2017. Modelling Fine Sediment Dynamics: Towards a Common Erosion Law for Fine Sand, Mud and Mixtures. Water 9, 564. https://doi.org/10.3390/w9080564.

Mengual, B., Le Hir, P., Rivier, A., Caillaud, M., Grasso, F., 2021. Numerical modeling of bedload and suspended load contributions to morphological evolution of the Seine Estuary (France). International Journal of Sediment Research 36, 723–735. https://doi.org/10.1016/j.ijsrc.2020.07.003.

Miller, K., Mountain, G., Wright, J., Browning, J., 2011. A 180-Million-Year Record of Sea Level and Ice Volume Variations from Continental Margin and Deep-Sea Isotopic Records. Oceanog. 24, 40–53. https://doi.org/10.5670/oceanog.2011.26.

Milliman, j.D., Syvitski, j.P.M., 1992. Gemorphic/Tectonic control of sediment discharge to Ocean: The importance of small mountainous rivers The journal of Geology, 525–544.

Mitchell, A.J., Uličný, D., Hampson, G.J., Allison, P.A., Gorman, G.J., Piggott, M.D., Wells, M.R., Pain, C.C., 2010. Modelling tidal current-induced bed shear stress and palaeocirculation in an epicontinental seaway: the Bohemian Cretaceous Basin, Central Europe. Sedimentology 57, 359–388. https://doi.org/10.1111/j.1365-3091.2009.01082.x.

Mojtahid, M., Jorissen, F.J., Garcia, J., Schiebel, R., Michel, E., Eynaud, F., Gillet, H., Cremer, M., Diz Ferreiro, P., Siccha, M., Howa, H., 2013. High resolution Holocene record in the southeastern Bay of Biscay: Global versus regional climate signals. Palaeogeography, Palaeoclimatology, Palaeoecology 377, 28–44. https://doi.org/10.1016/j.palaeo.2013.03.004.

Monbet, Y., Bassoullet, P., 1989. Bilan des connaissances océanographiques en rade de Brest. Rapport CEA/IPSN, code DERO/EL 89-23.

Montereale-Gavazzi, G., Roche, M., Degrendele, K., Lurton, X., Terseleer, N., Baeye, M., Francken, F., van Lancker, V., 2019. Insights into the Short-Term Tidal Variability of Multibeam Backscatter from Field Experiments on Different Seafloor Types. Geosciences 9, 34. https://doi.org/10.3390/geosciences9010034.

Moulin, M., Schnurle, P., Afilhado, A., Gallais, F., Dias, N., Evain, M., Soares, J., Fuck, R., Da Cruz Pessoa Neto, O., Viana, A., Aslanian, D., 2021. Imaging Early Oceanic Crust spreading in the Equatorial Atlantic Ocean: Insights from the MAGIC wide-angle experiment. Journal of South American Earth Sciences 111, 103493.

Murakoshi, N., Nakayama, N., Masuda, F., 1995. Diurnal inequality pattern of the tide in the upper Pleistocene Palaeo-Tokyo Bay: reconstruction from tidal deposits and growth-lines of fossil bivalves. Int Assoc Sediment Spec Publ 24, 289–300.

N

Nielsen, P., 1992. Coastal bottom boundary layers and sediment transport. Advanced series on Ocean Engineering. World Scientific.

O

Olariu, C., Steel, R.J., Dalrymple, R.W., Gingras, M.K., 2012. Tidal dunes versus tidal bars: The sedimentological and architectural characteristics of compound dunes in a tidal seaway, the lower Baronia Sandstone (Lower Eocene), Ager Basin, Spain. Sedimentary Geology 279, 134–155. https://doi.org/10.1016/j.sedgeo.2012.07.018.

Olivier, M.G., Leroux, E., Rabineau, M., Le Hir, P., Granjeon, D., Chataigner, T., Beudin, A., Muller, H., 2021. Numerical modelling of a Macrotidal Bay over the last 9,000 years: An interdisciplinary methodology to understand the influence of sea-level variations on tidal currents in the Bay of Brest. Continental Shelf Research 231, 104595. https://doi.org/10.1016/j.csr.2021.104595.

Ouahsine, A., Smaoui, H., Meftah, K., Sergent, P., Sabatier, F., 2013. Numerical study of coastal sandbar migration, by hydro-morphodynamical coupling. Environ Fluid Mech 13, 169–187. https://doi.org/10.1007/s10652-012-9252-5.

P

Palacio, C., Mayerle, R., Toro, M., Jimenez, N., 2005. Modelling of Flow in a Tidal Flat Area in the South-Eastern German Bight. Die Küste 69, 141–174.

Pasquaud, S., Vasconcelos, R.P., França, S., Henriques, S., Costa, M.J., Cabral, H., 2015. Worldwide patterns of fish biodiversity in estuaries: Effect of global vs. local factors. Estuarine, Coastal and Shelf Science 154, 122–128. https://doi.org/10.1016/j.ecss.2014.12.050.

Penaud, A., Ganne, A., Eynaud, F., Lambert, C., Coste, P.O., Herlédan, M., Vidal, M., Goslin, J., Stéphan, P., Charria, G., Pailler, Y., Durand, M., Zumaque, J., Mojtahid, M., 2020. Oceanic versus continental influences over the last 7 kyrs from a mid-shelf record in the northern Bay of Biscay (NE Atlantic). Quaternary Science Reviews 229, 106135. https://doi.org/10.1016/j.quascirev.2019.106135.

Petit-Maire, N., 1999. Natural variability of the Earth's environments: the last two climatic extremes (18 000 +/- 2 000 and 8 000 +/- 1 000 yrs BP). Sciences de la terre et des plantes / Earth & Planetary Sciences, 328-273.

Petton, S., Le Berre, D., Haurie, A., Pouvreau, S., 2016. HOMER Campaign : Mooring time series.

Petton, S., Le Roy, V., Bellec, G., Queau, I., Le Souchu, P., Pouvreau, S., 2021. Marine environmental station database of Daoulas bay.

Petton, S., Pouvreau, S., Dumas, F., 2020. Intensive use of Lagrangian trajectories to quantify coastal area dispersion. Ocean Dynamics 70, 541–559. https://doi.org/10.1007/s10236-019-01343-6.

Posamentier, H.W., Allen, G.P., 1993. Variability of the sequence stratigraphic model: effects of local basin factors. Sedimentary Geology 86, 91–109. https://doi.org/10.1016/0037-0738(93)90135-R.

Price, T.D., Ruessink, B.G., 2013. Observations and conceptual modelling of morphological coupling in a double sandbar system. Earth Surf. Process. Landforms 38, 477–489. https://doi.org/10.1002/esp.3293.

R

Rabineau, M., 2001. Un modele géometrique et stratigraphique des séquences de depôts quaternaires sur la marge du golfe du lion : enregistrement des cycles climatiques de 100 000 ans, Rennes, 394 pp.

Ray, R.D., Cartwright, D.E., 2007. Times of peak astronomical tides. Geophysical Journal International 168, 999–1004. https://doi.org/10.1111/j.1365-246X.2006.03293.x.

Reineck, H.-E., Wunderlich, F., 1968. Classification and origin of flaser and lenticular bedding. Sedimentology 11, 99–104. https://doi.org/10.1111/j.1365-3091.1968.tb00843.x.

Reynaud, J.-Y., Dalrymple, R.W., 2012. Shallow-Marine Tidal Deposits. In: Davis, R.A., Dalrymple, R.W. (Eds.) Principles of Tidal Sedimentology, vol. 13. Springer Science+Business Media B.V., Dordrecht, pp. 335–369.

Reynaud, J.-Y., Dalrymple, R.W., Vennin, E., Parize, O., Besson, D., Rubino, J.-L., 2006. Topographic Controls on Production and Deposition of Tidal Cool-Water Carbonates, Uzes Basin, SE France. Journal of Sedimentary Research 76, 117–130. https://doi.org/10.2110/jsr.2006.07.

Reynaud, J.-Y., James, N.P., 2012. The Miocene Sommières basin, SE France: Bioclastic carbonates in a tide-dominated depositional system. Sedimentary Geology 282, 360–373. https://doi.org/10.1016/j.sedgeo.2012.10.006.

Roberts, D.G., 2012. Regional geology and tectonics: Principles of geologic analysis. Elsevier Science & Technology Books, Amsterdam, Nederlands.

Roelvink, J.A., 2006. Coastal morphodynamic evolution techniques. Coastal Engineering 53, 277–287.

S

Seppä, H., Birks, H., 2001. July mean temperature and annual precipitation trends during the Holocene in the ennoscandian tree-line area: pollen-based climate reconstructions. The Holocene 11,5, 527–539.

Seton, M., Müller, R.D., Zahirovic, S., Gaina, C., Torsvik, T., Shephard, G., Talsma, A., Gurnis, M., Turner, M., Maus, S., Chandler, M., 2012. Global continental and ocean basin reconstructions since 200Ma. Earth-Science Reviews 113, 212–270. https://doi.org/10.1016/j.earscirev.2012.03.002.

Shanmugam, G., Shrivastava, S.K., Das, B., 2009. Sandy Debrites and Tidalites of Pliocene Reservoir Sands in Upper-Slope Canyon Environments, Offshore Krishna-Godavari Basin (India): Implications. Journal of Sedimentary Research 79, 736–756. https://doi.org/10.2110/jsr.2009.076.

Shaw, J., Todd, B.J., Li, M.Z., 2014. Geologic insights from multibeam bathymetry and seascape maps of the Bay of Fundy, Canada. Continental Shelf Research 83, 53–63. https://doi.org/10.1016/j.csr.2013.12.015.

Shields, A., 1936. Application of similarity principles and turbulence research to bed-load movement. Hydrodynamics Laboratory, California Institute of Technology 167, 43.

SHOM, Service Hydrographique Et Océanographique De La Marine., 2015a. Marnages sur les côtes françaises de La Manche et de l'Atlantique pour le coefficient 120.

SHOM, Service Hydrographique Et Océanographique De La Marine., 2015b. MNT Bathymétrique de façade Atlantique (Projet Homonim).

Siegle, E., Huntley, D.A., Davidson, M.A., 2004. Physical controls on the dynamics of inlet sandbar systems. Ocean Dynamics 54.

Simon, B., 2007. La marée océanique côtière. Institut océanographique, Paris, 433 pp.

Skogseid, J., Planke, S., Faleide, J.I., Pedersen, T., Eldholm, O., Neverdal, F., 2000. NE Atlantic continental rifting and volcanic margin formation. Geological Society of London, Special Publication, 295–326.

Smith, A.C., Wynn, P.M., Barker, P.A., Leng, M.J., Noble, S.R., Tych, W., 2016. North Atlantic forcing of moisture delivery to Europe throughout the Holocene. Scientific reports 6, 24745. https://doi.org/10.1038/srep24745.

Sømme, T.O., Helland-Hansen, W., Martinsen, O.J., Thurmond, J.B., 2009. Relationships between morphological and sedimentological parameters in source-to-sink systems: a basis for predicting semi-quantitative characteristics in subsurface systems. Basin Research 21, 361–387. https://doi.org/10.1111/j.1365-2117.2009.00397.x.

Soulsby, R., 1997. Dynamics of marine sands. Thomas Telford Publications, 249p.

Storms, J.E.A., Swift, D.J.P., 2003. Shallow-marine sequences as the building blocks of stratigraphy: insights from numerical modelling. Basin Research 15, 287–303. https://doi.org/10.1046/j.1365-2117.2003.00207.x.

Stéphan, P., Fichaut, B., Suanez, S., 2012. Les sillons de la rade de Brest et les marais maritimes associés. FRAC GPN, 137 pp.

Straume, E.O., Gaina, C., Medvedev, S., Hochmuth, K., Gohl, K., Whittaker, J.M., 2019. GlobSed: Updated total sediment thickness in the world's oceans. Geochemistry, Geophysics, Geosystems, 20.

T

Tessier, B., 1993. Upper intertidal rhythmites in the Mont-Saint-Michel Bay (NW France): Perspectives for paleoreconstruction. Marine Geology 110, 355–367. https://doi.org/10.1016/0025-3227(93)90093-B.

Tessier, B., 2012. Stratigraphy of Tide-Dominated Estuaries. In: Davis, R.A., Dalrymple, R.W. (Eds.) Principles of Tidal Sedimentology. Springer Science+Business Media B.V., Dordrecht.

Tessier, B., Billeaud, I., Sorrel, P., Delsinne, N., Lesueur, P., 2012. Infilling stratigraphy of macrotidal tide-dominated estuaries. Controlling mechanisms: Sea-level fluctuations, bedrock morphology, sediment supply and climate changes (The examples of the Seine estuary and the Mont-Saint-Michel Bay, English Channel, NW France). Sedimentary Geology 279, 62–73. https://doi.org/10.1016/j.sedgeo.2011.02.003.

Todd, B.J., Shaw, J., Li, M.Z., Kostylev, V.E., Wu, Y., 2014. Distribution of subtidal sedimentary bedforms in a macrotidal setting: The Bay of Fundy, Atlantic Canada. Continental Shelf Research 83, 64–85. https://doi.org/10.1016/j.csr.2013.11.017.

Toublanc, F., Brenon, I., Coulombier, T., 2014. Modélisation 3D de la dynamique des sédiments fins dans l'estuaire de la Charente (France) : évolution du bouchon vaseux et estimation des flux sédimentaires. XIIIèmes Journées Nationales Génie Côtier – Génie Civil, 513–522. https://doi.org/10.5150/jngcgc.2014.056.

Tosic, M., Martins, F., Lonin, S., Izquierdo, A., Restrepo, J.D., 2019. Hydrodynamic modelling of a polluted tropical bay: Assessment of anthropogenic impacts on freshwater runoff and estuarine water renewal. Journal of environmental management 236, 695–714. https://doi.org/10.1016/j.jenvman.2019.01.104.

Trentesaux, A., Stolk, A., Tessier, B., Chamleya, H., 1994. Surficial sedimentology of the Middelkerke Bank (southern North Sea). Marine Geology 121, 43–55.

Troadec, P., Le Goff, P., 1997. Etat des lieux et des milieux de la rade de Brest et de son bassin versant.

Tu, L.X., Thanh, V.Q., Reyns, J., Van, S.P., Anh, D.T., Dang, T.D., Roelvink, D., 2019. Sediment transport and morphodynamical modeling on the estuaries and coastal zone of the Vietnamese Mekong Delta. Continental Shelf Research 186, 64–76. https://doi.org/10.1016/j.csr.2019.07.015.

U

Uehara, K., Saito, Y., 2019. Tidal amplitude decreases in response to estuarine shrinkage: Tokyo Bay during the Holocene. Estuarine, Coastal and Shelf Science 225, 106225. https://doi.org/10.1016/j.ecss.2019.05.007.

Uehara, K., Saito, Y., Hori, K., 2002. Paleotidal regime in the Changjiang (Yangtze) Estuary, the East China Sea, and the Yellow Sea at 6 ka and 10 ka estimated from a numerical model. Marine Geology 183, 179–192.

Uehara, K., Scourse, J.D., Horsburgh, K.J., Lambeck, K., Purcell, A.P., 2006. Tidal evolution of the northwest European shelf seas from the Last Glacial Maximum to the present. J. Geophys. Res. 111. https://doi.org/10.1029/2006JC003531.

V

van de Lageweg, W.I., Feldman, H., 2018. Process-based modelling of morphodynamics and bar architecture in confined basins with fluvial and tidal currents. Marine Geology 398, 35–47. https://doi.org/10.1016/j.margeo.2018.01.002.

van Rijn, L., 1994. Sediment Transport, Part I: Bed Load Transport. J. Hydraul. Eng. 110(10), 1431–1456.

van Santen, R.B., Swart, H.E. de, van Dijk, T., 2011. Sensitivity of tidal sand wavelength to environmental parameters: A combined data analysis and modelling approach. Continental Shelf Research 31, 966–978. https://doi.org/10.1016/j.csr.2011.03.003.

van Vliet-Lanoë, B., Penaud, A., Hénaff, A., Delacourt, C., Fernane, A., Goslin, J., Hallégouët, B., Le Cornec, E., 2014. Middle- to late-Holocene storminess in Brittany (NW France): Part II – The chronology of events and climate forcing. The Holocene 24, 434–453. https://doi.org/10.1177/0959683613519688.

Verney, R., Lafite, R., Claude Brun-Cottan, J., Le Hir, P., 2011. Behaviour of a floc population during a tidal cycle: Laboratory experiments and numerical modelling. Continental Shelf Research 31, S64-S83. https://doi.org/10.1016/j.csr.2010.02.005.

Vilasi, N., Malandain, J., Barrier, L., Callot, J.-P., Amrouch, K., Guilhaumou, N., Lacombe, O., Muska, K., Roure, F., Swennen, R., 2009. From outcrop and petrographic studies to basin-scale fluid flow modelling: The use of the Albanian natural laboratory for carbonate reservoir characterisation. Tectonophysics 474, 367–392. https://doi.org/10.1016/j.tecto.2009.01.033.

Visser, R., 2002. Morphological modelling in the vicinity of groynes, an extended application in Delft3D-RAM including tidal impact, 129 pp.

W

Waeles, B., 2005. Modelisation morphodynamique de l'embouchure de la seine., Caen, 230 pp.

Wallis J., 1966. Hypoyhesis on the fux and refux of the sea. Phil. Trans. R. Soc. London, 263-289, 297-298.

Wang, P., 2012. Principles of Sediment Transport Applicable in Tidal Environments. In: Davis, R.A., Dalrymple, R.W. (Eds.) Principles of Tidal Sedimentology. Springer Science+Business Media B.V., Dordrecht.

Wang, S., Ge, J., Kilbourne, K.H., Wang, Z., 2020. Numerical simulation of mid-Holocene tidal regime and storm-tide inundation in the south Yangtze coastal plain, East China. Marine Geology 423, 106134. https://doi.org/10.1016/j.margeo.2020.106134.

Ward, S.L., Neill, S.P., Scourse, J.D., Bradley, S.L., Uehara, K., 2016. Sensitivity of palaeotidal models of the northwest European shelf seas to glacial isostatic adjustment since the Last Glacial Maximum. Quaternary Science Reviews 151, 198–211. https://doi.org/10.1016/j.quascirev.2016.08.034.

Webb, B.M., Marr, C., 2016. Spatial Variability of Hydrodynamic Timescales in a Broad and Shallow Estuary: Mobile Bay, Alabama. Journal of Coastal Research 32, 1374. https://doi.org/10.2112/JCOASTRES-D-15-00181.1.

Wells, M.R., Allison, P.A., Piggott, M.D., Gorman, G.J., Hampson, G.J., Pain, C.C., Fang, F., 2007a. Numerical Modeling of Tides in the Late Pennsylvanian Midcontinent Seaway of North America with Implications for Hydrography and Sedimentation. Journal of Sedimentary Research 77, 843–865. https://doi.org/10.2110/jsr.2007.075.

Wells, M.R., Allison, P.A., Piggott, M.D., Hampson, G.J., Pain, C.C., Gorman, G.J., 2010. Tidal Modeling of an Ancient Tide-Dominated Seaway, Part 1: Model Validation and Application to Global Early Cretaceous (Aptian) Tides. Journal of Sedimentary Research 80, 393–410. https://doi.org/10.2110/jsr.2010.044.

Wells, M.R., Allison, P.A., Piggott, M.D., Pain, C.C., Hampson, G.J., Dodman, A., 2007b. Investigating tides in the Early Pennsylvanian Seaway of NW Eurasia using the Imperial College Ocean Model. Geological Association of Canada,St. John's, Newfoundland Special paper 48, 363–387.

Wessel, P., W. H. F. Smith, R. Scharroo, J. Luis, and F. Wobbe, 2013. Generic Mapping Tools: Improved Version Released, EOS Trans. AGU, 94(45), 409–410. doi:10.1002/2013EO450001

Winter, C., Da Chiou, M., Riethmüller, R., Ernstsen, V.B., Hebbeln, D., Flemming, B.W., 2006. The concept of "representative tides" in morphodynamic numerical modelling. Geo-Mar Lett 26, 125–132. https://doi.org/10.1007/s00367-006-0031-5.

Woodroff, S., Horton, B., 2005. Holocene sea-level changes in the Indo-Pacific. Journal of Asian earth sciences 25, 29–43.

X

Xu, J.P., Wong, F.L., Kvitek, R., Smith, D.P., Paull, C.K., 2008. Sandwave migration in Monterey Submarine Canyon, Central California. Marine Geology 248, 193–212. https://doi.org/10.1016/j.margeo.2007.11.005.

Y

Z

Zhang, J., Burgess, P.M., Granjeon, D., Steel, R., 2019. Can sediment supply variations create sequences? Insights from stratigraphic forward modelling. Basin Res 31, 274–289. https://doi.org/10.1111/bre.12320.

Zhang, X., Dalrymple, R.W., Lin, C.M., 2017. Facies and stratigraphic architecture of the late Pleistocene to early Holocene tide-dominated paleo-Changjiang (Yangtze River) delta. GSA Bulletin 130, 455–483. https://doi.org/10.1130/B31663.1.

Zuchuat, V., Steel, E., Mulligan, R.P., Collins, D.S., Green, J.M., 2022. Tidal dynamics in palaeo-seas in response to changes in physiography, tidal forcing and bed shear stress. Sedimentology. https://doi.org/10.1111/sed.12975. wfoundland Special paper 48, 363–387.

Annexes

Annexes (chapter 4):

A lot of validation work were already done by several authors (see part 4.3.1). A further validation is carried out. The model outputs are compared with 5 ADCP and the tide gauge of the Brest harbour (Annexe 1). It concerns a case with a spatialized roughness length (Annexe 2) and a uniform roughness length equal to 3.5mm (Annexe 3).

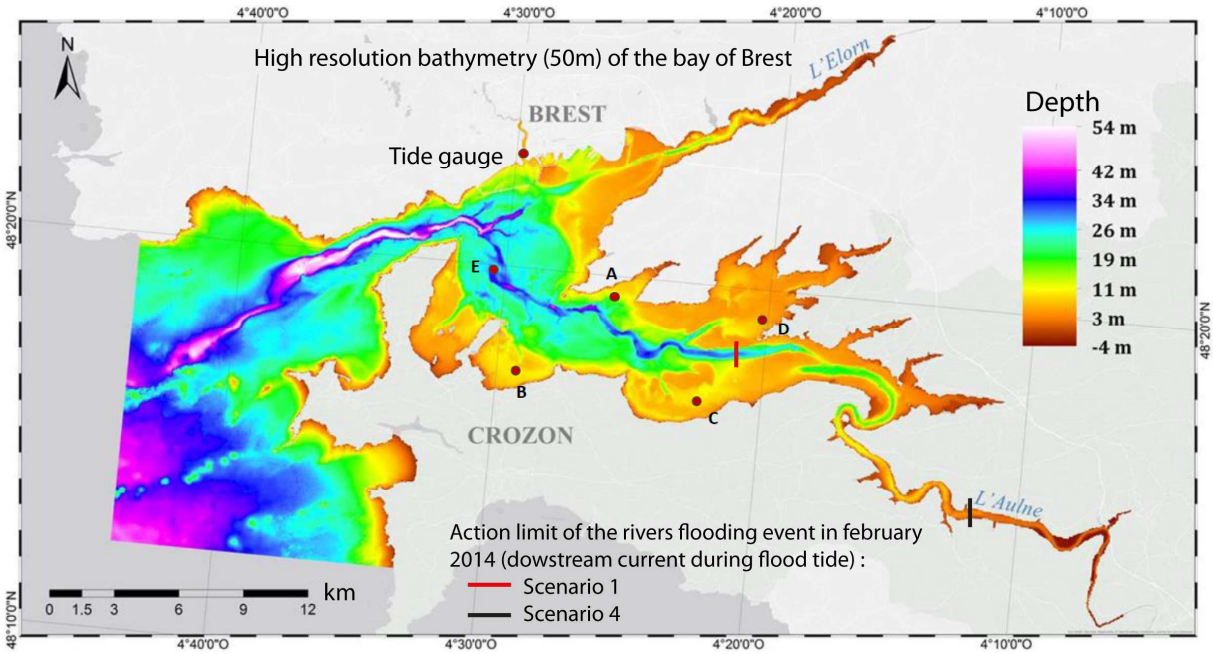

Annexe 1: High resolution bathymetry, with the position of all ADCP and the tidal gauge of Brest harbour. A, B, C, D recorded during 1 month (October 2014, Petton et al., 2016), E during 24 days (16 of July, ENSTA) and the tidal gauge during the entire year 2014. The action limit of one rivers flooding event during a flood of neap tide (February 2014, described in section 4.1) corresponds to black and red line.

Annexe 2: Validation of simulated currents with a spatialized Z0

Localisation	Variable	Percentage correlation (%)	RMSE	Willmott index
Tidal gauge	free surface	99	0,27m	0,93
ADCP A	U barotrope	70,3	0,1	0.47
	V barotrope	-11,2	0,06	0,37
ADCP B	U barotrope	61,7	0,04	0,57
	V barotrope	82,6	0,03	0,64
ADCP C	U barotrope	96,4	0,04	0,87
	V barotrope	75,9	0,02	0,62
ADCP D	U barotrope	96,6	0,05	0,82
	V barotrope	95,4	0,05	0,78
ADCP E	U barotrope	89,6	0,14	0,65
	V barotrope	97,5	0,16	0,74

Annexe 3: Validation of simulated currents with a uniform Z0 (3.5mm)

Localisation	Variable	Percentage correlation (%)	RMSE	Willmott index
ADCP D	U barotrope	95.9	0.05	0.81
	V barotrope	95.1	0.05	0.78
ADCP E	U barotrope	85.7	0.16	0.62
	V barotrope	94.4	0.23	0.67

The compared points reveal very slightly better values for the configuration with a spatialized roughness length. This justifies the simplification of the approach and the use of a uniform roughness length to facilitate comparison with past stages.

M2 and S2 ellipses:

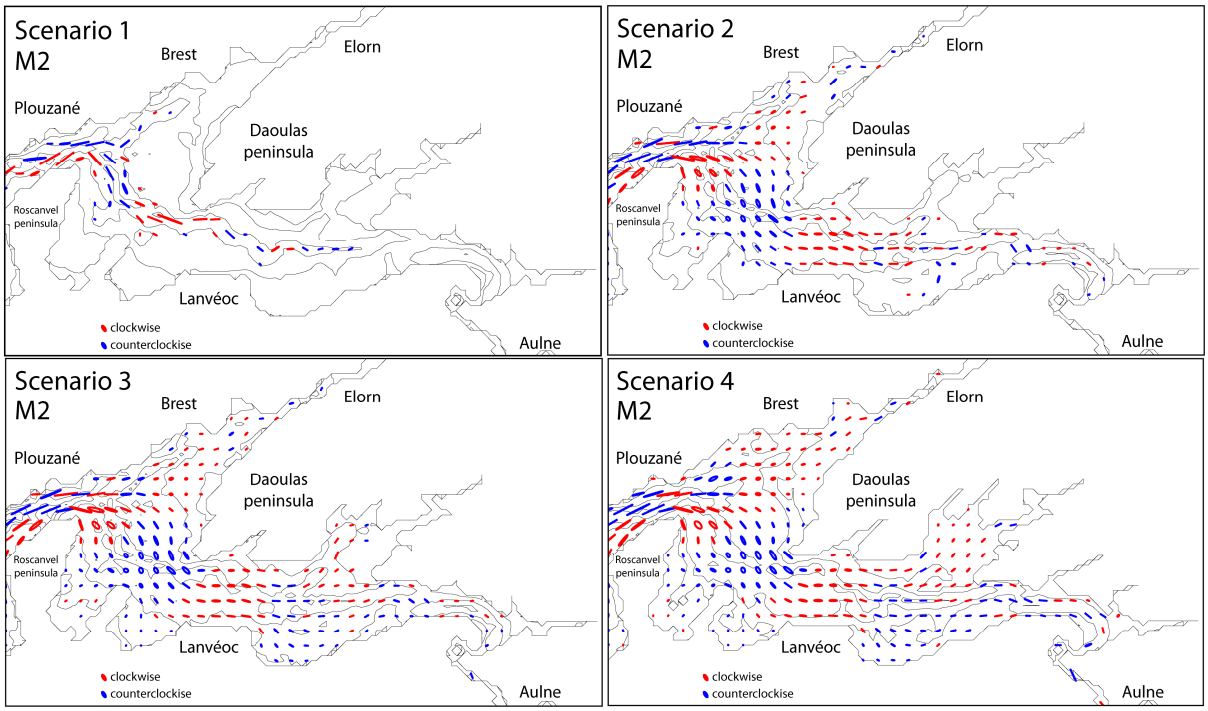

Annexe 4: M2 component ellipses for each scenario, calculated from the barotropic currents U and V.

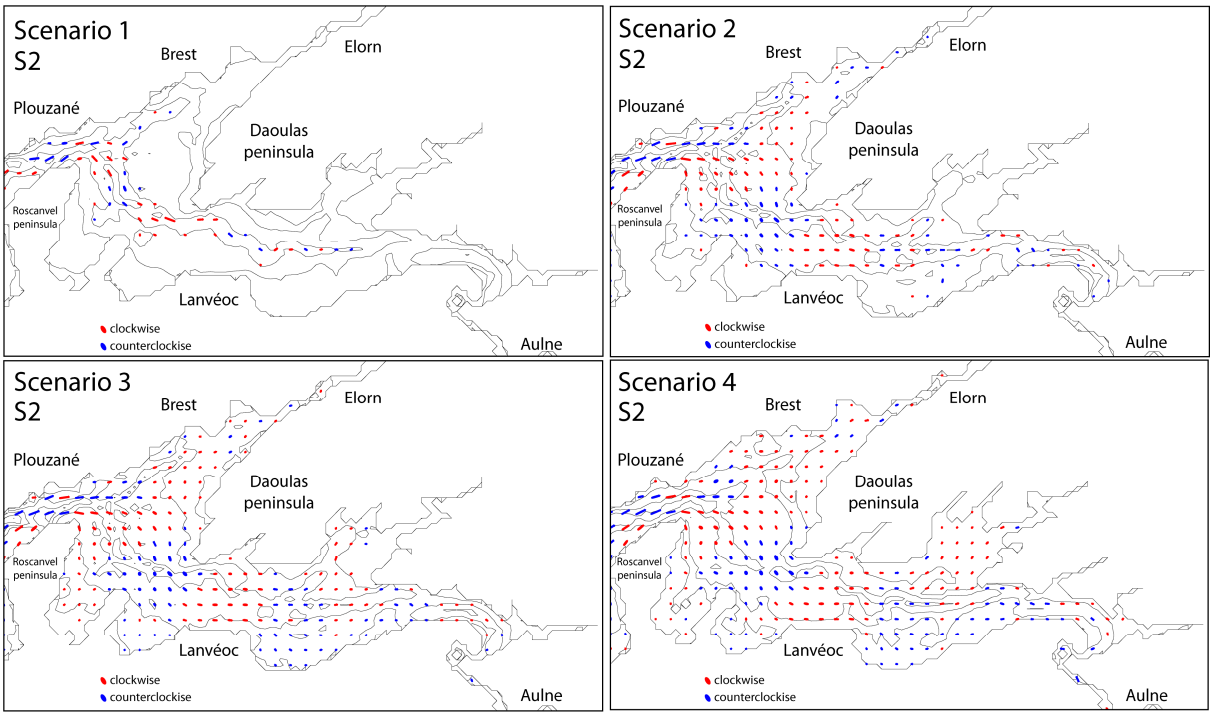

Annexe 5: S2 component ellipses for each scenario, calculated from the barotropic currents U and V.

Annexes (chapter 5):

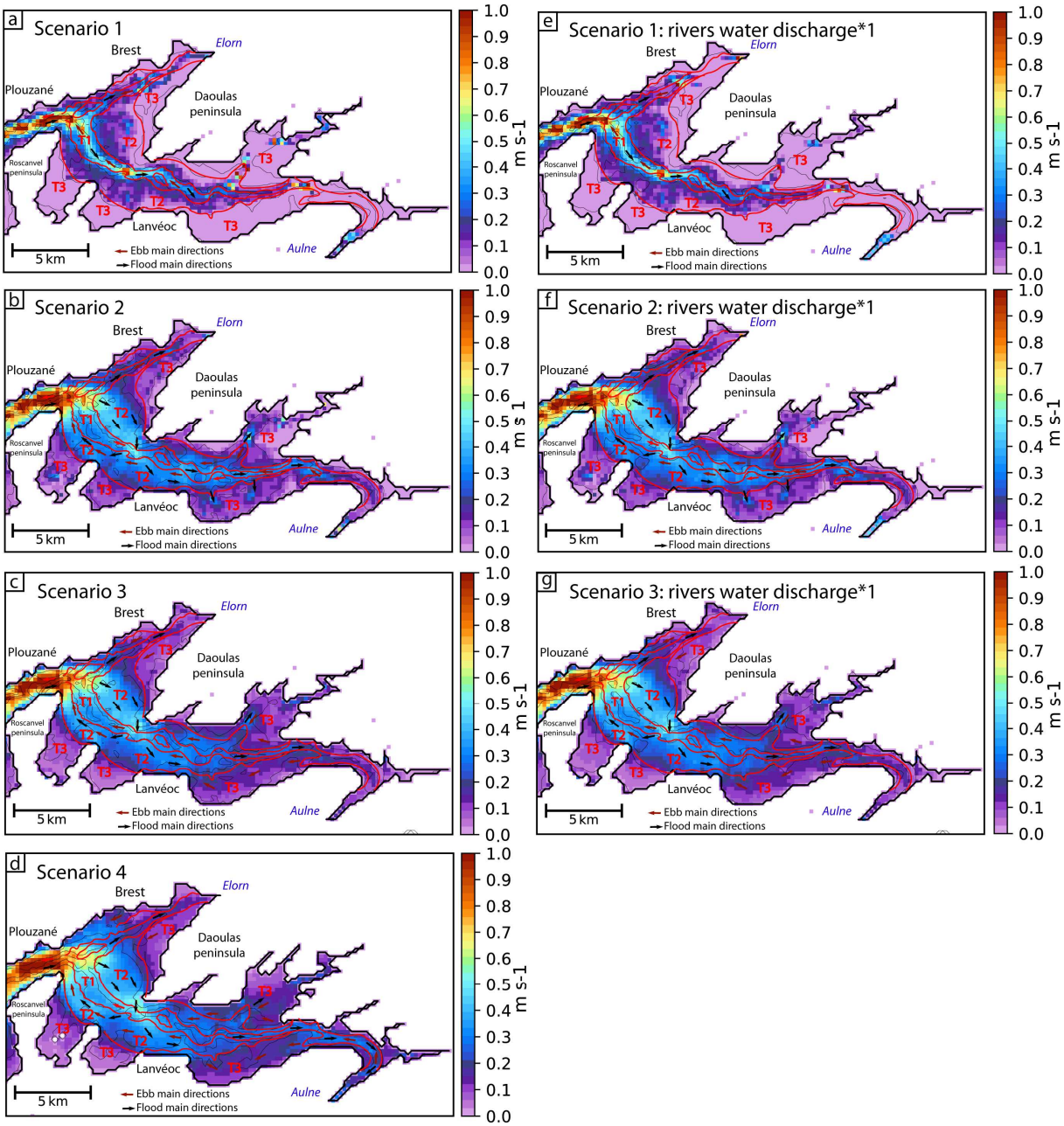

Annexe. 6: Bottom current percentile 90 over one year for a: scenario 1, b: scenario 2, c: scenario 3, d: scenario 4, e: scenario 1 with a water river discharge equal to scenario 4, f: scenario 2 with a water river discharge equal to scenario 4, g: scenario 3 with a water river discharge equal to scenario 4.

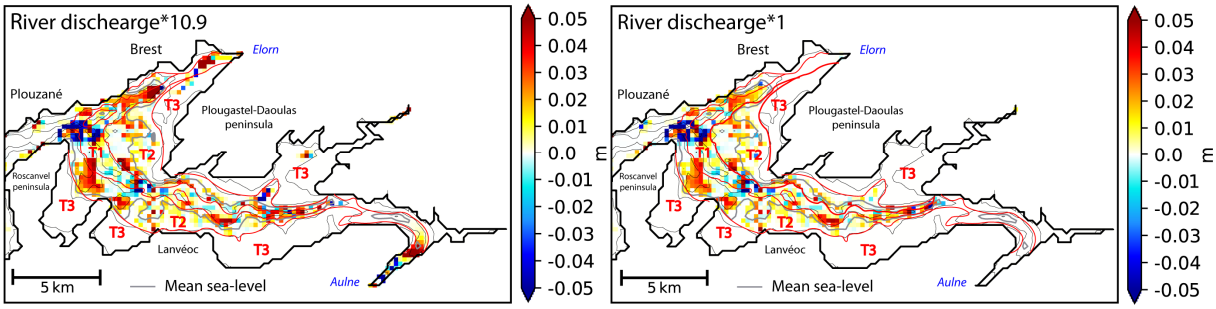

Annexe. 7: On the right, bathymetric evolution after 1 year for scenario 1 (9 ka BP) and on the left bathymetric evolution after 1 year for scenario 1, with a river water discharge equal to scenario 4. Red lines are morphological domain limits (T1, T2 T3) and the black line is the present-day coastline. Grey lines represent the mean sea level (-26 m).

Other annexes

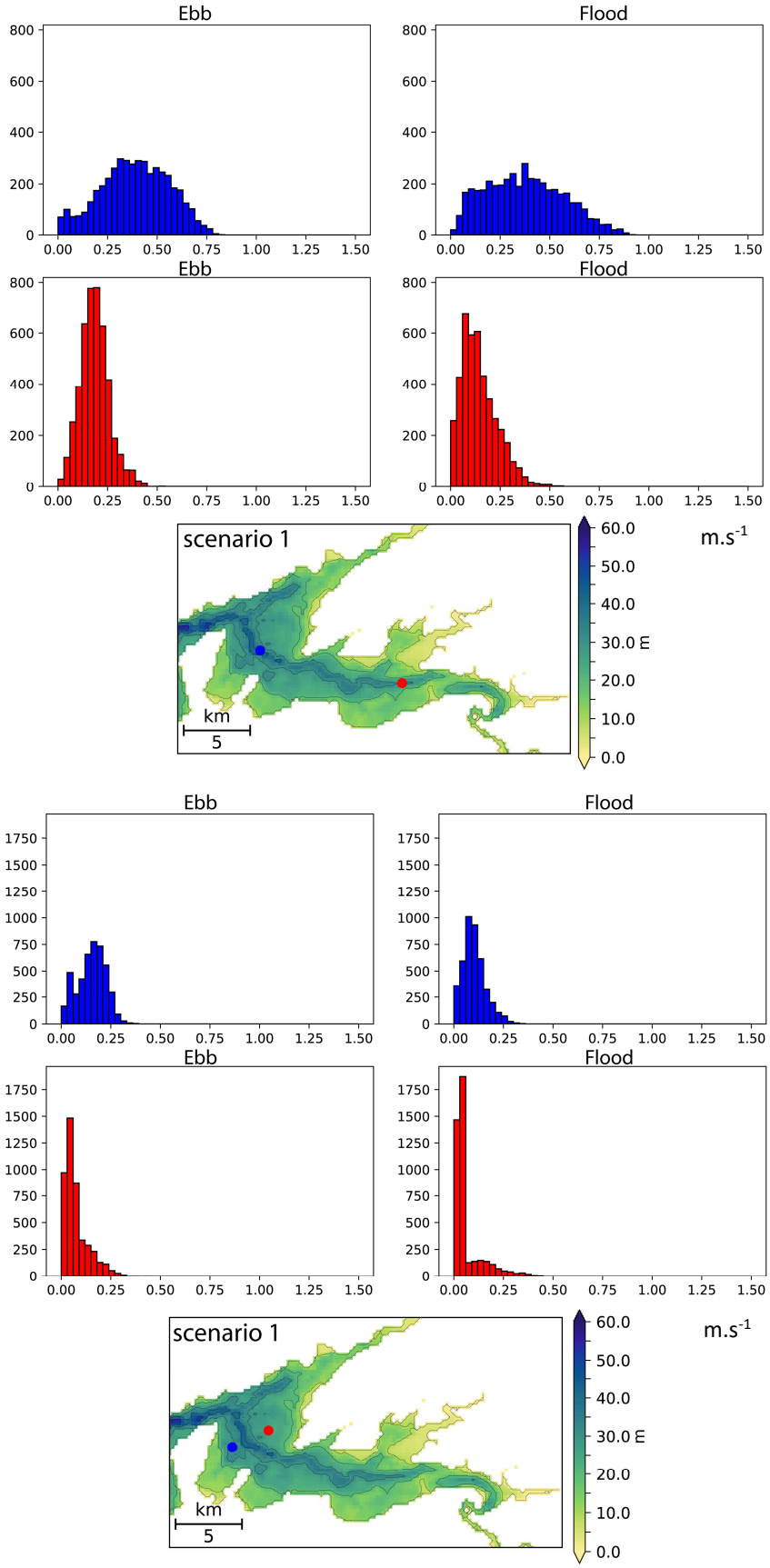

Annexe 8: Distribution of ebb and flood tides currents velocities over 1 year for scenario 1, calculated from simulations of chap. 4. On bottom, bathymetric map displaying sampling locations (red and blue).

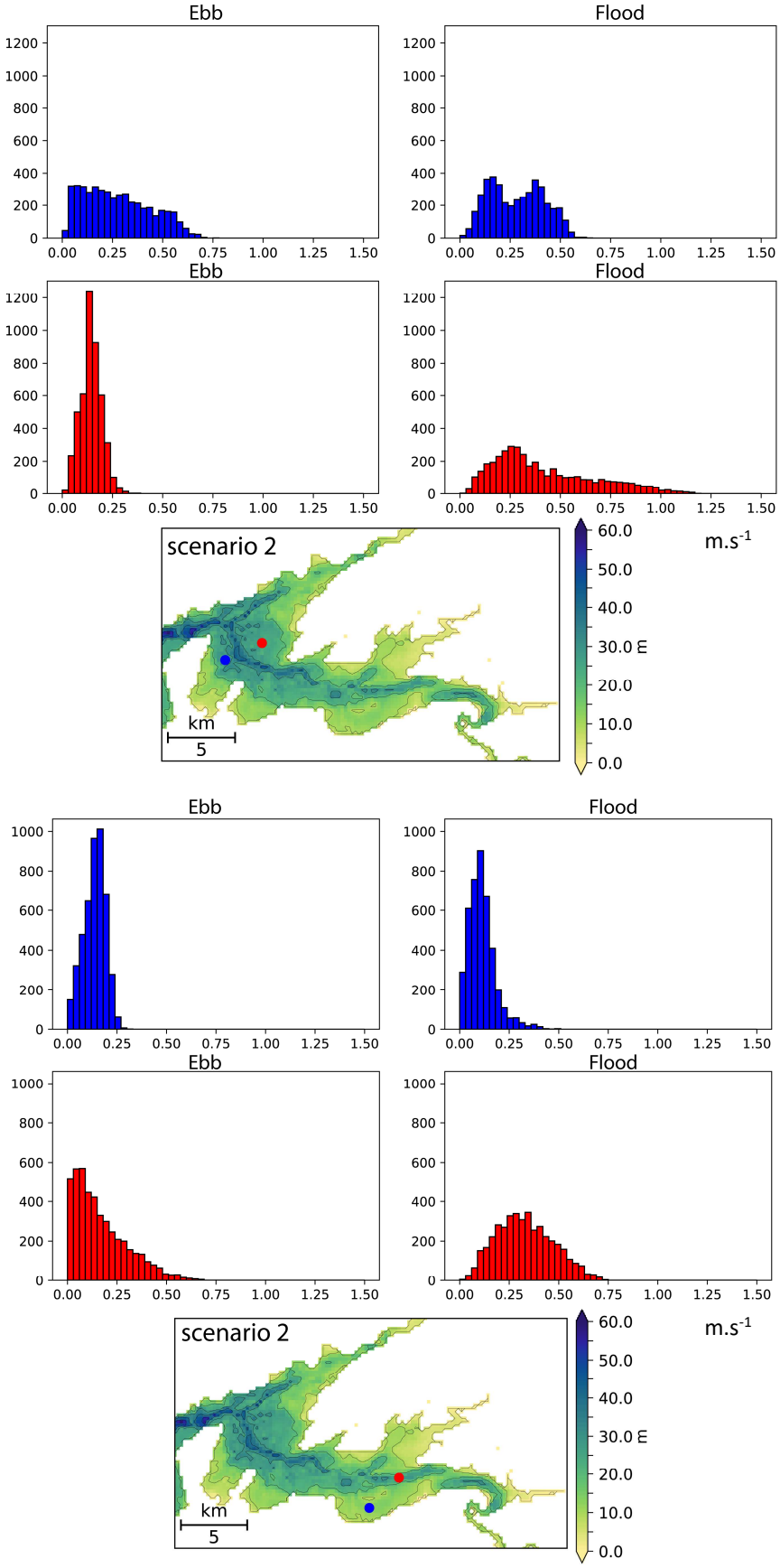

Annexe 9: Distribution of ebb and flood tides currents velocities over 1 year for scenario 2, calculated from simulations of chap. 4. On bottom, bathymetric map displaying sampling locations (red and blue).

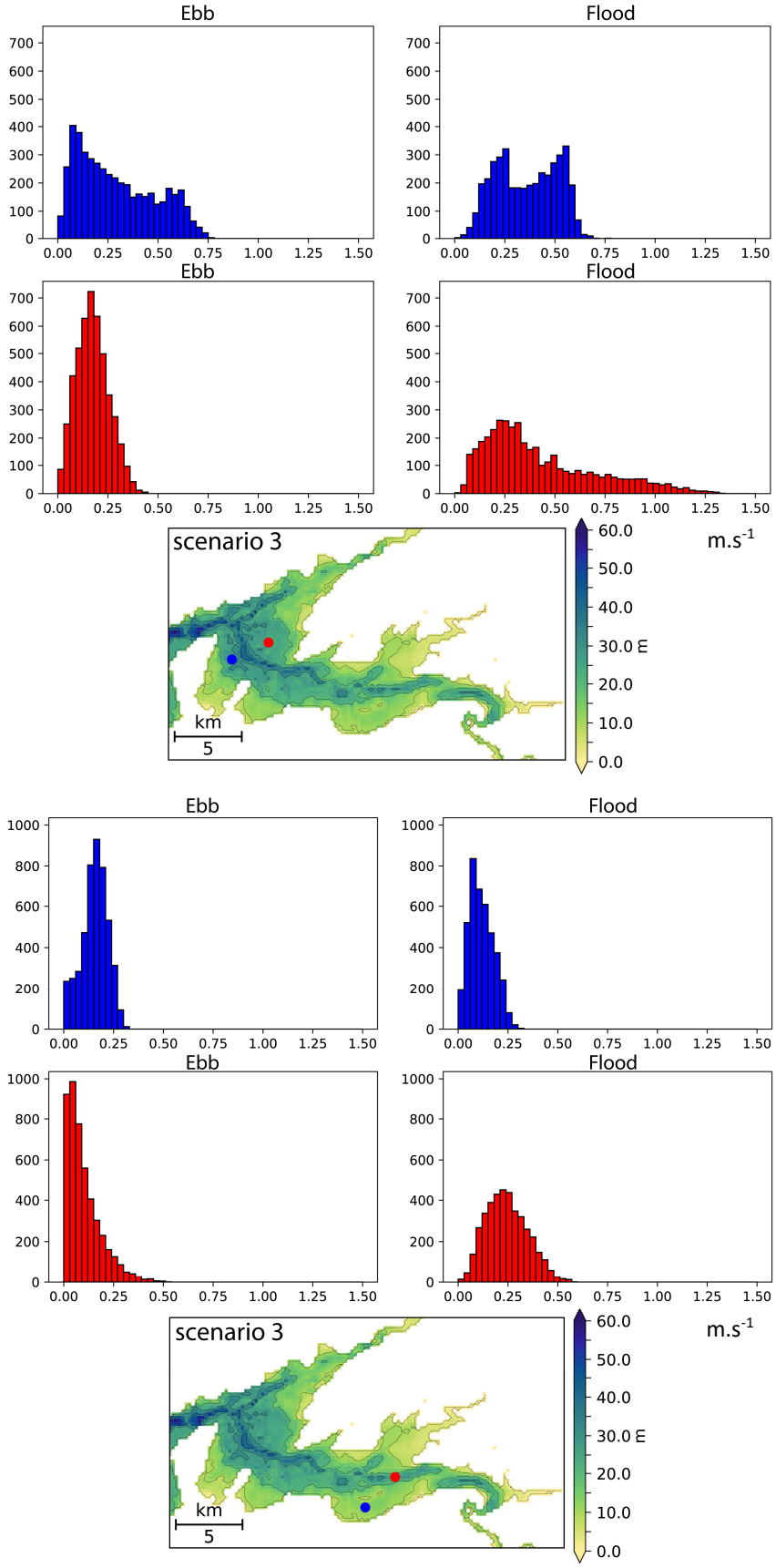

Annexe 10: Distribution of ebb and flood tides currents velocities over 1 year for scenario 2, calculated from simulations of chap. 4. On bottom, bathymetric map displaying sampling locations (red and blue).

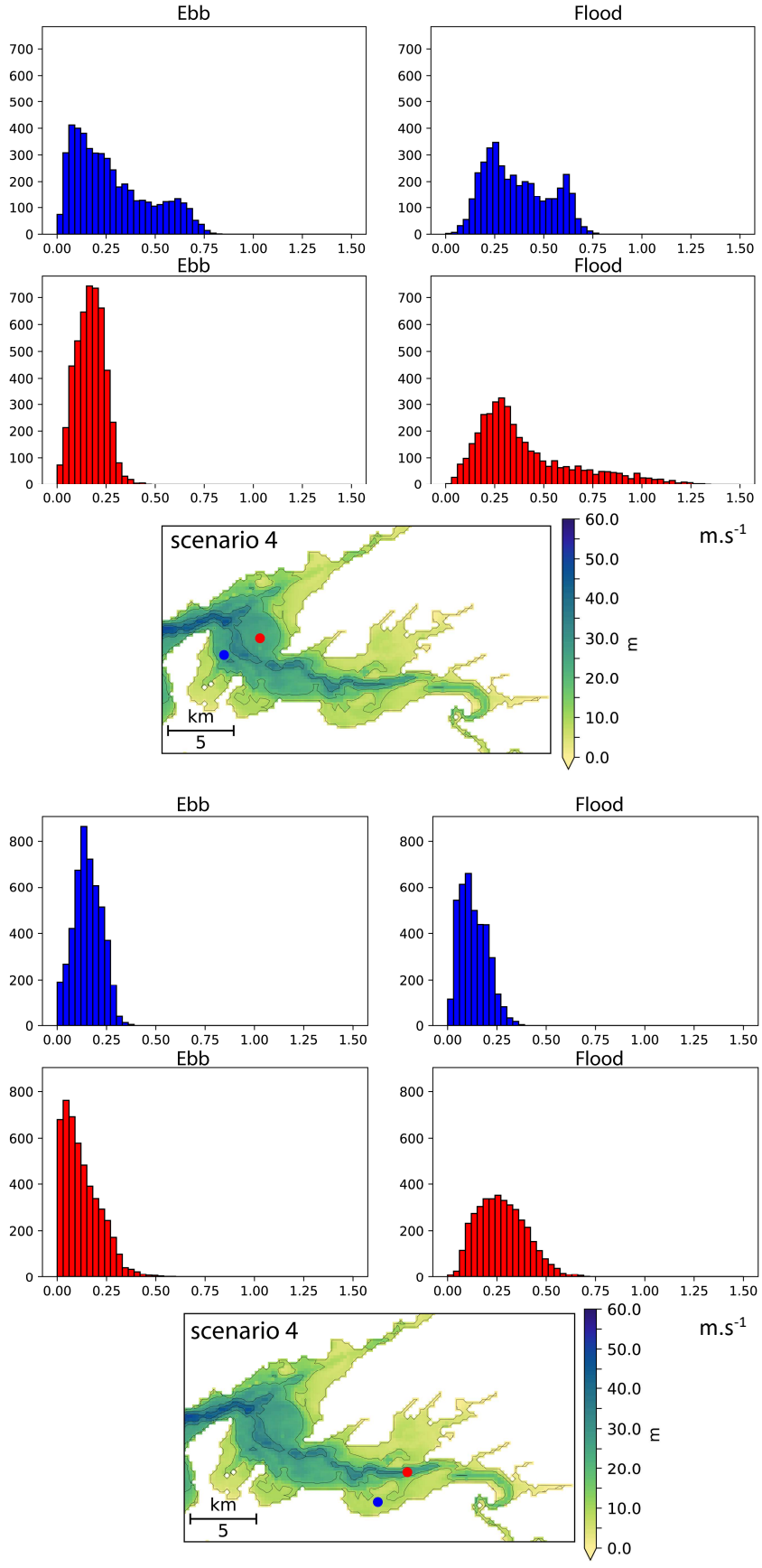

Annexe 11: Distribution of ebb and flood tides currents velocities over 1 year for scenario 2, calculated from simulations of chap. 4. On bottom, bathymetric map displaying sampling locations (red and blue).

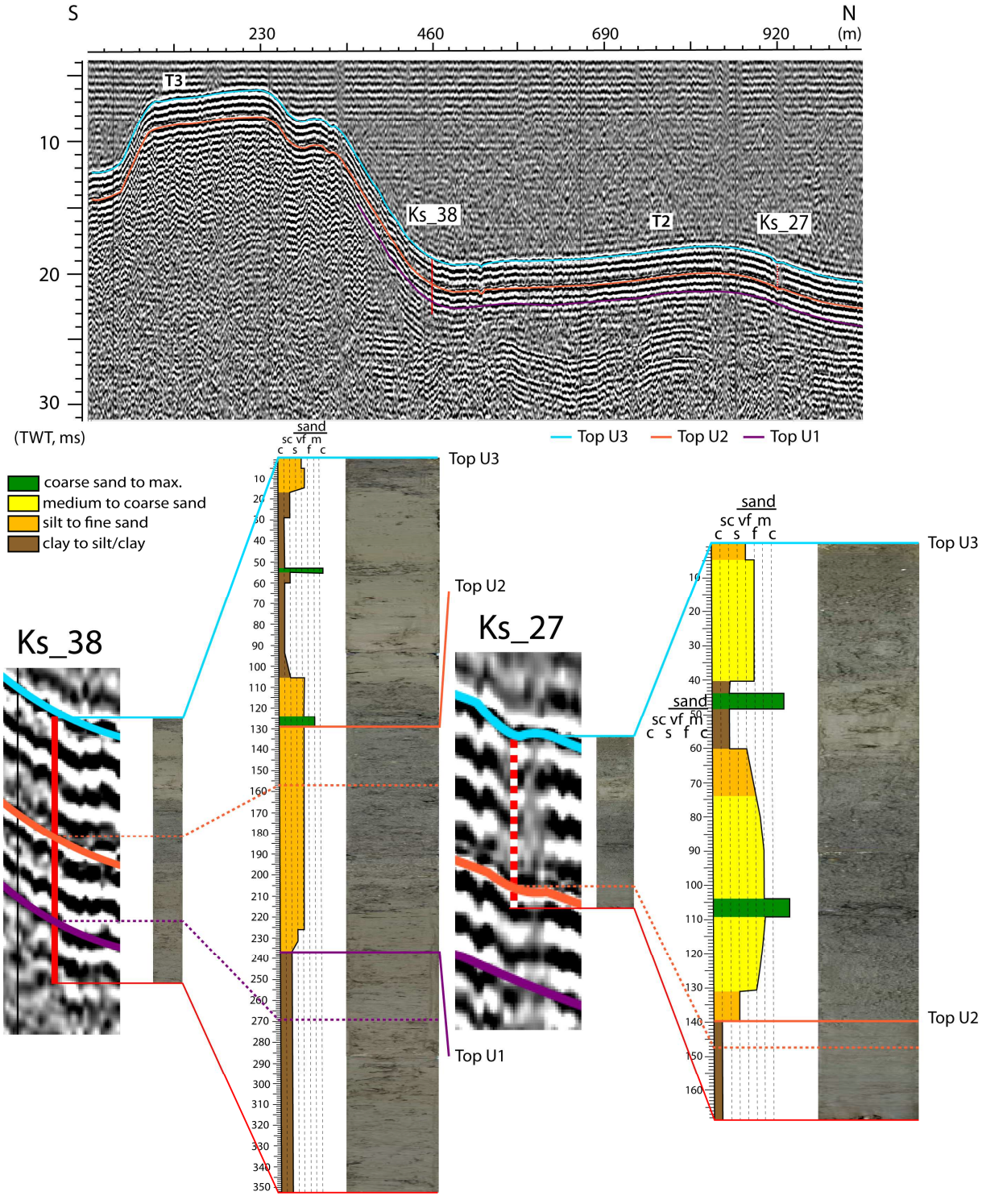

Annexe 12: (top) Interpreted seismic profile. (bottom) Photographs and lithologic log for cores Ks_38 and Ks_27. Dashed purple and orange lines are markers from seismic interpretation and full purple and orange lines represent the interpreted top of U1 and U2 (made to compensate the difference of resolution between cores and seismic profile).

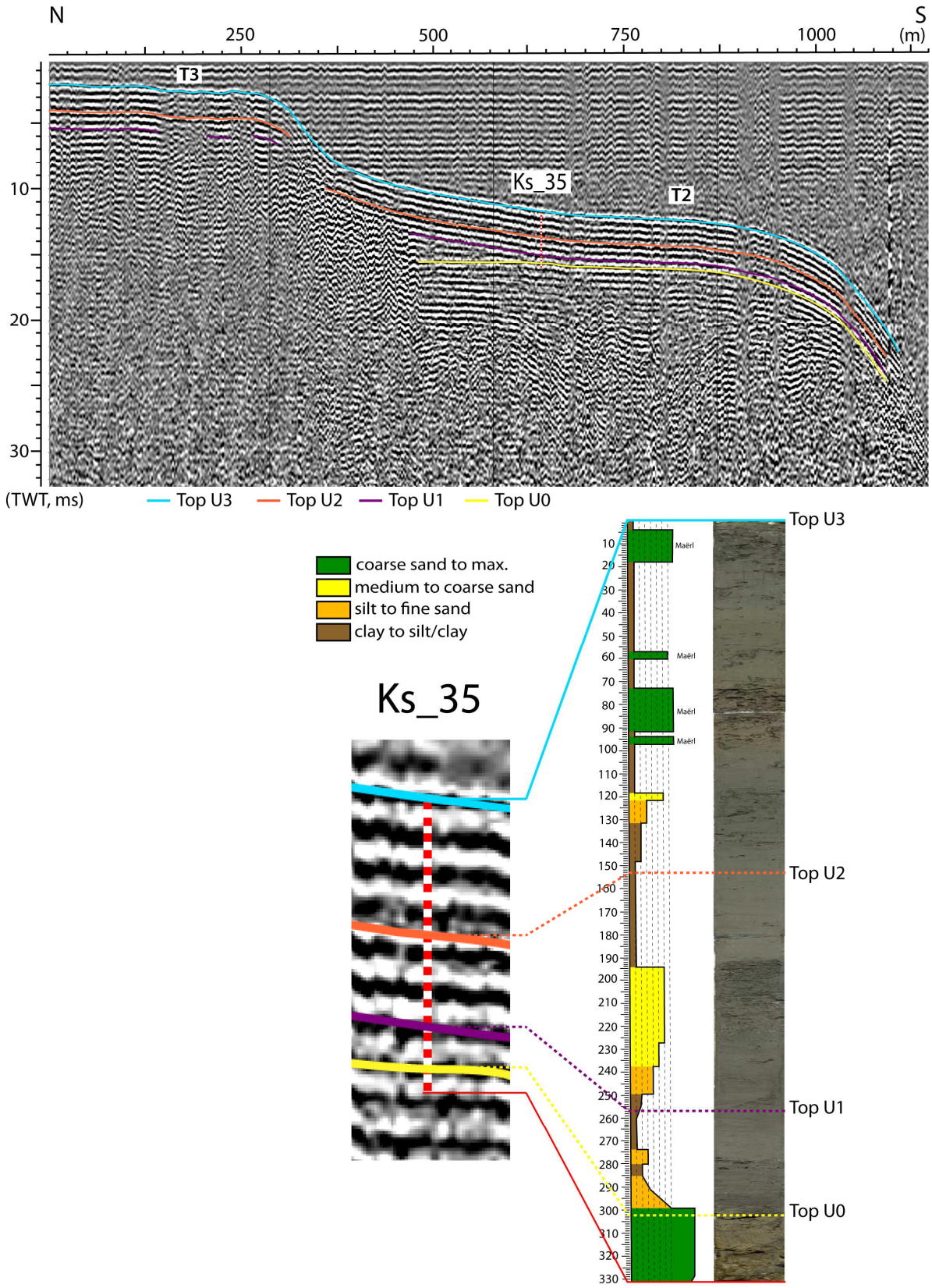

Annexe. 13: (top) Interpreted seismic profile. (bottom) Photograph and lithologic log for core Ks_35. Maël: only bioconstructions of Maërls.

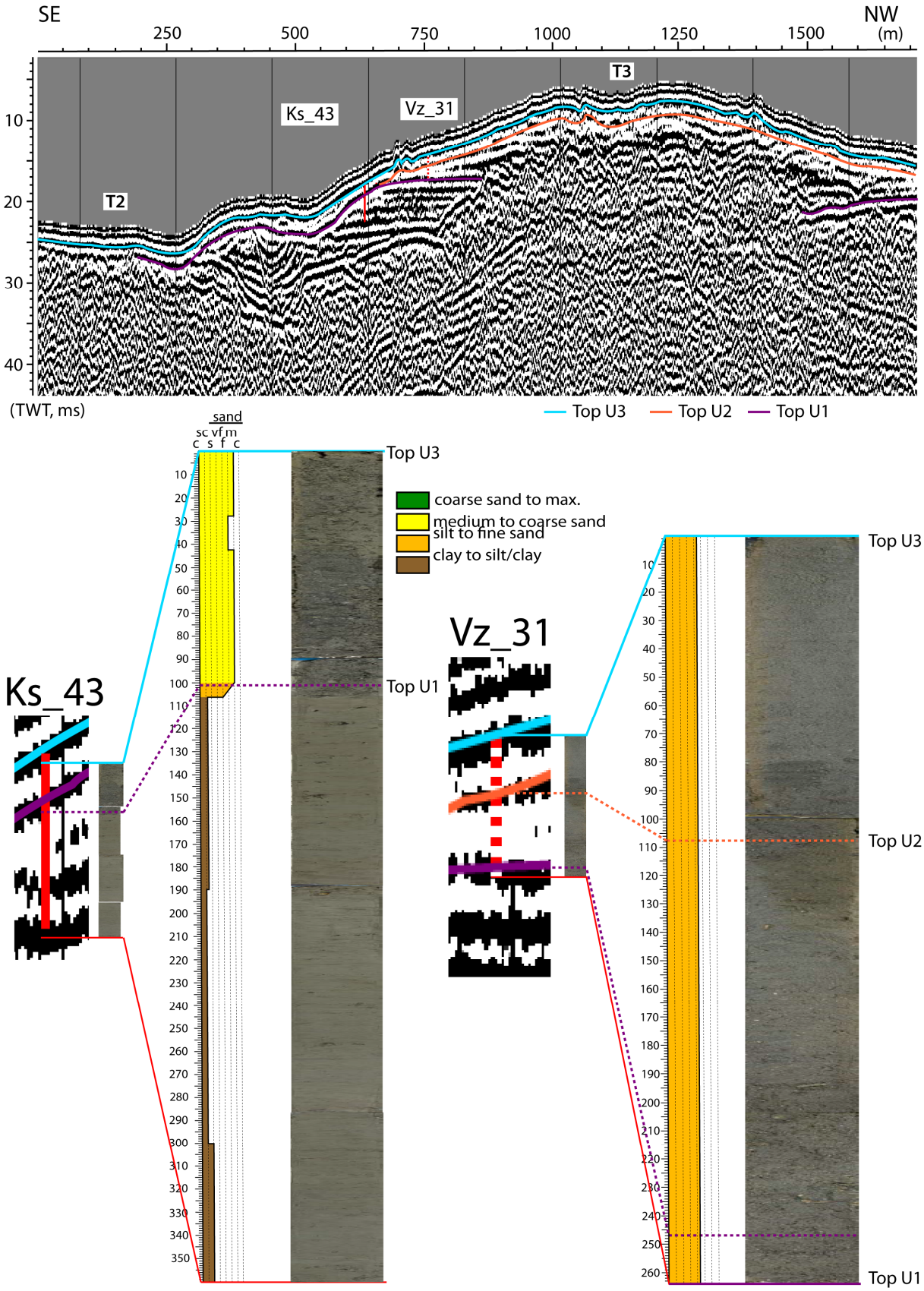

Annexe. 14: (top) Interpreted seismic profile. (bottom) Photographs and lithologic log for cores Ks_43 and Vz_31.

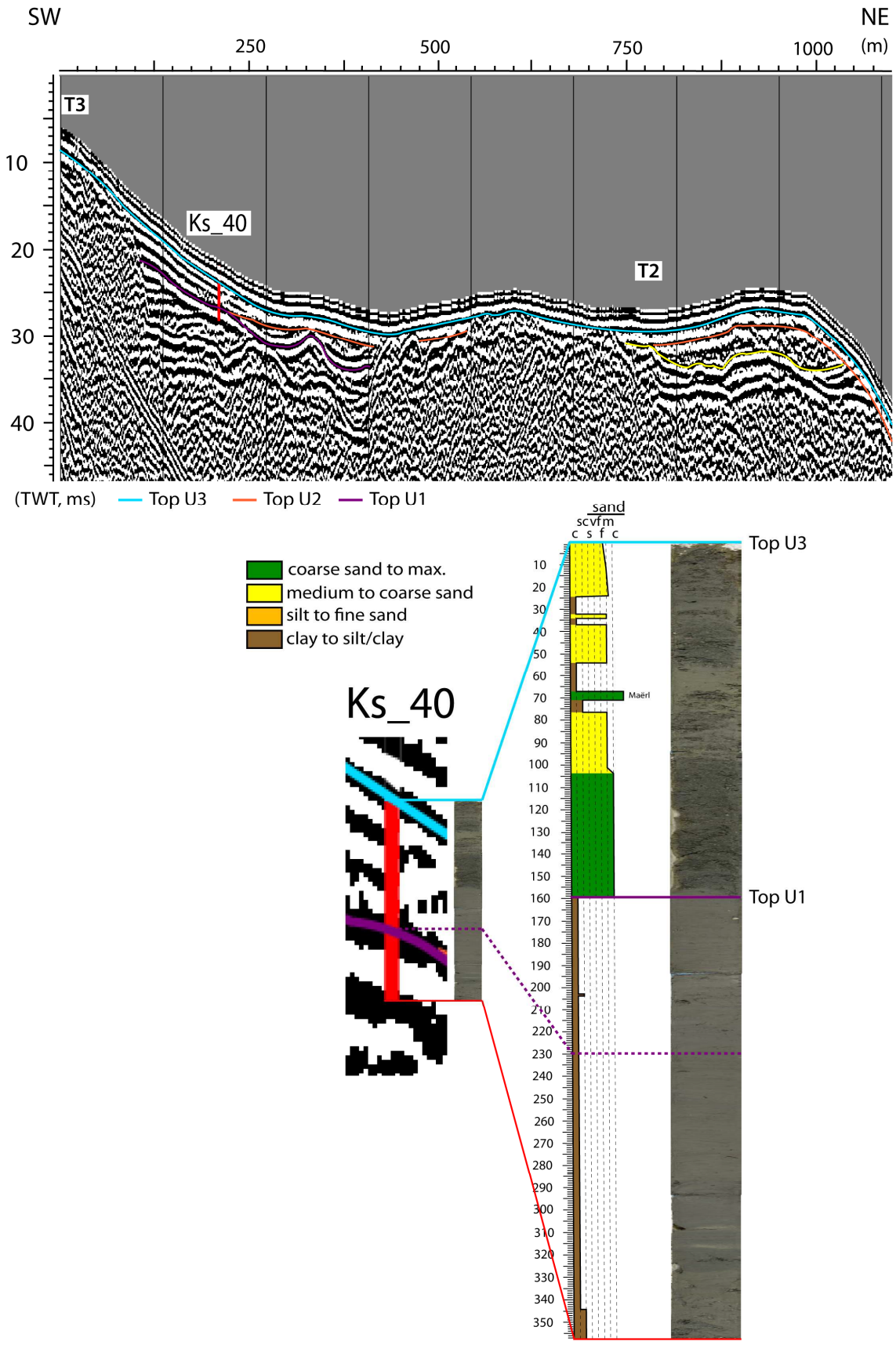

Annexe. 15: (top) Interpreted seismic profile. (bottom) Photograph and lithologic log for core Ks_40. Dashed purple line is marker from seismic interpretation and full purple line represents the interpreted top of U1 (made to compensate the difference of resolution between cores and seismic profile). Maërl: only bioconstructions of Maërls.

DOCTORAT SCIENCES BRETAGNE DE LA MER LOIRE ET DU LITTORAL

IFP Energies nouvelles

Ifremer

UBO Université de Bretagne Occidentale

Titre : Modélisation numérique de l'impact des courants tidaux sur le long-terme : application aux enregistrements sédimentaires Holocène de la rade de Brest.

Mots clés : Dynamiques sédimentaires, estuaire, courants de marée, modélisation hydrodynamique et hydro-sédimentaire, reconstructions paléo-environnementales

Résumé : L'impact de la marée sur les processus hydrodynamiques et le remplissage sédimentaire long-terme (quelques siècles à millénaires) des estuaires reste mal compris. Ces travaux de thèse sont une contribution à la compréhension de cet impact tidal et reposent sur une méthodologie en trois étapes appliquées à la rade de Brest, un estuaire macrotidal et protégé des vagues. (1) Des scénarii paléo-environnementaux représentatifs d'étapes clefs de la dernière transgression marine (~9 ka BP. à actuel) sont construits. (2) Les courants marins et l'impact de la marée sur les sédiments sont simulés pour chaque scénario avec le modèle hydrodynamique MARS3D, puis hydro-sédimentaire MUSTANG. (3) L'impact du forçage tidal sur l'érosion, le transport et le dépôt des sédiments est analysée en fonction de l'évolution de la morphologie de la rade suite à son ennoiement progressif au cours de l'Holocène. Au-delà des conclusions locales, l'étude a permis : (1) de confirmer le schéma conceptuel de dépôt de Dalrymple et al. (2012) à plusieurs stades d'une transgression ; (2) de montrer que la limite de dépôt entre les sédiments sableux et vaseux n'est pas égale à un seuil de profondeur d'eau, mais dépend de la distribution des courants, qui évoluent en fonction du niveau de la mer et de la largeur de la section active; (3) de confirmer une meilleure préservation des unités sédimentaires pendant les haut-niveaux marins (HST) que pendant les transgressions (TST) dans les estuaires dominés par la marée; (4) de mettre en place un laboratoire numérique réutilisable sur 9 ka. L'étude cherche ensuite à définir la (ou les) marée morphogène en rade de Brest au cours de l'Holocène. L'analyse de l'impact de la marée sur les variations du volume de sédiment a démontré que : (1) toutes les variations significatives se produisent durant les vives eaux fortes d'équinoxe et, dans de moindres proportions, durant les vives eaux modérées d'équinoxe et les vives eaux de solstice ; (2) les variations significatives se produisent quand la vitesse maximum de variation de la surface libre lors d'un cycle de flot et jusant dépasse ~1.25 $m.h^{-1}$. Les deux groupes de marée sont prometteurs pour déterminer deux marées morphogènes et obtenir un forçage simplifié pouvant reproduire l'évolution morphologique de l'estuaire sur un an. Ce qui permettrait de réaliser un changement d'échelle temporel et simuler la morphodynamique des estuaires sur de longues durées (quelques siècles à millénaires).

Title : Numerical modelling of the impact of tidal currents over the long-term: application to Holocene sedimentary records from the bay of Brest.

Keywords: Sedimentary dynamics, estuary, tidal currents, hydrodynamic and hydro-sediment modelling, paleo-environmental reconstructions

Abstract: The impact of tides on the hydrodynamic processes and the long-term (centuries to millennia) sediment infill of estuaries remains poorly understood. This thesis is a contribution to the understanding of this tidal impact, based on a three-step methodology applied to the bay of Brest, a macrotidal estuary protected from waves. (1) Paleoenvironmental scenarii representative of key stages of the last marine transgression (~9 ka BP. to present-day) are constructed. (2) Marine currents and tidal impact on sediment are simulated for each scenario with MARS3D hydrodynamic model, then MUSTANG hydro-sedimentary model. (3) The impact of tidal forcing on erosion, transport and deposition of sediments is analysed in relation to the evolution of the morphology of the bay following its progressive flooding during the Holocene. Beyond the local conclusions, the study allowed to: (1) confirm the conceptual deposition scheme of Dalrymple et al. (2012) at several steps of a transgression; (2) show that the depositional boundary between sandy and muddy sediments is not equal to a water depth threshold, but depends on currents distributions, which evolve according to sea-level variation and active flow section width; (3) confirm a better preservation of sedimentary units during high sea-level stages (HST) than during transgressions (TST) in tide dominated estuaries; (4) set up a reusable numerical laboratory over 9 ka. The study then seeks to define the morphogen tide(s) in the bay of Brest during the Holocene. The analysis of the impact of tides on sediment volume variations revealed that: (1) all significant variations occur during equinoctial strong spring tides and, in lesser proportions, during equinoctial moderate and both solstitial spring tides; (2) significant variations occur when the maximum sea surface variations rate, during an ebb and flood cycle, exceeds ~1.25 $m.h^{-1}$. The two tidal clusters are promising to determine two morphogen tides and to obtain a simplified forcing that can reproduce the morphological evolution of the estuary over one year. This would allow a temporal upscaling and to simulate the morphodynamic of estuaries over long periods (a few centuries to millennia).